Mechanics and Planning of Workpiece Fixturing and Robotic Grasping

Thesis by
Qiao Lin

In Partial Fulfillment of the Requirements
for the Degree of
Doctor of Philosophy

California Institute of Technology
Pasadena, California

1998

(Defended May 27, 1998)

Acknowledgements

I would like to thank my advisor, Dr. Joel W. Burdick, for his support and guidance. Throughout the course of this research, I have greatly appreciated his efforts in helping me achieve academic success as well as personal happiness. I would also like to thank Dr. Thomas K. Caughey for his encouragement and enlightening discussions, and thank the other members on my examining committee, Drs. Erik K. Antonsson, Curtis L. Collins, and Jerrold E. Marsden, for their valuable comments and suggestions. Special thanks go to Dr. Elon Rimon at Technion, Israel Institute of Technology, with whom I collaborated during this thesis research. The results from our pleasant collaboration have considerably improved the contents of Chapters 4, 5 and 6. Many helpful discussions with other faculty and students at Caltech are gratefully appreciated as well.

I would like to thank my parents, Zonghua and Wenqing, and my brothers, Shu and Kun, for their support and understanding. I am especially grateful to my wife, Jiuhong, whose love and patience have made this thesis possible. Thanks are also extended to my son, Haiying, for his allowing Daddy to work instead of playing with him.

Mechanics and Planning of Workpiece Fixturing and Robotic Grasping

by

Qiao Lin

In Partial Fulfillment of the
Requirements for the Degree of
Doctor of Philosophy

Abstract

This thesis addresses several key issues in mechanics and automated planning of workpiece fixturing and robotic grasping, including accurate and efficient modelling of compliance, well-defined and practically useful quality measures, and well-defined kinematic metric functions for rigid bodies.

The accurate and efficient modelling of compliant fixtures and grasps is considered. A stiffness matrix formula is derived using the overlap compliance representation for quasi-rigid bodies. In contrast to existing approaches using the linear contact model, this formula is well-suited to automated planning algorithms since it can incorporate realistic nonlinear contact models (e.g., the classical Hertz model), and can be directly computed from CAD data on basic geometric and material properties of the bodies. The formula is then used as a basis for a systematic analysis of local curvature effects on fixture stability. This analysis shows that destabilizing effects of local curvatures are practically negligible, and that curvature effects can be used to stabilize, sometimes significantly, an otherwise unstable fixture. The stiffness matrix formula is also used to show that stability analysis in general depends on the

choice of contact models, which offers additional evidence for the importance of using realistic contact models.

The stiffness and deflection quality measures are defined for compliant fixtures and grasps, and are applied to optimal planning. Unlike existing quality measures that rely on heuristic rules or depend on reference frame choices, the stiffness and deflection quality measures are theoretically sound. Equally important is that these quality measures accurately characterize functional performances which are important to practical fixturing applications, such as fixture stiffness and workpiece deflections. The stiffness and deflection quality measures are applied to optimal fixture and grasp planning, resulting in maximum-stiffness and minimum-deflection fixtures and grasps. The qualitative properties of optimal fixtures are characterized with respect to each quality measure, and efficient techniques are developed for finding such optimal fixtures.

The final key issue is concerned with formal well-definedness conditions and practical development methods for rigid body kinematic metric functions, such as norms, inner products, and distance metrics. Based on an intrinsic definition of the configuration space of a rigid body, the notion of objectivity is proposed to formalize the natural requirement that metric measurements be indifferent to the observers who perform the measurements. This notion is then used to clarify the fundamental physical implications of left, right and bi-invariant functions on $SE(3)$, and is further shown to be equivalent to the notion of frame-invariance. Based on these clarifications, several frame-invariant norms of rigid body velocities and wrenches, which have interesting physical interpretations, are defined.

Contents

List of Figures

List of Tables

Chapter 1

Introduction

1.1 Motivation

With vast advances in computer technology, flexible manufacturing has become an important trend in the manufacturing industries. A flexible manufacturing system consists of computer numerical-controlled (CNC) machine tools linked by a material-handling system, and operates as an integrated system under fully programmable control. Such systems are capable of manufacturing a wide variety of high-quality products at a low cost, and quickly adapting to changes in design, demand and product mix.

Fixturing is an essential part of flexible manufacturing systems. A *fixture* is a device that locates and holds a workpiece using a set of *fixture elements*. The fixture elements, or *fixels*, usually consist of clamps, locators and supports. The clamps actively apply forces on the workpiece, while the locators and supports, which apply reaction forces, are used to accurately locate the workpiece. While CNC machining and many computer-controlled material handling processes are highly automated and possess excellent adaptability, fixturing has remained one of the *least* automated manufacturing processes and often fails to accommodate the wide variety of part geometries to be processed. It is still common to see manufacturing systems with computerized

machining and inspection tools in which fixtures are designed and constructed by humans. The lack of automation makes workpiece fixturing rather costly and inefficient. According to an estimate [152], the cost of fixture design and fabrication for a flexible manufacturing system can amount to 10–20% of the total system cost. Given the huge expenditure on flexible manufacturing systems, it is evident that the automation of fixturing will result in enormous economic benefits.

To enable automated fixturing, it is crucial to automate the design of fixtures, which involves both hardware design and fixture planning. In the fixture planning process, a set of fixture elements is chosen for a given workpiece, and a plan is generated to position the fixture elements on the workpiece's surface. The foremost requirement of such a fixture plan is the complete restraint of the workpiece from undesirable motions. According to the nature of the manufacturing process for which the fixture is designed, the fixture plan must meet several other functional requirements, such as adequate stability and strength, sufficiently small deformation, accuracy and repeatability of workpiece location, freedom from interference between fixels and moving tools, and ease in fixture assembly and disassembly. Upon its generation, the fixture plan is verified by finite element methods and tested on prototype parts. If the plan is found to be invalid, the fixture planning process must be repeated.

Considerable progresses have been made in the innovation of fixture hardware. For example, *flexible fixtures*, such as modular fixtures, conformable fixtures and programmable clamps, have been introduced and are gaining popularity. However, fixture planning, a computationally intensive process that determines the deployment of hardware, has seriously lacked automation. A human designer is still commonly needed to select the fixture elements and come up with a fixture plan according to heuristic rules obtained from his or others' experience. Because of the lack of formal analysis, such an experience-

based plan often fails to meet the typically competing fixture requirements. Thus, many costly and time-consuming iterations are usually required to obtain a valid design. This is particularly true for complex workpieces since the fixturing of such workpieces typically requires prototyping, which is expensive. While attempts have been made at automated fixture planning based on analysis rather than human experience, the analysis methods are usually over-simplified and inaccurate. As a result, automated planning algorithms that are based on such inaccurate analysis methods are valid only in a limited number of applications. An automated fixture planning approach that is based on adequate analytical methods is thus clearly warranted.

Closely related to workpiece fixturing is the problem of robotic grasping, in which robotic fingers are placed on an object in order to achieve a firm grip of the workpiece. In particular, *grasp planning*, in which a plan is generated for finger placement, is dual to fixture planning in the sense that in both processes a set of contacts is sought that prevent undesirable motions of the grasped or fixtured object. The primary difference between fixturing and grasping is that strength, deformation and accuracy requirements are demanding for fixtures, while dexterity of manipulation is often important for grasps.

1.2 Objectives

The general objective of this thesis is to develop analytical and algorithmic tools that will eventually lead to automated planning systems for workpiece fixturing and robotic grasping which are based on *adequate and efficient* physical modelling. Compared with approaches that are based on experience-based heuristic rules or inaccurate analysis techniques, such planning systems use accurate physical models to evaluate the validity of fixture and grasp plans. In addition, the physical models are derived from first principles and can be

computed from CAD data of the workpiece and fixture elements. These features of the approach that is based on accurate and efficient modelling reduce the number of design iterations, and alleviate the need for trial-and-error experimentation in each design iteration. Therefore, the approach is amenable to automation and can generate better and more robust plans in a shorter time and at a lower cost. The following issues in the mechanics and planning of fixtures and grasps will be addressed in the thesis:

(1) Accurate and efficient modelling of compliance in fixtures and grasps.

(2) Well-defined quality measures for compliant fixtures and grasps which accurately characterize performance requirements determined from given manufacturing operations.

(3) Formal conditions and practical development methods for well-defined rigid-body kinematic metric functions, and their application to the development of frame-invariant norms of rigid body velocities and wrenches.

1.3 Contributions

This thesis first makes a contribution to accurate and efficient physical modelling by addressing the computation and analysis of compliance in fixturing and grasping. An *accurate* formula is derived for the fixture stiffness matrix that incorporates *realistic* contact models, such as the classical Hertz model. This formula is in contrast to existing formulas that are based on the linear-spring contact model, which is not supported by elasticity theory or experimental data. The stiffness matrix is expressed in *closed-form* in terms of basic geometric and material properties of the contacting bodies in a fixture, and can hence be *directly* computed from CAD data, including dimensional and shape specifications as well as elasticity constants. Thus, the stiffness matrix

formula is well-suited to automated fixture and grasp planning systems.

The stiffness matrix formula is used as a basis to systematically analyze how the stability of a fixture is influenced by the *local curvature* of the contacting bodies at the contacts. The thesis shows that destabilizing effects of local curvature are practically negligible, and that curvature effects can be used to stabilize, sometimes significantly, an otherwise unstable fixture. It is also shown that fixture stability analysis is generally affected by the *choice of contact models*, which further indicates the importance of using realistic contact models for compliance computation and analysis.

The second contribution of this thesis is the development of well-defined fixture quality measures and the application of these quality measures to optimal planning algorithms. The *stiffness quality measure* is defined as the worst-case characteristic stiffness of a fixture, and the *deflection quality measure* as the worst-case deflection of a fixtured workpiece in response to wrenches lying in a subset of the wrench space, called a *task wrench set*. While existing quality measures for grasps consisting of rigid bodies depend on the choice of reference frames, the stiffness and deflection quality measures explicitly address compliance and are *frame-invariant*. In addition, these quality measures are valid for general compliance models, and apply to two- and three-dimensional workpieces fixtured by any number of fingers. To allow efficient computation of the deflection quality measure, a practical approach is proposed to model a task wrench set, which represents a set of manufacturing operations, in terms of several types of primitive wrench sets that are easily computable.

The stiffness and deflection quality measures are applied to optimal fixture and grasp planning, resulting in maximum-stiffness and minimum-deflection fixtures and grasps. Focusing on three- and four-finger frictionless fixtures of polygonal objects, the qualitative properties of optimal finger arrangements are characterized, and practical algorithms are developed for finding *glob-*

ally optimal finger arrangements with respect to each quality measure. The maximum-stiffness and minimum-deflection fixtures as given in several examples are intuitively effective, thereby demonstrating that the stiffness and deflection quality measures can be practically useful.

In the third contribution, this thesis introduces and investigates the notion of *objective kinematic metric functions* for rigid bodies. Based on an intrinsic definition of the configuration space of a rigid body, the notion of objectivity is introduced to formalize the natural requirement that well-defined metric functions be *indifferent to observers* who perform metric measurements. The physical implications of invariance properties in $SE(3)$, the conventional configuration space of a rigid body, are then clarified in terms of the objectivity notion. It is shown that an objective kinematic function corresponds to a *family* of *left-invariant* metric functions on $SE(3)$, and that left invariance is necessary but not sufficient for objectivity. These observations indicate that bi-invariance is sufficient but not necessary for objectivity, and that right invariant functions in general do not satisfy the objectivity condition and should therefore be *avoided.*

Practical applications of objectivity are made convenient in terms of frame-invariance in the conventional configuration space where reference frames are used to describe rigid body motions. The thesis accurately clarifies the meaning of frame-invariance, and shows that frame-invariance is necessary and sufficient for ensuring objectivity. This in turn clarifies the relationship between frame-invariance and bi-invariance: bi-invariance is sufficient, but not necessary, for frame-invariance. In other words, bi-invariant functions only form a *subset* of frame-invariant functions.

Finally, supported by the equivalence between frame-invariance and objectivity, frame-invariant norms and pseudo-norms of rigid body velocities and wrenches are developed. These norms formalize the notion of "lengths" of

rigid body velocities and wrenches, and to the knowledge of this author, are the first frame-invariant methods for "length" measurement. The thesis gives norms that are induced from inner products, as well as norms that are not inducible from inner products. In both cases, the norms have interesting physical interpretations and are therefore practically useful, as demonstrated by their application to minimum-deflection fixtures and grasps.

1.4 Overview

This thesis uses the term *fixtures* to represent both fixtures and grasps, and the term *fingers* to represent both fixture elements and robotic fingers.

Chapter 2 reviews related research in automated planning of rigid fixtures and grasps, compliance modelling for fixturing and grasping, fixture and grasp quality measures and their application to optimal planning, and rigid body kinematic functions.

Following Chapter 3, which briefly reviews $SE(3)$ (the conventional configuration space of a rigid body), Chapter 4 addresses accurate and efficient modelling of compliance. Section 4.2 introduces several basic assumptions. Section 4.3 considers the modelling of compliant contacts, based on which Section 4.4 derives a closed-form fixture stiffness matrix formula that incorporates realistic contact models. The formula is then used to systematically analyze how fixture stability is influenced by the local curvature of the contacting bodies in Section 4.5, and how stability analysis is affected by the choice of contact model in Section 4.6.

Chapter 5 considers maximum-stiffness fixtures. Section 5.2 defines the principal rotational and translational stiffness parameters, and discusses their frame-invariance and physical interpretations. By meaningfully comparing the rotational and translational stiffnesses, Section 5.3 defines the stiffness

quality measure. Sections 5.4 and 5.5 finally use this quality measure to seek maximum-stiffness three- and four-finger fixtures of polygonal objects.

Chapter 6 addresses minimum-deflection fixtures. Section 6.2 defines the deflection quality measure in terms of frame-invariant velocity and wrench norms. Section 6.3 models task wrench sets by primitive wrench sets, and computes the deflection quality measure in the framework of this modelling scheme. The chapter concludes with section 6.4, which seeks minimum-deflection three- and four-finger fixtures of polygonal objects.

Chapter 7 introduces and investigates the notion of objectivity. Section 7.2 briefly reviews metric functions on manifolds. Section 7.3 gives an intrinsic definition to $\mathcal{C}$, the configuration space of a rigid body, while Section 7.4 represents $\mathcal{C}$ by $SE(3)$. Section 7.5 then defines the notion of objectivity in Euclidean space $\mathbb{E}^3$ and motivates Section 7.6, which defines the notion of objectivity in $\mathcal{C}$. Physical implications of invariance properties in $SE(3)$ are discussed in Section 7.7, followed by a discussion in Section 7.8 on the relations of objectivity to frame-invariance.

Chapter 8 develops several frame-invariant rigid body velocity and wrench norms. Following Section 8.3, which proves that there are no bi-invariant velocity and wrench norms, Section 8.4 proposes frame-invariant velocity norms, while Section 8.5 considers frame-invariant wrench norms that are induced from inner products. The chapter ends with Section 8.6, which presents an algorithm for computing the average wrench norm for planar bodies.

Finally, Chapter 9 summarizes the results of the thesis, discusses problems that remain open for future work, and indicates potential applications of the work reported in the thesis.

Chapter 2

Related Research

Fixturing automation plays an essential role in flexible manufacturing systems [5, 152, 161]. Research on fixturing automation has involved innovative hardware design, as well as automated fixture planning and the dual problem of automated grasp planning.

2.1 Hardware Innovation

While flexible fixturing devices such as computer-controlled vises [147] and numerically controlled clamps [161] have been proposed, fixturing hardware innovation has primarily involved conformable fixturing and modular fixturing. The *conformable fixturing* approach [18, 32, 46, 123], which utilizes fixture elements that are specially designed and fabricated to be capable of conforming to irregular workpiece shapes, can accommodate a wide variety of complex parts. Modular fixturing [60] is presently the most prominent flexible workholding approach. A *modular fixture* consists of a set of standard components including bases, locating and supporting pins, and clamping devices. These standard parts can be assembled as building blocks to form fixtures that are capable of holding a wide variety of part sizes and shapes. As widely recognized [2, 45, 47, 94, 171, 172], the use of modular fixtures can speed up the design and

construction of fixtures for batch manufacturing, which is typical of flexible manufacturing. Since modular fixtures can be disassembled and reused, their use can also reduce fixture storage and retrieval costs. These features make modular fixtures well-suited to flexible manufacturing systems. Modular fixturing systems have been commercially available from several manufacturers such as Bluco, Carr Lane and Jergens, and there are numerous research modular fixture kits, for example, [4, 10, 16, 17, 82, 143, 149, 155]. Research efforts on automated planning of modular fixtures will be reviewed below. The fixture modelling and planning methodologies proposed in this thesis are well-suited to modular fixturing, but they can also be applicable to dedicated fixtures that are used in large-volume manufacturing.

2.2 Automated Design or Planning Systems

Automated fixture design (or planning) systems can be knowledge-based or analysis-based. Knowledge-based fixture design expert systems [22, 37, 42, 91, 98, 111, 116, 144] rely on the knowledge of human experts and artificial intelligence techniques to select fixture elements, determine their positioning on the workpiece, and choose the clamping forces. Likewise, human knowledge and artificial intelligence are used in robotic grasping expert systems [13, 39, 165] to determine finger locations and devise a manipulation process. The knowledge-based approach attempts to mimic the decision process of a human expert, but does not address the fundamental physical principles based on which such decisions are made. Since this approach depends on human experience instead of first principles of science and engineering, the resulting fixture designs or grasp strategies are highly subjective and are not justified by physical laws. Consequently, these designs may not adequately meet given functional requirements.

Analysis-based automated design is built upon analytical modelling of fixtures and grasps. When adequate analytical models are used, the resulting designs will meet desired functional requirements. Along this line, a number of works (for example, [16, 26, 62, 76, 95, 170]) have been devoted to developing automated fixture design systems. Typically in these works, the 3-2-1 guideline [60] is used to determine the placement of the locating and support fixture elements, while geometric and kinematic methods are employed to ensure that the workpiece is completely restrained, has good workpiece location accuracy, and is free from interference between fixture elements and moving tools.

2.3 Methods for Automated Planning of Rigid Fixtures and Grasps

Automated fixture planning lies at the core of automated fixturing. A common approach to automated fixture planning, as well as the dual problem of automated grasp planning, treats workpieces and fixture elements (or robotic fingers) as rigid bodies. Fixtures and grasps consisting of such rigid bodies are said to be *rigid*. The planning of rigid fixtures and grasps can be based on kinematic or force constraint analysis. We review force-based methods in Sections 2.3.1 through 2.3.3, and review kinematic methods in Sections 2.3.4 through 2.3.6.

2.3.1 Force-Closure and Its Characterization

The notion of force-closure uses force constraint analysis to characterize the ability of a grasp to resist external disturbances. This notion was first introduced at the end of the nineteenth century by Reuleaux [132] in his work on mechanism kinematics, and has been widely used in grasp planning since the Ph.D. work of Salisbury [141]. Force-closure grasps are reviewed below.

It is well-known that any system of forces acting on a rigid object is equivalent to a generalized force, which is called a *wrench* and consists of a pure force and a torque. The set of all wrenches is called the *wrench space.* In a coordinate frame, a wrench can be written as a column vector $\boldsymbol{w} = (f, \tau)$, where f and τ are the force and torque components, respectively. A grasp is said to be *force-closure* if it can resist any wrench acting on the grasped object [109]. In other words, given any wrench applied to a force-closure grasp, each finger can apply a force at the contact such that the workpiece is in equilibrium.

The characterization of force-closure is well-developed for grasps where the contacts between the object and fingers are modelled as frictionless or frictional point contacts, or soft-finger contacts. In a *frictionless point contact*, the finger tip can only apply a force in the inward normal direction to the object's surface, while in a *frictional point contact* the finger force lies in a cone symmetric about the contact normal line. The soft-finger model [30] is similar to frictional point contact, but a torque about the contact normal can also be applied. Note that these primitive contact types can be used to describe, either precisely or approximately, more complex contacts. The characterization of force-closure can be given in terms of generating wrenches reviewed below. A *generating wrench* is a wrench due to a finger that applies, as appropriate, a unit force along the associated contact normal, or a unit force along one of two mutually orthogonal directions in the plane perpendicular to the contact normal, or a unit torque about the contact normal. Let the *generating-wrench matrix*, denoted W, be the matrix whose columns consist of the generating wrenches, expressed in a common coordinate frame, corresponding to all the fingers. Then a set of finger force magnitudes, denoted f, induces a wrench Wf. Given any external wrench $\boldsymbol{w}_{ext}$ acting on an object held in force-closure,

there exists f to satisfy the following equilibrium condition:

$$Wf + \boldsymbol{w}_{ext} = 0. \tag{2.1}$$

It follows that a grasp is force-closure if and only if its generating-wrench matrix, regarded as a map from the set of all possible magnitudes of finger force and torque components into the wrench space, is *surjective* [109]. Note that the elements of f are signed for frictional and force components, and are non-negative for force components normal to the object's surface. When all the contacts are *frictionless*, a grasp is force-closure if and only if the full collection of generating wrenches positively span the wrench space [142], or the origin lies in the *interior* of the convex hull of the generating wrenches [107]. The frictionless-contact conditions can be extended to planar grasps with frictionless point contacts [109]. Alternative force-closure tests have also been developed [12, 69, 113, 127, 128, 157].

The bounds on the number of fingers needed to achieve a force-closure grasp have been studies in the robotics literature. While it is well-known that four or seven frictionless point fingers are necessary to form a force-closure grasp of a two- or three-dimensional object without rotational symmetries [83, 132, 148], Mishra, Schwartz and Sharir [107] showed that six and twelve frictionless point fingers are sufficient. These bounds were tightened by Markenscoff, Ni, and Papadimitriou [96], who showed that four and seven frictionless point fingers are sufficient to form a force-closure grasp, respectively, of a bounded non-circular planar object whose boundary is piecewise smooth, and of a class of rather general three-dimensional objects, including all polyhedra.

2.3.2 Planning for Force-Closure

A majority of research on force-closure grasp planning has focused on frictional point fingers. Nguyen [113] proposed a geometric method for computing maximal regions of polygons where two fingers can be placed independently to achieve force-closure. This approach was extended by Faverjon and Ponce [40] to two-finger grasps of curved planar objects. Also addressing two-finger grasps of curved planar objects, Chen and Burdick [23] computed antipodal finger arrangements while Blake and Taylor considered more general finger positions that do not depend on the friction coefficient. Ponce and Faverjon [127] computed the sets of three-finger polygonal force-closure grasps, while Ponce et al. [128] computed three- and four-finger force-closure grasps of polyhedral objects. Park and Starr [121] considered synthesis of three-finger force-closure grasps of polygonal objects, while Mirtich and Canny [105] addressed optimal force-closure grasps of both two- and three-dimensional objects.

While frictional force-closure has been widely used in robotic grasping, it is not as often used in workpiece fixturing except for certain light-duty applications. Most robotic grasps are subjected to relatively light work loads. External forces due to such work loads are quite small and can hence be balanced by friction forces. On the other hand, manufacturing operations such as machining induce forces of magnitude as high as 20 KN (5000 lbf) [53]. Due to the large force magnitude, fixtures that are designed for such manufacturing operations usually do not rely on friction to achieve force-closure except for the special case of mechanical vises and chucks [27]. However, this does not preclude friction from being used to *enhance* fixtures that are force-closure without consideration of friction.

Frictionless force-closure has been used in both grasping and fixturing. Because of the large number (four or more) of fingers involved, research on the planning of frictionless force-closure is relatively sparse. Mishra, Schwartz and

Sharir [107] proposed algorithms for computing at least one force-closure finger arrangement for frictionless polyhedral objects, while Coelho and Grupen [29] cast frictionless force-closure planning as a control composition problem. Nguyen [113] computed maximal regions of polygons such that four fingers can be independently placed in each of these regions to form a frictionless force-closure grasp. Research efforts on planning frictionless force-closure fixtures have been reported in [9, 15, 27, 95, 166, 174, 175], and will be reviewed in Section 2.3.5 since frictionless force-closure is in fact equivalent to the kinematic notion of form-closure.

2.3.3 Force Analysis and Gravitational Stability

It is often necessary to determine the finger forces that are needed to balance an external wrench applied to a force-closure grasp. There is a rich volume of literature in such force analysis for robotic grasping, for example, [11, 19, 25, 70, 75, 164]. As pointed out by Trinkle [157], force-closure fixtures and grasps are typically statically indeterminate, i.e., given an applied wrench, the equilibrium equations are not sufficient to determine the finger forces. Since robotic fingers are actively controlled and always apply *known* forces, static indeterminacy is not a major problem for grasping. However, static indeterminacy makes fixture force analysis quite difficult since fixture elements, except for active clamps, only apply *unknown* reaction forces. Thus, additional assumptions, some of which may be unrealistic, are usually needed in fixture force analysis [15–17, 24, 57, 67, 76, 78, 87]. To resolve this problem, workpiece and fixel deformations must be considered.

A problem related to force-closure is the fixturing of multiple rigid bodies, which are constrained by fixture elements and subjected to gravity, in a *gravitationally stable state.* That is, any instantaneous motion that is allowed by the contact constraints will increase the gravitational potential energy of

the system. Research in this direction has been pursued by Trinkle and his coworkers [158, 159, 169]. Baraff, Mattikalli and Khosla [7] proved that the complexity of finding the smallest set of fixels to fixture a given collection of rigid bodies is NP-hard. A problem related to gravitational stability was studied by Mason, Rimon and Burdick [101, 102].

2.3.4 Form-Closure and Its Characterization

We now review kinematic methods for analysis and synthesis of rigid grasps and fixtures, which are commonly based on the notion of form-closure. A fixture or grasp is said to be *form-closure* if the kinematic constraints of the fingers completely prevent any instantaneous motion of the fixtured object. A form-closure fixture or grasp is also said to be *immobilizing* [137, 138], or to achieve *total restraint* [3].

Screw theory [109, 119] has been commonly used to analyze form-closure fixtures and grasps. Fixels or fingers are assumed to be in point contact with fixtured objects. In screw theory, the kinematic constraint on a workpiece by a contacting finger can be represented in terms of the generating wrench, denoted $\boldsymbol{\eta}$, corresponding to a unit finger force that is normal to the workpiece's surface and points into the workpiece. Any instantaneous motion, denoted by $\dot{q}$, is resisted by the contact if $\boldsymbol{\eta}^T \dot{q} < 0$, and is allowed by the contact if $\boldsymbol{\eta}^T \dot{q} \geqslant 0$. In other words, a contact prevents any motion of the workpiece on which the generating wrench associated with the contact does *negative* virtual work. It follows that a fixture is form-closure if there exists some contact at which $\boldsymbol{\eta}^T \dot{q} < 0$ for any instantaneous motion $\dot{q}$ [108], or equivalently, the set of inequalities $W^T \dot{q} \geqslant 0$ admits no nontrivial solution, where W is the matrix of generating wrenches [3].

In their investigation of immobilizing grasps [135, 137, 138], Rimon and Burdick discovered that the above screw-theory based conditions only iden-

tify a *subset* of form-closure grasps, which they called *first-order form-closure grasps.* Using a configuration space approach, they developed a theory, called *second-order mobility theory,* for the class of essential equilibrium grasps. An *essential equilibrium grasp* is a grasp in which the object is held in equilibrium, without the action of any external wrench, in such a way that all fingers must apply nonzero force to maintain equilibrium. In their theory, an integer index, called *second-order mobility index,* is used to account for the effects of curvature of the contacting bodies at the contact points. Given an essential equilibrium grasp that is not first-order form-closure, if the second-order mobility index is zero, then the grasp is form-closure. Such grasps whose form-closure is determined from the second-order mobility theory are called *second-order form-closure grasps.*

Rimon and Burdick [134, 137] also showed that *a grasp is frictionless force-closure if and only if it is first-order form-closure.* Due to this equivalence, the characterization of frictionless force-closure can be used to characterize form-closure. In particular, the bounds on the number of fingers needed to achieve a frictionless force-closure grasp (Section 2.3.1) also apply to first-order form-closure grasps. According to these bounds, four and seven fingers are respectively needed to hold a two- or three-dimensional object in first-order form-closure. Based on their second-order mobility theory, Rimon and Burdick improved these bounds for planar objects [134]. They showed that generic planar objects can be held in (first- or second-order) form-closure with three convex fingers that have sufficiently flat curvature. Further, if the curvature of the fingers can be chosen to be suitably concave, then form-closure can be achieved for generic planar objects with two fingers.

2.3.5 Planning for Form-Closure

Since frictionless force-closure and first-order form-closure are equivalent, methods for finding frictionless force-closure grasps (e.g., [29, 107, 113] as reviewed in Section 2.3.2) also lead to first-order form-closure grasps. This section primarily focuses on kinematically based methods for planning form-closure fixtures and grasps.

Mani and Wilson [95] presented a kinematic fixture synthesis method by examining the kinematic constraints provided by the combinations of triplets of contact lines. Bausch and Youcef-Toumi [9] defined the notion of "motion stops" associated with screw motions. As a measure of the fixture's geometric resistance to the screw motion, they characterize a first-order form-closure fixture by the condition that positive and negative motion stops exist for each screw motion that is reciprocal to five linearly independent lines of contact. In consequence, the fixture synthesis problem becomes one of finding a fixture that satisfies the motion stop criterion. Based on the frictionless force-closure characterization associated with Equation (2.1), Chou, Chandru and Barash [27] gave a first-order form-closure test for three-dimensional fixtures that requires solving a system of strict inequalities, and proposed a scheme for successively choosing clamps from a candidate set to achieve first-order form-closure in the horizontal plane. When the form-closure principle is applied to modular fixture planning, there are only a *finite* number of fixel arrangements since the fixels can only be located on a regular lattice structure. Brost and Goldberg [15], and Wallack and Canny [166] exploited this fact to develop algorithms for finding the entire collection of first-order form-closure modular fixtures of polygons. Zhuang, Goldberg and Wong [175] considered whether there exists a form-closure fixture plan for a given workpiece and modular fixture kit. Zhuang and Goldberg [174] addressed multiple-purpose fixtures—a multiple-purpose fixture is an arrangement of fixture elements which can

hold more than one part in first-order form-closure, and extended the notion to robust fixture design.

The planning of second-order form-closure grasps were considered by Ponce, Burdick and Rimon [126]. They showed that for planar objects whose boundary is described by polynomial splines, two-finger second-order form-closure grasps form a *discrete* set, while three-finger second-order form-closure grasps form a *two-dimensional* set. The set of three-finger second-order form-closure grasps were then computed using exact cell decomposition and homotopy continuation techniques.

2.3.6 Other Kinematic Considerations

In addition to immobilization of workpiece, other kinematic considerations have been given to fixture planning. In an approach related to second-order form-closure, Rimon and Blake [133] considered the "caging" problem, in which the object has some freedom to move but cannot escape the "cage" formed by the fingers. Addressing kinematic properties of fixture loading and unloading, Asada and By [3] proposed the notions of deterministic positioning, accessibility, detachability and formulated inequality tests for these notions. The notion of *deterministic positioning*, which is concerned with the accurate locating of the workpiece before the clamps are loaded, requires the workpiece to be at a *unique* location when in contact with all the locators. The notions of accessibility and detachability concern the ease of fixture loading and unloading. A workpiece is said to be *accessible* and *detachable* from a fixture if prior to clamping there exists at least one trajectory between the desired workpiece location in the fixture and an outside location, in which the workpiece motion does not conflict with geometrical constraints. Equivalent or alternative tests for these notions have been given by Chou, Chandru and Barash [27], King and Hutter [77], Bicchi [12], and Cai, Hu and Yuan [21].

The 3-2-1 rule for workpiece locating [60] is an experience-based kinematic guideline for the placement of locators on workpieces with plane surfaces. This rule states that a three-dimensional workpiece is located by six points on three planes. The first plane, which usually has the largest surface area, establishes the primary locating plane and is located by three supporting locators. The next largest surface establishes the secondary locating plane and is located with two locators. The final locator is placed on the tertiary plane to complete the location of the workpiece. Fixtures formed according to this rule usually involve more fixture elements (locators and clamps) than necessary, i.e., more than seven fixels are used to form a three-dimensional first-order form-closure fixture. In addition, the rule obviously applies only to workpieces with three suitable flat surfaces. Cai, Hu and Yuan [20] noted that three primary datum points are inadequate for fixturing deformable sheet metal products and proposed an "N-2-1" locating principle in which N ($N > 3$) contacts are used for primary locating.

2.4 Modelling of Compliance in Fixturing and Grasping

Automated planning of fixtures and grasps has primarily been based on the assumption of rigid bodies, as reviewed in Section 2.3. While rigid-body based fixture and grasp planning is acceptable in certain applications, it is inadequate in many fixturing applications. In particular, fixtures for machining operations are subjected to very high cutting forces. Workpieces in such fixtures usually experience deformations that are not negligible, as has been experimentally verified by Hockenberger and De Meter [56, 57]. These deformations must be examined to ensure machining accuracy [145], and the strength of workpieces must be analyzed to avoid any structural damage. While the rigid-body as-

sumption does not allow the computation of deformations, it also causes the problem of static indeterminacy. As discussed in Section 2.3.3, static indeterminacy makes the computation of reaction forces and evaluation of material strength very difficult.

Hence, compliance can play a significant or even dominant role in influencing fixture performance and must be carefully modelled to guarantee the fulfillment of fixturing functions. Three-dimensional finite element modelling has been used to analyze workpiece deformations and stresses in fixtures [28, 86, 103, 129, 149, 156]. Approaches that are based on ideas similar to finite elements have also been suggested (for example, Sinha and Abel [146], and Howard and Kumar [63] discretized the contact regions into a number of small elements). Compared with analytical methods, such discretization-based compliance modelling approaches are accurate, but are computationally expensive and in general do not offer insight into qualitative compliance behaviors of fixtures. Therefore, such methods are appropriate to be used as a verification method for final fixture designs, but not as well-suited for automated fixture planning, in particular for early planning stages.

Closed-form, analytical compliance models are efficient and well-suited to automated fixture planning. The simplest analytical compliance model is based on the linear-spring contact model, which represents a compliant contact as a linear spring attached to the grasped object that is assumed to be rigid. This approach has been widely used to analyze compliant grasps. Among the first to study compliant grasps, Hanafusa and Asada [52] presented a two-dimensional analysis in which a potential function, based on the shape of the object, is used to determine stable positions for a three-finger robot hand. The frictionless fingers were loaded with linear springs and were angularly even-spaced at 120°. Baker, Fortune and Grosse [6] extended the work of Hanafusa and Asada by allowing the angular spacing between the

fingers to vary, and showed that when there is no friction and the fingers' angular spacings are fixed, generally no stable grasping can be achieved for polygonal objects. In these two works, local curvature effects were implicitly included so that stability was achieved by three frictionless fingers. Cutkosky and Wright [33] considered different compliant finger-tip models, and studied the effects of these models on grasp stability. They indicated that stability depends on finger-tip models, initial finger forces as well as local curvatures of finger tips. Kerr and Sanger [74] considered grasps with frictional point fingers whose compliant properties are modelled by linear springs. Nguyen [114] addressed the stiffness and stability of planar and three-dimensional objects grasped by frictional or frictionless fingers modelled by "virtual springs", and showed that a force-closure grasp can be made stable by appropriately choosing "virtual springs". He also demonstrated that the stiffness matrix depends on local curvature as well as whether the fingers stick or slide on the object. Also modelling the fingers by linear springs, Howard and Kumar [64] considered stability of planar grasps, while Donoghue, Howard and Kumar [35] investigated stable workpiece fixturing. Both studies developed stiffness matrix formulas that include the dependence on local contact geometry. However, the authors did not address how to compute the elastic coefficients of the linear springs.

In related work, Whitney [168] proposed the notion of remote center of compliance, which indicates that a mating operation has the best chance of success if the compliance matrix associated with the grasped part is diagonal at the point where the part first touches a mating component. Cutkosky and Kao [31] addressed computing grasp stiffness matrices by including the contributions of the hand and finger mechanisms in addition to the finger tips, and also considered the synthesis problem of specifying servo gains at the joints to achieve a desired stiffness matrix. Howard, Zefran and Kumar [65], and Zefran and Kumar [173] considered the differential geometric properties of

stiffness matrices for mechanical systems that are not in an equilibrium state, but did not consider the modelling of contact compliance. Loncaric [93], and Patterson and Lipkin [122] investigated structures of stiffness and compliance matrices of a robotic manipulator modeled as an elastically supported rigid body. In this work, we derive via a more general approach the characteristic compliance parameters considered by Patterson and Lipkin, and use them to define a fixture quality measure.

While the linear spring compliance model has been widely used in the robotics community, it is not supported by elasticity theory or experimental data. No systematic procedures have been proposed to position the linear spring elements that model contact compliance. Further, the linear spring stiffness coefficients must be determined from experiments, as there are no theoretical models to compute these coefficients from first principles. For automated fixture planning algorithms that would accurately compute fixture arrangements, fixture geometries, fixture reaction forces, and fixtured object deflections from CAD models, these shortcomings of the linear spring model are significant.

A compliance model that is more accurate and more systematically deployable than the linear spring model is clearly needed. This model should afford a closed-form formula that is amenable to analysis and efficient computation. This thesis uses overlap functions [48, 136] to model compliant contacts and derive a closed-form stiffness matrix that incorporates realistic contact models, such as the classical Hertz model. As indicated by Hockenberger and De Meter [58, 59, 104], spherical-tipped locators and clamps are often used to restrain workpieces during machining, and contact region deformation is one of the predominant modes of workpiece displacement for structurally rigid workpieces. These circumstances can be accurately addressed by the Hertz model, and thus offer evidence that the incorporation of the Hertz model in the fixture

stiffness matrix formula is of great practical interest.

2.5 Fixture and Grasp Quality Measures

Quality measures are scalar-valued functions that quantify the effectiveness of grasps and fixtures. In fixture and grasp planning, it is necessary to use quality measures to identify optimal fixel or finger arrangements. To generate fixture and grasp plans that optimally meet given functional requirements, quality measures must faithfully characterize these requirements.

Prior work on quality measures has mostly focused on rigid robotic grasps. Li and Sastry [90] suggested several quality measures for force-closure grasps which are either based on the smallest singular value of the generating-wrench matrix (Section 2.3.1), or ellipsoids in the wrench space modelling manipulation tasks. The quality measure for frictionless force-closure grasps proposed by Kirkpatrick, Mishra, and Yap [79] is defined to be the radius of the maximal ball inscribed in the convex hull of the generating wrenches. This quality measure was extended by Ferrari and Canny [41] to frictional force-closure grasps. While above generating-wrench based quality measures have interesting physical and geometrical properties, they suffer from a major deficiency in their dependence on the choice of reference frames used to express the generating-wrench matrix. When evaluated using these quality measures, a grasp that is optimal under one choice of reference frame may fail to be optimal under another. Several authors have devised schemes to avoid this problem. Markenscoff and Papadimitriou [97] minimized the worst-case finger forces needed to balance any external unit force acting at a specified point in the object. The approach proposed by Mirtich and Canny [105] first computes the grasps that best counteract pure forces, and then selects among these grasps the one which best resists pure torques. Teichmann [151] modified the quality

measure of Kirkpatrick, Mishra, and Yap [79] to the radius of the largest ball inscribed in the convex hull of the generating wrenches with respect to all choices of coordinate frames, but did not discuss the physical interpretation of the approach.

While the above quality measures characterize the overall effectiveness of grasps in withstanding work loads, one may alternatively focus on the margin by which grasp contact constraints are satisfied. Ji and Roth [70] minimized the dependence on friction of the equilibrium finger forces, while Trinkle [157] considered the smallest of the (normalized) equilibrium finger forces. Other quality measures along this line include those proposed by Kerr and Roth [75], Chen, Walker and Cheatham [24], Bicchi [12], and Varma and Tasch [162]. A general discussion of desired properties of grasp quality measures, and a review of several existing quality measures and their application in optimal planning were presented by Mishra [106].

The potentially important role played by compliance in many grasping and fixturing operations calls for the development of quality measures that take these effects into consideration. However, quality measures for compliant grasps and fixtures are rather scarce. While the quality measure proposed by Ponce, Burdick and Rimon [126] applies to three-finger immobilizing rigid grasps, it offers insight into the rotational stiffness of such grasps when compliance is introduced. Prattichizzo, Salisbury and Bicchi [131] defined robustness measures that quantify a compliant grasp's sensitivity to perturbations of a given work load. Cutkosky and Kao [31] pointed out that the eigenvalues of the grasp stiffness matrix provides information on grasp stability. Donoghue, Howard and Kumar [35] proposed using a weighted square sum of the displacement components of a fixtured object induced by a given applied wrench. However, both stiffness matrix eigenvalues and the square sum of the displacement components are *dependent* upon the choice of reference frames.

This thesis builds upon prior work and presents two quality measures for compliant fixtures and grasps. These quality measures are *frame-invariant*, and have interesting physical properties that make them well-suited for fixture and grasp planning. The *stiffness quality measure* focuses on the structure of stiffness matrices. Rather than using the eigenvalues of stiffness matrices, the quality measure is defined based on the frame-invariant principal stiffness parameters of Patterson and Lipkin [122] which we derive in a more general framework. On the other hand, the *deflection quality measure* characterizes deformations of fixtured or grasped objects that are subjected to general disturbances or well-understood work loads. While the deflection quality measure characterizes workpiece deformations, they are based on the *quasi-rigid body* representation of compliance (Section 4.2), rather than general finite element methods as used in other minimum-deformation fixture planning approaches [103, 129]. Thus, the deflection quality measure can be efficiently evaluated and is well-suited to automated fixture and grasp planning.

2.6 Rigid Body Kinematic Metric Functions

Kinematic metric functions for rigid bodies are frequently needed to develop quality measures for fixtures, grasps and other manipulation procedures. It may be desired to measure the "distance" between two locations of a rigid body. There may be a need to measure the "length" of a rigid body velocity or wrench, and/or the "angle" between two rigid body velocities or wrenches. These are all examples of kinematic metric functions, which are real-valued functions of rigid body locations, velocities, and wrenches. Since the practical needs for kinematic metric functions frequently arise, it is important to consider fundamental conditions and practical development methods for well-defined metric functions. Central to well-definedness is the issue of

frame-invariance—the invariance of metric functions to the choice of reference frames.

In the recent years, the effects of choices of coordinate frames on rigid body kinematic metric functions have received much attention from researchers in robotics and other related engineering disciplines. The efforts in developing frame-invariant distance metrics, which form a subset of general metric functions addressed in this thesis, have been relatively successful. Latombe [85, Chapter 2] used the standard distance metric of $\mathbb{R}^3$ to induce two distance metrics on the c-space. Let $\mathcal{B} \in \mathbb{R}^3$ be the region occupied by a rigid body with respect to some body-fixed frame. Given two locations g_1 and g_2 of the body frame relative to a world frame, their distance is defined by $\rho(g_1, g_2) = \max_{r \in \mathcal{B}} \|g_1(r) - g_2(r)\|$, which is frame-invariant. Latombe also employed the Hausdorff distance [50] to define a different distance metric. Kazerounian and Rastegar [73] presented a similar approach by defining a distance metric to be a weighted average of $\|g_1(r) - g_2(r)\|$ over the entire region $\mathcal{B}$. Martinez and Duffy [100] studied these metrics in more detail, and proposed an alternative one that applies to the special case of planar motions. Larochelle and McCarthy [84] considered an approximately bi-invariant distance metric of planar motions which are approximated by pure three-dimensional rotations. This work was extended to spatial displacements by Etzel and McCarthy [38].

A distance metric can also be defined by use of a Riemannian metric. As an inner product of tangent vectors, a Riemannian metric allows one to measure the "length" of a curve in the c-space. Then, the distance between two configurations is defined to be the length of the shortest curve connecting them. Park [120] systematically investigated this approach, while Tchon and Duleba [150] presented a similar investigation. By the lack of bi-invariant Riemannian metrics, Park proved that there exist no differentiable bi-invariant distance metrics on $SE(3)$. He then defined a left (or right) invariant distance

metric using a left (or right) invariant Riemannian metric, which is essentially the Euclidean inner product of two tangent vectors represented as vectors in $\mathbb{R}^6$. In addition, explicit formulas were derived for these distances by use of Riemannian manifold theory. He observed that the left invariant distance is invariant to change of world frame, while the right invariant distance is not influenced by change of body frame. However, he did not indicate well-definedness or applicability conditions for these distances, only remarking that if one frame can be somewhat naturally chosen, then one should use a distance that is not affected by the choice of the other frame.

Several issues pertaining to inner products of rigid body velocities and wrenches have been identified, either directly or indirectly. Duffy [36] showed the fallacy of the definition of two instantaneous motions or wrenches being orthogonal as their representations as vectors in $\mathbb{R}^6$ being orthogonal. He pointed out that this notion of orthogonality depends on the choice of frames as well as the length scale used to compare translations and rotations. Li [88] showed that several manipulability measures based on the grasp Jacobian are frame-dependent and are hence not "well-posed". Note that the use of a Jacobian for this purpose implicitly assumes an inner product structure discussed by Duffy [36]. A similar frame-dependence problem was identified in works on quality measures, for example, Ferrari and Canny [41], Kirkpatrick et al. [79]. In these works, the radii of wrench balls, which are used to define quality measures, depend on frame choices because of the use of the frame-dependent Euclidean wrench norm.

This thesis considers frame-invariant solutions to the practical problems mentioned above. The approach is based on a fundamental understanding of well-definedness, and in particular frame-invariance, of kinematic metric functions afforded by the general principle of objectivity [99]. The physical implications of the invariance properties in $SE(3)$ are clarified and their re-

lations to objectivity and frame-invariance are investigated. Frame-invariant norms, which may or may not be induced from inner products, of velocities and wrenches are proposed. Because of their interesting physical interpretations, these norms can be potentially useful in practical applications.

Chapter 3

Conventional Configuration Space Representation

This chapter introduces notation, and reviews the conventional representation of rigid body kinematics. Some basic results in manifold theory are first reviewed as follows, since the discussion of the configuration space representation makes extensive use of these results.

3.1 Smooth Manifolds

Manifolds are the generalization of curves and surfaces in $\mathbb{R}^3$. This section reviews smooth manifolds, and their tangent and cotangent bundles. Other relevant notions on manifolds will be reviewed in the subsequent chapters when specifically needed. Detailed exposition of manifold theory can be found in References [1, 14].

Let M be a set, which is *not* necessarily a subset of $\mathbb{R}^k$ ($k > 0$ is an integer). A *chart on* M is a pair (ϕ, U) where ϕ is a bijection from a subset $U \subset M$ to an open subset of $\mathbb{R}^n$. Two overlapping charts (ϕ, U) and (ψ, V) are said to be C^∞*-related* if $\psi^{-1} \circ \phi$ is a diffeomorphism where it is defined. Recall that a *diffeomorphism* between two open subsets of $\mathbb{R}^n$ is a smooth (i.e., C^∞-

differentiable) bijection whose inverse is also smooth. An *atlas* is a collection of C^∞-related charts $\{(\phi_i, U_i)\}$ such that $M = \cup_i U_i$. The set M is said to be a *smooth manifold of dimension* n if it admits a smooth atlas $\{(\phi_i, U_i)\}$ such that $V_i = \phi_i(U_i)$ are open subsets of $\mathbb{R}^n$. The map ϕ_i^{-1} or the pair (ϕ_i^{-1}, V_i) is also called a *parametrization* of the subset $U_i \in M$.

Let M be a smooth manifold of dimension n. A smooth curve *at* $x \in M$ is a smooth function $c\colon (-\epsilon, \epsilon) \to M$, with $\epsilon > 0$, such that $c(0) = x$. Two curves c_1 and c_2 in M at x are said to be *tangent* if $\frac{d}{dt}\big|_{t=0} \phi \circ c_1(t) = \frac{d}{dt}\big|_{t=0} \phi \circ c_2(t)$ for some chart (ϕ, U) around x. It can be shown that the notion of tangency is independent of the choice of chart. Tangency at x is an *equivalence relation* among curves at x. A *tangent vector* v to M at x is an equivalence class of curves at x; the curves in the equivalence class are said to be along v or have velocity v. If c is a curve with velocity v, then $\frac{d}{dt}\big|_{t=0} \phi \circ c(t) \in \mathbb{R}^n$ is called the *coordinates* of v induced from the chart (ϕ, U) or parametrization $(\phi^{-1}, \phi(U))$. These coordinates are customarily written as a column vector. Note that if M is a subset of $\mathbb{R}^k$, then $\dot{c}(0) = \frac{dc}{dt}\big|_{t=0}$ is the same for all curves c in an equivalence class. Thus a tangent vector v can be naturally identified with $\dot{c}(0)$, where c is any curve along v. One hence recovers the usual notion of tangent vectors to a surface in $\mathbb{R}^k$. A tangent vector will be denoted by $\dot{c}(0)$ even if M is not a subset of $\mathbb{R}^k$.

The *tangent space*, denoted T_xM, to M at x, is the set of all tangent vectors at x. The tangent space has a vector space structure induced from $\mathbb{R}^n$. The *tangent bundle* of M is a manifold of dimension $2n$ defined by $TM = \cup_{x \in M} T_xM$. The *cotangent space*, denoted T_x^*M, to M at x, is by definition the dual of the tangent space T_xM. That is, a *cotangent vector* (or *covector*) $\alpha \in T_x^*M$ is a real-valued linear functional on T_xM. The *cotangent bundle* is a manifold of dimension $2n$ defined by $T^*M = \cup_{x \in M} T_x^*M$. The *coordinates*, denoted $\bar{\alpha}$ and written as a column vector, of a covector $\alpha \in T_x^*M$ are given

by the equation $\bar{\alpha}^T \bar{v} = \alpha(v)$ for all $v \in T_x M$, where $\bar{v}$ is the coordinates of v.

3.2 Conventional Rigid Body Kinematic Representation

Reference frames have been conventionally used to describe rigid body motions. This approach, while not intrinsic, is convenient for practical calculations and will be used in this thesis. An exception will be made in Chapter 7, where the objectivity notion entails intrinsic description of rigid body kinematics.

3.2.1 Conventional Configuration Space

This section reviews the conventional configuration space representation [109]. Let $\mathcal{B}$ denote a rigid body, whose configuration is conventionally specified in terms of two reference frames. The *world frame*, denoted $\mathcal{F}_W$, is a stationary reference frame. The *body frame*, denoted $\mathcal{F}_B$, is a reference frame fixed to $\mathcal{B}$. The location, $g = \left(\begin{smallmatrix} R & d \\ 0 & 1 \end{smallmatrix}\right)$, of $\mathcal{F}_B$ relative to $\mathcal{F}_W$ specifies $\mathcal{B}$'s *configuration*. Here $d \in \mathbb{R}^3$ is the position of $\mathcal{F}_B$'s origin, and R is a 3×3 proper orthogonal matrix whose columns are unit vectors along $\mathcal{F}_B$'s coordinate axes. The set of all possible locations of $\mathcal{F}_B$ relative to $\mathcal{F}_W$ is called the (conventional) *configuration space*, or *c-space* of $\mathcal{B}$ and is denoted by $SE(3)$.

Given a configuration $g_0 = \left(\begin{smallmatrix} R_0 & d_0 \\ 0 & 1 \end{smallmatrix}\right) \in SE(3)$, the c-space can be parametrized around g_0 using *hybrid coordinates* $q = (d, \theta) \in \mathbb{R}^3 \times \mathbb{R}^3$ by

$$\varphi(q) = \begin{pmatrix} R(\theta) & d \\ 0 & 1 \end{pmatrix} \in SE(3), \tag{3.1}$$

where $R(\theta) = \exp(\widehat{\theta})R_0$ and the operator $\widehat{(\cdot)}$ maps $\theta \in \mathbb{R}^3$ to a skew-symmetric matrix $\widehat{\theta}$ such that $\widehat{\theta}v = \theta \times v$ for all $v \in \mathbb{R}^3$. In this parametrization, g_0 has coordinates $q_0 = (d_0, 0)$. Note that if $\theta \neq 0$, then $\exp(\widehat{\theta})$ is a rotation, of magnitude $\|\theta\|$, about a line that is aligned along θ and passes through $\mathcal{F}_W$'s origin.

It can be shown that hybrid parametrizations around a collection of points in $SE(3)$ can be inverted to form an atlas of C^∞-related charts. Therefore, $SE(3)$ is a smooth manifold of dimension six. Note that the conventional c-space representation depends on the choice of reference frames, and that different frame choices induce different hybrid coordinates. Suppose that $\bar{\mathcal{F}}_B$ and $\bar{\mathcal{F}}_W$ are chosen as body and world frames, respectively, where the location of $\bar{\mathcal{F}}_B$ is $g_B = \left(\begin{smallmatrix} R_B & d_B \\ 0 & 1 \end{smallmatrix}\right)$ with respect to $\mathcal{F}_B$, and that of $\bar{\mathcal{F}}_W$ is $g_W = \left(\begin{smallmatrix} R_W & d_W \\ 0 & 1 \end{smallmatrix}\right)$ with respect to $\mathcal{F}_W$. Then, $g = \left(\begin{smallmatrix} R(\theta) & d \\ 0 & 1 \end{smallmatrix}\right)$ ($\mathcal{F}_B$'s location relative to $\mathcal{F}_W$) transforms to $\bar{g}$ ($\bar{\mathcal{F}}_B$'s location relative to $\bar{\mathcal{F}}_W$) so that the same location of the body is represented. It can be shown that $\bar{g} = \left(\begin{smallmatrix} R(\bar{\theta}) & \bar{d} \\ 0 & 1 \end{smallmatrix}\right)$, where

$$\begin{aligned} \bar{d} &= R_W^T(d - d_W + R(\theta)d_B), \qquad \text{and} \\ \bar{R}(\bar{\theta}) &= \exp(\bar{\theta})\,(R_W^T R_0 R_B) = R_W^T R(\theta) R_B. \end{aligned} \tag{3.2}$$

This introduces a change of parametrization: $q = f(\bar{q})$, where $\bar{q} = (\bar{d}, \bar{\theta}) \in \mathbb{R}^3 \times \mathbb{R}^3$.

3.2.2 Tangent and Cotangent Bundles of $SE(3)$

Since $SE(3)$ is a six-dimensional smooth manifold, tangent and cotangent spaces to $SE(3)$ are six-dimensional vector spaces. The unions of all tangent spaces and cotangent spaces are the tangent and cotangent bundles of $SE(3)$, respectively. Given $g_0 \in SE(3)$, a tangent vector $\mathbf{v} \in T_{g_0}SE(3)$ is a *velocity*,

or *instantaneous displacement*, of $\mathcal{B}$. Such a tangent vector can also be used to approximate a displacement of $\mathcal{B}$ which is finite but is sufficiently small. This approximation approach will be used throughout this thesis for the displacement of a fixtured workpiece due to a given manufacturing operation. Dually, the cotangent space, $T^*_{g_0}SE(3)$, is comprised of covectors to $SE(3)$ at g_0. A covector $\boldsymbol{\alpha} \in T^*_{g_0}SE(3)$ is a *generalized force*, or *wrench*, acting on the object. In the following various representations of tangent vectors and covectors are reviewed, including hybrid, body, spatial, and screw coordinates.

Hybrid Velocities and Wrenches

The hybrid parametrization of $SE(3)$ around $g_0 = \left(\begin{smallmatrix} R_0 & d_0 \\ 0 & 1 \end{smallmatrix}\right)$, as given in Equation (3.1), induces the following representation of tangent vectors: each $\dot{q}_h = (v_h, \omega_h) \in \mathbb{R}^3 \times \mathbb{R}^3$, called a *hybrid velocity*, maps to $\left(\begin{smallmatrix} \widehat{\omega_h} R_0 & v_h \\ 0 & 0 \end{smallmatrix}\right) \in T_{g_0}SE(3)$. The vectors v_h and ω_h have familiar interpretations. Both specified in $\mathcal{F}_W$, v_h is the velocity of the origin of $\mathcal{F}_B$, and ω_h is the angular velocity of $\mathcal{F}_B$. With tangent vectors represented by hybrid velocities, a covector $\boldsymbol{\alpha} \in T^*_{g_0}SE(3)$ is represented by a *hybrid wrench*, denoted $\boldsymbol{w}_h = (f_h, \tau_h) \in \mathbb{R}^3 \times \mathbb{R}^3$, such that $\boldsymbol{w}_h^T \dot{q}_h = \boldsymbol{\alpha}(\mathbf{v})$ for all $\mathbf{v} \in T_{g_0}SE(3)$. Corresponding to the physical interpretation of hybrid velocities, f_h and τ_h, both viewed in $\mathcal{F}_W$, are a force and a torque at the origin of $\mathcal{F}_B$, respectively.

Hybrid velocities and wrenches depend on choices of reference frames. Suppose that the frames $\bar{\mathcal{F}}_B$ and $\bar{\mathcal{F}}_W$ are used as world and body frames. Then corresponding to the change of parametrization $q = f(\bar{q})$ determined by Equations (3.2), hybrid velocities and wrenches are transformed to

$$\dot{q}_h = Df(\bar{q}_0)\dot{\bar{q}}_h \quad \text{and} \quad \bar{\boldsymbol{w}}_h = Df^T(\bar{q}_0)\boldsymbol{w}_h, \tag{3.3}$$

where the Jacobian of f at $\bar{q}_0 = f^{-1}(q_0)$ is given by

$$Df(\bar{q}_0) = \begin{pmatrix} R_W & \widehat{R_0 d_B} R_W \\ 0 & R_W \end{pmatrix}. \tag{3.4}$$

Observe that since d_W and R_B do not appear in the Jacobian, a translation of $\mathcal{F}_W$ or a rotation of $\mathcal{F}_B$ does not affect the transformation.

Body Velocities and Wrenches

Hybrid velocities and wrenches are an intuitive representation of tangent and cotangent vectors. Among other representations that can be convenient are the body and spatial representations. First consider body velocities and wrenches.

Recall that given a hybrid velocity $\dot{q}_h = (v_h, \omega_h)$ and hybrid wrench $\boldsymbol{w}_h = (f_h, \tau_h)$, the vectors v_h, ω_h, f_h, and τ_h are given coordinates in $\mathcal{F}_W$. If these coordinates are given in $\mathcal{F}_B$, then they become a *body velocity*, denoted $\dot{q}_b = (v_b, \omega_b)$, and a *body wrench*, denoted $\boldsymbol{w}_b = (f_b, \tau_b)$. The body and hybrid representations are related by

$$\dot{q}_h = T_{bh}\dot{q}_b \quad \text{and} \quad \boldsymbol{w}_h = T_{bh}\boldsymbol{w}_b, \tag{3.5}$$

where

$$T_{bh} = \mathrm{diag}(R_0, R_0) \tag{3.6}$$

is a block-diagonal matrix. When $\bar{\mathcal{F}}_B$ and $\bar{\mathcal{F}}_W$ are chosen as reference frames,

body velocities and wrenches transform according to

$$\dot{q}_b = \mathrm{Ad}_{g_B}\, \dot{\bar{q}}_b \quad \text{and} \quad \bar{\boldsymbol{w}}_b = \mathrm{Ad}_{g_B}^T\, \boldsymbol{w}_b, \tag{3.7}$$

where Ad_{g_B} is the *adjoint map* associated with g_B given by

$$\mathrm{Ad}_{g_B} = \begin{pmatrix} R_B & \widehat{d_B} R_B \\ 0 & R_B \end{pmatrix}. \tag{3.8}$$

Body velocities and wrenches have the following formal interpretation. Given a tangent vector $\mathbf{v} \in T_{g_0}SE(3)$, the tangent vector $g_0^{-1}\mathbf{v} \in T_eSE(3)$, where $e \in SE(3)$ is the identity rigid transformation, takes the form $g_0^{-1}\mathbf{v} = \left(\begin{smallmatrix} \widehat{\omega_b} & v_b \\ 0 & 0 \end{smallmatrix}\right)$, where $v_b, \omega_b \in \mathbb{R}^3$. It can be shown that $\dot{q}_b = (v_b, \omega_b)$ is precisely the body velocity corresponding to $\mathbf{v}$. The body wrench corresponding to $\boldsymbol{\alpha} \in T_{g_0}SE(3)$ is then determined by $\boldsymbol{w}_b^T \dot{q}_b = \boldsymbol{\alpha}(\mathbf{v})$ for all $\mathbf{v} \in T_{g_0}SE(3)$. Note that unlike the hybrid representation, body velocities and wrenches *cannot* be induced from a parametrization of $SE(3)$.

Spatial Velocities and Wrenches

Dual to the body representation, tangent vectors and covectors can be represented by spatial velocities and spatial wrenches. A tangent vector $\mathbf{v} \in T_{g_0}SE(3)$ can be represented by $\mathbf{v}g_0^{-1} = \left(\begin{smallmatrix} \widehat{\omega_s} & v_s \\ 0 & 0 \end{smallmatrix}\right) \in T_eSE(3)$ for some $v_s, \omega_s \in \mathbb{R}^3$. The *spatial velocity* corresponding to $\mathbf{v}$ is given by $\dot{q}_s = (v_s, \omega_s)$. It can be shown that while ω_s is the angular velocity of $\mathcal{F}_B$ as specified in $\mathcal{F}_W$, v_s is the velocity, specified in $\mathcal{F}_W$, of a point in $\mathcal{B}$ that coincides with the origin of $\mathcal{F}_W$ at the time of instantaneous motion. The *spatial wrench*, denoted $\boldsymbol{w}_s = (f_s, \tau_s)$ and corresponding to $\boldsymbol{\alpha} \in T_{g_0}SE(3)$, is determined by $\boldsymbol{w}_s^T \dot{q}_s = \boldsymbol{\alpha}(\mathbf{v})$ for all $\mathbf{v} \in T_{g_0}SE(3)$. Note that f_s and τ can be interpreted as a force and torque

specified with respect to $\mathcal{F}_W$ and acting at the origin of $\mathcal{F}_W$. The spatial and body representations are related by

$$\dot{q}_s = \mathrm{Ad}_{g_0}\, \dot{q}_b, \quad \text{and} \quad \boldsymbol{w}_b = \mathrm{Ad}_{g_0}^T\, \boldsymbol{w}_s. \tag{3.9}$$

where the adjoint Ad_{g_0} can be computed from the formula (3.8).

Similar to the body representation, the spatial representation *cannot* be induced from a parametrization of $SE(3)$. Unlike the hybrid and body representations, spatial velocities and wrenches will not be used extensively in this thesis. However, their suitability for use in rigid body metric functions will be examined in Chapter 7.

Screw Coordinates of Velocities and Wrenches

Tangent vectors and covectors afford geometric interpretations in terms of screw coordinates. The screw description can be given either in the body frame or spatial frame, based on body or spatial coordinates. The screw coordinates associated with a body or spatial velocity $\dot{q} = (v, \omega)$ consist of a *screw axis* l, a *pitch* h, and a *screw magnitude* θ. The velocity can be described as an instantaneous rotation by an amount θ about l, followed by an instantaneous translation along l by an amount θh. If $\omega \neq 0$, the screw coordinates are given by $l = \{\omega \times v/\|\omega\|^2 + a\omega : a \in \mathbb{R}\}$, $h = \omega^T v/\|\omega\|^2$, and $\theta = \|\omega\|$. Therefore, the screw axis is a line directed along ω and passing through the point $\omega \times v/\|\omega\|^2$. If $\omega = 0$, then $l = \{0 + av : a \in \mathbb{R}\}$ and $\theta = \|v\|$, while h is said to be infinite.

Dually, the screw coordinates of a body or spatial wrench $\boldsymbol{w} = (f, \tau)$ also consist of a *screw axis* l, a *pitch* h, and a *screw magnitude* F. The wrench is equivalent to a force of magnitude F along the directed line l and a torque of magnitude Fh about l. If $f \neq 0$, then $l = \{f \times \tau/\|f\|^2 + af : a \in \mathbb{R}\}$, $h = f^T\tau/\|f\|^2$, and $F = \|f\|$. The screw axis is hence a line directed along f

and passing through the point $f \times \tau / \|f\|^2$. If $f = 0$, then $l = \{0 + a\tau : a \in \mathbb{R}\}$, $F = \|\tau\|$, and h is infinite.

3.2.3 Representation of Planar Motions

In the special case that the object is restricted to move in a plane, choose the z-axes of the world and body frames to be perpendicular to the plane. Then the configuration space, now denoted $SE(2)$, is a three-dimensional manifold. The body's configuration is given by $g = \left(\begin{smallmatrix} R & d \\ 0 & 1 \end{smallmatrix}\right) \in SE(2)$, where $d \in \mathbb{R}^2$ and R is a 2×2 proper orthogonal matrix. In the hybrid parametrization (3.1), $q = (d, \theta) \in \mathbb{R}^2 \times \mathbb{R}$, and $R(\theta) = \exp(-\theta J)$, where

$$J = \begin{pmatrix} 0 & 1 \\ -1 & 0 \end{pmatrix}. \tag{3.10}$$

In the hybrid, body and spatial representations, linear velocities and force components become vectors in $\mathbb{R}^2$, while angular velocities and torques become scalars. The transformation rules and representation relationships as given in Equations (3.3), (3.5), (3.7) and (3.9) remain to hold. However, the Jacobian $Df(\bar{q}_0)$ and transformation matrix T_{bh} now become

$$Df(\bar{q}_0) = \begin{pmatrix} R_W & JR_0 d_B \\ 0 & 1 \end{pmatrix} \quad \text{and} \quad T_{bh} = \operatorname{diag}(R_0, 1), \tag{3.11}$$

while the adjoint matrix associated with $g_B = \left(\begin{smallmatrix} R_B & d_B \\ 0 & 1 \end{smallmatrix}\right) \in SE(2)$ takes the form

$$\mathrm{Ad}_{g_B} = \begin{pmatrix} R_B & Jd_B \\ 0 & 1 \end{pmatrix}. \tag{3.12}$$

The following notational convention concludes the review of conventional c-space representation. For convenience, elements of $SE(3)$ or $SE(2)$ will be referred to by their hybrid coordinates. Likewise, tangent vectors or covectors will also be referred to by their hybrid or body representations. Therefore, notations such as $q = (d, \theta) \in SE(3)$, $\dot{q} = (v, \omega) \in T_{q_0}SE(3)$, and $\boldsymbol{w} = (f, \tau) \in T^*_{q_0}SE(3)$ will be conveniently used when there is no risk of confusion.

Chapter 4

Accurate Modelling of Compliant Fixtures and Grasps

4.1 Introduction

As indicated in Chapter 2 (Section 2.4), compliance modelling that is based on linear-spring models is not supported by experiments or elasticity theory, and there is a strong need for a compliance model which is more accurate and more systematically deployable than the linear-spring models. Such a model should offer a closed-form formula amenable to analysis and efficient computation, and be supported by experimental data and results from elasticity theory. This chapter develops a general compliance model that possesses such desired features using overlap functions. The use of overlap functions has been proposed by Gesley [48] and by Rimon and Burdick [136], and this chapter extends their work. Realistic nonlinear contact models (such as the Hertz model) are formulated using overlap functions, and then applied to the computation and analysis of the fixture stiffness matrix. The resulting stiffness matrix formula admits nonlinear as well as linear contact models. When applied to the linear-spring model, the formula agrees with the prior results of Nguyen [114]. When applied to the experimentally verified and theoreti-

cally justified Hertz contact model [54], the stiffness matrix offers a realistic description of fixture compliance.

Since the Hertzian stiffness matrix can be calculated from first principles, it can be automatically determined from the material and geometrical properties of the contacting bodies. This is in contrast with the linear-spring stiffness coefficients, which are determined in an ad-hoc way. Further, the Hertzian stiffness matrix is used to investigate the significance of surface curvature effects to overall fixture stiffness. Curvature effects have recently been suggested as a means for reducing the number of fingers needed to fixture an object [34, 134], and these effects have been deployed by Ponce for fixturing polyhedral objects [125]. The analysis in this chapter supports the use of these effects in certain circumstances. It will be shown that destabilizing curvature effects are practically negligible, while stabilizing curvature effects may desirably be quite significant. This chapter also study the influence of different choices of contact models on the qualitative stability of a fixture. It will be demonstrated that while stability analyses according to the linear-spring model and the more realistic Hertz model can be qualitatively similar, the two models may in general lead to qualitatively different stability results.

This chapter needs a parametrization of the configuration space of a rigid body. The hybrid parametrization as given in Equation (3.1) will be conveniently used. Accordingly, hybrid velocities and wrenches are used, which are induced from the hybrid parametrization, to represent tangent vectors and covectors. This chapter is organized as follows. Section 4.2 introduces some basic assumptions on compliant fixtures. Section 4.3 then discusses the modelling of compliant contacts with overlap functions, and reviews the Hertz theory in the context of overlap functions. Section 4.4 derives a closed-form formula for the stiffness matrix using overlap functions. The formula is used in Section 4.5 to analyze the effects of local curvature on the stability of a

fixture, and in Section 4.6 to analyze the impact of different choices of contact model on the stability of a fixture.

4.2 Basic Assumptions

This section introduces a few basic assumptions on compliant fixtures. A *fixture* or *grasp* consists of an object, denoted $\mathcal{B}$, contacted by m fingers $\mathcal{A}_1, \ldots, \mathcal{A}_m$. It is assumed that the contacts are *frictionless*, that in the absence of deformations the each finger touches the object at an *isolated point*, and that boundaries of the bodies near the contact points are *smooth*. In addition, we make the key assumption that the bodies are *quasi-rigid*, i.e., deformations due to compliance effects are assumed to be localized to the vicinity of the contact points, so that the overall motion of $\mathcal{B}$ relative to the fingers can be described using rigid body kinematics. The quasi-rigidness assumption holds with reasonable accuracy provided that the bodies do not possess slender structures. It is also assumed that the quasi-rigid fingers $\mathcal{A}_i$ are *stationary*. This allows one to focus on the overall motion of the quasi-rigid body $\mathcal{B}$ in terms of $\mathcal{B}$'s configuration space. Recall from Section 3.2.1 that a configuration of $\mathcal{B}$, regarded as a rigid body, is a location of a body-fixed frame $\mathcal{F}_B$ relative to a stationary world frame $\mathcal{F}_W$. The final assumption is that the object is held in an equilibrium fixture, as reviewed below.

As a fixtured object $\mathcal{B}$ is in frictionless contact with the fingers, the i^{th} finger applies a force $F_i N_i$, where F_i is the magnitude of the force, and N_i is the unit normal at the i^{th} contact pointing into $\mathcal{B}$. This force applies a wrench, given by $F_i \boldsymbol{\eta}_i$ with respect to the origin of $\mathcal{F}_B$, where $\boldsymbol{\eta}_i = \begin{pmatrix} N_i \\ Rr_i \times N_i \end{pmatrix}$, called the *generating wrench* at the i^{th} contact, is the wrench due to a unit finger force. In this formula, r_i is the position of the i^{th} contact point in $\mathcal{F}_B$, while R is the orientation of $\mathcal{F}_B$ relative to $\mathcal{F}_W$. The fixture is called an *equilibrium fixture*

if in the absence of a disturbing wrench, the finger forces satisfy the following equilibrium condition:

$$F_1\boldsymbol{\eta}_1 + \cdots + F_2\boldsymbol{\eta}_m = 0. \tag{4.1}$$

Let $\nu_i = F_i / \sum_{j=1}^{m} F_j$ be the normalized force magnitudes. Then it follows that an arrangement of the fingers forms an equilibrium fixture if and only if there exist scalars ν_i such that

$$\nu_1\boldsymbol{\eta}_1 + \cdots + \nu_m\boldsymbol{\eta}_m = 0, \qquad 0 \leqslant \nu_i \leqslant 1 \quad \text{and} \quad \sum_{i=1}^{m} \nu_i = 1. \tag{4.2}$$

In words, if the zero wrench can be expressed as a convex combination of the generating wrenches, there exist suitable finger force magnitudes which generate an equilibrium fixture.

4.3 Modeling Contact Compliance

This section introduces a general approach to modelling a compliant contact based on the notion of overlap, and reviews the classical Hertz theory in the context of the overlap approach. We focus on a particular contact and omit the subscript i as appropriate.

4.3.1 The Overlap Representation

Let an object $\mathcal{B}$ be in point contact with a stationary finger $\mathcal{A}$. When $\mathcal{B}$ is displaced towards $\mathcal{A}$, the surfaces of the two bodies deform in the vicinity of the contacts. One wishes to ignore the details of surface deformation, and model the resultant contact force as a function of the displacement of $\mathcal{B}$. Such a model

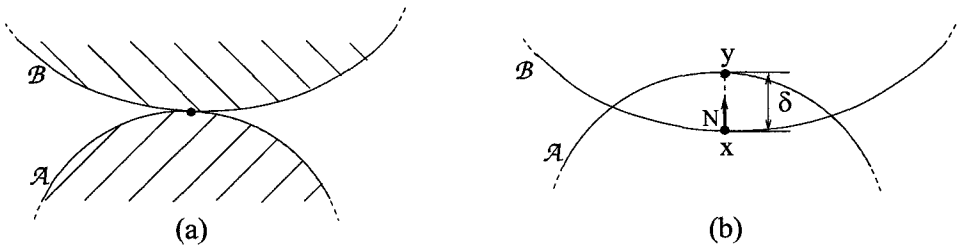

Figure 4.1: (a) An initial point contact. (b) After a relative approach of δ.

is based on *overlap functions* [136] as follows. Let $\mathcal{B}(q)$ denote the subset of $\mathbb{R}^3$ occupied by the undeformed shape of $\mathcal{B}$, when $\mathcal{B}$ is at a configuration q. Let the boundaries of $\mathcal{B}(q)$ and the undeformed shape of $\mathcal{A}$ be denoted $\partial\mathcal{B}(q)$ and $\partial\mathcal{A}$. Rather than solve for the surface deformation, imagine that the rigid shape of $\mathcal{B}$ freely penetrates the rigid shape of $\mathcal{A}$. The *overlap* between $\mathcal{B}(q)$ and $\mathcal{A}$, denoted $\delta(q)$, is defined as the minimum amount of translation that would separate $\mathcal{B}$ from $\mathcal{A}$. At the initial contact configuration $\mathcal{B}(q)$ and $\mathcal{A}$ intersect at an isolated point, and $\delta(q) = 0$. Similarly, $\delta(q)$ is zero at configurations where $\mathcal{B}(q)$ is disjoint from $\mathcal{A}$. When $\mathcal{B}(q)$ overlaps the finger $\mathcal{A}$, there exists a unique *overlap segment*[1] with endpoints $x \in \partial\mathcal{B}(q)$ and $y \in \partial\mathcal{A}$, such that $\delta = \|x - y\|$ (Figure 4.1). Moreover, the normals to $\partial\mathcal{B}(q)$ and $\partial\mathcal{A}$ at x and y are collinear with the overlap segment. The overlap $\delta(q)$ is generally a nonlinear function of q, and is smooth at points q where $\delta(q) > 0$.

The overlap δ is known in the contact mechanics literature as the *relative approach* of the two bodies [49, 72]. Also in agreement with the contact mechanics literature, the contact force is assumed to act along the overlap segment $\overline{xy}$. The force's magnitude, denoted F, is assumed to depend on the overlap in terms of a function f,

$$F = f(\delta). \tag{4.3}$$

[1]The overlap segment is unique for all sufficiently small overlaps δ [136].

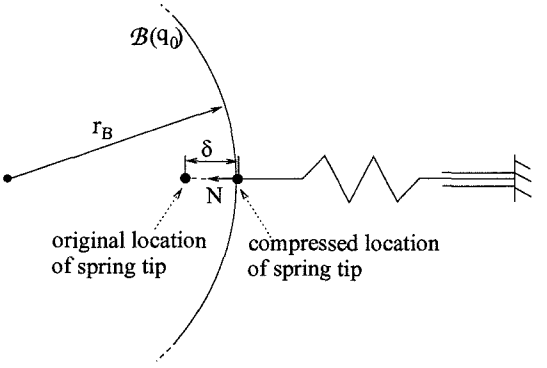

Figure 4.2: Linear spring model.

The function f is required to be differentiable, zero when its argument is zero, and positive when its argument is positive. (In particular, the derivative $f'(\delta)$ is positive at $\delta = 0$.) To summarize, the contact force has magnitude $F = f(\delta)$ and direction $N(x)$, where $N(x)$ is the inward-pointing unit normal to $\mathcal{B}$ at the endpoint x of the overlap segment (Figure 4.1).

Linear spring example. To provide a sense of continuity with the existing literature [52, 114, 125], consider the case of an object held by m linear springs. As illustrated in Figure 4.2, each spring is assumed to act along a *fixed* direction which is aligned with $\mathcal{B}$'s surface normal at the contact. At the equilibrium, the overlap $\delta(q_0)$ is the net compression of the i^{th} spring, and the magnitude of the spring force is $F = k\delta(q_0)$, where k is the spring stiffness. Thus in the linear-spring case f is simply linear in δ. However, our focus is on modelling the naturally occurring compliance in contacting bodies, for which the Hertz contact model is more suitable.

4.3.2 The Hertz Contact Model

The Hertz contact model (1882) describes the elastic interactions between two contacting quasi-rigid bodies [54, 72], and has been experimentally verified by several investigators [43]. This section summarizes the Hertz model, showing that it corresponds to a particular choice of the compliance function (4.3) in

terms of the overlap.

The Hertz theory addresses the non-conforming contact problem. When the non-conforming bodies $\mathcal{B}$ and $\mathcal{A}$ are brought into contact, they touch initially at a single point or a line, depending on their initial shapes. Under the action of the load, they deform and touch over a finite area (termed the *contact area*) surrounding the point or line of first contact, while the undeformed shapes of $\mathcal{B}$ and $\mathcal{A}$ have an overlap δ. The interactive normal tractions in the contact area are called the *contact pressure*, and the integral of the contact pressure gives the magnitude of the net contact force.

First consider the *point contact* case, where the bodies initially contact at a point. Let $N(x)$ be the inward unit normal to the surface of $\mathcal{B}$ at x, and $N(y)$ the outward unit normal to the surface of $\mathcal{A}$ at y. The *curvature matrices* (or Weingarten maps [153]) of $\mathcal{B}$ and $\mathcal{A}$ at the initial contact point, $x_0 = y_0$, are given by

$$L_B = -DN(x)\big|_{x=x_0} \quad \text{and} \quad L_A = DN(y)\big|_{y=y_0},$$

respectively. Recall that the curvature matrix at some point of a surface, when acting upon a tangent vector, measures the rate of change of the unit outward normal to the surface along the tangent vector. The reciprocals of the eigenvalues of the curvature matrix restricted to the tangent space are called the *principal radii of curvature* of the surface. The *relative curvature matrix* of the surfaces of $\mathcal{B}$ and $\mathcal{A}$ at $x_0 = y_0$ is defined by $L_{rel} = L_A + L_B$. The reciprocals of the eigenvalues of L_{rel} (again restricted to the tangent space), denoted by r_{rel1} and r_{rel2} ($r_{rel1} \geqslant r_{rel2}$), are called the *principal radii of relative curvature*. It is assumed that L_{rel} is *positive definite*, which guarantees that the bodies initially contact at a single point.

In the Hertz theory, the boundary of the contact area is assumed to be an

ellipse with principal semi-axes a and b ($a \geqslant b$). For non-conforming contact, a and b are very small when compared with the characteristic dimension of the bodies, the magnitude of the bodies' principal radii of curvature, as well as the magnitude of the principal radii of relative curvature. The *eccentricity ratio* of the contact area, defined by $e = (1 - b^2/a^2)^{\frac{1}{2}}$, is determined from the equation

$$\frac{(1-e^2)^{-1}\mathbf{E}(e) - \mathbf{K}(e)}{\mathbf{K}(e) - \mathbf{E}(e)} = \frac{r_{rel1}}{r_{rel2}}, \tag{4.4}$$

where $\mathbf{K}(e)$ and $\mathbf{E}(e)$ are complete elliptic integrals.

The contact force magnitude, the maximum pressure $p_{\max}$ over the contact area and $c = \sqrt{ab}$, which together with e determines a and b, are given as follows in terms of the overlap δ.

$$f(\delta) = (4/3)\beta_1(e)E^* r_e^{\frac{1}{2}} \delta^{\frac{3}{2}}, \tag{4.5}$$

$$p_{\max} = (2/\pi)\beta_2(e)E^*(\delta/r_e)^{\frac{1}{2}}, \tag{4.6}$$

$$c = \beta_3(e)(r_e\,\delta)^{\frac{1}{2}}, \tag{4.7}$$

where $r_e = (r_{rel1}r_{rel2})^{1/2}$. In these formulas, E^* is determined from basic material properties as follows.

$$\frac{1}{E^*} = \frac{1-\nu_A^2}{E_A} + \frac{1-\nu_B^2}{E_B},$$

where E_B and E_A are Young's moduli, and ν_A and ν_B are Poisson's ratios of

$\mathcal{B}$ and $\mathcal{A}$. The coefficients β_i, which approach 1 as $e \to 0$, are given by

$$\beta_1(e) = \frac{\pi}{\sqrt{2}e\mathbf{K}^{\frac{3}{2}}(e)}\Phi^{\frac{1}{4}}(e),$$
$$\beta_2(e) = \frac{\pi e}{2\sqrt{2}(1-e^2)^{\frac{1}{2}}\mathbf{K}^{\frac{1}{2}}(e)}\Phi^{-\frac{1}{4}}(e),$$
$$\beta_3(e) = \frac{\sqrt{2}(1-e^2)^{\frac{1}{2}}}{e\mathbf{K}^{\frac{1}{2}}(e)}\Phi^{\frac{1}{4}}(e),$$
$$\Phi(e) = (\mathbf{K}(e) - \mathbf{E}(e))((1-e^2)^{-1}\mathbf{E}(e) - \mathbf{K}(e)).$$

Observe that the compliance function (4.5) is of the form $f(\delta) = c\delta^{3/2}$, which implies that *the Hertz contact model corresponds to a particular choice of the function $f(\delta)$ in the overlap model* (4.3). It is also practically important to note that, this compliance function, along with the formulas (4.6) and (4.7), are fully specified in terms of the relative curvature and material properties at the contact.

In deriving Equation (4.5), the local deformations near the contact point are calculated by regarding each body as an elastic half space loaded over a small elliptical region of its plane surface. This treatment, which can be justified by the smallness of the contact area, allows one to ignore the detailed shape of the body outside the local contact region. A local displacement field computed this way decays with distance ρ from the contact point as $1/\rho$. Thus, with the natural assumption that the elastic half space is "fixed at infinity", i.e., the displacement approaches zero as $\rho \to \infty$, one finds the local deformations (in particular, the displacement of the contact point) of each surface.

Now consider the *line contact* problem. The elastic properties of planar objects can be approximately modelled by cylinders whose cross section is the desired planar shape. Such cylinders will contact along a line, and the loading

per unit length of the contact will be taken as a model for planar contact. For simplicity, neglect the effects of the bodies' finite length . Instead of the overlap δ, it is more convenient to use the resultant contact force F (per unit length) as the independent variable. Then the maximum pressure $p_{\max}$ and the half-width a of the contact area, which is a narrow strip along the initial contact line, are given by

$$p_{\max} = (\frac{E^* F}{\pi r_{rel}})^{\frac{1}{2}}, \tag{4.8}$$

$$a = (\frac{\pi E^*}{4 F r_{rel}})^{\frac{1}{2}}, \tag{4.9}$$

where the relative radius of curvature r_{rel} is determined by $1/r_{rel} = 1/r_B + 1/r_A$, with r_B and r_A the radii of $\mathcal{B}$ and $\mathcal{A}$ at the contact (positive if convex).

To determine the compliance relationship, i.e., the dependence of δ on F, one may again regard each body as an elastic half space loaded over an infinitely long narrow strip. Unfortunately, a major difficulty arises from the limitations of two-dimensional elasticity theory. The displacement field now decays with the distance ρ from the contact point as $\ln \rho$, and the assumption of the half-space being "fixed at infinity" leads to an infinitely large displacement at the contact point. Therefore, to obtain finite local deformations, one must choose a datum point which is at a finite distance from the contact point. For instance, choose a datum point for each body such that it lies on the inward contact normal at a distance ℓ_B (or ℓ_A) from the contact point. Then one can show that the overlap δ is given by

$$\delta = F\Big\{\frac{(1-\nu_B^2)}{\pi E_B}\big(\ln\frac{\pi E^* \ell_B^2}{4F r_{rel}} - \frac{\nu_B}{1-\nu_B}\big) + \frac{(1-\nu_A^2)}{\pi E_A}\big(\ln\frac{\pi E^* \ell_A^2}{4F r_{rel}} - \frac{\nu_A}{1-\nu_A}\big)\Big\}. \tag{4.10}$$

As noted by Johnson [71] and Poritsky [130], the logarithmic dependence on ℓ_B and ℓ_A makes the compliance relationship reasonably insensitive to the choice of datum points.

The compliance relationships given by (4.5) and (4.10) are all *nonlinear* in terms of the overlap δ. While the linear spring model is generally not appropriate, there are special circumstances where a linear relationship can be approximately used. For a circular cylinder of finite length in non-conforming contact with a pair of diametrically opposed bodies, Nikpur and Gohar [115] review approximate formulas including linear or nearly linear spring relationships. In the context of fixturing or grasping, if contacts resemble this structure, the linear spring model can be used with reasonable accuracy. Otherwise, the linear spring model is generally *not* justified.

When the bodies are conforming, the Hertzian conditions are no longer satisfied. It is no longer adequate to consider only local deformations, and the overall deformation of at least one of the bodies must be considered. The determination of the functional relationship (4.3) becomes very difficult. In general this function is no longer in closed form and must be found numerically or experimentally. A special type of conforming contact was investigated by Goodman and Keer [49]. They investigated the problem of an elastic sphere indenting an elastic spherical cavity, whose radius is only slightly larger than the sphere's. Their numerical results showed a moderately harder load-overlap relationship than predicted by the Hertz model. Since the Hertz model will predict a moderately softer contact than actually prevails, it may be possible to treat contacts of this type by the Hertz theory and obtain a conservative estimate of contact compliance.

It is important to note that the overlap representation (4.3) is valid under more general circumstances than those assumed by Hertz theory. For example, the surfaces do not have to be smooth at the contact, and the size of the

contact area does not have to be always small compared with the size of the bodies, although in the former case $\delta(q)$ may fail to be differentiable. So long as the contacts are frictionless and the relative approach of the elastic bodies is reasonably well-defined and small, the resultant contact force can be expressed as a function of the overlap. This understanding is key to the ensuing discussion of geometric effects in fixture stability.

Finally, notice that realistic modelling of contact compliance, for instance using the Hertz model, is still desirable even if one wishes to use a linear model. Since linear models are in general not theoretically supported, they often have to be determined experimentally. Obviously, the dependence on experimental data is a serious limiting factor on automated fixture or grasp planning algorithms. Thus as an alternative to the experimental approach, a linear model may be determined from a realistic model. Specifically, let $F = f(\delta)$ be a nonlinear model that can be computed from first principles. Choose an overlap value δ_0, at which value the fixture is expected to be preloaded. Then a linear model, $F = k\delta$, can be obtained by setting $k = f'(\delta_0)$, which is called a *tangent modulus*, or $k = f(\delta_0)/\delta_0$, which is called a *secant modulus*. The use of a secant modulus will be illustrated in Example 4.6.1.

4.4 Computation of the Stiffness Matrix

We have thus far developed a contact modelling scheme in which the direction and magnitude of the i^{th} finger force depend on the object's configuration via the overlap $\delta_i(q)$. Based on this scheme, this section derives a formula for the stiffness matrix of an equilibrium fixture in terms of the overlap functions and their derivatives. Then the computation of the terms which appear in the stiffness matrix formula will be discussed.

4.4.1 A Formula for the Stiffness Matrix

First, it will be useful to express the elastic potential of an m-finger fixture as a function of the overlap functions $\delta_i(q)$. Recall that $F_i = f_i(\delta_i)$ is the magnitude of the i^{th} finger force associated with a given compliance model (such as the Hertz model). Then the elastic potential energy of the system consisting of an object $\mathcal{B}$ fixtured by fingers $\mathcal{A}_1, \ldots, \mathcal{A}_m$ is

$$\Pi(q) = \sum_{i=1}^{m} \int_0^{\delta_i(q)} f_i(\sigma) d\sigma. \tag{4.11}$$

Since f_i is assumed differentiable and $\delta_i(q)$ is smooth at points q where $\delta_i(q) > 0$, the potential Π is differentiable at configurations where all the contacts are loaded.

Suppose that in the absence of any external wrench, $\mathcal{B}$ is held in an equilibrium fixture under the action of *nonzero* force by each finger. The nonzero finger forces are called *preloading forces.* The condition for equilibrium is that $\mathcal{B}$'s configuration, denoted q_0, be a *critical point* of the elastic potential. That is, the gradient[2] of Π must vanish at q_0. Taking the derivative of Π gives the following condition for an equilibrium fixture:

$$\nabla\Pi(q_0) = \sum_{i=1}^{m} f_i(\delta_i(q_0)) \nabla\delta_i(q_0) = 0. \tag{4.12}$$

As discussed in detail below, each summand in (4.12) is the wrench generated by a finger force corresponding to an overlap $\delta_i(q_0)$.

The *stiffness matrix* of an equilibrium fixture is defined as the Hessian,

[2]For the purposes of this thesis, it suffices to understand the *gradient* of g: $M \to \mathbb{R}$ (M is a manifold) as $\nabla\bar{g}$ where $\bar{g} = g \circ \varphi$ for a chart φ on M, and the *Hessian* of g as $D^2\bar{g}$ (this actually defines a Hessian independent of charts at a point where $\nabla\bar{g}$ vanishes). For brevity g and $\bar{g}$ will be notationally identified.

$K = D^2\Pi(q_0)$, of the elastic potential energy $\Pi(q)$ at q_0. Since $\nabla\Pi(q_0) = 0$ at an equilibrium fixture, the behavior of Π in the vicinity of q_0 is determined by K. If K is positive definite, then q_0 is a local minimum point of Π, and the fixture is stable [136]. While there exist stable fixtures whose stiffness matrix is only positive semi-definite, such fixtures are not generic and cannot adequately resist external disturbances. Therefore, we only consider stable equilibrium fixtures with positive definite stiffness matrices, and refer to them simply as *stable fixtures.* The stiffness matrix also specifies the load-overlap relationship as follows. A sufficiently small displacement of $\mathcal{B}$ can be approximated by a tangent vector (or rigid body velocity) $\dot{q}$. Corresponding to the displacement $\dot{q}$, the fingers react with a restoring wrench which is approximately given by $\boldsymbol{w} = K\dot{q}$. Thus K is a linear mapping from $T_{q_0}SE(3)$ to $T^*_{q_0}SE(3)$, which specifies for a given displacement $\dot{q}$ of $\mathcal{B}$ the fingers' wrench $\boldsymbol{w}$.

To compute the stiffness matrix, $\nabla\Pi(q)$ can be differentiated to obtain the following formula.

Lemma 4.4.1. *Let $\mathcal{B}$ be held in an m-finger equilibrium fixture at a configuration q_0, such that the i^{th} finger applies a non-zero force of magnitude $F_i = f_i(\delta_i(q_0))$, where $\delta_i(q_0)$ is the overlap at the i^{th} contact. Then the stiffness matrix of the fixture is*

$$K = K_1 + K_2 = \sum_{i=1}^{m} f_i'(\delta_i(q_0))\nabla\delta_i(q_0)\nabla\delta_i^T(q_0) + \sum_{i=1}^{m} f_i(\delta_i(q_0))D^2\delta_i(q_0), \tag{4.13}$$

where $f_i' = df_i(\delta_i)/d\delta_i$.

In the formula, K_1 and K_2 depend on the initial overlaps $\delta_i(q_0)$. Moreover, it will be seen that both summands depend on the contact point locations and contact normal directions. But K_2 additionally depends on the surface

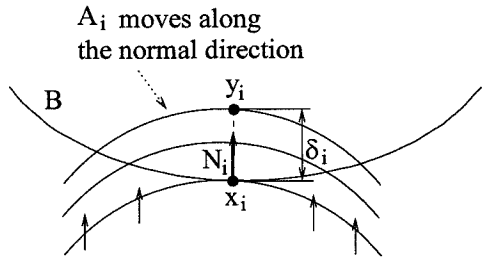

Figure 4.3: During normal loading both x_i and N_i remain unchanged.

curvature at the contacts. We say that K_1 accounts for first-order geometrical effects, while K_2 accounts for second-order, or surface curvature, effects. If K_1 alone is positive definite, the fixture is said to be *stable to first-order.* Otherwise, if the entire matrix K is positive definite, the fixture is said to be *stable to second-order.* Note that K_1 is at least positive semidefinite, since by construction $f_i'(\delta_i(q_0)) > 0$. Note, as well, that according to the equilibrium condition (4.12) the gradients $\nabla\delta_i(q_0)$ are linearly dependent at q_0. Hence for K_1 to be positive definite (and the fixture first-order stable), the number of contacts must be at least four in two dimensions and at least seven in three dimensions. Any stable fixture with a smaller number of contacts must involve curvature effects and be stable to second-order. We now turn to the computation of the terms $\delta_i(q_0), \nabla\delta_i(q_0)$ and $D^2\delta_i(q_0)$ which appear in the stiffness matrix formula.

4.4.2 Computation of the Overlaps $\delta_i(q_0)$

In the computation of the preloading overlaps $\delta_i(q_0)$, the following two assumptions are made. Recall that x_i is the endpoint of the overlap segment on the boundary of $\mathcal{B}$, and that N_i is the inward-pointing unit normal at x_i. It is assumed that starting from known initial contact points, the loaded contacts are achieved by pressing the fingers along the contact normals. As illustrated in Figure 4.3, the location of x_i and the direction of N_i remain unchanged during such a process. The quantities x_i and N_i for the loaded fixture are therefore

assumed to be known. Second, we restrict our attention to the following class of *essential equilibrium fixtures*. By definition, an equilibrium fixture is essential if *all* the fingers are *necessary* for maintaining the equilibrium. That is, in an essential fixture all the fingers must apply nonzero force in order to guarantee a zero net wrench on $\mathcal{B}$. The essential fixtures constitute a large class of fixtures: almost all two-dimensional fixtures by up to four fingers and three-dimensional fixtures by up to seven fingers are essential [135].

Essential fixtures afford an equivalent characterization that can be used for the computation of preloading finger forces and overlaps. Suppose that in an equilibrium fixture, the preloading finger forces are $f_i(\delta_i(q_0))$, where $\delta_i(q_0)$ are preloading overlaps. Define the *total preload* of the fixture to be $f_T = \sum_{i=1}^{m} f_i(\delta_i(q_0))$. Then the normalized preloading finger forces $\nu_i = f_i(\delta_i(q_0))/f_T$ satisfy the equilibrium condition (4.2), i.e., $\sum_{i=1}^{m} \nu_i \boldsymbol{\eta}_i = 0$, where $\boldsymbol{\eta}_i$ are the generating wrenches at the contacts. The following lemma characterizes essential fixtures in terms of ν_i.

Lemma 4.4.2 ([135]). *A fixture is essential if and only if the normalized preloading finger forces ν_i are nonzero and unique.*

According to this lemma, if a fixture is essential, then the normalized preloading finger forces can be computed, which then determine the magnitude of the preloading finger forces by the relationship $F_i = \nu_i f_T$, where the total preload f_T is yet to be determined. The overlaps $\delta_i(q_0)$ are then found by inverting the compliance functions f_i, $\delta_i(q_0) = f_i^{-1}(F_i)$.

Example 4.4.1. For two-dimensional or three-dimensional fixtures involving two and three fingers, the normalized finger-force magnitudes can be determined as follows. For two fingers the equilibrium condition $\nu_1 \boldsymbol{\eta}_1 + \nu_2 \boldsymbol{\eta}_2 = 0$ directly implies that $\nu_1 = \nu_2 = 1/2$. For three fingers the equilibrium condition is $\nu_1 \boldsymbol{\eta}_1 + \nu_2 \boldsymbol{\eta}_2 + \nu_3 \boldsymbol{\eta}_3 = 0$. It can be verified by direct substitution that the

solution is $\nu_i = N_{i+1} \times N_{i+2}$ for $i = 1, 2, 3$, where index addition is performed modulo 3. In this expression, N_i is the inward unit normal at the i^{th} contact, and the cross-product for vectors $v_1, v_2 \in \mathbb{R}^2$ is taken as $\det([v_1, v_2])$.

It remains to determine the total preload f_T for a given fixture. One needs to choose a suitable preloading level so that under work load, the contacts between the object and fingers are maintained and the material strength requirements of the contacting bodies are satisfied. First we briefly review some relevant notions from material strength theory [154]. The *stress* at a point in a body is the force per unit area over some differential cross-sectional area containing this point. Two important types of stress are normal and shear stresses. *Normal stress* arises from forces perpendicular to a cross-sectional area, while *shear stress* arises from forces lying in the plane of a cross-sectional area. The maximum value of the shear stress over all cross-sectional areas at all points of a body is called the *maximum shear stress* and is denoted τ_{max}. To ensure that no permanent deformation or plastic yield occurs in a material such as steel or aluminum, τ_{max} must not exceed the *yield stress* of the material. Much like Young's modulus and Poisson's ratio, the yield stress, denoted σ_{yield}, is a basic material property.

Hertz theory relates the maximum shear stress, τ_{max}, to the maximum pressure in the contact area, $p_{\max}$, by the formula $\tau_{max} = \zeta p_{\max}$ where $\zeta = 0.31$ for a point contact and $\zeta = 0.3$ for a line contact [72]. For an m-finger fixture, the allowable pressure can be determined by the condition

$$\max_{1 \leqslant i \leqslant m} \zeta \, p_{\max i} = \gamma \, \sigma_{yield}, \tag{4.14}$$

where $0 < \gamma < 1$ is called the *preloading factor*. This parameter is used to ensure that the maximum shear stress is below σ_{yield}, so that the material remains elastic under work load. For this reason γ should be sufficiently less

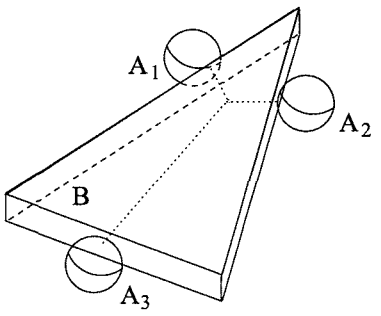

Figure 4.4: A three-finger fixture of a triangular object (the supporting plane is not shown).

than unity. On the other hand, γ should be considerably greater than zero to make the fixture stiffer, and to prevent contact breakage under work load. The condition (4.14) determines the preloading level as follows. According to formula (4.6), $p_{\max i} = d_i \delta_i^{1/2}$ where d_i is listed below. Substituting for $p_{\max i}$ in (4.14) leads to the expression: $\max_{1 \leqslant i \leqslant m} \{\zeta d_i \delta_i^{1/2}\} = \gamma \sigma_{yield}$. Using formula (4.5), each finger-force magnitude is given by $F_i = c_i \delta_i^{3/2} = \nu_i f_T$, where c_i is listed below and the ν_i's are the normalized finger force magnitudes which have been already computed. Substituting $\delta_i^{1/2} = (f_T \nu_i / c_i)^{1/3}$ gives: $\left(\max_{1 \leqslant i \leqslant m} \{\zeta d_i (\nu_i / c_i)^{1/3}\}\right) {f_T}^{1/3} = \gamma \sigma_{yield}$, in which f_T is the only unknown. Solving for f_T gives the formula:

$$f_T = \min_{1 \leqslant i \leqslant m} \frac{c_i (\gamma \sigma_{yield})^3}{\nu_i (\zeta d_i)^3}, \tag{4.15}$$

where $c_i = \frac{4}{3} \beta_1(e) E^* r_e^{1/2}$ and $d_i = \frac{2}{\pi} \beta_2(e) E^* r_e^{-1/2}$. The resulting formula determines the total preloading level in terms of material properties, first-order geometrical quantities (which determine ν_i), and relative curvature at the m contacts.

Example 4.4.2. Figure 4.4 shows an essential three-finger fixture of a triangular object made of a thick plate. Assuming that the base edge of the triangle makes an angle of 75° with the other edges, the normalized finger

forces for this fixture are $\nu_1 = \nu_2 = 0.4$ and $\nu_3 = 0.2$. The object and fingers are made of an aluminum alloy with Young's modulus $E = 73 \times 10^9$ Pa, Poisson's ratio $\nu = 0.33$, and yield stress $\sigma_{yield} = 345 \times 10^6$ Pa. Then $E^* = 41 \times 10^9$ Pa. If the fingers have identical spherical tips of radius 2 cm, then $r_{rel1} = r_{rel2} = 2$ cm and $\beta_j = 1$ for $j = 1, 2, 3$. Thus, $c_i = 7.72 \times 10^9\,\text{Pa} \times \text{cm}^{1/2}$ and $d_i = 184 \times 10^9\,\text{Pa} \times \text{cm}^{-1/2}$ for all contacts. Choosing the preloading factor as $\zeta = 0.7$, one obtains $f_T = 1466$ N from (4.15). Then the formula $F_i = \nu_i f_T$ gives the individual preloading finger forces $F_1 = F_2 = 582$ N and $F_3 = 302$ N. Using the relation $\delta_i(q_0) = (F_i/c_i)^{2/3}$, one finds the preloading overlaps $\delta_1(q_0) = \delta_2(q_0) = 17.9$ micro meters and $\delta_3(q_0) = 11.5$ micro meters.

4.4.3 Computation of the Overlap Gradients $\nabla\delta_i(q_0)$

The following lemma gives the formula for the overlap gradient $\nabla\delta_i(q_0)$. In anticipation of the derivation of $D^2\delta_i(q_0)$, we explicitly write the dependence of the various terms in the formula on $\mathcal{B}$'s configuration q.

Lemma 4.4.3 ([135]). *Let $\mathcal{B}(q)$ have an overlap of $\delta_i(q) > 0$ with $\mathcal{A}_i$. Let $x_i(q)$ be the endpoint of the overlap segment on the boundary of $\mathcal{B}$, and let $N(x_i(q))$ be the inward-pointing unit normal to the boundary of $\mathcal{B}$ at x_i. Then the gradient of δ_i at $q = (d, \theta)$ is:*

$$\nabla\delta_i(q) = -\begin{pmatrix} N(x_i(q)) \\ R(\theta)r_i(q) \times N(x_i(q)) \end{pmatrix}, \tag{4.16}$$

where $r_i(q)$ is the point $x_i(q)$ expressed in the body frame $\mathcal{F}_B$, and $R(\theta)$ is the orientation of $\mathcal{F}_B$ relative to the world frame $\mathcal{F}_W$.

We are now in a position to further explain the meaning of Equation (4.12), $\sum_{i=1}^{m} f_i(\delta_i)\nabla\delta_i = 0$. It follows from (4.16) that $-\nabla\delta_i(q)$ is the wrench gen-

erated by a unit finger-force, acting on $\mathcal{B}$ at the point x_i along the direction $N(x_i)$. Since the finger-force magnitude due to an overlap of δ_i is $F_i = f_i(\delta_i)$, the vector $f_i(\delta_i)\nabla\delta_i$ is the wrench generated by the i^{th} finger due to an overlap of δ_i. Thus, condition (4.12) matches the standard equilibrium condition (4.1), that in the absence of external wrenches the net wrench exerted by the fingers must vanish.

4.4.4 Computation of the Overlap Hessians $D^2\delta_i(q_0)$

The last term in the stiffness matrix for which one needs a formula is the Hessian $D^2\delta_i(q_0)$. Here the derivation of the formula is summarized with details provided in the appendix. Let $q(t)$ be a c-space curve such that $q(0) = q_0$ and $\dot{q}(0) = \dot{q}$, where $\dot{q}$ is a general tangent vector in $T_{q_0}SE(3)$. To derive a formula for $D^2\delta_i(q_0)$, consider the quadratic form: $\dot{q}^T D^2\delta_i(q_0)\,\dot{q} = \dot{q}^T \frac{d}{dt}\big|_{t=0} \nabla\delta_i(q(t))$. To simplify the derivation, decompose the tangent space into the direct sum of two subspaces, $T_{q_0}SE(3) = V_1 \oplus V_2$. The subspace V_1 is tangent to the level-set $S_i = \{q : \delta_i(q) = \delta_i(q_0)\}$, and is given by $V_1 = \{\dot{q} : \nabla\delta_i^T(q_0)\,\dot{q} = 0\}$. This subspace is the set of instantaneous motions of $\mathcal{B}$ that keep δ_i unchanged. The subspace V_2 is tangent to the line denoted l_i, which passes through q_0 in the direction $(N_i, 0)$, where $N_i = N(x_i(q_0))$. This line corresponds to a pure translational motion of $\mathcal{B}$ along the direction N_i. The subspace V_2 is given by $V_2 = \{\dot{q} : \dot{q} = \alpha(N_i, 0),\ \alpha \in \mathbb{R}\}$, and is spanned by instantaneous pure translations of $\mathcal{B}$ along the direction N_i.

The key observation is that $\nabla\delta_i$ remains constant during pure translation of $\mathcal{B}$ along an interval of the line l_i centered at q_0. As illustrated in Figure 4.5(a), in physical space this translation corresponds to a penetration of $\mathcal{B}$ along the overlap segment. The direction N_i of the overlap segment, which is also the direction of the unit normal to $\mathcal{B}$ at $x_i = x_i(q_0)$, remains unchanged during this penetration. Similarly, the location of r_i, $\mathcal{B}$'s endpoint of the overlap segment

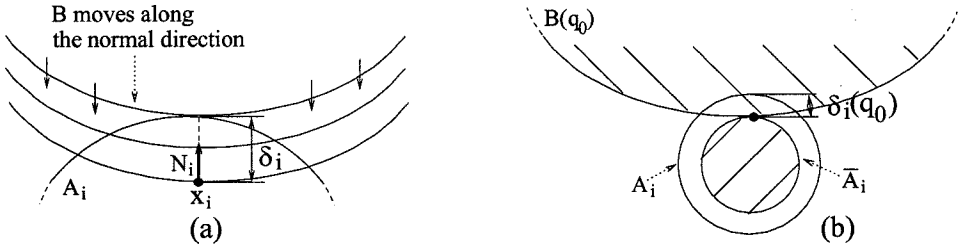

Figure 4.5: (a) During normal penetration both x_i and N_i remain unchanged. (b) The imaginary finger $\bar{\mathcal{A}}_i$ obtained by uniformly compressing $\mathcal{A}_i$ by $\delta_i(q_0)$.

expressed in $\mathcal{F}_B$, and the orientation matrix R of $\mathcal{B}$, also remain unchanged during this motion. Thus $\nabla\delta_i$ given in (4.16) remains constant during this motion, and consequently $D^2\delta_i(q_0)$ vanishes along the subspace V_2. Thus one only needs to compute $D^2\delta_i(q_0)$ along V_1.

To compute the derivative of $\nabla\delta_i(q)$ along V_1, let $q(t)$ be a c-space curve in $\mathcal{S}_i$, such that $q(0) = q_0$ and $\dot{q}(0) = \dot{q} \in V_1$. To evaluate $\frac{d}{dt}\big|_{t=0}\nabla\delta_i(q(t))$, imagine that the physical finger $\mathcal{A}_i$ is replaced with a rigid finger $\bar{\mathcal{A}}_i$, obtained by uniformly compressing $\mathcal{A}_i$ by the amount $\delta_i(q_0)$ (Figure 4.5(b)). Then $\mathcal{B}(q_0)$, which originally overlaps $\mathcal{A}_i$, is in point contact with $\bar{\mathcal{A}}_i$. Further, since the trajectory $q(t)$ lies in $\mathcal{S}_i$, $\mathcal{B}$ moves along $q(t)$ while maintaining contact with $\bar{\mathcal{A}}_i$. Such a motion is called a *roll-slide motion* of $\mathcal{B}$ along the surface of $\bar{\mathcal{A}}_i$. Since $\mathcal{S}_i$ is a level-set of $\delta_i(q)$, $\nabla\delta_i(q)$ is a normal vector field for $\mathcal{S}_i$. Hence $\dot{q}^T\frac{d}{dt}\nabla\delta_i(q(t))$ is a scalar multiple of the *curvature* of $\mathcal{S}_i$ along $\dot{q}$. A formula for the curvature of $\mathcal{S}_i$ is known, since $\mathcal{S}_i$ can be interpreted as the boundary of the c-space obstacle[3] corresponding to $\bar{\mathcal{A}}_i$. Using the formula for the curvature of such a boundary [139], one obtains: $\dot{q}^T\frac{d}{dt}\big|_{t=0}\nabla\delta_i(q(t)) = \dot{q}^T Q_i \dot{q}$, with the

[3]The *c-space obstacle* corresponding to a stationary body $\mathcal{A}$ is the collection of configurations q such that $\mathcal{B}(q)$ intersects the body $\mathcal{A}$.

6×6 matrix Q_i given by

$$Q_i = \begin{pmatrix} I & -\widehat{p}_i \\ 0 & \widehat{N}_i \end{pmatrix}^T \begin{pmatrix} -L_{\bar{A}_i}\bar{L}_{reli}^{-1}L_{B_i} & L_{\bar{A}_i}\bar{L}_{reli}^{-1} \\ \bar{L}_{reli}^{-1}L_{\bar{A}_i} & \bar{L}_{reli}^{-1} \end{pmatrix} \begin{pmatrix} I & -\widehat{p}_i \\ 0 & \widehat{N}_i \end{pmatrix} + \begin{pmatrix} 0 & 0 \\ 0 & (\widehat{N}_i^T\widehat{p}_i)_s \end{pmatrix}, \tag{4.17}$$

where by definition $(A)_s = \frac{1}{2}(A^T + A)$. In this formula, the following notation is used: $x_i = x_i(q_0)$, $r_i = r_i(q_0)$, $N_i = N(x_i(q_0))$, and $p_i = R_0 r_i$. Also, L_{B_i} is the curvature matrix of $\mathcal{B}$ at x_i, $L_{\bar{A}_i}$ is the curvature matrix of $\bar{\mathcal{A}}_i$ at x_i, and $\bar{L}_{reli} = L_{B_i} + L_{\bar{A}_i}$ is the relative curvature of $\mathcal{B}$ and $\bar{\mathcal{A}}_i$ at x_i.

To extend the derivative of $\nabla\delta_i(q)$ from V_1 to the entire tangent space $T_{q_0}SE(3)$, we construct in the appendix a projection matrix P_i. This matrix maps a tangent vector $\dot{q} \in T_{q_0}SE(3)$ to its unique component $\dot{q}_1 \in V_1$, corresponding to the direct-sum decomposition $T_{q_0}SE(3) = V_1 \oplus V_2$. The following proposition gives the formula for P_i and provides the resulting formula for $D^2\delta_i(q_0)$.

Proposition 4.4.4. *Let $\mathcal{B}(q_0)$ have an overlap of $\delta_i(q_0) > 0$ with $\mathcal{A}_i$. Using the hybrid parametrization* (3.1)*, the 6×6 Hessian matrix of the overlap function δ_i is:*

$$D^2\delta_i(q_0) = P_i^T Q_i P_i \quad \textit{where } P_i = \begin{pmatrix} I - N_i N_i^T & N_i N_i^T \widehat{p}_i \\ 0 & I \end{pmatrix}, \tag{4.18}$$

and Q_i is given in (4.17).

The proposition is proved in the appendix. Under a normal loading process, the quantities N_i and $p_i = R_0 r_i$ are identical to the respective quantities prior to the loading process. Similarly, the curvature matrix L_{B_i} is identical to the

curvature matrix of $\mathcal{B}$ at the original contact point x_i. As for the curvature matrix $L_{\bar{A}_i}$, it can be shown that $L_{\bar{A}_i} = [L_A^{-1}(y_i) - \delta_i(q_0)I]^{-1}$, where $L_A(y_i)$ is the curvature of the undeformed finger at the endpoint y_i of the overlap segment. In a normal loading process y_i is identical to the point of $\mathcal{A}_i$ which was in contact with $\mathcal{B}$ prior to the loading process (Figure 4.3), hence $L_A(y_i)$ is known. Thus all the terms in (4.18) are computable from the corresponding geometrical quantities prior to the loading process.

For planar fixtures the Hessian formula has the following simpler form. Let r_{B_i} and r_{A_i} denote the radius of curvature of the planar bodies $\mathcal{B}$ and $\mathcal{A}_i$ at their original contact point x_i. Then the radius of curvature of the imaginary finger $\bar{\mathcal{A}}_i$ is $r_{\bar{A}_i} = r_{A_i} - \delta_i(q_0)$, and Proposition 4.4.4 simplifies to the following formula for $D^2\delta_i(q_0)$.

Corollary 4.4.5. *For a planar fixture, the* 3×3 *Hessian matrix of the overlap function* δ_i *takes the form:*

$$D^2\delta_i(q_0) = \frac{1}{r_{\bar{A}_i} + r_{B_i}} \begin{pmatrix} N_i N_i^T - I & (r_{B_i} - \rho_i)JN_i \\ (r_{B_i} - \rho_i)(JN_i)^T & (r_{\bar{A}_i} + \rho_i)(r_{B_i} - \rho_i) \end{pmatrix}, \qquad (4.19)$$

where $r_{\bar{A}_i} = r_{A_i} - \delta_i(q_0)$, $\rho_i = -(R_0 r_i) \times N_i$, *and* $J = \left(\begin{smallmatrix} 0 & 1 \\ -1 & 0 \end{smallmatrix}\right)$.

The stiffness matrix of a linear-spring system. As an example, the stiffness matrix will be computed for m linear springs holding an object in equilibrium. Assume that each spring has a "point finger" at its tip, and that $\mathcal{B}$'s radius of curvature at the i^{th} contact is r_{B_i} (Figure 4.2). Using formula (4.13), one has to compute the matrix $K = \sum_{i=1}^m f_i'(\delta_i(q_0))\nabla\delta_i(q_0)\nabla\delta_i(q_0)^T + \sum_{i=1}^m f_i(\delta_i(q_0))D^2\delta_i(q_0)$. As discussed in Section 4.3.1, $f_i(\delta_i(q_0)) = k_i\delta_i(q_0)$ and $f_i'(\delta_i(q_0)) = k_i$ for a linear spring. Using formula (4.16) for the gradient of δ_i, $\nabla\delta_i(q_0) = (N_i, \tau_i)$, where $\tau_i = R_0 r_i \times N_i \in \mathbb{R}$. Since the tips of the springs are point fingers, $r_{\bar{A}_i} = 0$ can be substituted in (4.19). Since the sum

of the finger forces vanishes at an equilibrium fixture, one can also substitute $\sum_{i=1}^{m} k_i \delta_i(q_0) N_i = 0$ in (4.19). These substitutions give the formula:

$$K = \sum_{i=1}^{m} k_i \begin{pmatrix} N_i N_i^T & \tau_i N_i \\ \tau_i N_i^T & \tau_i^2 \end{pmatrix} - \sum_{i=1}^{m} \frac{k_i \delta_i(q_0)}{r_{B_i}} \begin{pmatrix} I - N_i N_i^T & \rho_i J N_i \\ \rho_i (J N_i)^T & \rho_i (\rho_i - r_{B_i}) \end{pmatrix}.$$

The resulting formula for K agrees with the stiffness matrix formula derived by Nguyen for the same linear-spring system [114]. Further, by a similar substitution process one can obtain the stiffness matrix formula derived by Ponce for linear springs with spherical tips holding a polyhedral object [125].

To summarize, closed-form formulas have been found for $\delta_i(q_0)$, $\nabla\delta_i(q_0)$, and $D^2\delta_i(q_0)$. Substituting these formulas into Formula (4.13) gives a closed-form expression for the stiffness matrix. The resulting expression explicitly depends on the geometry of the contacts (i.e. the contact points, contact normals, and relative curvatures), and allows the use of any particular overlap model. When applied to the realistic nonlinear Hertz contact model, the stiffness matrix formula provides an accurate description of fixture compliance in terms of basic material properties of the object and fingers. When applied to the linear-spring model, the stiffness matrix formula admits arbitrary piecewise smooth object and linear-spring tips, and it agrees with the specialized formulas derived by Nguyen [114] and Ponce [125].

4.5 Effects of Contact Geometry

This section compares the contribution of first and second-order geometrical effects to fixture stiffness and stability. After a preliminary scaling operation of the stiffness matrix, we characterize the conditions under which second-order effects provide stiffness comparable to the stiffness provided by first-

order effects. Then the relative contribution of curvature to fixture stability is analyzed, and several examples are given to illustrate the results. The following *spectral matrix norm* will be used to compare order of magnitude of matrices. The spectral norm of a matrix A is defined by $\|A\| = \lambda_{\max}^{1/2}(A^TA)$, where $\lambda_{\max}(A^TA)$ is the largest eigenvalue of the matrix A^TA. If A is symmetric then $\|A\| = \max\{|\lambda_i(A)|\}$ over the eigenvalues $\lambda_i(A)$ of A. Given a symmetric matrix A, we write $A > 0$ when A is positive definite, and $A \geqslant 0$ when A is positive semidefinite.

4.5.1 Significance of Curvature Effects

The stiffness matrix of an equilibrium fixture is given in Equation (4.13) as $K = K_1 + K_2$, where K_1 depends only on first-order geometrical quantities while K_2 additionally depends on the bodies' curvature. In order to derive the conditions under which K_2 is comparable with K_1, it is convenient to scale the stiffness matrix into a dimensionless matrix denoted $\widetilde{K}$. We construct a scaling matrix S, such that the matrix $\widetilde{K} = S^TKS = S^TK_1S + S^TK_2S$ has the property that $\|S^TK_1S\|$ is of the order-of-magnitude of unity. To that end, we define two characteristic parameters. First recall that f_T, the total preload, is given by $f_T = \sum_{i=1}^{m} f_i(\delta_i(q_0))$. The first parameter, called the *characteristic contact stiffness* k_0, is a constant of the order-of-magnitude of the derivatives $f_i'(\delta_i(q_0))$. We also define an auxiliary parameter, called the *characteristic preloading overlap* δ_0, as the quotient $\delta_0 = f_T/k_0$. Note that δ_0 has the same order of magnitude as the preloading overlaps $\delta_i(q_0)$. The second parameter, denoted l, is a characteristic length of $\mathcal{B}$.

Choosing a 6×6 scaling matrix $S = \frac{1}{\sqrt{k_0}}\,\mathrm{diag}(I, \frac{1}{l}I)$, the nondimensionalized stiffness matrix is $\widetilde{K} = S^TKS = \widetilde{K}_1 + \widetilde{K}_2$. The dimensionless first- and

second-order terms, $\widetilde{K}_1 = S^T K_1 S$ and $\widetilde{K}_2 = S^T K_2 S$, take the form

$$\widetilde{K}_1 = GDG^T \quad \text{and} \quad \widetilde{K}_2 = \sum_{i=1}^{m} \nu_i \Psi_i, \tag{4.20}$$

where $\nu_i = \frac{f_i(\delta_i(q_0))}{f_T}$ are the normalized preloading finger force magnitudes, $G = \operatorname{diag}(I, \frac{1}{l} I)\,[\nabla\delta_1(q_0), \cdots, \nabla\delta_m(q_0)]$, $D = \operatorname{diag}\left(\frac{f_1'(\delta_1(q_0))}{k_0}, \ldots, \frac{f_m'(\delta_m(q_0))}{k_0}\right)$, and $\Psi_i = \delta_0 \operatorname{diag}(I, \frac{1}{l} I)\, D^2\delta_i(q_0)\, \operatorname{diag}(I, \frac{1}{l} I)$. Note that ν_i are in general not unique unless the fixture is essential.

From now on we focus on the i^{th} contact and omit the subscript i where appropriate. Let Ψ_{11}, Ψ_{12}, and Ψ_{22} be the block-entries of Ψ. Then evaluation of formula (4.18) for $D^2\delta_i(q_0)$ gives the following expressions for the block-entries of Ψ:

$$\begin{aligned} \Psi_{11} &= -\delta_0 \mathcal{L}_{\bar{A}} \bar{L}_{rel}^{-1} \mathcal{L}_B, \qquad \Psi_{12} = \frac{\delta_0}{l} \mathcal{L}_{\bar{A}} \bar{L}_{rel}^{-1} (\mathcal{L}_B \widehat{p} + \widehat{N}), \\ \Psi_{22} &= \frac{\delta_0}{l^2} \left\{ \widehat{N}^T \bar{L}_{rel}^{-1} \widehat{N} - \widehat{p}^T \mathcal{L}_{\bar{A}} \bar{L}_{rel}^{-1} \mathcal{L}_B \widehat{p} + \left(\widehat{N} \bar{L}_{rel}^{-1} (\mathcal{L}_{\bar{A}} - \mathcal{L}_B) \widehat{p} \right)_S \right\}, \end{aligned} \tag{4.21}$$

where $\mathcal{L}_{\bar{A}} = (I - NN^T)\, L_{\bar{A}}\, (I - NN^T)$ and $\mathcal{L}_B = (I - NN^T)\, L_B\, (I - NN^T)$. Recall that N is the unit contact normal, that $L_{\bar{A}}$ and L_B are the curvature matrices of $\bar{\mathcal{A}}$ and $\mathcal{B}(q_0)$ at the contact, and that $\bar{L}_{rel} = L_{\bar{A}} + L_B$ is the relative curvature matrix.

It can be observed that $\|\widetilde{K}_1\| = \|GDG^T\|$ is of the order-of-magnitude of unity. Consequently, the second-order effects are much smaller than the first-order effects when the condition $\|\Psi\| \ll 1$ holds true, or equivalently, when $\|\Psi_{jl}\| \ll 1$ for $j, l = 1, 2$. These conditions are characterized in the following proposition. We write $x = \mathcal{O}(1)$ if either $|x| \ll 1$ or $|x| \sim 1$.

Proposition 4.5.1. *The second-order effects satisfy* $\|\Psi_{jl}\| \ll 1$ *for* $j, l = 1, 2$, *when the following two conditions hold.*

(1) $\delta_0\|L_{\bar{A}}\| \ll 1$ *and* $\delta_0\|L_B\| \ll 1$.

(2) $\frac{\|L_{\bar{A}}\|}{\|\bar{L}_{rel}\|} = \mathcal{O}(1)$, $\frac{\|L_B\|}{\|\bar{L}_{rel}\|} = \mathcal{O}(1)$, *and* $\frac{\|\bar{L}_{rel}^{-1}\|}{l^2\|\bar{L}_{rel}\|} = \mathcal{O}(1)$.

The proposition is proved in the appendix. To gain a more intuitive understanding of the conditions, the proposition is applied to planar fixtures to obtain.

Corollary 4.5.2. *For a contact in a planar fixture, let* $r_{\bar{A}}$ *and* r_B *be the radii of curvature of* $\bar{\mathcal{A}}$ *and* $\mathcal{B}$*, and let* $\bar{r}_{rel} = (1/r_{\bar{A}} + 1/r_B)^{-1}$*. The second-order effects are much smaller than the first-order effects when the following two conditions hold.*

(1) $\delta_0 \ll |r_{\bar{A}}|$ *and* $\delta_0 \ll |r_B|$.

(2) $\bar{r}_{rel}/r_{\bar{A}} = \mathcal{O}(1)$, $\bar{r}_{rel}/r_B = \mathcal{O}(1)$, *and* $\bar{r}_{rel}/l = \mathcal{O}(1)$.

Observe that condition (1), $\delta_0 \ll |r_{\bar{A}}|$ and $\delta_0 \ll |r_B|$ (or $\delta_0\|L_{\bar{A}}\| \ll 1$ and $\delta_0\|L_B\| \ll 1$), is not restrictive at all. This condition requires that the bodies' radii of curvature at the contact be much larger than δ_0, which is satisfied by all practical contacts. Condition (2) imposes an upper bound on $\bar{r}_{rel}$ (a lower bound on $\|\bar{L}_{rel}\|$). Since $\bar{r}_{rel}$ increases as the surfaces at the contact approach a closer match, condition (2) asserts that as long as the surfaces do not match too closely, second-order effects are relatively small in their order of magnitude. On the other hand, when condition (2) is violated, one may possibly have significant second-order effects, and this case is discussed below.

4.5.2 Effects of Local Curvature on Fixture Stability

Recall that the positive definiteness of the stiffness matrix K implies fixture stability. Since $\widetilde{K} = S^T K S$ where S is non-singular, the positive definiteness of $\widetilde{K}$ also implies fixture stability. The matrix $\widetilde{K}$ consists of two summands, $\widetilde{K} = \widetilde{K}_1 + \widetilde{K}_2$, such that $\widetilde{K}_1 = GDG^T$ with $D = \text{diag}\left(\frac{f_1'(\delta_1(q_0))}{k_0}, \ldots, \frac{f_m'(\delta_m(q_0))}{k_0}\right)$.

Since by construction $f_i'(\delta_i(q_0)) > 0$, the matrix D is positive definite and consequently $\widetilde{K}_1$ is positive semidefinite. Thus, the first-order effects are always *stabilizing*. To investigate the influence of $\widetilde{K}_2 = \sum_{i=1}^{m} \nu_i \Psi_i$ on fixture stability, we continue to focus on the i^{th} contact and drop the index i for brevity. The matrix Ψ associated with the contact can be decomposed into the sum $\Psi = \Psi_a + \Psi_b$, such that $\Psi_a \geqslant 0$ while Ψ_b is indefinite but very small. The decomposition is given in the following lemma, which is proved in the appendix.

Lemma 4.5.3. *Let $\mathcal{L}_S = \mathcal{L}_B \widehat{p} + \widehat{N}$. Then the matrix Ψ given in* (4.21) *can be written as:*

$$\begin{aligned}\Psi &= \Psi_a + \Psi_b \\ &= \begin{pmatrix} \delta_0 \mathcal{L}_{\bar{A}}{}^T \bar{L}_{rel}^{-1} \mathcal{L}_{\bar{A}} & \frac{\delta_0}{l} \mathcal{L}_{\bar{A}} \bar{L}_{rel}^{-1} \mathcal{L}_S \\ \frac{\delta_0}{l} \mathcal{L}_S{}^T \bar{L}_{rel}^{-1} \mathcal{L}_{\bar{A}} & \frac{\delta_0}{l^2} \mathcal{L}_S{}^T \bar{L}_{rel}^{-1} \mathcal{L}_S \end{pmatrix} + \begin{pmatrix} -\delta_0 \mathcal{L}_{\bar{A}} & 0 \\ 0 & \frac{\delta_0}{l^2} \big(-\widehat{p}^T \mathcal{L}_B \widehat{p} + (\widehat{N}\widehat{p})_s \big) \end{pmatrix}.\end{aligned} \tag{4.22}$$

In this decomposition, Ψ_a is positive semidefinite, and provided that $\delta_0 \|L_{\bar{A}}\| \ll 1$ and $\delta_0 \|L_B\| \ll 1$, the matrix Ψ_b satisfies $\|\Psi_b\| \ll 1$.

The lemma implies that Ψ_a is always stabilizing, while any possibly destabilizing curvature effects must come from Ψ_b. To discuss the influence of Ψ_b on fixture stability, let us first consider fixtures which are stable to first-order. In such fixtures the possibly destabilizing effects of Ψ_b are usually too small to destabilize the fixture, as made precise in the following proposition.

Proposition 4.5.4. *Let a fixture be first-order stable* (i.e. $\tilde{K}_1 > 0$). *Then the fixture is stable* (i.e. $\tilde{K} = \tilde{K}_1 + \tilde{K}_2 > 0$), *when the following condition holds true:*

$$\sigma_{min}^2(G) \min_{1 \leqslant i \leqslant m} \frac{f_i'(\delta_i(q_0))}{k_0} \gg \max_{1 \leqslant i \leqslant m} \left\{ \delta_0 \|L_{\bar{A}i}\|, \delta_0 \|L_{Bi}\|, \frac{\delta_0}{l} \right\}, \tag{4.23}$$

where $G = \mathrm{diag}(I, \frac{1}{l}I)[\nabla\delta_1(q_0), \cdots, \nabla\delta_m(q_0)]$ *and* $\sigma_{min}(G)$ *is the smallest singular value of* G.

The proof appearing in the appendix shows that $\lambda_{\min}(\widetilde{K}_1)$ is bounded from below by the left side of (4.23), while $\|\Psi_b\|$ is bounded from above by the right side of (4.23). Thus $\lambda_{\min}(\widetilde{K}_1) \gg \|\Psi_b\|$ and $\widetilde{K}$ is consequently positive definite. Note that condition (4.23) is usually not restrictive, for the following reason. At a first-order stable equilibrium fixture, the convex hull of the normalized finger wrenches contains the origin in its interior (Equation (4.12)). As long as the volume of the wrenches' convex hull is not too small (i.e., as long as the wrenches do not approximately lie on a lower dimensional subspace of wrench space), $\sigma_{min}(G)$ is of the order of unity. Further, in practical fixtures the derivatives $f_i'(\delta_i(q_0))$ are of the same order-of-magnitude, and $\min_{1\leqslant i\leqslant m}\{f_i'(\delta_i(q_0))\}$ is therefore of the order of k_0. The left side of (4.23) is thus of the order of unity, while the factor δ_0 on the right side of (4.23) always satisfies $\delta_0 \ll 1$. Thus under usual circumstances (4.23) holds true, and *first-order stability typically implies stability.* On the other hand, when condition (4.23) is violated, a fixture which is stable to first-order can actually be unstable due to curvature effects. An example of this phenomenon is provided in Figure 4.6 below.

Next consider the relative influence of curvature effects in second-order stable fixtures. In such fixtures $\widetilde{K}_1 \geqslant 0$, and curvature effects supply the stabilizing forces along the kernel of $\widetilde{K}_1$. one wishes to characterize the condition under which the forces produced by $\widetilde{K}_2$ are comparable to the forces produced by $\widetilde{K}_1$. The following proposition describes this condition, and its proof appears in the appendix.

Proposition 4.5.5. *Let a fixture be second-order stable, such that* $\delta_0\|L_{\bar{A}}\| \ll 1$ *and* $\delta_0\|L_B\| \ll 1$. *Then the stabilizing curvature effects are comparable to the stabilizing first-order effects when* $\|\bar{L}_{rel}\|/(\frac{\delta_0}{l^2}) = \mathcal{O}(1)$, *since in this case*

$\|\Psi_a\| \sim 1$ *while* $\|\Psi_b\| \ll 1$.

The proposition implies that the stabilizing second-order effects become more pronounced as $\|\bar{L}_{rel}\|$ decreases (as the contacting surfaces achieve a better match). In particular, *when the two surfaces fit sufficiently closely, the stabilizing second-order effects can become comparable with the first-order effects.* Such significant stabilizing second-order effects are illustrated below. The result has a practical implication for fixture design. It has been shown that curvature effects can reduce the number of fixtures needed to immobilize an object [34, 134]. But up until now it has not been clear how much force can be produced by curvature effects, compared to forces generated by first-order effects. The above analysis indicates that by proper selection of the fixtures' curvature, fixtures that exploit curvature effects can be as stiff as fixtures that exploit only first-order effects. However, in many applications the usually softer curvature-effects may be adequate, and such close curvature matching is not necessary.

Finally, the proposition yields the following corollary when applied to planar fixtures.

Corollary 4.5.6. *For a contact in a planar fixture, if* $\delta_0 \ll |r_A|$ *and* $\delta_0 \ll |r_B|$, *any possibly destabilizing curvature effects are very small. On the other hand, let* $\kappa = r\delta_0/l^2$ *for non-concave surfaces and* $\kappa = (\frac{r}{l})^2(\frac{\delta_0}{\Delta r})$, *where* $r = \min\{|r_A|, |r_B|\}$, *and* $\Delta r = ||r_B| - |r_A|| \ll r$. *Then the stabilizing curvature effects are significant if* $1/\kappa = \mathcal{O}(1)$.

As will be illustrated by Example 4.5.3, the scalar function κ predicts whether second-order effects are significant. For this reason it is called the *curvature effect indicator.*

4.5.3 Examples of Local Curvature Effects

This section illustrates the computation of the Hertzian stiffness matrix, and discuss the influence of curvature effects in several examples. The first example illustrates that second-order effects can destabilize a fixture which is neutrally stable to first-order. (Second-order effects, recall, typically do not destabilize a fixture which is first-order stable.) The second example shows that second-order effects can stabilize a fixture which is neutrally stable to first-order. The last example illustrates that with an appropriate contact geometry, the stabilizing curvature effects can be made quite significant. The following is a list of assumptions and formulas for the examples.

In all the examples the fingers are assumed to be identical and have a spherical tip. The objects are made of a thick plate and lie on a supporting plane. Hence one can compute the 3×3 stiffness matrix corresponding to motions of the objects on the supporting plane. The Hertz contact model (Equations (4.5–4.7)) will be used to compute the dimensionless stiffness matrix and compare first- and second-order effects. According to Section 4.3.2, the maximum shear stress in a body is given by $\tau_{max} = 0.31 p_{\max}$. The finger placements in the examples possess geometric symmetry, and form essential fixtures. Therefore, the compliance functions are the same at the contacts: $f_i(\delta_i) = f(\delta_i)$. In addition, the normalized preloading finger forces are uniquely given by $\nu_i = 1/m$, where m is the number of fingers. The total preload can then be determined from formula (4.15) as follows:

$$f_T = \frac{m}{6}\mu_p^3 \beta_1(e) E^* r_e^2 \qquad \text{where} \quad \mu_p = \frac{\pi \gamma \sigma_{yield}}{0.31 \beta_2(e) E^*}. \tag{4.24}$$

Recall that in the formula $r_e = (r_{rel1} r_{rel2})^{1/2}$ where r_{reli} are the principal radii of relative curvature at each contact. The preloading finger forces are

then given by $f(\delta_i(q_0)) = f_T/m$, which gives the preloading overlaps $\delta_i(q_0) = \frac{1}{4}\mu_p^2 r_e$, and the preloading contact stiffnesses $f'(\delta_i(q_0)) = \mu_p \beta_1(e) E^* r_e$. In each example, set $k_0 = \frac{m}{2} f_i'(\delta_i(q_0))$ and $\delta_0 = f_T/k_0$. Therefore,

$$k_0 = \frac{m}{2}\mu_p \beta_1(e) E^* r_e \quad \text{and} \quad \delta_0 = \frac{1}{3}\mu_p^2 r_e. \tag{4.25}$$

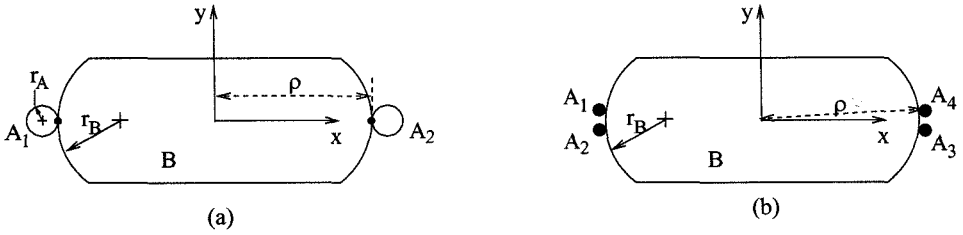

Figure 4.6: (a) Top view of an object fixtured by two spherical fingers. (b) The same object fixtured by four fingers in a way which may become unstable.

Example 4.5.1. Figure 4.6(a) shows a symmetric object $\mathcal{B}$ made of a thick plate and fixtured by two spherical fingers of radius r_A. The origin of the body frame $\mathcal{F}_B$ is chosen at the center of the object, with orientation aligned with the world frame. The object has a radius of curvature $r_B > 0$ in the horizontal direction, and being flat in the vertical direction, has an infinite radius of curvature in the vertical direction. Thus, $r_{rel1} = (1/r_A + 1/\infty)^{-1} = r_A$ and $r_{rel2} = (1/r_A + 1/r_B)^{-1}$, from which $r_e = r_A(r_B/(r_A + r_B))^{1/2}$. Substituting this formula and $m = 2$ into Equations (4.24) and (4.25) determines the total preload f_T and scaling parameters k_0 and δ_0. By choosing $l = 2\rho$, where $\rho > 0$ is the distance from $\mathcal{F}_B$'s origin to the contacts, one can find the dimensionless stiffness matrix $\widetilde{K} = S^T K S$, where K is computed according to Lemma 4.4.1, with the terms $\nabla\delta_i(q_0)$ and $D^2\delta_i(q_0)$ computed from Lemma 4.4.3 and Corollary 4.4.5. The resulting first- and second-order summands of $\widetilde{K}$ are given by $\widetilde{K}_1 = \text{diag}(2, 0, 0)$ and $\widetilde{K}_2 = \delta_0\,\text{diag}(0, -1/(r_A + r_B), (r_B - \rho)(r_A + \rho)/4\rho^2(r_A + r_B))$. The dimensionless stiffness matrix thus takes the

form:

$$\widetilde{K} = \mathrm{diag}\left(2, -\frac{\delta_0}{r_A + r_B}, \frac{\delta_0 (r_B - \rho)(r_A + \rho)}{4\rho^2 (r_A + r_B)}\right).$$

Since $\widetilde{K}_1 = \mathrm{diag}(2, 0, 0)$, the first-order effects are neutral with respect to translations of $\mathcal{B}$ along the y-axis and rotations of $\mathcal{B}$ about the origin. The second-order effects, while small, destabilize the fixture with respect to y-translations of $\mathcal{B}$. These effects destabilize (if $r_B < \rho$) or stabilize (if $r_B > \rho$) the fixture with respect to rotations of $\mathcal{B}$ about the origin. This example explains why a coin fixtured by two frictionless fingers tends to slip away from the fingers [30, 114].

Finally, Figure 4.6(b) shows the same object fixtured by four "point fingers." Assuming a fixed positive preload f_T, the four finger wrenches positively span the origin, and the fixture is stable to first-order. However, the fingers contact the object at points which are close to the contact points of the two-finger fixture of Figure 4.6(a), for which curvature effects introduce instability along y-translations. Since $\widetilde{K}_1$ and $\widetilde{K}_2$ vary continuously with the geometrical parameters, there is a small neighborhood about the original contact points in which the destabilizing effects of $\widetilde{K}_2$ still dominate the stabilizing effects of $\widetilde{K}_1$. Figure 4.6(b) illustrates such a contact arrangement, in which the fixture is still unstable, even though the fixture is stable to first-order. Inspection of $\widetilde{K}_2$ further reveals that as f_T increases, the destabilizing effect of $\widetilde{K}_2$ increases, which also agrees with [30, 114].

Example 4.5.2. Figure 4.7 shows an equilateral triangular object fixtured by three spherical fingers of radius r_A. The origin of $\mathcal{F}_B$ is chosen at the center of the object. For this fixture, $r_{rel1} = r_{rel2} = (1/r_A + 1/\infty)^{-1} = r_A$, which implies that $r_e = r_A$, and $\beta_j(e) = 1$ for $j = 1, 2$. Substituting these formulas along

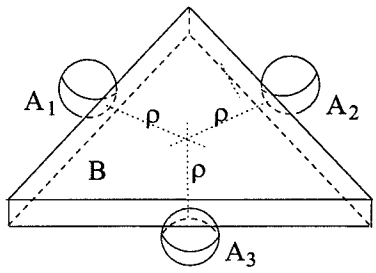

Figure 4.7: Fixturing an equilateral triangle by three spherical fingers (the supporting plane is not shown).

with $m = 3$ into Equations (4.24) and (4.25) determines the total preload f_T and scaling parameters k_0 and δ_0. Also for nondimensionalization, choose a characteristic object length to be $l = 2\rho$, where $\rho > 0$ is the distance of $\mathcal{F}_B$'s origin from the contacts. Using Lemmas 4.4.1 and 4.4.3 along with Corollary 4.4.5 to compute the dimensionless stiffness matrix $\widetilde{K} = S^T K S$, one obtains

$$\widetilde{K}_1 = \text{diag}(1,\, 1,\, 0) \quad \text{and} \quad \widetilde{K}_2 = \text{diag}\left(0,\, 0,\, \frac{\delta_0(\rho + r_A)}{4\rho^2}\right).$$

While the fixture is not stable by considering only the first-order effects, it is stable after the second-order effects are included, since $\widetilde{K} = \widetilde{K}_1 + \widetilde{K}_2$ is positive definite. As r_A increases, the stabilizing influence of $\widetilde{K}_2$ becomes more pronounced. This is consistent with the fact that the nonlinear spring relationship becomes harder as r_A grows. While the second-order effects are less significant than the first-order effects, they may provide adequate stabilization for many applications.

Example 4.5.3. This example illustrates how local curvature effects can be used to *significantly* stabilize an otherwise unstable fixture. Figure 4.8 shows a top view of an object $\mathcal{B}$ made of a thick plate. The boundary of $\mathcal{B}$ consists of three circular arcs cut from the plate, each of radius $r_B = -r$ where $r = 3l$. The body frame $\mathcal{F}_B$ is chosen at the center of the object, with orientation

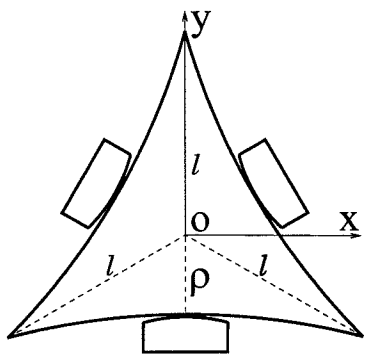

Figure 4.8: Top view of a curved triangular object fixtured by three similarly curved fingers.

aligned with the world frame. The parameter ρ, the distance of the body frame origin from the contacts, is given by $\rho = \frac{1}{2}(\sqrt{4r^2 - 3l^2} - 2r + l) = 0.372l$. The object is fixtured by three fingers with spherical tips of radius $r_A = r - \Delta r$, where $0 < \Delta r \ll r$. The contact normals are oriented along the object's lines of symmetry, which are 120° apart. Letting $\epsilon = \frac{\Delta r}{r}$ and neglecting small quantities when appropriate, the relative radii of curvature are $r_{rel1} = (1/r_A + 1/r_B)^{-1} = r/\epsilon$ and $r_{rel2} = (1/r_A + 1/\infty)^{-1} = r$, from which $r_e = r/\sqrt{\epsilon}$. Thus, noting that $m = 3$, one can determine the total preload f_T and scaling parameters k_0 and δ_0 from Equations (4.24) and (4.25). Lemmas 4.4.1 and 4.4.3, and Corollary 4.4.5 can be used to compute the dimensionless stiffness matrix $\widetilde{K} = S^T K S$:

$$\widetilde{K}_1 = \text{diag}(1,\, 1,\, 0) \quad \text{and} \quad \widetilde{K}_2 = \text{diag}\left(\xi_T,\, \xi_T,\, \xi_R\right),$$

where $\xi_T = \frac{2\mu_p^2}{3(4\epsilon\sqrt{\epsilon}+\mu_p^2)}$ and $\xi_R = \frac{4\mu_p^2(r+\rho)^2}{3(4\epsilon\sqrt{\epsilon}+\mu_p^2)l^2}$. The terms ξ_T and ξ_R in $\widetilde{K}_2$ measure the contribution of second-order effects to the translational and rotational stiffness of the fixture. Since the contacting surfaces tend to match perfectly when the value of Δr is very small, one needs to check if a, the length of the contact area's major semi-axis, is small compared with the radii of curvature

of the surfaces and the object's characteristic dimension. From Formula (4.7) one can find $a/r = \beta_3(e)\mu_p/2\sqrt{\epsilon}(1-e^2)^{\frac{1}{4}}$. Further, the ratio $\delta_0/\Delta r = \frac{1}{3}\mu_p^2\epsilon^{-3/2}$ can be computed, from which the curvature effect indicator (Corollary 4.5.6) is given by $\kappa = (r/l)^2(\delta_0/\Delta r)$.

For concreteness, suppose that the fingers are rigid and the object is made of an aluminum alloy with $E = 73$ GPa, $\nu = 0.33$, and $\sigma_{yield} = 345$ MPa. Thus, $E^* = E/(1-\nu^2) = 81.9$ GPa. Let $\gamma = 0.7$, i.e., the fixture is preloaded to 70% of the material capacity. Then the parameters ξ_T and ξ_R, along with the curvature effect indicator κ, and the ratios $\delta_0/\Delta r$, a/r and a/l, are computed for different values of ϵ in Table 4.1. The small values of a/r and a/l as listed in the table indicate that the Hertz model applies with reasonable accuracy. Moreover, when ϵ is sufficiently small, or the bodies' curvature achieves a close match, κ is of the order of unity even though $\delta_0/\Delta r \ll 1$. By Corollary 4.5.6, the second-order stabilizing effects are significant. Indeed, this is confirmed by the values of ξ_R, which are in the order of unity for small values of ϵ. Thus, as the fingers' curvature approaches the object's curvature, the forces generated by second-order effects become comparable with the forces generated by first-order effects.

Table 4.1: Compliant behaviors of the fixture for various values of ϵ.

ϵ	κ	ξ_T	ξ_R	a/r	a/l	$\delta_0/\Delta r$
0.01	0.927	0.048	1.087	0.081	0.242	0.103
0.02	0.418	0.022	0.510	0.066	0.197	0.046
0.03	0.260	0.014	0.322	0.058	0.173	0.029
0.04	0.185	0.010	0.230	0.053	0.158	0.021
0.05	0.142	0.008	0.177	0.049	0.147	0.016

4.6 Impact of the Choice of Contact Model on Stability Analysis

This section considers the impact of the choice of contact models on qualitative stability analysis results. We are interested in determining whether the prediction of fixture stability is *model-dependent*, i.e., the prediction of fixture stability or instability depends the choice of contact models. It will be shown that while the stability of some fixtures propagates within a class of contact models, *fixture stability analysis is in general model-dependent.* Even for those fixtures that behave qualitatively the same with respect to different contact models, their stability may differ significantly in a quantitative way.

Recall from Section 4.5.1 that the dimensionless stiffness matrix takes the form $\widetilde{K} = \widetilde{K}_1 + \widetilde{K}_2$, where $\widetilde{K}_1 = GDG^T$, and $\widetilde{K}_2 = \sum_{i=1}^{m} \nu_i \Psi_i$. According to Lemma 4.5.3, the second-order term can be further decomposed into $\widetilde{K}_2 = U + V$, where $U = \sum_{i=1}^{m} \nu_i \Psi_{a_i}$ and $V = \sum_{i=1}^{m} \nu_i \Psi_{b_i}$. In this decomposition, U is positive semidefinite and always stabilizing, while V accounts for the possibly destabilizing curvature effects. Our analysis of fixtures whose stability is insensitive to contact model choices will be based on the following key observation. The matrix G, and for essential fixtures the matrix $\widetilde{K}_2$, are *model-independent*, i.e., they are determined solely by the contact geometry and remain the same for all contact models.

First consider the stability of first-order stable fixtures under different contact models. Note that first-order stability, i.e., $\widetilde{K}_1 = GDG^T > 0$, is a model-independent notion since G is model-independent and D, provided $\delta_i(q_0) > 0$, is positive definite for all contact models. By Proposition 4.5.4, if the condition (4.23) is satisfied with respect to a contact model, then $\widetilde{K} = \widetilde{K}_1 + \widetilde{K}_2 > 0$, and in this case first-order stability implies stability. This immediately leads to the following corollary.

Corollary 4.6.1. *Suppose that a fixture is first-order stable. Then the fixture is stable for all contact models that satisfy the following condition:*

$$\sigma_{min}^2(G) \min_{1 \leqslant i \leqslant m} \frac{f_i'(\delta_i(q_0))}{k_0} \gg \max_{1 \leqslant i \leqslant m} \{\delta_0 \|L_{\bar{A}i}\|, \delta_0 \|L_{Bi}\|, \frac{\delta_0}{l}\}.$$

Now consider the impact of contact model choices on second-order stable fixtures. Recall that second-order stability means that $\widetilde{K}_1 + \widetilde{K}_2 > 0$ while the first-order term $\widetilde{K}_1$ is only positive semidefinite. We first consider the special case where there are no destabilizing curvature effects. Decompose the second-order term into $\widetilde{K}_2 = U + V$, where $U = \sum_{i=1}^m \nu_i \Psi_{a_i}$ and $V = \sum_{i=1}^m \nu_i \Psi_{b_i}$, with Ψ_{a_i} and Ψ_{b_i} given by Lemma 4.5.3. Since $U \geqslant 0$, any destabilizing curvature effects are accounted for by V. Moreover, V is model-independent for essential fixtures. We thus immediately arrive at

Lemma 4.6.2. *Let a fixture be essential. If $V = 0$, then the stability of fixture is independent of the choice of contact models.*

This scenario is often possible in practice when there is symmetry in both the bodies' geometry and the finger positions. This is illustrated by the fixtures in Examples 4.5.2 and 4.5.3, where destabilizing curvatures effects are indeed absent.

When destabilizing curvature effects are present, we consider the case where curvature effects are insignificant as discussed in Proposition 4.5.1. The following proposition, which is proved in the appendix, gives a condition under which second-order stable fixtures remain stable for a class of contact models.

Proposition 4.6.3. *Consider an essential fixture that satisfies the geometric conditions $\frac{\|L_{\bar{A}_i}\|}{\|\bar{L}_{rel_i}\|} = \mathcal{O}(1)$, $\frac{\|L_{B_i}\|}{\|\bar{L}_{rel_i}\|} = \mathcal{O}(1)$, and $\frac{\|\bar{L}_{rel_i}^{-1}\|}{l^2\|\bar{L}_{rel_i}\|} = \mathcal{O}(1)$ at each contact. Suppose that the fixture is second-order stable with respect to a given contact*

model such that the following inequality holds:

$$\sigma_0^2(G) \min_{1\leqslant i\leqslant m} \frac{f_i'(\delta_i(q_0))}{k_0} \gg \max_{1\leqslant i\leqslant m} \{\delta_0\|L_{\bar{A}i}\|, \delta_0\|L_{Bi}\|, \frac{\delta_0}{l}\},$$

where $\sigma_0(G)$ is the smallest nonzero singular value of G. Then the fixture is stable for all contact models under which the above inequality remains to hold.

This proposition does not address the situation where there exist significant curvature effects. Since significant curvature effects are practically always stabilizing, it is conjectured that the stability of fixtures with such effects are insensitive to the choice of contact models. This conjecture is currently still under investigation.

We have thus far shown that under certain conditions the stability of essential fixtures as well as first-order stable fixtures are qualitatively insensitive to the particular contact model that is chosen for stability analysis. But it should be realized that such fixtures in general behave quite differently with respect to different contact models. Therefore, for accurate modelling in automated planning algorithms, an appropriately chosen contact model must be used. In particular, the Hertz model, which is theoretically sound and experimentally verified, is in general more appropriate than the linear model. The following example shows the quantitative differences between the two models.

Example 4.6.1. Again consider the fixture in Example 4.5.2 (Figure 4.7) with a preloading overlap $\delta_i(q_0) = \delta$. The translational and rotational stiffnesses of this fixture with respect to the concurrency point are given by

$$k_T = \frac{3}{2}f'(\delta), \qquad k_R = \frac{3(\rho + r)f(\delta)}{l^2},$$

respectively. Let δ_s be the allowable preloading overlap, i.e., the corresponding

maximum shear stress in the bodies equals the yield stress σ_{yield}. Consider a linear model whose spring constant is defined as a secant modulus: $k = f(\delta_s)/\delta_s = \frac{4}{3}E^*\sqrt{r\delta_s}$. Then the translational and rotational stiffnesses with respect to the linear model are

$$\bar{k}_T = \frac{3}{2}k, \qquad \bar{k}_R = \frac{3(\rho + r)k\delta}{l^2},$$

respectively. The following ratios can hence be computed.

$$\frac{k_T}{\bar{k}_T} = \frac{3}{2}(\frac{\delta}{\delta_s})^{\frac{1}{2}}, \qquad \frac{k_R}{\bar{k}_R} = (\frac{\delta}{\delta_s})^{\frac{1}{2}}.$$

Therefore, the behavior of the fixture is quite different as δ is significantly different from δ_s. We also see that even if one wishes to use a linear model, the spring constant can often be derived from the Hertz model.

If a fixture is neither essential nor first-order stable, its stability may even be qualitatively different, as shown by the following example.

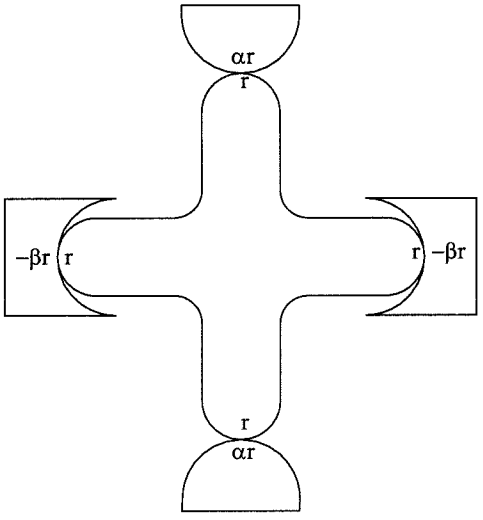

Figure 4.9: A four-finger fixture whose stability analysis is model-dependent.

Example 4.6.2. Consider a fixture of an object as shown in Figure 4.9. For simplicity assume that the contacting surfaces are all spherical. The object has identical local geometry at the contacts, with radius of curvature r. There are a pair of identical convex fingers with radius αr and a pair of concave fingers with radius $-\beta r$, where α and β are both positive constants with $\beta > 1$. Using the Hertz model, the compliance relationships corresponding to the convex and concave fingers can be written as

$$f_1(\delta) = \frac{4}{3}\sqrt{\frac{\alpha r}{\alpha+1}}E^*\delta^{\frac{3}{2}}, \quad \text{and} \quad f_2(\delta) = \frac{4}{3}\sqrt{\frac{\beta r}{\beta-1}}E^*\delta^{\frac{3}{2}},$$

respectively. Using a linear model and assuming an identical spring constant k for all contacts, the compliance relationships are

$$\bar{f}_1(\delta) = \bar{f}_2(\delta) = k\delta.$$

Let the preloading overlaps be δ_1 and δ_2 for the two types of contacts, respectively. Write the stiffness matrix corresponding to the Hertz model, while the formula corresponding to the linear model can be obtained by replacing f_1 and f_2 with $\bar{f}_1$ and $\bar{f}_2$, respectively.

$$K = \begin{pmatrix} K_{11}^{(1)} & 0 \\ 0 & 0 \end{pmatrix} + \begin{pmatrix} K_{11}^{(2)} & 0 \\ 0 & K_{22}^{(2)} \end{pmatrix},$$

where $K_{11}^{(1)} = \text{diag}(2f_1'(\delta_1),\, 2f_2'(\delta_2))$, $\|K_{11}^{(2)}\| \ll \|K_{11}^{(1)}\|$, and $K_{22}^{(2)} = f_1(\delta_1)\,(\rho -$

$r)\xi_R$ with

$$\xi_R = \frac{\rho/r - \beta}{\beta - 1}\frac{f_2(\delta_2)}{f_1(\delta_1)} - \frac{\rho/r + \alpha}{\alpha + 1}.$$

Choose $\rho > r$. Then the fixture is stable if $\xi_R > 0$, or unstable if $\xi_R < 0$. Note that for the Hertz model and the linear model, we have

$$\frac{f_2(\delta_2)}{f_1(\delta_1)} = (\frac{\delta_2}{\delta_1})^{\frac{3}{2}}, \quad \text{and} \quad \frac{\bar{f}_2(\delta_2)}{\bar{f}_1(\delta_1)} = \frac{\delta_2}{\delta_1},$$

respectively. As shown in Table 4.2, as the relevant parameters assume different values, ξ_R and $\bar{\xi}_R$, where $\bar{\xi}_R$ is computed from the same formula as ξ_R except that $\bar{f}_1$ and $\bar{f}_2$ are used instead of f_1 and f_2, can have opposite signs. That is, while the fixture is stable with respect to one model, it may be unstable with respect to the other.

Table 4.2: Qualitative differences in stability.

α	β	ρ/r	δ_2/δ_1	ξ_R	$\bar{\xi}_R$
2	1.5	4.5	0.35	-0.0667	0.4688
3	1.5	9.5	5	0.075	-0.2628

Summary:

This chapter used the overlap representation to formulate the theoretically and experimentally justified Hertz model, and derived a closed-form formula for the fixture stiffness matrix. This formula allows for direct computation of the stiffness matrix from geometric and material properties of the fixture, and can incorporate the Hertz model and other realistic contact models. The closed form of the stiffness matrix formula also allowed a systematic analysis of the

effects of local curvature on fixture stability. It was shown that while curvature effects may destabilize first-order stable fixtures, these destabilizing effects are practically very small. On the other hand, curvature effects can provide significant stabilizing effects, as illustrated by an example. This chapter also analyzed the impact of contact model choices on fixture stability. I was shown that under certain conditions, first-order fixtures, as well as second-order stable essential fixtures, are insensitive to certain classes of contact models. However, in general, stability analysis is model-dependent, and this fact was illustrated by Example 4.6.2. The practical utility of the stiffness matrix formula will be demonstrated in the next two chapters, where the formula is applied to computing the fixture stiffness matrix in planning optimal fixtures.

Chapter 5

Maximum-Stiffness Fixtures and Grasps

5.1 Introduction

Chapter 2 indicated that quality measures for compliant fixtures have been lacking, and that most previous works on quality measures for rigid bodies suffer the fundamental deficiency of dependence on reference frame choices. These problems are addressed in this and next chapters, which develop frame-invariant, physically meaningful quality measures for compliant fixtures, and apply them to optimal fixture planning.

This chapter focuses on optimal fixtures and grasps that exhibit *maximal stiffness.* We are interested in such fixtures and grasps since the stiffness, or rigidity, of a candidate fixture or grasp is often a suitable measure of effectiveness. The compliant behaviors of fixtures are represented by their stiffness matrices, and it is therefore natural to define quality measures by exploring the structure of stiffness matrices. Since the eigenvalues of the fixture stiffness matrix depend on choices of reference frames, other stiffness parameters that are *frame-invariant* should be sought.

The approach described in this chapter is based on six invariant scalars

called the *principal translational and rotational stiffnesses.* These parameters were first identified by Patterson and Lipkin [122] using screw theory. The same parameters can be derived using a different approach that is described in this chapter. The relation between the two approaches will be discussed, and a novel geometrical interpretation will be given to the principal stiffnesses. To allow meaningful comparison of the stiffness parameters, the rotational stiffnesses is converted into equivalent translational stiffnesses according to considerations of the object's maximal displacement and equivalence of elastic energy. Based on the resulting set of comparable parameters, the *stiffness quality measure* is defined, and applied to planning *maximum-stiffness fixtures and grasps* of polygonal objects by three and four fingers. In both cases practical methods are developed for computing the *globally optimal* finger arrangement, and provide examples which show that the resulting optimal fixtures are indeed intuitively effective fixtures.

As indicated in Chapter 3, tangent vectors and covectors to $SE(3)$ can be represented in different ways. For convenience, *body velocities and body wrenches* (specified in a body frame $\mathcal{F}_B$) will be used in this chapter as well as the following chapters. The fixture stiffness matrix, denoted K, will also be specified with respect to body coordinates. That is, the relationship $\boldsymbol{w} = K\dot{q}$ holds, where $\dot{q}$ is a body velocity and $\boldsymbol{w}$ a body wrench. Using (3.5), the ensuing results in body coordinates can be expressed in terms of hybrid coordinates. In particular, quantities that are frame-invariant in body coordinates remain frame-invariant in hybrid coordinates[1].

[1]We do not use spatial coordinates in frame-invariance considerations, since as will be shown in Chapter 7, spatial coordinates are inappropriate for these purposes.

5.2 Principal Stiffness Parameters

This section identifies several frame-invariant parameters of compliant fixtures, which will be used to define the stiffness quality measure in the next section. From the wrench-displacement relationship $\boldsymbol{w} = K\dot{q}$ and the change-of-frame formulas (3.7) for body coordinates, the fixture stiffness matrix can be shown to obey the following transformation rule:

$$\bar{K} = \mathrm{Ad}_{g_B}^T \, K \, \mathrm{Ad}_{g_B}, \tag{5.1}$$

where $\bar{K}$ is the stiffness matrix specified with respect to a new body frame $\bar{\mathcal{F}}_B$ located at $g_B \in SE(3)$ relative to $\mathcal{F}_B$, Ad_{g_B} is the adjoint map associated with g_B given by (3.8) or (3.12). It follows that the eigenvalues of K, which could provide insight into the stiffness matrix, are *frame-dependent* since Ad_{g_B} is in general not orthogonal. To find frame-invariant stiffness parameters, we partition K, and $C = K^{-1}$, called the *compliance matrix* of the fixture, along translational and rotational motions.

$$K = \begin{pmatrix} K_{11} & K_{12} \\ K_{12}^T & K_{22} \end{pmatrix} \quad \text{and} \quad C = \begin{pmatrix} C_{11} & C_{12} \\ C_{12}^T & C_{22} \end{pmatrix}, \tag{5.2}$$

where the entries K_{ij} are 3×3 matrices in the 3D case. In the 2D case, the dimensions of K_{11}, K_{12} and K_{22} become 2×2, 2×1 and 1×1, respectively. We will focus on *stable fixtures whose stiffness matrices are positive definite*, since other fixtures are considered ineffective.

Given any tangent vector $\dot{q} = (v, \omega)$, the notation $(K\dot{q})_1 = K_{11}v + K_{12}\omega$ and $(K\dot{q})_2 = K_{12}^T v + K_{22}\omega$ will be used for convenience. Similarly, we write $(C\boldsymbol{w})_1 = C_{12}f + C_{22}\tau$ and $(C\boldsymbol{w})_2 = C_{12}^T f + C_{22}\tau$ for any wrench $\boldsymbol{w} = (f, \tau)$.

5.2.1 Definition of the Principal Stiffness Parameters

The first set of stiffness parameters is defined on a tangent subspace on which the stiffness matrix has a frame-invariant structure. This subspace is given by

$$V = \{\dot{q} \in T_{q_0}SE(3) \ : \ f = (K\dot{q})_1 = 0\},$$

where q_0 is the equilibrium fixture configuration of $\mathcal{B}$. In words, the subspace V consists of small displacements of $\mathcal{B}$ which cause the fingers to react in such a way as to generate a pure net torque on the body. Using the partition of K yields $V = \{(v, \omega) : v = -K_{11}^{-1}K_{12}\omega\}$, from which it follows that V can be parametrized in terms of $\omega \in \mathbb{R}^3$ as[2]

$$V = \left\{\dot{q} = P\omega : \omega \in \mathbb{R}^3\right\} \quad \text{where} \quad P = \begin{pmatrix} -K_{11}^{-1}K_{12} \\ I \end{pmatrix}. \tag{5.3}$$

Let K_V denote the restriction of the stiffness matrix K to the subspace V. We now derive an expression for K_V. The stiffness matrix K is a linear operator from $T_{q_0}SE(3)$ to $T_{q_0}^*SE(3)$, and $\dot{q}^T K\dot{q}$ is consequently a symmetric bilinear operator on $T_{q_0}SE(3)$. Since the vectors in V are parametrized by ω, (5.3) implies that $\omega^T K_V \omega = \omega^T P^T K P \omega$ for arbitrary ω. Thus K_V has the representation $K_V = P^T K P = K_{22} - K_{12}^T K_{11}^{-1} K_{12}$. In addition, the pure torque corresponding to $\dot{q} \in V$ is given by $(K\dot{q})_2 = K_V\,\omega$.

Under the body representation, K_V is not affected by choice of world frame. Consider now a new body frame $\bar{\mathcal{F}}_B$, and use overbars to denote objects associated with this frame. The linear operator K_V has the following invariance property.

[2] K_{11} is invertible since, in general, the principal sub-matrices of a positive definite matrix are positive definite and therefore invertible.

Proposition 5.2.1. *Let V and $\bar{V}$ be the subspaces parametrized by* (5.3) *with respect to the old and new body frames. Let K_V and $\bar{K}_V$ be the restriction of the respective stiffness matrix to V and $\bar{V}$. Then K_V and $\bar{K}_V$ obey the orthogonal transformation $\bar{K}_V = R_B^T K_V R_B$, where R_B is the rotation matrix from $\mathcal{F}_B$ to $\bar{\mathcal{F}}_B$. Hence, the eigenvalues of K_V are* frame-invariant.

Proof. Using the stiffness matrix transformation rule (5.1) and formula (3.8) for Ad_{g_B}, the components of the stiffness matrix $\bar{K}$ are: $\bar{K}_{11} = R_B^T K_{11} R_B$, $\bar{K}_{12} = R_B^T(K_{12}+K_{11}\widehat{d_B})R_B$, and $\bar{K}_{22} = R_B^T(K_{22}+K_{12}^T\widehat{d_B}-\widehat{d_B}K_{12}-\widehat{d_B}K_{11}\widehat{d_B})R_B$. Substituting these expressions into $\bar{K}_V = \bar{K}_{22} - \bar{K}_{12}^T\bar{K}_{11}^{-1}\bar{K}_{12}$ gives $\bar{K}_V = R_B^T K_V R_B$. □

The second set of stiffness parameters is defined from the dual consideration of a subspace of wrenches on which the compliance matrix C has a frame-invariant structure. This subspace is given by:

$$W = \left\{ \boldsymbol{w} \in T_{q_0}^* SE(3) : \omega = (C\boldsymbol{w})_2 = 0 \right\}.$$

The subspace W thus consists of external wrenches whose action on $\mathcal{B}$ causes it to move with pure translation. The subspace W can be parametrized in terms of $f \in \mathbb{R}^3$ as

$$W = \left\{ \boldsymbol{w} = Qf : f \in \mathbb{R}^3 \right\} \quad \text{where} \quad Q = \begin{pmatrix} I \\ -C_{22}^{-1}C_{12}^T \end{pmatrix}. \tag{5.4}$$

According to this parametrization, the pure translation induced by a wrench $\boldsymbol{w} \in W$ takes the form $v = (C\boldsymbol{w})_1 = C_W f$, where C_W is the restriction of C to the subspace W given by $C_W = Q^T C Q = C_{11} - C_{12}C_{22}^{-1}C_{12}^T$. To express C_W in terms of the stiffness matrix, the inversion formula of a partitioned matrix

can used to write

$$\begin{pmatrix} C_{11} & C_{12} \\ C_{12}^T & C_{22} \end{pmatrix}^{-1} = \begin{pmatrix} C_W^{-1} & -C_{11}^{-1}C_{12}\Delta^{-1} \\ -\Delta^{-1}C_{12}^T C_{11}^{-1} & \Delta^{-1} \end{pmatrix},$$

where $\Delta = C_{22} - C_{12}^T C_{11}^{-1} C_{12}$. Since $C^{-1} = K$, the uniqueness of a matrix inverse implies that

$$C_W = K_{11}^{-1}. \tag{5.5}$$

With respect to a new body frame $\bar{\mathcal{F}}_B$, the submatrix K_{11} transforms to $\bar{K}_{11} = R_B^T K_{11} R_B$. We therefore immediately arrive at the following invariance property of C_W:

Proposition 5.2.2. *Let W and $\bar{W}$ be the subspaces parametrized by* (5.4) *with respect to the old and new body frames. Let C_W and $\bar{C}_W$ be the restriction of the respective compliance matrix to W and $\bar{W}$. Then C_W and $\bar{C}_W$ obey the orthogonal transformation $\bar{C}_W = R_B^T C_W R_B$, where R_B is the rotation matrix from $\mathcal{F}_B$ to $\bar{\mathcal{F}}_B$. Hence, the eigenvalues of C_W are* frame-invariant.

Propositions 5.2.1 and 5.2.2 lead to the following observations. The behavior of K on the tangent subspace V characterizes the *rotational stiffness* of the fixture. In response to an instantaneous displacement in V, the reaction wrench is a pure torque. In addition, the reaction torque varies by at most a pure rotation corresponding to different choices of frames. Similarly, the behavior of C on the wrench subspace W characterizes the *translational compliance* of the fixture. A wrench in W generates a pure translation of $\mathcal{B}$, which is the same up to a rotation with respect to different frames. Based on these observations, the following frame-invariant principal parameters of K can be

defined.

Definition 5.2.1 (Principal Stiffnesses). Let K be the fixture stiffness matrix, and $C = K^{-1}$ the compliance matrix. Let K_V and C_W be the restriction of K and C to the subspaces V and W. Then the *principal rotational stiffnesses* of the fixture are the eigenvalues μ_i $(i = 1, 2, 3)$ of $K_V = K_{22} - K_{12}^T K_{11}^{-1} K_{12}$, and the *principal translational stiffnesses* of the fixture are the eigenvalues σ_i $(i = 1, 2, 3)$ of $C_W^{-1} = K_{11}$.

For planar fixtures the principal stiffness parameters have the following physical interpretation. It can be shown that every planar fixture has a *unique* location of an object frame origin, given by

$$d_B = JK_{11}^{-1}K_{12}, \tag{5.6}$$

such that when $\bar{\mathcal{F}}_B$ is placed at this location, $\bar{K}$ takes the *block-diagonal* form $\bar{K} = \text{diag}(R_B^T K_{11} R_B, \mu)$. That is, for planar fixtures the translational and rotational effects are *decoupled* about this special point, called the *center of compliance* of the fixture [114]. The principal translational and rotational stiffnesses of a planar fixture are physically the translational and rotational stiffnesses about the center of compliance. For 3D fixtures, there is generally no such center of compliance, and the stiffness matrix in general cannot be made block-diagonal. However, it is important to note that the principal stiffness parameters are still well-defined and frame-invariant in the 3D case.

5.2.2 Screw Coordinates Interpretation

While searching for a 3D analog of the center of compliance, Patterson and Lipkin [122] were the first to recognize the existence of the principal stiffness

parameters. They used screw coordinates, and we now show that our principal parameters are equivalent to the ones derived by Patterson and Lipkin.

Consider a tangent vector $\dot{q}_i = P\omega_i \in V$, where ω_i is a unit eigenvector of K_V associated with the eigenvalue μ_i. Correspondingly, one has a pure torque given by $\tau = (K\dot{q}_i)_2 = \mu_i\omega_i$. From the review of screw coordinates in 3.2.2, the tangent vector $\dot{q}_i$ induces a *pure-torque wrench of magnitude* μ_i *about the screw axis of* $\dot{q}_i$. On the other hand, for $\boldsymbol{w}_i = Qf_i \in W$ where f_i is a unit eigenvector of C_W associated with the eigenvalue σ_i^{-1}, we have $v = (C\boldsymbol{w}_i)_1 = \sigma_i^{-1}f_i$. Hence, the wrench $\boldsymbol{w}_i$ generates a *pure-translation displacement of magnitude* σ_i^{-1} *along the screw axis of* $\boldsymbol{w}_i$. The principal stiffness parameters can now be interpreted in terms of screw coordinates. Every stiffness matrix K has six frame-invariant screw axes. A displacement of $\mathcal{B}$ along the first three axes results in a pure torque which acts on $\mathcal{B}$ along the same axis of magnitude which is determined by the rotational stiffness μ_i $(i = 1, 2, 3)$. A wrench applied to $\mathcal{B}$ along the other three axes results in a pure translation of $\mathcal{B}$ along the same axis, and the magnitude of the translation is determined by the translational stiffness σ_i $(i = 1, 2, 3)$.

5.2.3 Geometric Interpretation

We now interpret the principal stiffness parameters in terms of the geometry of two level-sets. The first is a level-set in the tangent space, defined by $\mathcal{S} = \{\dot{q} \in T_{q_0}SE(3) : \Phi(\dot{q}) = 1\}$, where $\Phi(\dot{q}) = \frac{1}{2}\dot{q}^T K\dot{q}$. The second is a level-set in the wrench space, defined by $\mathcal{T} = \{\boldsymbol{w} \in T^*_{q_0}SE(3) : \Psi(\boldsymbol{w}) = 1\}$, where $\Psi(\boldsymbol{w}) = \frac{1}{2}\boldsymbol{w}^T C\boldsymbol{w}$. These level sets consist of tangent vectors or wrenches that induce unit elastic energy, and geometrically represent a five-dimensional ellipsoidal surface in the six-dimensional tangent or wrench space. The shape of these ellipsoidal surfaces varies as different coordinate frames are used. However, these surfaces possess frame-invariant features which correspond to

the principal stiffness parameters.

First consider the level-set $\mathcal{S}$. For each fixed ω, the subset of $\mathcal{S}$ with this particular value of ω is denoted $\mathcal{S}_\omega$. Each subset $\mathcal{S}_\omega$ is a level-set of the function $\Phi_\omega(v) \triangleq \Phi(v,\omega)$, in which ω is a fixed parameter and only v is a variable. Rewriting $\Phi(v,\omega)$ as a function of v only gives:

$$\Phi_\omega(v) = \frac{1}{2}(v + K_{11}^{-1}K_{12}\omega)^T K_{11}(v + K_{11}^{-1}K_{12}\omega) + \frac{1}{2}\omega^T K_V \omega.$$

Hence for each fixed ω, the level-set $\mathcal{S}_\omega = \{v : \Phi_\omega(v) = 1\}$ is a two-dimensional ellipsoidal surface with principal semi-axes of lengths $((2 - \omega^T K_V\, \omega)/\sigma_i)^{1/2}$ $(i = 1,2,3)$. Since the quadratic form $\omega^T K_V\, \omega$ is frame-invariant, these lengths are frame-invariant. In particular, when $\omega = 0$, these lengths are simply given by $\sqrt{2/\sigma_i}$ $(i = 1,2,3)$. In other words, the principal translational stiffnesses σ_i determine the frame-invariant shape of the intersection of $\mathcal{S}$ with the pure-translation subspace given by $\omega = 0$. This feature can be easily visualized in 2D fixtures as will be described shortly.

The level-set $\mathcal{S}$ possesses another frame-invariant geometrical feature. Consider the projection, denoted $\mathcal{S}_{v=0}$, of the set $\mathcal{S}$ onto the pure-rotation subspace given by $v = 0$. It can be verified that the boundary of $\mathcal{S}_{v=0}$ (called the *silhouette* of $\mathcal{S}$ along the direction of projection) is the projection of the points on $\mathcal{S}$ at which the vector normal to $\mathcal{S}$ has zero v-components. The latter set is denoted $\mathcal{S}_n$. Since $\mathcal{S}$ is a level-set of the function $\Phi(v,\omega)$, $\mathcal{S}_n$ is determined by the condition $(\nabla\Phi(\dot{q}))_1 = 0$. This condition implies that $\mathcal{S}_n = \{(v,\omega) \in \mathcal{S} : v = -K_{11}^{-1}K_{12}\omega\} = \{(v,\omega) \in \mathcal{S} : \frac{1}{2}\omega^T K_V \omega = 1\}$. Thus, the projection of the set $\mathcal{S}$ onto the subspace $v = 0$ is given by

$$\mathcal{S}_{v=0} = \{(v,\omega) :\ v = 0 \text{ and } \frac{1}{2}\omega^T K_V \omega \leqslant 1\}.$$

The projection set is a three-dimensional ellipsoid with principal semi-axes of length $\sqrt{2/\mu_i}$, where μ_i $(i = 1, 2, 3)$ are the frame-invariant eigenvalues of K_V. In other words, the principal rotational stiffness parameters are precisely the semi-axis lengths of the ellipsoid formed by projecting $\mathcal{S}$ onto the pure-rotation subspace given by $v = 0$.

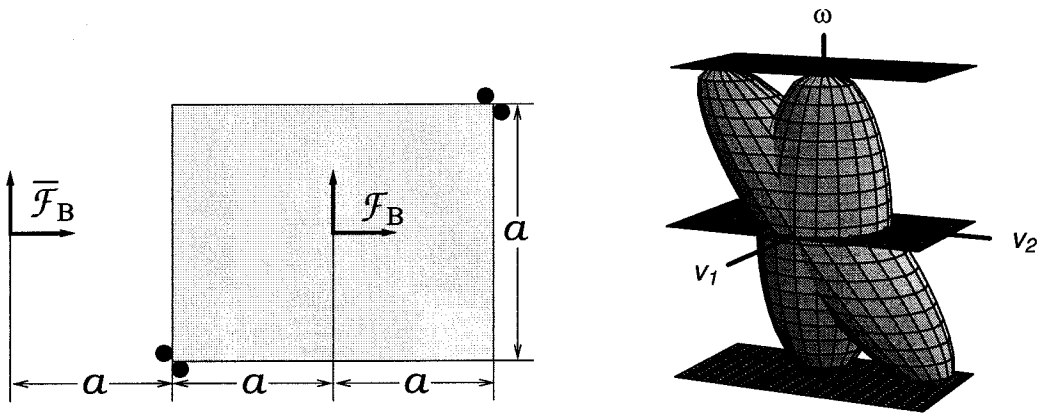

(a) Four-finger fixture of a rectangle (b) Elastic energy ellipsoids

Figure 5.1: The elastic energy ellipsoids in $T_{q_0}SE(3)$ of a fixture.

We now describe, in terms of planar fixtures, the above frame-invariant features of the level set $\mathcal{S}$, which becomes a two-dimensional ellipsoidal surface in $\mathbb{R}^3$. Figure 5.1(b) shows two such ellipsoids for the 4-finger fixture of a rectangle shown in Figure 5.1(a). The upright ellipsoid corresponds to the frame $\mathcal{F}_B$, while the slanted ellipsoid corresponds to the frame $\bar{\mathcal{F}}_B$. As can be observed from the figure, the lengths of the principal semi-axes of each horizontal cross section of $\mathcal{S}$ are frame-invariant. Similarly, the projection of $\mathcal{S}$ onto the ω-axis is bounded by two points, whose ω-coordinates are $\pm\sqrt{2/\mu}$. These two points are frame-invariant, and $\mathcal{S}$ is always bounded by the two horizontal planes $\omega = \pm\sqrt{2/\mu}$.

The frame-invariant features of the level set $\mathcal{T}$, which is a five-dimensional ellipsoidal surface in the six-dimensional wrench space, can be analogously identified and are summarized as follows. Each subset of $\mathcal{T}$ with a fixed value

of f, denoted $\mathcal{T}_f$, is a two-dimensional ellipsoidal surface whose principal semi-axes are equal to $(\mu_i(2 - f^T K_{11}^{-1} f))^{1/2}$ $(i = 1, 2, 3)$ and are frame-invariant. In particular, when $f = 0$ the principal semi-axes of $\mathcal{T}_f$ are given by $\sqrt{2\mu_i}$ for $i = 1, 2, 3$. The projection of $\mathcal{T}$ onto the wrench subspace determined by $\tau = 0$ is given by

$$\mathcal{T}_{\tau=0} = \{(f, \tau) : \tau = 0 \text{ and } \frac{1}{2} f^T K_{11}^{-1} f \leqslant 1\},$$

which is a three-dimensional ellipsoid whose principal semi-axes have frame-invariant lengths of $\sqrt{2\sigma_i}$ $(i = 1, 2, 3)$.

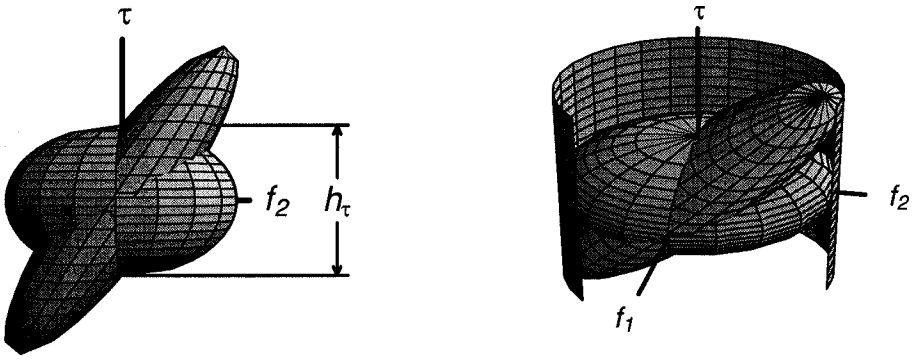

(a) $\mathcal{T}$ intersects the τ-axis at the same points: $h_\tau = 2\sqrt{2\mu}$

(b) $\mathcal{T}$ is inscribed in the same elliptic cylinder

Figure 5.2: The elastic energy ellipsoid in $T^*_{q_0}SE(3)$.

For planar fixtures $\mathcal{T}$ is a two-dimensional ellipsoidal surface in $\mathbb{R}^3$. For the fixture given in Figure 5.1(a), the frame-invariant features of $\mathcal{T}$ are shown in Figure 5.2, where the upright and slanted ellipsoids again correspond to the frames $\mathcal{F}_B$ and $\bar{\mathcal{F}}_B$, respectively. It can be seen that the ellipsoid $\mathcal{T}$ intersects the τ-axis, which is chosen to be the vertical axis, at two points whose τ-coordinates are $\pm\sqrt{2\mu}$, as shown in Figure 5.2(a). In addition, regardless of frame choices, the horizontal projection of $\mathcal{T}$ is the planar ellipse $\frac{1}{2} f^T K_{11}^{-1} f \leqslant 1$. Hence, with respect to arbitrarily chosen coordinate frames, $\mathcal{T}$ is always

inscribed in the vertical cylinder whose base set is this ellipse, as shown in Figure 5.2(b).

Also note that the *volume* of the ellipsoids is frame-invariant, since the volume is determined by $\det(K)$ which is frame-invariant [90]. However, no use is made of the volume in the stiffness quality measure.

5.3 The Stiffness Quality Measure

This section defines a frame-invariant quality measure for compliant fixtures based on the principal stiffness parameters. First we must find a way to meaningfully compare the translational and rotational stiffnesses of a fixture. Our approach is based on the object's maximal displacement and the elastic energy associated with this maximal displacement.

Let $\dot{q} = \alpha(v, \omega)$ be an infinitesimal displacement of $\mathcal{B}$, where $\alpha > 0$ is a scalar, $\|\omega\| = 1$ if $\omega \neq 0$, and $\|v\| = 1$ if $\omega = 0$. The maximal displacement of any point in $\mathcal{B}$ will be simply called the *maximal displacement* of $\mathcal{B}$. Clearly, such a maximal displacement is a measure of the object's deflection resulting from elastic deformations. Moreover, since $\mathcal{B}$ has bounded dimension, this maximal displacement always exists and is independent of frame choice. If $\omega = 0$, the maximal displacement of $\mathcal{B}$ is simply α. If $\omega \neq 0$, let $\rho_{\max}(\dot{q})$ be the greatest distance from the instantaneous screw axis associated with $\dot{q}$ to $\mathcal{B}$'s boundary points. Then $\mathcal{B}$'s maximal displacement is $\alpha(\rho_{\max}(\dot{q})^2 + (v \cdot \omega)^2)^{1/2}$, where $v \cdot \omega$ is the pitch of $\dot{q}$. In the case of planar fixtures the vector ω is perpendicular to v, and the maximal displacement of $\mathcal{B}$ is $\alpha\rho_{\max}(\dot{q})$, where $\rho_{\max}(\dot{q})$ is the maximal distance from $\mathcal{B}$'s instantaneous center of rotation to $\mathcal{B}$'s boundary points. We now convert the rotational stiffnesses to equivalent translational stiffnesses using the object's maximal displacement.

First consider planar fixtures, where there is only a single principal rota-

tional stiffness parameter, denoted by μ. To compare μ with the translational stiffness parameters σ_1, σ_2, we define a parameter which has the units of translational stiffness and whose equivalence with the principal rotational stiffness μ is determined as follows. As discussed in Section 5.2, μ is associated with rotations of $\mathcal{B}$ about the fixture's center of compliance. Corresponding to a rotation of $\mathcal{B}$ with magnitude α about the center of compliance, $\mathcal{B}$'s maximal displacement is given by $\alpha\rho_{\max}$, and the amount of elastic energy induced by the maximal displacement is $\frac{1}{2}\mu\alpha^2$. Suppose that $\mathcal{B}$ undergoes a translation of $\alpha\rho_{\max}$, which obviously results in the same maximal displacement. As this translation occurs, it may be imagined that $\mathcal{B}$, instead of being fixtured by the fingers, is attached to a linear spring aligned with the direction of translation. We define the constant of this spring, denoted μ_{eq}, as *equivalent* to the principal rotational stiffness μ, if the elastic energy of the linear spring resulting from the (imaginary) translation equals $\frac{1}{2}\mu\alpha^2$. Thus, the equation $\frac{1}{2}\mu_{eq}(\rho_{\max}\alpha)^2 = \frac{1}{2}\mu\alpha^2$ leads to the following expression for the equivalent stiffness μ_{eq}:

$$\mu_{eq} = \frac{\mu}{\rho_{\max}^2}. \tag{5.7}$$

The parameter μ_{eq} has the same units as the translational stiffnesses σ_i and its equivalence is also based on the physically meaningful principle of elastic energy. The three parameters can now be meaningfully compared, and the quality measure can be defined to be: $Q_{stiff} = \min\{\sigma_1, \sigma_2, \mu_{eq}\}$.

Next the quality measure will be defined for 3D fixtures. Like the planar case, we define stiffness parameters which are equivalent to the principal rotational stiffnesses μ_i. Let ω_i be a unit-magnitude eigenvector of K_V associated with μ_i, and let $\alpha > 0$ be a scalar. Then the displacement of $\mathcal{B}$ represented by the vector $\alpha\omega_i$ is $\dot{q}_i = \alpha P\omega_i$. Using formula (5.3) for P, we write $\dot{q}_i = \alpha(v_i, \omega_i)$

where $v_i = -K_{11}^{-1}K_{12}\omega_i$. When $\mathcal{B}$ is subjected to the displacement $\dot{q}_i$, the amount of induced elastic energy is given by $\frac{1}{2}\mu_i\alpha^2$, and the maximal displacement of $\mathcal{B}$ is given by $\alpha(\rho_{\max_i}^2 + (v_i \cdot \omega_i)^2)^{1/2}$, where $\rho_{\max i} = \rho_{\max}(\dot{q}_i)$. Now imagine the situation where the object, while attached to a linear spring, undergoes a pure translation by the amount of this maximal displacement in the direction of the spring. The stiffness coefficient of the linear spring, denoted μ_{eq_i}, is defined as *equivalent* to the principal rotational stiffness μ_i, if the elastic energy of the spring due to the translation equals $\frac{1}{2}\mu_i\alpha^2$. Hence, by requiring that $\frac{1}{2}\mu_{eq_i}\left(\alpha\sqrt{\rho_{\max_i}^2 + (v_i \cdot \omega_i)^2}\right)^2 = \frac{1}{2}\mu_i\alpha^2$, we obtain the following formula for μ_{eq_i}:

$$\mu_{eq_i} = \frac{\mu_i}{\rho_{\max_i}^2 + (v_i \cdot \omega_i)^2} \quad \text{for } i = 1, 2, 3. \tag{5.8}$$

As in the 2D case, the equivalent stiffness parameters have the same units as the translational stiffnesses. Therefore, the quality measure is defined for 2D and 3D fixtures as follows.

$$Q_{stiff} = \begin{cases} \min\{\sigma_1, \sigma_2, \mu_{eq}\} & \text{(2D case)} \\ \min\{\sigma_{\min}, \mu_{eq_{\min}}\} & \text{(3D case)} \end{cases} \tag{5.9}$$

where $\sigma_{\min} = \min\{\sigma_1, \sigma_2, \sigma_3\}$ and $\mu_{eq_{\min}} = \min\{\mu_{eq_1}, \mu_{eq_2}, \mu_{eq_3}\}$.

As discussed in Section 5.2.1, the principal stiffness parameters characterize the stiffness of a given fixture, and Q_{stiff}, called the *stiffness quality measure*, characterizes the *worst-case* stiffness of the fixture. The worst-case stiffness is determined by a trade-off between the worst-case translational and rotational stiffnesses. The worst-case translational stiffness is characterized by the smallest principal translational stiffness $\sigma_{\min}$, and the worst-case rotational

stiffness by the smallest equivalent rotational stiffness $\mu_{eq_{\min}}$ (or μ_{eq} in the 2D case). In characterizing the worst-case rotational stiffness by $\mu_{eq_{\min}}$ (or μ_{eq}), the principal rotational stiffness parameters are meaningfully compared with the translational stiffness parameters by considering equivalence of elastic energy based on the object's maximal displacement. Note that Q_{stiff} has the following properties. First, Q_{stiff} is valid for fixtures of 2D and 3D objects by any number of fingers. Second, the fixtures can be modeled by any compliance model, since Q_{stiff} depends only on the stiffness matrix of the fixture. Third, Q_{stiff} is *invariant* with respect to change of world and object reference frames. Last, the optimal fixture of an object is the *maximum-stiffness fixture*, i.e., Q_{stiff} is *maximized* to allow the highest worst-case stiffness.

5.4 Three- and Four-Finger Fixtures of Polygonal Objects: A Characterization

The stiffness quality measure, and the deflection quality measure that will be developed in the next chapter, will be applied to optimal fixturing of polygonal objects. This section is to lay the necessary foundation for these applications. While the quality measures can be used with stiffness matrices computed from any contact model with or without inclusion of friction and other effects, the overlap-based compliance model as developed in Chapter 4 will be used for stiffness matrix computation.

To apply optimization algorithms for finding the optimal fixture of a given object, we need to *parametrize* the set of all possible finger arrangements, which is called the *contact configuration space*. For a planar fixture, it may be natural to parametrize each finger location by its scalar distance from a reference point along the object's boundary. However, three- and four-finger equilibrium fixtures of polygons can be parametrized in a more convenient

form. Based on a parametrization of the contact c-space, the stiffness matrix, and hence the quality measure, become parametrized. Optimization algorithms can then be developed to find the parameter values corresponding to the optimal fixture.

5.4.1 Three-Finger Stable Equilibrium Fixtures

When a polygonal object is fixtured by three frictionless fingers, each finger must lie on a different edge of the object. Therefore, we can consider triplets of edges. A triplet of edges is said to be *admissible* if the inward-pointing normals to these edges positively span the plane. We need only consider admissible edge-triplets because of the following properties that characterize *equilibrium fixtures* by three frictionless fingers. The contact normals must positively span the origin, and the lines collinear with the contact normals must be concurrent, i.e., intersect at a common point. We discard three-finger fixtures where a finger is placed at a vertex and simultaneously contacts two edges, since such fixtures are weak in strength and cannot be modelled by the Hertz model and other realistic contact models.

We now invoke the computation method as described in Chapter 4 to compute the stiffness matrix of three-finger equilibrium fixtures. In the following lemma which is proved in Appendix B.2.1, N_i denotes the unit normal to an edge of $\mathcal{B}$ at the i^{th} contact, pointing into $\mathcal{B}$ and specified in $\mathcal{F}_B$. Further, $k_i = f_i'(\delta_i(q_0))$ where the compliance function f_i corresponds to a **general** (linear or nonlinear) contact model. Also recall that the *circumscribing circle* of a triangle is the circle which passes through the triangle's vertices (Figure 5.3).

Lemma 5.4.1. *Let three disc fingers of radius r hold a polygonal object $\mathcal{B}$ on an edge-triplet in a frictionless equilibrium fixture. Choose the origin of the body frame $\mathcal{F}_B$ at the concurrency point of the lines of the contact normals.*

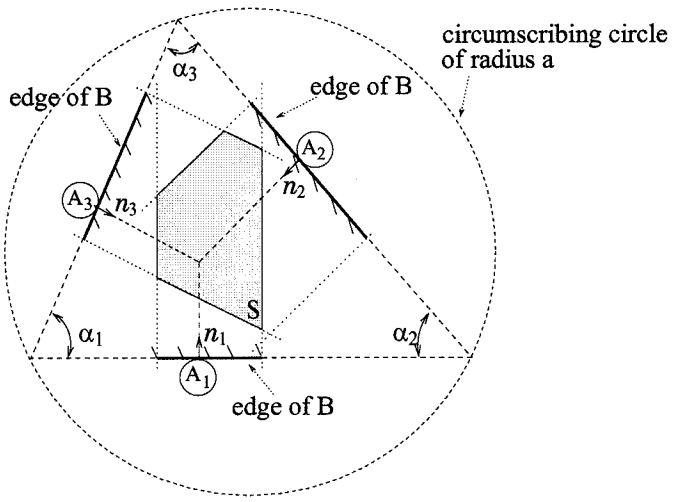

Figure 5.3: Three fingers on an triplet of edges.

Then for a general contact model, the fixture is stable and its stiffness matrix is given by

$$K = \mathrm{diag}(\sum_{i=1}^{3} k_i N_i N_i^T, \mu) \quad \textit{where } \mu = f_T(2a\zeta + r). \tag{5.10}$$

In the expression for μ, f_T *is the* total preload, *given by* $f_T = \sum_{i=1}^{3} f_i(\delta_i(q_0))$; a *is the radius of the triangle's circumscribing circle; and* $\zeta = \frac{\prod_{i=1}^{3} \sin\alpha_i}{\sum_{i=1}^{3} \sin\alpha_i}$ *is determined from the triangle's three interior angles, denoted* α_i $(i = 1, 2, 3)$.

It follows from this lemma that *the collection of stable equilibrium fixtures associated with a given admissible edge-triplet can be parametrized by the position of the concurrency point of the contact normals.* Such concurrency point positions form a *bounded convex polygonal region*, denoted S, which can be obtained by intersecting three strips orthogonal to the edges, as shown in Figure 5.3. Moreover, the lemma asserts that K is block-diagonal when $\mathcal{F}_B$'s origin is at the concurrency point of the contact normals. Since this property uniquely characterizes the center of compliance (Equation (5.6)), the concurrency point is at the fixture's center of compliance. Thus, the two eigenvalues

of the 2×2 matrix $K_{11} = \sum_{i=1}^{3} k_i N_i N_i^T$ are the translational stiffnesses σ_1,σ_2, and μ is the rotational stiffness of the fixture.

The parameters σ_1,σ_2, and μ must be positive so that K is positive definite. In the parameter $\mu = f_T(2a\zeta + r)$, a and r are positive constants, while ζ is a positive constant in compressive fixtures where the fingers push towards the concurrency point[3]. Assuming the usual case of a compressive fixture, μ is positive when f_T is strictly positive. The condition $f_T > 0$ implies that the fixture must be *preloaded* for stability. We therefore assume that *f_T, and hence $f_i(\delta_i(q_0))$, have specified positive values for all possible finger placements.* This is a reasonable assumption, since in practice one often wishes to compare different fixtures corresponding to a common preloading level determined by the task specifications and material strength requirements. Under this assumption, *μ is a positive constant on a given admissible edge-triplet.*

We finally perform an order-of-magnitude analysis of μ by comparing the ratio μ/l^2 with σ_i, where l is $\mathcal{B}$'s characteristic dimension. First degenerate edge-triplets are excluded in which the three edges are almost parallel to each other. Typical edge-triplets are non-degenerate, and inspection of the matrix K_{11} reveals that its eigenvalues σ_1 and σ_2 are of the same order of magnitude as the stiffness coefficients $k_j = f_j'(\delta_j(q_0))$. This condition can be written as $\sigma_i \sim k_j$. According to (5.10), $\mu/l^2 = f_T(2a\zeta + r)/l^2$, where $f_T \sim k_j \delta_j(q_0)$. Thus, $(\mu/l^2)/\sigma_i \sim \mu/k_j l^2 \sim \delta_j(q_0)(2a\zeta + r)/l^2$. Since $\zeta \leqslant 1/4$, $a/l \sim 1$ and $\delta_j(q_0)/l \ll 1$, we have $(\mu/l^2)/\sigma_i \sim \delta_j(q_0)/l \ll 1$. Therefore,

$$\frac{\mu}{l^2} \ll \sigma_i. \tag{5.11}$$

This relationship is true for a *general* contact model, and will be useful in com-

[3] ζ is negative in expansive fixtures where the fingers push away from the concurrency point.

puting the stiffness and deflection quality measures for three-finger fixtures.

5.4.2 Four-Finger Stable Equilibrium Fixtures

Having characterized three-finger fixtures, four-finger fixtures of polygons will now be considered. Since a four-finger fixture of a polygonal object involves three or four edges, we can consider all four-finger placements on triplets and quadruplets of edges. The following parametrization of four-finger fixtures on a particular edge combination will prove convenient to be used in optimization algorithms. Let O be the origin of $\mathcal{F}_B$ and let e_i be the edge containing the i^{th} contact. Then the i^{th} contact is parametrized by the signed distance, denoted s_i, from O to the line containing the i^{th} contact normal. In other words, s_i is the moment of the unit normal N_i, specified in a body frame $\mathcal{F}_B$, with respect to O. A point $s = (s_1, s_2, s_3, s_4)$ specifies a particular placement of four fingers, and the collection of all four-finger fixtures on a given edge combination is a *bounded convex polytope*, denoted $\mathcal{P}$, in $\mathbb{R}^4$.

If a fixture in $\mathcal{P}$ is an equilibrium fixture, its stiffness matrix can be computed from Formula (4.13), which is expressed in terms of body coordinates in Appendix B.1. Depending on whether the first-order term in the stiffness matrix is positive definite, the fixture may be first- or second-order stable. It can be shown that for a polygon fixtured by four disc fingers, the second-order effects are small compared with the first-order effects. This implies that the optimal fixture is expected to be first-order stable. Thus, optimal fixture planning can focus on the set of first-order stable fixtures in $\mathcal{P}$. This subset of $\mathcal{P}$ is characterized in the following lemma, which is proved in Appendix B.2.2. In the lemma, $h_i = (N_i, s_i)$ is the wrench generated by N_i, which can be interpreted as a unit force, and $d_i(s) = \det([h_{i+1}, h_{i+2}, h_{i+3}]) \pmod 4$.

Lemma 5.4.2. *An arrangement $s \in \mathcal{P}$ of four fingers on a polygon $\mathcal{B}$ forms a first-order stable equilibrium fixture if and only if $d_1(s)$, $-d_2(s)$, $d_3(s)$ and*

$-d_4(s)$ are all nonzero and have the same sign. To the first order, the stiffness matrix in this case approximately takes the form

$$K = \begin{pmatrix} \sum_{i=1}^{4} k_i N_i N_i^T & \sum_{i=1}^{4} k_i s_i N_i \\ \sum_{i=1}^{4} k_i s_i N_i^T & \sum_{i=1}^{4} k_i s_i^2 \end{pmatrix}, \tag{5.12}$$

where N_i is the inward unit normal at the i^{th} contact, $k_i = f_i'(\delta_i(q_0))$, and the function f_i represents a general (linear or nonlinear) contact model.

The lemma implies that the collection of (first-order) stable equilibrium fixtures is the union $\mathcal{D} = \mathcal{D}_1 \cup \mathcal{D}_2$, where

$$\mathcal{D}_1 = \mathcal{P} \cap \left\{ s \in \mathbb{R}^4 : \; d_1(s), -d_2(s), d_3(s), -d_4(s) < 0 \right\}, \tag{5.13}$$

$$\mathcal{D}_2 = \mathcal{P} \cap \left\{ s \in \mathbb{R}^4 : \; d_1(s), -d_2(s), d_3(s), -d_4(s) > 0 \right\}. \tag{5.14}$$

We observe that each function d_i is linear in s. Hence, each $\mathcal{D}_i$ is a *bounded convex polytope* in $\mathbb{R}^4$. For a given edge combination we may separately search the convex polytopes $\mathcal{D}_1$ and $\mathcal{D}_2$ for the optimal finger arrangement.

Finally, consider the computation of the principal stiffnesses. By definition, the translational stiffnesses σ_i are the eigenvalues of the submatrix $K_{11} = \sum_{i=1}^{4} k_i s_i N_i^T$, where K_{11} has been computed from (5.12). The rotational stiffness is given by $\mu = K_{22} - K_{12}^T K_{11}^{-1} K_{12}$. Substitution of the submatrices K_{ij} given in (5.12) yields

$$\mu(s) = \sum_{i=1}^{4} k_i s_i^2 - \Big(\sum_{i=1}^{4} k_i s_i N_i^T\Big)\Big(\sum_{i=1}^{4} k_i N_i N_i^T\Big)^{-1} \sum_{i=1}^{4} k_i s_i N_i. \tag{5.15}$$

Unlike the case of three-finger fixtures, μ, along with σ_i for a four-finger fixture

is a complex function of s when a nonlinear contact model is used. This is because in that case $k_i = f_i'(\delta_i(q_0))$ will generally depend on s. To simplify the optimization problems to follow, we will assume, for four-finger fixtures of polygons employing a given edge combination, each contact is represented via a compliance function that is linear in the overlap: $f_i(\delta_i) = k_i\delta_i$, where each elasticity constant k_i is constant on a given edge. Under this assumption, the translational stiffness parameters σ_i become constants for all stable equilibrium fixtures on the given edge combination. In the mean time, it can be shown that $\mu(s)$ is a *non-negative* quadratic function of s. That is, the quadratic part of $\mu(s)$ is positive semidefinite.

5.5 Maximum-Stiffness Fixtures of Polygons

Having properly characterized three- and four-finger stable equilibrium fixtures, we are now in a position to consider maximum-stiffness fixtures, i.e., fixtures that maximize the stiffness quality measure. While our optimization procedure is based on overlap-based compliance computation, it is important to note that the stiffness quality measure is valid with stiffness matrices computed from general contact models, which may or may not take into consideration friction effects and possibly non-local deformations.

5.5.1 Maximum-Stiffness Three-Finger Fixtures

As characterized in 5.4.1, three-finger equilibrium fixtures on a give admissible triplet of edges of a polygonal object can be parametrized by the concurrency point of the contact normals. Moreover, when the total preload f_T is specified, the rotational stiffness μ is a constant regardless of the position of the concurrency point. According to (5.11), $\mu/l^2 \ll \sigma_i$ for a non-degenerate edge-triplet.

Since $\rho_{\max}/l \sim 1$, the equivalent stiffness μ_{eq} as defined in (5.7) satisfies

$$\mu_{eq} = \frac{\mu}{\rho_{\max}^2} = (\frac{\mu}{l^2})(\frac{\rho_{\max}}{l})^2 \ll \sigma_i.$$

It follows that $\min\{\sigma_1, \sigma_2, \mu_{eq}\} = \mu_{eq}$, and therefore

$$Q_{stiff} = f_T \frac{2a\zeta + r}{\rho_{\max}^2}. \tag{5.16}$$

The quality measured is dominated by the equivalent rotational stiffness in the case of three-fingered fixtures because such fixtures are highly "translationally" stiff about the concurrency point.

In (5.16), the numerator is constant for a given admissible edge-triplet. Hence Q_{stiff} is maximized when $\rho_{\max}^2$ is minimized. It is important to note that this observation holds for *general* contact models since formula (5.16) is based on general contact models. This observation also agrees with intuition, since the fixture with the smallest $\rho_{\max}$ generates the smallest deflection of $\mathcal{B}$ due to a unit torque, which means that the fixture has the largest equivalent rotational stiffness about the concurrency point. To compute the fixture which minimizes $\rho_{\max}^2$ on a given edge-triplet, we parametrize the equilibrium fixtures on the edge-triplet by the coordinates of the concurrency point, denoted p. The domain of p is a convex polygonal region S as shown in Figure 5.3. Thus for each $p \in S$ there exist finger placements such that p is the concurrency point of the contact normals. Let $\rho_{\max}(p)$ be the distance from p to the farthest vertex of $\mathcal{B}$. Then $\rho_{\max}^2(p) = \max\{\|v_i - p\|^2\}$ over the vertices $v_1, ..., v_n$ of $\mathcal{B}$. It can be verified the $\rho_{\max}^2(p)$ is a convex function. Since the region S is convex, the minimization of $\rho_{\max}^2(p)$ over S is a standard *convex minimization* problem, which can be solved by efficient ϵ-approximate algorithms in $O(n \log \epsilon)$ steps

[112].

Example 5.5.1. When $\mathcal{B}$ is a triangular object, the minimizer of $\rho^2_{\max}$ over S, and hence the maximum-stiffness fixture, can be determined graphically. First find the smallest disc which contains the triangle. Let p_0 denote the center of this disc. As shown in Figure 5.4(a), if the region S contains the point p_0, then the optimal concurrency point is at p_0. Otherwise, p_0 lies outside S. It can be shown that in this case $\mathcal{B}$ is necessarily an obtuse triangle, and p_0 is at the midpoint of the triangle's longest edge. The region S is a parallelogram determined by the other two edges, and the optimal concurrency point is at the center of the smallest disc which contains $\mathcal{B}$, such that the disc's center lies in S. It can be shown that this is the point where the half-line which starts at p_0 along the perpendicular bisector of the longest edge first intersects the region S. This scenario is shown in Figure 5.4(b).

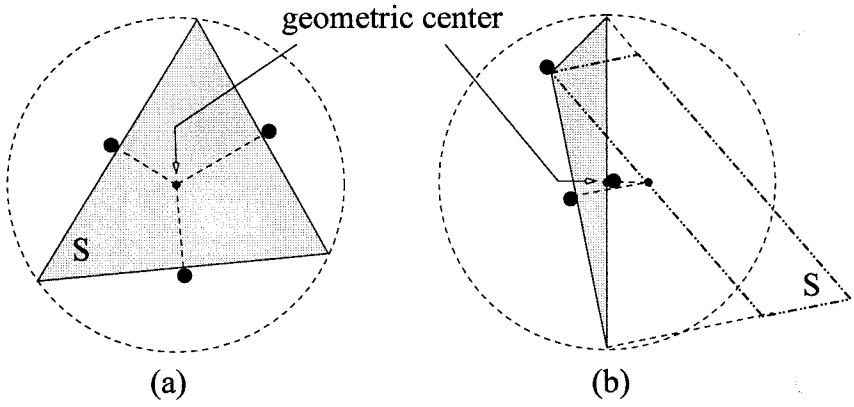

Figure 5.4: Maximum-stiffness three-finger fixtures of two triangular objects, in which the geometric center lies (a) inside S and (b) outside S.

To compute the globally maximum-stiffness fixture, we have to evaluate (5.16) on the admissible edge-triplets of $\mathcal{B}$. Inspection of (5.16) reveals the following characteristics of the globally optimal fixture. In (5.16), while the total preload f_T is taken to be the same for all edge triplets, the quantities a and ζ are *different* for different edge triplets. Therefore, whether the

maximum-stiffness fixture on a given edge-triplet is the global optimum over all edge-triplets depends on the distance $\rho_{\max}$, as well as the *shape* (characterized by ζ) and the *size* (characterized by a) of the triangle determined by the given edge triplet. For the quality measure to assume a large value, $\rho_{\max}$ is preferred to be *small*, while a and ζ are preferred to be *large*. A large value of a generally means that the fingers *spread apart* in the fixture. It can be verified that the shape parameter ζ is bounded by $\zeta \leqslant 1/4$, with equality holding for an equilateral triangle. Thus, the edges in the triplet are preferred to be *oriented evenly*. In the ideal case, the edges form an equilateral. It is important to note that the parameters $\rho_{\max}$, a, and ζ *combine* to determine the fixture quality; a single parameter alone is *not* sufficient for this purpose. These observations will be illustrated in two examples. In the examples, the limiting case of zero finger radii is assumed for simplicity. Further, the center of the smallest disc containing $\mathcal{B}$ is called the *geometric center* of $\mathcal{B}$, and the radius of the disc is called the *radius* ρ_0 of $\mathcal{B}$.

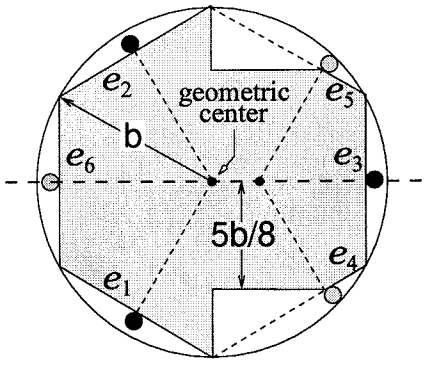

Figure 5.5: Maximum-stiffness three-finger fixtures of an polygon.

Example 5.5.2. Consider the maximum-stiffness three-finger fixturing of the polygonal object whose convex hull is a regular hexagon. The geometric center and radius of the polygon are given by the center and radius of the hexagon's circumscribing circle. Hence, $\rho_0 = b$. We consider two edge-triplets (e_1, e_2, e_3) and (e_4, e_5, e_6). These two edge combinations determine two congruent tri-

angles, for which the combined effect on Q_{stiff} of shape and size is given by $a\zeta = \frac{\sqrt{3}}{4}b$. The optimal concurrency point of the triplet (e_1, e_2, e_3) coincides with the geometric center. Thus, $\rho_{\max} = \rho_0$ and $Q_{stiff} = \frac{\sqrt{3}}{2}(\frac{f_T}{b})$ for this fixture. On the other hand, the optimal concurrency point of (e_3, e_4, e_5) lies on the line of symmetry of $\mathcal{B}$, at a distance $\frac{\sqrt{3}}{6}b$ from the geometry center. For this finger arrangement, it can be shown that $\rho^2_{\max} = \frac{19}{12}b^2$ and $Q_{stiff} = \frac{6\sqrt{3}}{19}(\frac{f_T}{b})$. We see that while the triangles associated with the two edge-triplets have the same shape and size, the different distance of the optimal concurrency point from the farthest vertices of $\mathcal{B}$ lead to different quality measure values. Consequently, the optimal fixture on (e_1, e_2, e_3) is better than the optimal fixture on (e_4, e_5, e_6).

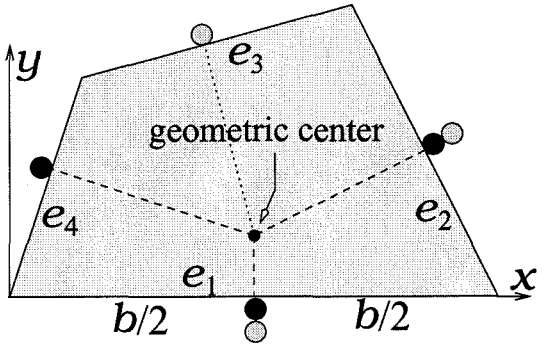

Figure 5.6: Maximum-stiffness three-finger fixtures of a quadrilateral.

Example 5.5.3. Consider the maximum-stiffness three-finger fixture of the quadrilateral shown in Figure 5.6. The vertices of the quadrilateral have coordinates $(0, 0)$, $(b, 0)$, $(0.7b, 0.6b)$ and $(0.15b, 0.45b)$ with respect to the frame shown in the figure. The radius of the quadrilateral is $\rho_0 = 0.5154b$, and the geometric center is located at $(0.5b, 0.125b)$. For the admissible edge-triplets (e_1, e_2, e_3) and (e_1, e_2, e_4), the maximum-stiffness finger locations are shown in the figure. The concurrency points of these fixtures both coincide with the geometric center. However, the combined effect of shape and size is $a\zeta = 0.1376b$ for (e_1, e_2, e_3), and $a\zeta = 0.1664b$ for (e_1, e_2, e_4). Consequently,

these fixtures have different quality measure values. For the maximum-stiffness fixture on (e_1, e_2, e_3) we have $Q_{stiff} = 1.0359 f_T/b$, while for the optimal fixture on (e_1, e_2, e_4) we have $Q_{stiff} = 1.2526 f_T/b$. The optimal finger arrangement on (e_1, e_2, e_4) gives the global maximum-stiffness fixture of this object.

5.5.2 Formulating the Maximum-Stiffness Four-Finger Fixture Problem

We now turn to maximum-stiffness four-finger fixtures of polygons. The optimization problem is formulated in this section, which is followed by a technique for solving the optimization problem and then by several examples.

In considering maximum-stiffness four-finger fixtures, $k_i = \text{const}$ is assumed, while stiffness parameters σ_i and μ are parametrized in Section 5.4.2. Therefore, for a particular edge combination, σ_i are constant regardless of the contact parameters s_i, while $\mu(s)$ is a non-negative quadratic function. To compute the stiffness quality measure, we also need a formula for the equivalent stiffness $\mu_{eq} = \mu/\rho^2_{\max}$, where $\rho_{\max}$ is the distance from the fixture's center of compliance to the farthest vertex of $\mathcal{B}$. Let p denote the fixture's center of compliance. Then according to (5.6), $p = JK_{11}^{-1}K_{12}$. Substituting for K_{ij} given by Lemma 5.4.2 yields:

$$p(s) = J(\sum_{i=1}^{4} k_i N_i N_i^T)^{-1} \sum_{i=1}^{4} k_i s_i N_i,$$

which is *linear in* s. Now, $\rho^2_{\max}(p(s)) = \max\{\|v_i - p(s)\|^2\}$ where $v_1, ..., v_n$ are the vertices of $\mathcal{B}$'s convex hull. Since $p(s)$ is linear in s, $\rho^2_{\max}(p(s))$ is the maximum of n *positive definite quadratic functions* in s. The maximum value

of the quality measure Q_{stiff} is given on a particular edge combination by

$$Q_{stiff} = \min\left\{\sigma_1, \sigma_2, \max_{s\in\mathcal{D}_1\cup\mathcal{D}_2}\{\frac{\mu(s)}{\rho^2_{\max}(p(s))}\}\right\},$$

where $\mathcal{D}_1$ and $\mathcal{D}_2$ are given by (5.13) and (5.14), respectively.

Before presenting an optimization procedure, we mention some characteristics of the maximum-stiffness four-finger fixture on a given edge combination. First, $\sigma_{\min} = \min\{\sigma_1, \sigma_2\}$ is constant on a given edge combination, and the formula $Q_{stiff} = \min\{\sigma_1, \sigma_2, \mu_{eq}\}$ indicates that $Q_{stiff} \leqslant \sigma_{\min}$ on a given edge combination. Hence, if in the course of maximizing $\mu_{eq}(s)$ some s^* is found such that $\mu_{eq}(s^*) \geqslant \sigma_{\min}$, this s^* is necessarily the optimal finger arrangement on the given edge combination. Second, $\sigma_{\min}$ is the smallest eigenvalue of the matrix $K_{11} = \sum_{i=1}^4 k_i N_i N_i^T$. Hence $Q_{stiff} \leqslant \sigma_{\min} \leqslant \frac{1}{2}\operatorname{tr}(\sum_{i=1}^4 k_i N_i N_i^T) = \frac{1}{2}\sum_{i=1}^4 k_i$, where $\operatorname{tr}(\cdot)$ is the trace operator. To improve this bound, the contact normals N_i are preferred to be *evenly oriented.* In particular, if the material constants are uniform with $k_i = k$, then $\sigma_{\min} \leqslant 2k$, and equality holds when the contact normals are 90° apart, namely, the edge combination forms a rectangle. Next we discuss the parameters that influence $\mu_{eq}(s)$. Since $\mu_{eq}(s) = \mu(s)/\rho^2_{\max}(p(s))$, the parameter $\rho_{\max}$ is desired to be *small* while μ is preferred to be *large.* But μ is the fixture's rotational stiffness about the center of compliance, and is given by $\mu = \sum_{i=1}^4 k_i \bar{s}_i^2$, where $\bar{s}_i$ is the i^{th} contact's moment about the center of compliance. Thus, for μ to assume a large value, each $|\bar{s}_i|$ is desired to be large. This indicates that the fingers should *spread apart* as much as possible with respect to the center of compliance. To summarize, for a fixture to have good stiffness quality, it is preferred that the edges be evenly oriented to make $\sigma_{\min}$ large; that the fingers spread apart with respect to the center of compliance to make μ large; and that the distance from the fixture's center of compliance to $\mathcal{B}$' farthest vertex be small to make $\rho_{\max}$

small. These parameters *combine* to determine the maximum-stiffness fixture.

5.5.3 Computation of Global Maximum-Stiffness Four-Finger Fixtures

Section 5.5.2 formulated the problem of optimal four-finger fixturing of a polygonal object in terms of a collection of subproblems in which $\mu_{eq}(s) = \frac{\mu(s)}{f(s)}$ is maximized over $\mathcal{D}$, where μ and f are positive semidefinite quadratic functions with $f(s) > 0$ whenever $s \in \mathcal{D}$, and the domain $\mathcal{D}$ is a convex polyhedral subset of $\mathbb{R}^4$.

We are interested in finding the global maximum of $\mu_{eq}(s)$ over $\mathcal{D}$. While μ_{eq} is a nonconvex and strongly nonlinear function whose global maximum may in general be very difficult to find, there is a technique that guarantees to find the global optimum. The technique is presented as follows, and is proved in Appendix B.3. Define a scalar function $\psi\colon \mathbb{R} \to \mathbb{R}$ by

$$\psi(t) = \max_{s \in \mathcal{P}} \phi(t, s),$$

where $\phi(t, s) = \mu(s) - tf(s)$. The following lemma indicates that the maximization of $\mu_{eq}(s)$ over $\mathcal{D}$ is equivalent to the computation of the unique zero of this scalar function.

Proposition 5.5.1. *The scalar function $\psi(t)$ is strictly monotonic decreasing and has a unique positive zero. In addition, maximizing $\mu_{eq}(s)$ over $\mathcal{D}$ is equivalent to finding the zero of ψ in the following sense. A positive number $t^* > 0$ satisfies $\psi(t^*) = 0$ if and only if $t^* = \max_{s \in \mathcal{D}} \mu_{eq}(s)$. In this case, a contact configuration $s^* \in \mathcal{D}$ maximizes $\phi(t^*, s)$, regarded as a function of s, over $\mathcal{D}$ if and only if it maximizes $\mu_{eq}(s)$ over $\mathcal{D}$.*

It follows from this proposition that the maximization of $\mu_{eq}(s)$ over $\mathcal{D}$

is equivalent to solving for the unique root of the scalar equation $\psi(t) = 0$. Note that to evaluate ψ at some t, we need to maximize a quadratic function of s, which is in general *indefinite*, i.e., the matrix associated with the quadratic term in this function has positive *and* negative eigenvalues. Indefinite quadratic programming (IQP) is unfortunately NP-hard, and the known algorithms are exponential in the number of variables. For example, References [44, 163] describe an indefinite quadratic minimization algorithm which takes $O(l(\frac{m(m+1)}{\sqrt{\epsilon}})^p)$ steps, where m is the number of variables and p the number of negative eigenvalues of the quadratic objective function. In this bound, l is the time it takes to solve a convex quadratic optimization problem of the same size, which is $O(n \log \epsilon)$ where n is the number of linear constraints in the polytope $\mathcal{D}$. Since in our case $m = 4$ and $p \leqslant 4$, the number of steps is linear in the number of constraints, with a somewhat large constant determined by the dimension $m = 4$. Thus, given m being small, our approach provides a practical procedure which *guarantees* to find the *global optimum* at a reasonable computational cost despite the strongly nonlinear and nonconvex nature of the stiffness quality measure.

5.5.4 Examples of Maximum-Stiffness Four-Finger Fixtures

In the following examples point fingers with uniform elasticity constants $k_i = k$ are assumed for simplicity.

Example 5.5.4. Figure 5.7 shows a rectangular object $\mathcal{B}$ of size $2a \times 2b$. When $\mathcal{B}$ is fixtured by four fingers, each finger must contact a different edge of $\mathcal{B}$. The contact normals are 90° apart, and $\sigma_{\min}$ achieves its upper bound: $\sigma_{\min} = 2k$ for all finger arrangements. Now consider the equivalent rotational stiffness, $\mu_{eq} = \mu/\rho^2_{\max}$. Given any equilibrium fixture of $\mathcal{B}$, the lines of the contact

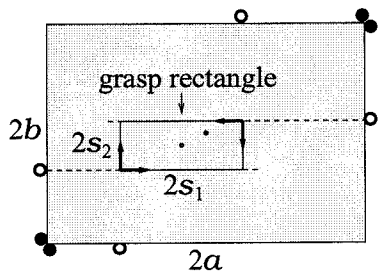

Figure 5.7: Four-finger fixtures of a rectangular object, with the maximum-stiffness fixture shown in solid circles.

normals form a rectangle, which is called the *fixture rectangle* to distinguish it from the rectangular object. It can be verified that the fixture's center of compliance is located at the center of the fixture rectangle [114]. Moreover, the rotational stiffness is given by $\mu = 2k(\bar{s}_1^2 + \bar{s}_2^2)$, where $\bar{s}_1$ and $\bar{s}_2$ are the half-length and half-width of the fixture rectangle. Clearly, when the fingers are placed at the ends of the object's edges with $\bar{s}_1 = a$ and $\bar{s}_2 = b$ as shown in the figure, μ achieves its maximum value: $\mu = 2k(a^2 + b^2)$. Indeed, this fixture obeys the rule that the fingers should spread apart with respect to the center of compliance. Also, the center of compliance for this fixture coincides with $\mathcal{B}$'s center of symmetry, and the distance from the center of compliance to $\mathcal{B}$'s farthest vertex is minimized: $\rho_{\max} = \sqrt{a^2 + b^2}$. This indicates that the same finger placement also maximizes the equivalent rotational stiffness: $\mu_{eq} = \mu/\rho_{\max}^2 = 2k$. It follows that the finger arrangement shown with solid circles is the globally optimal fixture, with maximal value of $Q_{stiff} = 2k$.

Example 5.5.5. Figure 5.8 shows an isosceles triangle whose base edge is of length $2b$ and whose legs form an angle 2α. We focus on the placement of two fingers on the base edge (called *base fingers*), and one finger on each side edge (called *side fingers*). Using Lemma 5.4.2, $\sigma_{\min} = 2k\cos\alpha^2$, which is constant for all the equilibrium fixtures on this edge combination. We now discuss the maximization of $\mu_{eq} = \mu/\rho_{\max}^2$. It can be shown that for any placement of a base finger at an interior point of the base edge, there exists an alternative

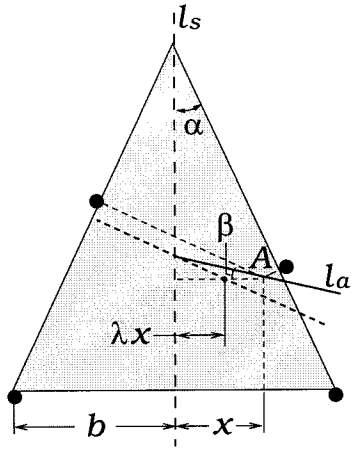

Figure 5.8: Four-finger fixtures of an isosceles triangle.

placement of a higher μ_{eq} value, such that both base fingers are located at the base's endpoints. Thus we may restrict our attention to finger arrangements where the base fingers are at the endpoints of the base edge.

Let A be the intersection point of the side fingers' force lines. By symmetry, we need only consider finger arrangements in which the point A lies in the right half-plane bounded by the line of symmetry ℓ_s (Figure 5.8). Let x denote the distance between A and ℓ_s. With the stiffness matrix computed from Lemma 5.4.2, it can be shown that $\mu/k = 2a^2 + 2x^2 \sin^2\alpha/(1+\sin^2\alpha)$, and that the center of compliance is located on the same horizontal line as the point A, at a distance $x\sin^2\alpha/(1+\sin^2\alpha)$ from ℓ_s (Figure 5.8). Now consider a *fixed* value of x, i.e., the side fingers move in a way such that the point A, along with the center of compliance, is at a fixed distance to the line ℓ_s. Then μ_{eq} is maximized as the center of compliance moves onto the bisector of the left side edge, since with μ a constant, this minimizes $\rho_{\max}$ for the given x. Thus, we can focus on the following one-parameter family of fixtures: the intersection A lies on the ray ℓ_a, which originates from the center of the triangle's circumscribing circle and is oriented relative to the base edge at an angle $\beta = \tan^{-1}(\frac{\sin^2\alpha\tan\alpha}{1+\sin^2\alpha})$ (Figure 5.8). As x increases, $\mu(x)$ and $\rho_{\max}(x)$, both increasing, compete to

determine the variation of $\mu_{eq}(x) = \mu(x)/\rho^2_{\max}(x)$. It can be shown that when $\alpha \leqslant 27.5°$, $\mu_{eq}(x)$ is maximized at $x = 0$ with $\mu_{eq}(0) = 2k\sin^2 2\alpha$; otherwise, $\mu_{eq}(x)$ is maximized at $x = b$. The fixture given by $x = 0$ is intuitively good: the leg fingers are symmetric and the corresponding contact normals intersect at the center of the circumscribing circle. The fixture with $x = b$ is discarded because it does not form an equilibrium fixture[4]. While μ_{eq} is not maximized at $x = 0$ when $\alpha < 27.5°$, it can be shown that $\mu_{eq}(0)/\mu_{eq}(b) \geqslant 0.95$ for all $0° < \alpha < 90°$. Hence, the intuitively good fixture given by $x = 0$ precisely or approximately maximizes μ_{eq} for all values of α. To summarize, since $\mu_{eq}(0) = 2k\sin^2 2\alpha \geqslant \sigma_{\min}$ as $\alpha \geqslant 30°$, the intuitive fixture with $x = 0$ is optimal as $\alpha \geqslant 27.5°$, with $Q_{stiff} = 2k\cos^2\alpha$ for $\alpha \geqslant 30°$ and $Q_{stiff} = 2k\sin^2 2\alpha$ for $27.5° \leqslant \alpha \leqslant 30°$. The fixture with $x = 0$ is approximately optimal with $Q_{stiff} = 2k\sin^2 2\alpha$ when $\alpha < 27.5°$.

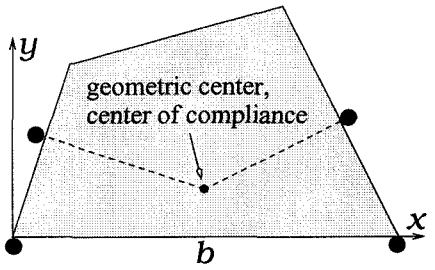

Figure 5.9: Global maximum-stiffness fixture of a quadrilateral.

Example 5.5.6. In the previous examples, the symmetry of the objects allowed analytical analysis of the optimal finger arrangement. For a general polygonal object it is necessary to use the numerical procedure outlined in Proposition 5.5.1. This example considers the maximum-stiffness four-finger fixturing of the quadrilateral used in Example 5.5.3 for the three-finger case. Recall that the vertices of this quadrilateral have coordinates $(0, 0)$, $(b, 0)$,

[4]Note that the positivity of the principal stiffness quality measure does *not* imply that the fixture is in equilibrium, since the positive definiteness of the stiffness matrix can be formally computed even for a non-equilibrium fixture and may still be positive definite.

$(0.7b, 0.6b)$ and $(0.15b, 0.45b)$, and that the geometric center has coordinates $(0.5b, 0.125b)$. By considering all feasible edge combinations we can find the maximum-stiffness fixture associated with each combination, and further determine the globally optimal fixture, which is shown in Figure 5.9. For this fixture, $\sigma_{\min} = 1.684k$ and $\mu_{eq} = 1.882k$, hence $Q_{stiff} = 1.684k$. In addition, the center of compliance of this fixture coincides with the geometric center of the object. Therefore, the optimal finger arrangement maximizes μ_{eq} by minimizing $\rho_{\max}$, and by spreading apart the two fingers on the base edge to allow μ to assume a large value.

Summary:

This chapter described the principal translational and rotational stiffnesses of compliant fixtures and grasps, and used them to define the frame-invariant stiffness quality measure. The quality measure is defined as the smallest of these parameters, where the rotational stiffnesses are made comparable with the translational stiffnesses based on the equivalence of elastic energy and the fixtured object's maximal displacement. This quality measure applies to both two- and three-dimensional compliant fixtures modelled by general compliance models and employing any number of fingers. The stiffness quality measure was applied to maximum-stiffness fixtures of polygonal objects by three and four fingers. In each case the qualitative properties of the optimal fixture were characterized, and efficient algorithms were developed for graphically or numerically finding the optimal fixture. The examples of maximum-stiffness fixtures were intuitively effective, which indicates that the quality measure is potentially useful in practical applications. While the stiffness quality measure uses the object's maximal displacement to scale the principal rotational stiffnesses, it does not directly assess the object's deflection. Such assessment may be desirable in practice since workpiece deflections often have a direct impact on manufacturing tolerances. The deflection quality measure addresses this

issue and will be discussed in the next chapter.

Chapter 6

Minimum-Deflection Fixtures and Grasps

6.1 Introduction

In the stiffness quality measure, the maximal displacement of a fixtured object was used for the comparison of rotational and translational stiffnesses. However, the stiffness quality measure does not directly characterize the object's deflection in response to work loads. This chapter addresses the evaluation of fixture effectiveness *directly* based on object deflections. This consideration has strong practical relevance, since it has been theoretically (Shawki and Abdel-aal [145]) and experimentally (Hockenberger De Meter [56, 57]) shown that workpiece deflections are a major source of geometric error in machining operations, and that proper choice of fixel geometry and layout can significantly reduce such deflections.

Menassa and DeVries [103], and Pong, Barton, Cohen [129] considered optimal fixturing by minimizing workpiece deformations computed from three-dimensional finite element analysis. This approach offers excellent accuracy, but is very time-consuming and expensive. More efficient methods for minimum-deflection fixture planning are therefore preferred, especially in early planning

stages when workpiece designs and process plans are frequently modified. To address this need, a fixture quality measure is defined that characterizes deflections of quasi-rigid workpieces.

The *deflection quality measure* is defined as the *norm* of the object's worst-case displacement due to an external wrench lying in a subset of wrench space, called *task wrench set*, which models a set of manufacturing operations. While it is natural to use the notion of norms to characterize the magnitude of instantaneous rigid body velocities and wrenches, the Euclidean velocity and wrench norms that have been traditionally used vary with choices of reference frames. Quality measures that are based on Euclidean norms are frame-dependent and therefore lead to inconsistency in identifying optimal fixtures. We have developed frame-invariant, physically meaningful velocity and wrench norms based on the notion of objectivity (Chapter 7). Some of these norms are used in this chapter, and will be discussed in more detail in Chapter 8.

Two types of task wrench sets will be considered. The first type is relevant to fixturing applications where external wrenches can be applied in all directions at various magnitudes. In this case, the task wrench set is given in terms of the *unit wrench ball*, which consists of wrenches whose norms are less than or equal to unity. Kirkpatrick, Mishra and Yap [79], Ferrari and Canny [41], and Teichmann [151] have used wrench norms to define quality measures for rigid grasps. However, the Euclidean wrench norm used in these works depend on reference frame location, whereas we use *frame-invariant* wrench and rigid body velocity norms. The deflection quality measure defined with respect to the unit wrench ball can be easily computed, and will be applied to *minimum-deflection* three- and four-finger fixtures of polygonal objects.

Task wrench sets of the second type are those that model specific manufacturing operations. Since fixtures are often designed for specific manufacturing operations, work loads that arise from these operations are well-specified. In

this case, the task wrench sets should model specific manufacturing operations in an accurate and efficient manner. The deflection quality measure becomes *task-dependent* when applied to such task wrench sets. Task-dependent quantification of fixture effectiveness has been relatively scarce. Brost and Peters [16] proposed a quality criterion that is based on the fixels' maximal reaction force with respect to specified tasks. Li and Sastry [89] considered a task-dependent approach to robotic grasping. Modelling tasks by ellipsoids in the wrench space, they defined a quality measure which is the radius of the largest task ellipsoid that can be embedded in the set of wrenches resistible by finger forces up to a given magnitude. While their approach is geometrically interesting and may be appropriate in certain grasping applications, wrenches that arise from practical manufacturing operations such as metal cutting generally do not form an ellipsoidal set.

A scheme will be developed for modelling task wrench sets for manufacturing operations. A collection of *primitive task wrench sets* will first be proposed, which can be used to model such basic machining operations as drilling and milling. These primitives are then used as building blocks to model more complex manufacturing operations. This approach offers an accurate and efficient means to task-dependent minimum-deflection fixturing. In particular, efficient computation can be performed, without exhaustive consideration of sample points resulting from discretization techniques, for cutting forces that move along a family of continuous paths and vary in a range of directions.

6.2 The Deflection Quality Measure

While the stiffness quality measure uses the maximal displacement of a fixtured object for comparing rotational and translational stiffnesses, the deflection quality measure defined in this section directly assesses the object's deflection.

We first introduce several velocity and wrench norms and pseudo-norms.

6.2.1 Velocity and Wrench Norms and Pseudo-Norms

Characterization of deflections of quasi-rigid bodies entails the use of norms or pseudo-norms of rigid body velocities and wrenches. While such notions will be considered in a fundamental and systematic manner in Chapters 7 and 8, for the sake of deflection characterization we introduce a few specific norms and pseudo-norms that are frame-invariant and have interesting physical interpretations.

Norms or pseudo-norms formalize the notion of *length*, or *magnitude* of vectors in a vector space. A *pseudo-norm* on a vector space V is a real-valued function on V that is non-negative, homogeneous and satisfies the triangle inequality. A *norm* is a positive definite pseudo-norm. While widely used, the Euclidean norms of velocities and wrenches, defined by $\|\dot{q}\| = (\dot{q}^T\dot{q})^{1/2}$ and $\|\boldsymbol{w}\| = (\boldsymbol{w}^T\boldsymbol{w})^{1/2}$, respectively, unfortunately depend on choices of reference frames. Since this drawback will inevitably lead to inconsistent results, we need to use velocity and wrench norms and pseudo-norms that are frame-invariant.

The RMS and Maximum Velocity Norms and Pseudo-Norms

Given a body velocity $\dot{q} = (v, \omega)$, define a real-valued function by

$$\|\dot{q}\|_{rms} = \Big(\int_{\mathcal{B}} \nu(r) |v + \omega \times r|^2 dV \Big)^{\frac{1}{2}}, \tag{6.1}$$

where $\mathcal{B}$ also denotes the region of $\mathbb{R}^3$ occupied by the object with respect to $\mathcal{F}_B$, r represents the location of points in $\mathcal{B}$, $\nu(r) \geqslant 0$ is a weighting function satisfying $\int_{\mathcal{B}} \nu(r) dV = 1$, and $|x| = (x^T x)^{1/2}$ for all $x \in \mathbb{R}^3$. As will be shown

in 8.4, $\|\dot{q}\|$ *is a frame-invariant pseudo-norm on the tangent space.* Since $|v + \omega \times r|$ is the velocity magnitude of the point r, $\|\dot{q}\|$ is the *root-mean-square*[1] *(rms)* of the velocities of $\mathcal{B}$'s points with respect to the weighting function $\nu(r)$. Therefore, $\|\dot{q}\|$ will be called the *rms velocity pseudo-norm.* For example, choose $\nu(r) = \sum_{i=1}^{n} \nu_i \delta(r - r_i)$, where r_i represent a collection of $\mathcal{B}$'s feature points that are important for manufacturing accuracy, $\nu_i > 0$ and $\sum_{i=1}^{k} \nu_i = 1$, and δ denotes the Dirac delta function. Then, the rms pseudo-norm gives the root-mean-square of the velocities of these feature points.

The rms velocity pseudo-norm can be computed from

$$\|\dot{q}\|_{rms} = (\dot{q}^T M \dot{q})^{\frac{1}{2}} \quad \text{where} \quad M = \int_{\mathcal{B}} \nu(r) \begin{pmatrix} I & -\widehat{r} \\ \widehat{r} & -\widehat{r}^2 \end{pmatrix} dV \tag{6.2}$$

is the *weighting matrix.* As will be shown in Chapter 8 (Section 8.4), when the weighting function ν satisfies a positive definiteness condition, $\|\dot{q}\|$ becomes a norm, which is called the *velocity rms-norm.*

The reason for which a pseudo-norm, rather than a norm, is in general allowed is that during the execution of manufacturing operations we may need to monitor the displacements of only a small number of points. For example, during a drilling operation we may be only interested in the displacement of the point at which a hole is to be drilled. In this case, certain displacements of $\mathcal{B}$ cause no displacement of the feature point, and are therefore unimportant to manufacturing accuracy. A pseudo-norm which filters out such displacements would then be justified.

Now consider a velocity pseudo-norm that gives the maximal displacement of a set of feature points. Given body velocity $\dot{q} = (v, \omega)$, the following is a *frame-invariant* pseudo-norm (see 8.4), called the *maximum velocity pseudo-*

[1]When $\nu(r)$ is the mass density of $\mathcal{B}$, $\|\dot{q}\|_{rms}^2$ is proportional to $\mathcal{B}$' kinetic energy. However, this interpretation will not be used in this chapter.

norm:

$$\|\dot{q}\|_{\max} = \max_{r \in \Omega_B} |v + \omega \times r|, \tag{6.3}$$

where $\Omega_B \subset \mathcal{B}$ is a set of feature points of the object. This pseudo-norm has an attractive physical interpretation: $\|\dot{q}\|_{\max}$ gives the *maximal velocity*, or *maximal instantaneous displacement*, of $\mathcal{B}$'s feature points as $\mathcal{B}$ has velocity $\dot{q}$. When Ω_B contains at least three non-collinear points, $\|\dot{q}\|_{\max}$ becomes a norm and will be called the *maximum velocity norm.*

The computation of the maximum velocity pseudo-norm is discussed in 8.4 for general objects, and is considered below for an object $\mathcal{B}$ where the convex hull of its feature-point set Ω_B is a polyhedron. Let I_V be an index set for the polyhedron's vertices. For a body velocity $\dot{q} = (v, \omega)$, the velocity of a vertex $i \in I_V$ with body coordinates r_i is $u_i = v - \widehat{r}_i \omega$. Hence, $|u_i|^2 = \dot{q}^T A_i \dot{q}$ where $A_i = [I_3 \ -\widehat{r}_i]^T [I_3 \ -\widehat{r}_i]$, and

$$\|\dot{q}\|^2_{\max} = \max_{i \in I_V} \dot{q}^T A_i \dot{q}. \tag{6.4}$$

In most applications, the displacements of the points in the fixtured object $\mathcal{B}$ are very small. Thus, a displacement of $\mathcal{B}$ can be approximated by a tangent vector $\dot{q}$. The pseudo-norm $\|\dot{q}\|$ then indicates the size, or length, of the displacement, and measures how far $\mathcal{B}$ is displaced from its original location. Motivated by this observation, we define $\|\dot{q}\|$ as the *deflection* of $\mathcal{B}$ corresponding to the displacement $\dot{q}$. In particular, $\|\dot{q}\|_{rms}$ is called the *rms-deflection*, and $\|\dot{q}\|_{\max}$ the *max-deflection* of $\mathcal{B}$.

The RMS Wrench Norm

We now introduce an interesting wrench norm which is discussed in 8.4 in more detail. Let the weighting function ν satisfy the positive definiteness condition of Definition 8.4.1. Then the weighting matrix M, as given by (6.2), is positive definite and $\|\dot{q}\|_{rms}$ becomes the rms velocity norm. A *frame-invariant* wrench norm, called the *wrench rms-norm*, can be induced from this velocity norm by

$$\|\boldsymbol{w}\|_{rms} = \sup\Big\{ \frac{|\boldsymbol{w}^T \dot{q}|}{\|\dot{q}\|_{rms}} : \ \dot{q} \in T_{q_0} SE(3) \Big\} = (\boldsymbol{w}^T M^{-1} \boldsymbol{w})^{1/2}. \tag{6.5}$$

The rms-norm of a body wrench $\boldsymbol{w} = (f, \tau)$ acting on $\mathcal{B}$ has the following physical interpretation that explains the name of the norm. Imagine that $\boldsymbol{w}$ is *generated* by a *distributed pure force*, denoted $\mathsf{f}(r)$ where $r \in \mathcal{B}$, with respect to the given weighting function ν. That is, $f = \int_{\mathcal{B}} \nu(r)\mathsf{f}(r)dV$ and $\tau = \int_{\mathcal{B}} \nu(r)\, r \times \mathsf{f}(r)dV$. Denote by $\mathcal{D}^2_{\boldsymbol{w}}$ the set of such distributed forces such that for each f in $\mathcal{D}^2_{\boldsymbol{w}}$, the integral $\int_{\mathcal{B}} \nu(r)|\mathsf{f}(r)|^2 dV$ is finite. Then

$$\|\boldsymbol{w}\|_{rms} = \inf\Big\{ \Big(\int_{\mathcal{B}} \nu(r)|\mathsf{f}(r)|^2 dV \Big)^{\frac{1}{2}} : \ \mathsf{f} \in \mathcal{D}^2_{\boldsymbol{w}} \Big\}.$$

Therefore, $\|\boldsymbol{w}\|_{rms}$ is, with respect to the weighting function ν, the *greatest lower bound for the root-mean-square of the magnitudes of distributed forces that generate* $\boldsymbol{w}$.

6.2.2 The Deflection Quality Measure

Based on frame-invariant velocity and wrench norms as well as the notion of object deflection, this section presents a frame-invariant fixture quality measure that characterizes the worst-case deflection of the object in response to work loads. Similar to the stiffness quality measure, we focus on *stable fixtures*

with positive definite stiffness matrices.

To consider the deflection of a candidate fixture of a workpiece $\mathcal{B}$, assume that the wrench acting on $\mathcal{B}$ belongs to a *compact* subset of the wrench space $T^*_{q_0}SE(3)$. This subset of the wrench space, denoted W, is called the *task wrench set* for the fixture. The forces generated by a given set of manufacturing operations, such as machining, assembly and inspection, can be modelled by a task wrench set. The assumption that task wrench sets are compact is justified since practical manufacturing forces always have *finite* magnitude. In the simplest case, task wrench sets can consist of only a small number of wrenches. For example, in a perfectly performed drilling operation, the task wrench set contains a single wrench consisting of a torque and a thrust force. However, task wrench sets are in general much more complex, and typically contain an infinite number of wrenches. Section 6.3 considers constructing task wrench sets in terms of building blocks that can be efficiently computed.

When a wrench $\boldsymbol{w} \in W$ is applied to a fixtured object $\mathcal{B}$, an infinitesimal displacement of $\mathcal{B}$ is generated according to the relationship $\dot{q} = C\boldsymbol{w}$, where $C = K^{-1}$ is the fixture's compliance matrix. The deflection corresponding to this displacement is $\|\dot{q}\|$, determined from a velocity pseudo-norm described above. The effectiveness of the fixture can be quantified by the following quality measure:

$$\Delta_W = \sup_{\boldsymbol{w} \in W} \|C\boldsymbol{w}\|. \tag{6.6}$$

This quality measure, called the *deflection quality measure*, characterizes the *worst-case deflection of the workpiece under the action of any wrench that lies in the given task wrench set.* Clearly, since deflections are desired to be small, a fixture that has a small value of Δ_W is considered effective.

Suppose that in a fixturing application a tolerance ϵ is given, i.e., the de-

flection of the object, when measured in terms of a velocity pseudo-norm $\|\cdot\|$, must not exceed ϵ. The deflection quality measure Δ_W has three interesting applications corresponding to this specified tolerance. First, if a set of manufacturing operations is modelled by a task wrench set W, then the quality measure can be used for *design verification*: the candidate fixture is valid if $\Delta_W \leqslant \epsilon$. Second, the quality measure can be used to determine the *load capacity* of a given fixture. Suppose that a set of manufacturing applications can be modelled as $W = \{\alpha \boldsymbol{w} : \boldsymbol{w} \in W_0,\ 0 \leqslant \alpha \leqslant \alpha_{\max}\}$, where W_0 is a nominal task wrench set and $\alpha_{\max}$ represents the load capacity. Then the tolerance requirement implies that

$$\alpha \sup_{\boldsymbol{w} \in W_0} \|C\boldsymbol{w}\| \leqslant \epsilon,$$

which determines the maximal capacity of work loads that can be safely applied to the fixture:

$$\alpha_{\max} = \frac{\epsilon}{\sup_{\boldsymbol{w} \in W_0} \|C\boldsymbol{w}\|}.$$

The third application of the quality measure is optimal fixturing. Suppose that a set of fixtures is parameterized by a vector $s \in \mathcal{P}$. Thus, the compliance matrix takes the parametrized form $C(s)$, and the optimal fixture can be found among the given set of candidates and verify its validity:

$$\min_{s \in \mathcal{P}} \sup_{\boldsymbol{w} \in W} \|C(s)\,\boldsymbol{w}\| \leqslant \epsilon.$$

The computation of the deflection quality measure for general task wrench sets will be discussed in 6.3. Here we consider the case where the task wrench

set is taken to be the *unit wrench ball*: $W = \{\boldsymbol{w} \in T^*_{q_0}SE(3) : |\!|\!|\boldsymbol{w}|\!|\!| \leqslant 1\}$, where $|\!|\!|\cdot|\!|\!|$ is a wrench norm. Assume that in (6.6) a velocity norm, rather than a pseudo-norm, is used. Then the deflection quality measure can be written as

$$\Delta_W = \sup\{\|C\boldsymbol{w}\| : \boldsymbol{w} \in T^*_{q_0}SE(3),\ |\!|\!|\boldsymbol{w}|\!|\!| \leqslant 1\} = \sup\left\{\frac{\|C\boldsymbol{w}\|}{|\!|\!|\boldsymbol{w}|\!|\!|} : \boldsymbol{w} \in T^*_{q_0}SE(3)\right\}.$$

Since $C = K^{-1}$ where K is the fixture stiffness matrix, using change of variables $\boldsymbol{w} = K\dot{q}$ in the above formula leads to $\Delta_W = 1/Q_{defl}$ where

$$Q_{defl} = \inf\{|\!|\!|K\dot{q}|\!|\!| :\ \dot{q} \in T_{q_0}SE(3),\ \|\dot{q}\| \leqslant 1\} = \inf\left\{\frac{|\!|\!|K\dot{q}|\!|\!|}{\|\dot{q}\|} : \dot{q} \in T_{q_0}SE(3)\right\} \tag{6.7}$$

Because of the simple relationship between Q_{defl} and Δ_W, Q_{defl} will also be called the *deflection quality measure*, as suggested by the notation. Clearly, an effective fixture is expected to have a large value of Q_{defl}. Provided that frame-invariant norms are used, they are both *frame-invariant.*

While Δ_W, with W taken to be the unit wrench ball, characterizes the worst-case deflection of the object under the action of wrenches lying in the unit wrench ball, Q_{defl} is the worst-case magnitude of the restoring wrench corresponding to all displacements lying in the unit displacement ball. However, it is important to note that the velocity and wrench balls are in general *not* Euclidean spheres in $\mathbb{R}^6$. Corresponding to frame-invariant norms, these balls are *frame-invariant* in the sense that regardless of choices of reference frames, the boundary points on these balls always have unit norm. This is to be distinguished from previous works (e.g., [41, 79, 151]) on quality measures for rigid grasps, where frame-dependent wrench balls were used.

In practice, one first computes the stiffness matrix K, and then obtains the compliance matrix C by inverting K. Therefore, when W is taken to be the unit wrench ball and deflections are computed in terms of a velocity norm, the deflection quality measure formulation (6.7), which defines Q_{defl} in terms of the unit velocity ball, is more convenient. In the remainder of this section we compute Q_{defl} using the velocity and wrench norms introduced in 6.2.1.

First consider the computation with the rms velocity and wrench norms, in which case Q_{defl} characterizes the worst-case rms-deflection of $\mathcal{B}$ over the rms-norm unit wrench ball. Denote the smallest eigenvalue of a symmetric matrix A by $\lambda_{\min}(A)$. From (6.2) and (6.5) we have $\|\dot{q}\|_{rms} = \dot{q}^T M \dot{q}$, and $\|K\dot{q}\|_{rms} = \dot{q}^T K M^{-1} K \dot{q}$. Letting $x = M^{1/2}\dot{q}$, we can rewrite (6.7) as

$$Q_{defl}^2 = \inf_{\dot{q}\in\mathbb{R}^6} \frac{(K\dot{q})^T M^{-1}(K\dot{q})}{\dot{q}^T M \dot{q}} = \inf_{x\in\mathbb{R}^6} \frac{x^T \widetilde{K}^2 x}{x^T x},$$

where $\widetilde{K} = M^{-1/2} K M^{-1/2}$ is called the *scaled stiffness matrix.* Thus, for the rms velocity and wrench norms, the quality measure is given by the *smallest eigenvalue of the scaled stiffness matrix* $\widetilde{K}$:

$$Q_{defl} = \lambda_{\min}(\widetilde{K}). \tag{6.8}$$

Next compute Q_{defl} with respect to the maximum velocity norm and wrench rms-norm. The use of the maximum velocity norm allows the quality measure to indicate $\mathcal{B}$'s worst-case max-deflection, which is just the maximal displacement of $\mathcal{B}$'s body points. While computing Q_{defl} with the maximum velocity norm is complicated for general objects, the formula (6.4) allows efficient computation for objects with polyhedral convex hulls. Using this formula

and the wrench rms-norm formula (6.5) yields

$$Q_{defl}^2 = \inf_{\dot{q}\in\mathbb{R}^6} \frac{\dot{q}^T K M^{-1} K \dot{q}}{\max_{i\in I_V} \dot{q}^T A_i \dot{q}} = \min_{i\in I_V} \inf_{\dot{q}\in\mathbb{R}^6} \frac{\dot{q}^T K M^{-1} K \dot{q}}{\dot{q}^T A_i \dot{q}}.$$

Introducing the change of variables $y = M^{-1/2} K \dot{q}$ yields

$$Q_{defl} = \left(\max_{i\in I_V} \lambda_{\max}(M^{\frac{1}{2}} K^{-1} A_i K^{-1} M^{\frac{1}{2}})\right)^{-\frac{1}{2}}.$$

Thus, Q_{defl} can be efficiently computed from a collection of eigenvalue problems for 6×6 symmetric matrices.

6.3 Representation of Task Wrench Sets

To plan optimal fixtures for manufacturing operations, forces that arise from manufacturing operations must be modelled in an accurate and efficient fashion. A natural approach is to use appropriate subsets of the wrench space to represent such manufacturing forces. This section proposes several primitive task wrench sets which accurately represent manufacturing forces while possessing reasonably simple geometry to allow efficient computation. Using these primitive wrench sets as building blocks, we will be able to represent more complex manufacturing operations.

6.3.1 Primitive Task Wrench Sets

We now consider the building blocks for task representation: primitive task wrench sets. In developing such wrench sets, one needs to bear in mind that the forces arising from a manufacturing operation typically vary in both magnitude and direction during the manufacturing process, and that it is usually

difficult to precisely determine these forces. For example, in the milling operation illustrated in Figure 6.1, the cutter exerts a force on the workpiece. While the magnitude of the cutting force can be estimated from machining power, the direction of the force is difficult to determine. Thus, the force may be assumed to lie in the sector (shown in the figure), which moves along the cutting path with the cutter. To study the effects of machining operations on the fixture, it is in general necessary to consider all conceivable positions and directions of the cutting force. While a discrete set of positions and directions can be considered [16], this approach can be computationally costly, in particular for three-dimensional fixtures. Therefore, it is desirable to develop a procedure for conveniently modelling task wrench sets. The modelling of tasks for robotic grasping was considered by Li and Sastry [89] using ellipsoids in the wrench space. We propose using different types of primitive wrench sets whose adequacy for workpiece fixturing is based on the following observations.

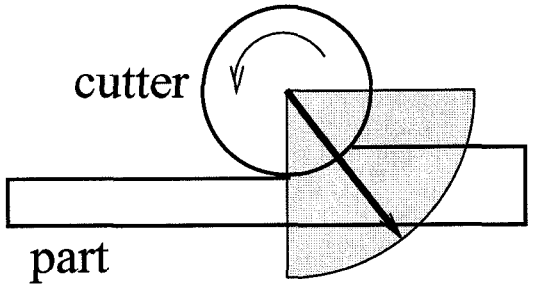

Figure 6.1: Cutting force in a milling operation.

First consider assembly fixtures, which are also known as assembly pallets. As a fixtured part hits a motion stop during its transfer from station to station, it will be quickly decelerated. Due to this deceleration, the part is subjected to an inertial force acting at the center of mass. Thus the task wrench set is simply a collection of known pure forces.

Next consider fixtures for machining purposes. As shown in the milling example given above, machining operations exerts a wrench, which in general

consists of a force and a torque, on the workpiece. Due to uncertainties, the wrench may not be completely known, and in general varies as the cutter moves. However, the force component of the wrench can often be considered to be in a given range of directions, with known magnitude along each direction. That is, the force component lies in a given compact set independent of the wrench's position. Such a compact set may be conservatively used even when the magnitude or direction range of the force component changes during the machining operation. Since the force domain is fixed, the task wrench set is a subset of the cylinder (interior points included) in the wrench space based on the fixed force component set. For instance consider the milling operation shown in Figure 6.1. As shown in Figure 6.2(a), with respect to the frame $\bar{\mathcal{F}}_B$, the force domain is a sector given by $F = \{(f\cos\phi, f\sin\phi) : -\frac{\pi}{4} \leqslant \phi \leqslant \frac{\pi}{4},\ 0 \leqslant f \leqslant \rho_f\}$. The task wrench set is a subset of the cylinder based on F and is shown in Figure 6.2(b).

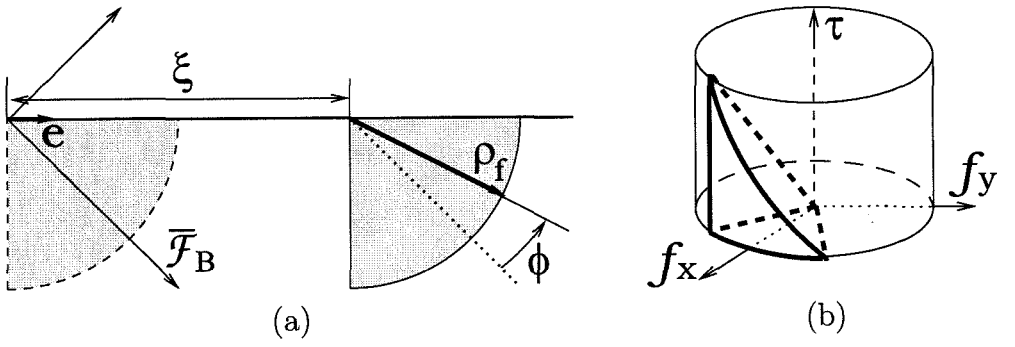

Figure 6.2: Task primitive for milling operation.

These observations suggest that we model task wrench sets as subsets of cylinders in the wrench space, whose base sets are compact sets in the space of force components. First consider two types of primitive force domains. Let $\bar{\mathcal{F}}_B$ be a body frame. With respect to this frame, let n be a unit vector, $S = \{f \in \mathbb{R}^3 : f^T f \leqslant \rho_f^2\}$ a sphere, and $H = \{f \in \mathbb{R}^3 : n^T f \leqslant \rho_h\}$ a half-space with boundary normal to n, where $\rho_f \geqslant 0$, $\rho_h \in \mathbb{R}$ and $\alpha \in [0, \pi]$ are

constants. A force domain F is said to be of *Type I-3D* if $F = S \cap \Gamma$, and of *Type II-3D* if $F = H \cap \Gamma$, where $\Gamma = \{f \in \mathbb{R}^3 : \ n^T f \geqslant |f| \cos\alpha\}$ is a circular cone which is symmetric about n. When $n = (0, 0, 1)$, i.e., F is symmetric about the f_z-axis (Figure 6.3), F is said to be in *canonical form.* In body coordinates, F is independent of the choice of world frame. Since any change of body frame may only result in a rigid rotation of F, the *shape* of F remains the *same* for all frame choices.

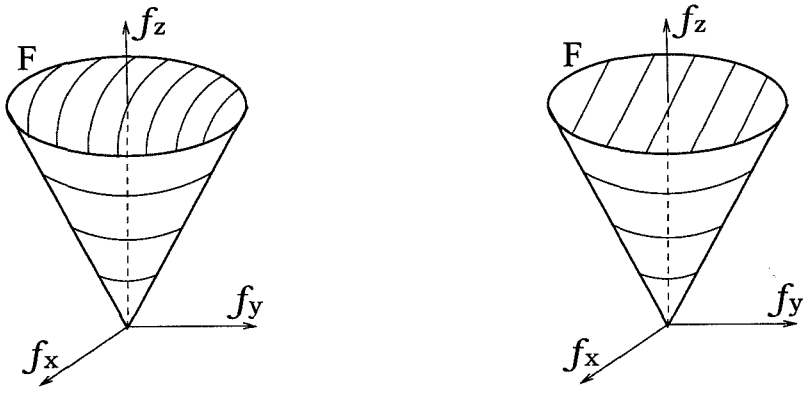

(a) Type I-3D (b) Type II-3D

Figure 6.3: Canonical forms of force domain.

Now consider a general form for primitive wrench sets using body wrenches in the body frame $\bar{\mathcal{F}}_B$. A *primitive wrench set* is a subset of the wrench space of the form

$$\bar{W} = \{(f, (\Phi\xi) \times f + \Psi f + \tau_0) \in T^*_{q_0} SE(3) : \ f \in F, \ \xi \in P\},$$

where Φ and Ψ are appropriately dimensioned constant matrices, τ_0 is a constant vector and $\xi \in P$ is a parameter vector. The parameter domain P is taken as a *compact polygonal set.* Note that we assume $P \subset \mathbb{R}^2$ since cutting forces can only be applied on the workpiece's boundary, and that we do *not* make any assumptions on the convexity of P.

Observe that the torque component of a primitive wrench in general consists of three terms. The first term accounts for the contribution of a moving pure force ($\Phi\xi$ gives the position of f), the second term gives a torque that is related to the force component in some specified manner, and the third term is a constant torque. Specific examples of these terms can be found in Examples 6.3.1–6.3.4.

Geometrically, a primitive wrench set is a parametrized subset of a solid cylinder in the wrench space whose base set is F and whose generators are orthogonal to F. This is illustrated in Figure 6.2(b), which shows the primitive wrench set for the milling operation of Figure 6.1. The following two examples give some practically useful primitive wrench sets for three-dimensional workpiece fixturing.

Example 6.3.1. In Figure 6.4 are shown two force cones that move over a polygonal region in space. The cones are both in canonical form with respect to the body frame $\bar{\mathcal{F}}_B$. The parameter domain is a planar region, specified with coordinate axes ξ_1 and ξ_2. Then this primitive wrench set is given by $\bar{W} = \{(f, (\Phi\xi) \times f) \in T^*_{q_0}SE(3) : \ f \in F, \ \xi \in P\}$, where $\Phi = [e_1, e_2]$ with e_1 and e_2 being unit vectors, specified in $\bar{\mathcal{F}}_B$, along the ξ_1 and ξ_2 axes.

Example 6.3.2. Figure 6.5 shows a model of drilling operations. In this model a force of constant magnitude ρ_f and a torque of constant magnitude ρ_τ are aligned along a line ℓ, which lies in a cone as shown. It is seen that the base set F is of Type I-3D, and that $\bar{W} = \{(f, (\rho_\tau/\rho_f)f) \in T^*_{q_0}SE(3) : \ f \in F\}$.

Now consider the special case of planar fixtures. The wrench space is 3-dimensional with scalar torque components. The parameter domain P for primitive wrench sets is now a line segment. The Type I-3D force domain reduces to *Type I-2D* (the intersection of a disc with a planar cone), and Type II-3D reduces to *Type II-2D* (the intersection of a half-plane with a

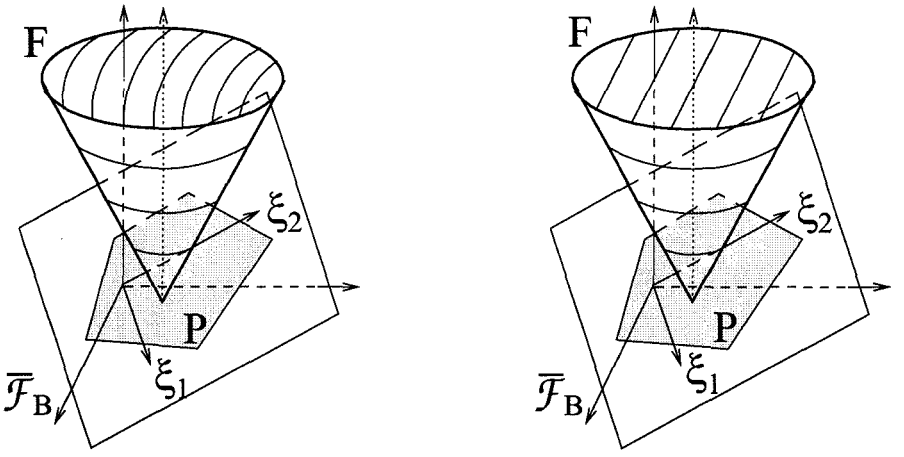

Figure 6.4: Force cones moving over a polygon.

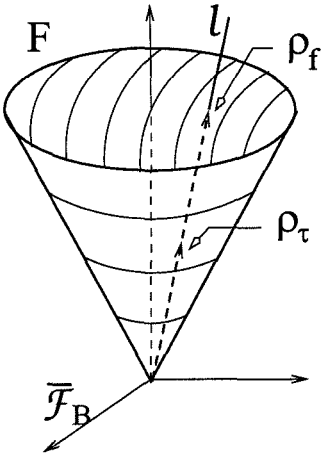

Figure 6.5: A model for drilling operations.

planar cone). Choose canonical forms of F such that it is symmetric with respect to the f_x-axis, as shown in Figure 6.6.

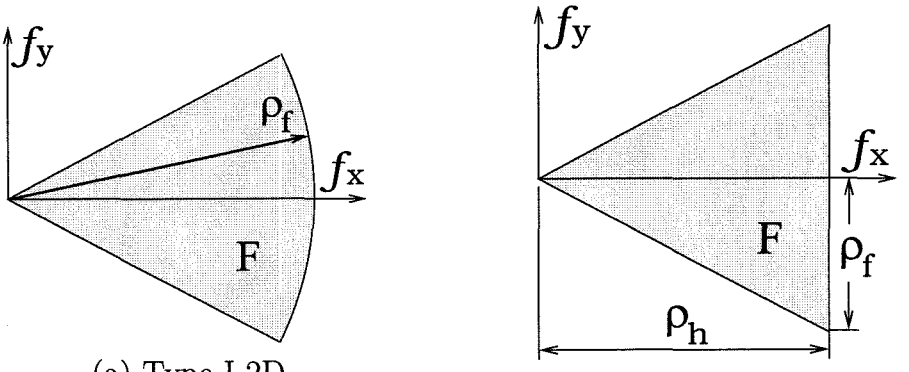

(a) Type I-2D (b) Type II-2D

Figure 6.6: Canonical forms of two-dimensional force domain.

Example 6.3.3. As shown in Figure 6.7, two task primitives are given where a force sector and a force cone, both in canonical forms, move along a line segment P, respectively. Then in the frame $\bar{\mathcal{F}}_B$, the primitive wrench sets are of the form $\bar{W} = \{(f, \xi e \times f) \in \mathbb{R}^3 : \ f \in F, \ \xi \in P\}$, where e is a unit vector along P.

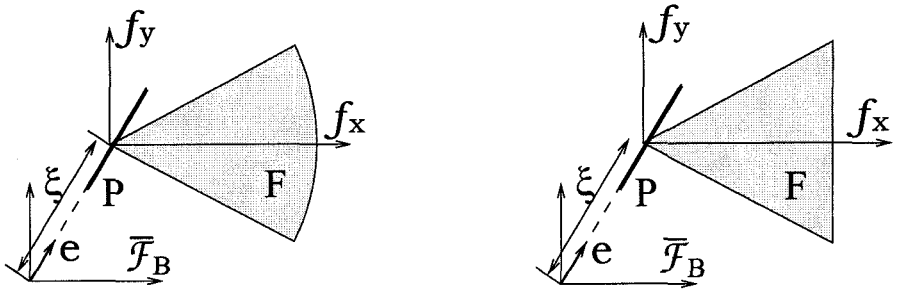

(a) (b)

Figure 6.7: Planar force cones moving along a line segment.

Example 6.3.4. Figure 6.8 shows a model of drilling operations for planar fixtures. This primitive wrench set takes the form $\bar{W} = \{(f, \tau_d) \in \mathbb{R}^3 : \ |f| \leqslant \rho_f\}$.

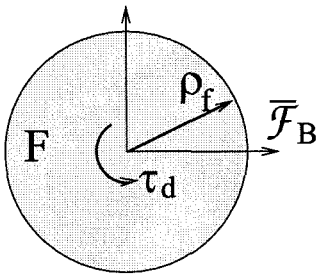

Figure 6.8: A model for drilling operation in planar case.

We have thus far defined a collection of primitive task wrench sets that can be used to model basic manufacturing operations. The following subsections use the primitive task wrench sets to compute the deflection quality measure as applied to given manufacturing operations. These primitive sets will also be used to verify whether under work loads the workpiece and fingers in a fixture can maintain proper contact and satisfy material strength requirements.

6.3.2 Deflection Quality Measure and Contact Maintainability Condition

Section 6.2.2 defined the deflection quality measure (Equation (6.6)), where workpiece deflections were represented in terms of pseudo-norms of rigid body velocities. The maximum velocity pseudo-norm defined in Equation (6.3) gives the maximal displacement of the workpiece's feature points. This physical meaning is very attractive in practical fixturing applications, and will therefore be used in the task-model based deflection computation.

The deflection quality measure will now be reformulated with respect to the maximum velocity pseudo-norm in a form more convenient for task-model based computation. Corresponding to a rigid displacement $\dot{q} = (v, \omega)$, the displacement of a point $r \in \Omega_B$, where Ω_B is $\mathcal{B}$'s feature-point set, can be written as $u_r = v + \omega \times r = D_r \dot{q}$, where $D_r = [-\widehat{r},\ I]$. Thus, in response to a task wrench $\boldsymbol{w} \in W$, the displacement of r is $u_r(\boldsymbol{w}) = D_r C \boldsymbol{w}$, where C is the

fixture compliance matrix. The deflection quality measure (Equation (6.6)) can thus be written as

$$\Delta_W = \max_{\boldsymbol{w}\in W} \max_{r\in\Omega_B} |u_r(\boldsymbol{w})| = \max_{r\in\Omega_B} \max_{\boldsymbol{w}\in W} |u_r(\boldsymbol{w})|.$$

Assume that Ω_B, *the feature-point set of* $\mathcal{B}$, *contains only a finite number of points in the object.* This is a reasonable assumption since in practice manufacturing accuracy can usually be monitored in terms of a finite number of feature points. Under this assumption, we can for each $r \in \Omega_B$ focus on $\max_{\boldsymbol{w}\in W} |u_r(\boldsymbol{w})|$, which is the maximal displacement of r with respect to all wrenches in the task wrench set W.

During a manufacturing process, we also need to ensure that the workpiece and fingers maintain proper contact. In terms of overlap-based compliance modelling, the overlaps must remain non-negative, and must not be excessively large so as to satisfy material strength requirements. From theory of strength of materials [154], for a material to remain elastic, the *maximum shear stress* in the material must not exceed the material's *yield stress.* From Chapter 4, the maximum shear stress in the contacting bodies can be expressed as a function of the overlap. It follows that the *allowable overlap*, which is the maximal overlap allowed by material strength, can be determined from the contact geometry and material properties.

Now consider the approximation of the overlap at each contact when the fixture is under work loads. When the object undergoes a small displacement $\dot{q}$ away from an equilibrium configuration q_0, the change of the overlap at the i^{th} contact is approximately $\nabla\delta_i^T(q_0)\dot{q}$. Note that when $\dot{q}$ is given in body coordinates, $\nabla\delta_i(q_0)$, which can be interpreted as a wrench, should also be given in body coordinates. In response to a task wrench $\boldsymbol{w}$, the overlap at the i^{th} contact is approximately $\delta_i(q_0) + \Delta\delta_i(\boldsymbol{w})$, where $\delta_i(q_0)$ is the preloading over-

lap (when $\boldsymbol{w}$ is not applied), and $\Delta\delta_i(\boldsymbol{w}) = \nabla\delta_i^T(q_0)C\boldsymbol{w}$. For the object and fingers to maintain proper contact and satisfy material strength requirements, the following condition must hold:

$$0 \leqslant \delta_i(q_0) + \Delta\delta_i(\boldsymbol{w}) \leqslant \delta_{maxi} \tag{6.9}$$

where δ_{maxi} is the allowable overlap for the contact.

6.3.3 Formulation Using Primitive Wrench Sets

In order to allow efficient computation of the deflection quality measure and contact maintainability condition with respect to given manufacturing operations, efficient representation of manufacturing forces is needed. This can be achieved by modelling the task wrench set in terms of primitive wrench sets.

Let W be a given task wrench set, and let $\bar{W}_1, \ldots, \bar{W}_m$ be primitive wrench sets

$$\bar{W}_i = \{(f_i, (\Phi_i\xi_i) \times f_i + \Psi_i f_i + \tau_{0_i}) \in T^*_{q_0}SE(3) : \ f_i \in F_i, \ \xi_i \in P_i\},$$

expressed in the intermediate body frames $\bar{\mathcal{F}}_{B1}, \ldots, \bar{\mathcal{F}}_{Bm}$ displaced from $\mathcal{F}_B$ by $g_1, \ldots, g_m$, respectively. We say that W *is modelled by* $\bar{W}_i$ if for each $\boldsymbol{w} \in W$, there exist $\bar{\boldsymbol{w}}_i \in \bar{W}_i$ such that

$$\boldsymbol{w} = \sum_{i=1}^{m} \mathrm{Ad}_{g_i}^{-T}\, \bar{\boldsymbol{w}}_i, \tag{6.10}$$

where the transformation rule (3.7) has been used to express $\bar{\boldsymbol{w}}_i$ with respect to the body frame $\mathcal{F}_B$. Thus, the task wrench set is given by a primitive

wrench set, or the Minkowski sum of several primitive wrench sets.

To compute the deflection quality measure, we can focus on computing $\max_{\boldsymbol{w}\in W} |u_r(\boldsymbol{w})|$, or equivalently, $\max_{\boldsymbol{w}\in W} |u_r(\boldsymbol{w})|^2$, where $u_r(\boldsymbol{w}) = D_r C \boldsymbol{w}$, for a particular point $r \in \Omega_B$. Let $\boldsymbol{w}$ be given in terms of primitive wrenches by (6.10), where each $\bar{\boldsymbol{w}}_i$ is determined by its force component $f_i \in F_i$ and parameter vector $\xi_i \in P_i$. The displacement $u_r(\boldsymbol{w})$ depends on $f = (f_1, \ldots, f_m) \in F = F_1 \times \cdots \times F_m$ and $(\xi_1, \ldots, \xi_m) \in P = P_1 \times \cdots \times P_m$. By using the structure of primitive wrench sets, $u_r(\boldsymbol{w})$ can be rewritten in the form

$$u_r(f, \xi) = \sum_{i=1}^{m} A_i(\xi_i)\, f_i + b(\xi) = \sum_{i=1}^{m} Z_i(f_i)\, \xi_i + y(f),$$

where $A_i(\xi_i)$, $b(\xi)$, $Z_i(f_i)$, and $y(f)$ are matrix- or vector-valued functions. It follows that $|u_r|^2$ is a *convex* function when either f or ξ is fixed. Since the maximum of a convex function is achieved at an *extreme point* of the *convex hull* of its domain, $|u_r(f, \xi)|^2$ achieves its maximum at an extreme point of the convex hull of P when f is fixed. Now, $\max_{\boldsymbol{w}\in W} |u_r(\boldsymbol{w})|^2 = \max_{f\in F} \max_{\xi\in P} |u_r(f, \xi)|^2$. Thus, the global maximum of $|u_r|^2$ can be obtained by finding its maxima with respect to f for each of the vertices of the convex hull of P. Let ξ_0 denote such a vertex, and consider $\phi(f) \triangleq u_r(f, \xi_0)$. Dropping for brevity the argument ξ_0 from A_i and b_i, which are now *constant*, we can focus on $\max_{f\in F} |\phi(f)|^2$, where

$$\phi(f) = \sum_{i=1}^{m} A_i\, f_i + b. \tag{6.11}$$

Now consider the computational verification of the contact maintainability condition (6.9) with respect to all wrenches in the task wrench set. For this

purpose we need to determine whether the following inequalities hold at each contact:

$$\delta(q_0) + \min_{\boldsymbol{w} \in W} \Delta\delta(\boldsymbol{w}) \geqslant 0 \quad \text{and} \quad \delta(q_0) + \max_{\boldsymbol{w} \in W} \Delta\delta(\boldsymbol{w}) \leqslant \delta_{max},$$

where the contact-indexing subscript have been dropped for simplicity. Recall that $\Delta\delta(\boldsymbol{w}) = \eta^T C \boldsymbol{w}$, with $\eta = \nabla\delta(q_0)$, is the overlap change at the j^{th} contact. Therefore, we need to find the maximum and minimum of the overlap variation $\Delta\delta(\boldsymbol{w})$ over the task wrench set.

When the task wrench set is modelled by the primitive wrench sets $\bar{W}_1$, $\ldots$,$\bar{W}_m$ according to (6.10), we have $\Delta\delta(\boldsymbol{w}) = \sum_{i=1}^{m} \eta^T C \operatorname{Ad}_{g_i}^{-T} \bar{\boldsymbol{w}}_i$, i.e., $\Delta\delta$ is *linear* in $\bar{\boldsymbol{w}}_i$. This fact allows the use of a formulation similar to that of the deflection quality measure. We can again focus on a particular vertex ξ_0 of the convex hull of the composite parameter domain P, and maximize or minimize $\psi(f) \triangleq \Delta\delta(f, \xi_0)$ given by

$$\psi(f) = \sum_{i=1}^{m} h_i^T f_i + c, \tag{6.12}$$

where h_i and c are determined by ξ_0.

Since $\phi(f)$ is convex quadratic and $\psi(f)$ is affine, the maximizers of $\phi(f)$, as well as the maximizers and minimizers of $\psi(f)$, belong to $\operatorname{ext}(F) = \operatorname{ext}(F_1) \times \cdots \times \operatorname{ext}(F_m)$, where $\operatorname{ext}(F)$ and $\operatorname{ext}(F_i)$ are the set of extreme points of F and F_i, respectively. Each $\operatorname{ext}(F_i)$ can be partitioned in the form $\operatorname{ext}(F_i) = \overline{F}_i \cup \widetilde{F}_i$, where $\overline{F}_i$ is a *discrete* set and $\widetilde{F}_i$ a *continuous set.* Suppose that f_{1_0} is an element of $\overline{F}_1$. Then for maximizing $\phi(f)$ over $\{f_{1_0}\} \times \widetilde{F}_2 \times \cdots \times \widetilde{F}_m$, the function may be recast as $\phi(f_2, \ldots, f_m) = \sum_{i=2}^{m} A_i f_i + (A_1 f_{1_0} + b)$. By reasoning along this line, we can ignore the discrete sets $\overline{F}_i$ without loss of

generality and focus on maximizing $\phi(f)$, or maximizing and minimizing $\psi(f)$, over $\widetilde{F}_1 \times \cdots \times \widetilde{F}_m$. Now, consider the typical form of the sets $\widetilde{F}_i$. Let F_i be a primitive force domain described in Section 6.3.1. Then $\widetilde{F}_i$ is either a circular arc or a spherical patch with a circular boundary, and is determined by the following two constraints:

$$f_i^T f_i = \rho_{fi}^2 \quad \text{and} \quad n_i^T f_i \geqslant \rho_{fi} \cos \alpha_i, \tag{6.13}$$

where all the quantities except f_i are constant.

6.3.4 Extreme Overlap Variations

To find extreme overlap variations, we need to find the maximum and minimum of the function ψ defined in (6.12). Since ψ is an affine function of f, and the constraints $f_i \in \widetilde{F}_i$ and $f_j \in \widetilde{F}_j$ are independent when $i \neq j$, the maximization or minimization of ψ can be carried out by maximizing or minimizing each component linear function $\psi_i(f_i) = h_i^T f_i$ over $\widetilde{F}_i$, whose typical form is given by (6.13).

The solution can be found in a straightforward way. Note that the maximizer or minimizer of $\psi_i(f_i)$ subject to the constraint that $f_i^T f_i = \rho_{fi}^2$ is given by $f_i^* = \pm(\rho_{fi}/|h_i|)h_i$. If f_i^* satisfies the inequality in (6.13), then it is the solution over $\widetilde{F}_i$, with the optimal value of ψ_i given by $\psi_i(f_i^*) = \pm\rho_{fi}|h_i|$. On the other hand, if f_i^* does not satisfy the inequality constraint, then the maximizer or minimizer of ψ_i must occur on the boundary of $\widetilde{F}_i$, which is a circle (for three-dimensional force domains) or consists of two points (for two-dimensional domains), and can be easily found.

6.3.5 Maximal Particle Displacements

To find the maximal displacement of a particle of $\mathcal{B}$ with respect to a given task wrench set, we need to find the maximum of the function $\phi(f_1, \ldots, f_m)$, as defined in Equation (6.11), over $\widetilde{F}_1 \times \cdots \times \widetilde{F}_m$.

Since ϕ is a convex quadratic function, whose maximum over $\widetilde{F}_i$ determined by the constraints (6.13) remains maximal over the region determined by $f_i^T f_i \leqslant \rho_{fi}^2$ and $n_i^T f_i \geqslant \rho_{fi} \cos\alpha_i$. Thus, we need to solve a *convex quadratic maximization* problem subjected to *multiple convex quadratic constraints.* Several algorithms have been developed for such optimization problems (e.g., [8]), and can be used to find the global maximum of $\phi(f)$.

We now discuss the following important special case where the task wrench set is modelled by a single task primitive. In this case, we wish to maximize $\phi(f) = |Af + b|^2$ over $\widetilde{F}$ which is given by the constraints that $f^T f = \rho_f^2$ and $n^T f \geqslant \rho_f \cos\alpha$.

The maximization problem affords a particularly simple solution when the force domain is planar ($f \in \mathbb{R}^2$). The constraints in this case can be parameterized by $f = (\cos\theta, \sin\theta)^T$, where $\theta \in [-\alpha, \alpha]$. For maximizing $\phi(f)$, it is necessary that $(Af + b)^T \frac{\partial}{\partial\theta}(Af + b) = 0$, i.e.,

$$(-a_1^T \sin\theta + a_2^T \cos\theta)(a_1 \cos\theta + a_2 \sin\theta + b) = 0,$$

where $A = [a_1,\ a_2]$. Substituting $\sin\theta = (1-t^2)/(1+t^2)$ and $\cos\theta = 2t/(1+t^2)$ yields a quartic equation in t, which can be solved to find the maximizer of ϕ.

Now consider the case where $f \in \mathbb{R}^3$. If the maximizer of ϕ lies on the boundary of $\widetilde{F}$, i.e., the inequality constraint for $\widetilde{F}$ holds as an equality, then the technique for the two-dimensional case can be invoked since $\widetilde{F}$'s boundary is a circle. Thus, it remains to consider the case where ϕ is maximized at

an interior point of $\widetilde{F}$ and the inequality constraint is inactive. Omitting the constant term, ϕ can be rewritten as $\phi(f) = \frac{1}{2} f^T G f + d^T f$, where $G = 2A^T A$ and $d = 2A^T b$. The global maximizer of ϕ over $\widetilde{F}$ is a local (but not necessarily global) maximizer of ϕ over the sphere $f^T f = \rho_f^2$. These local maximizers can be determined by the following stationarity conditions:

$$(G - \mu I) f + d = 0 \quad \text{and} \quad f^T f = \rho_f^2,$$

where $\mu > 0$ is an undetermined Lagrange multiplier. Let U be an orthogonal matrix such that $D = U \Lambda U^T$, where Λ is a diagonal matrix whose diagonal entries are the eigenvalues of D. Introducing change of variables $x = U^T f$ and letting $c = -U^T d$ lead to

$$(\Lambda - \mu I) x = c \quad \text{and} \quad x^T x = \rho_f^2. \tag{6.14}$$

The solution of these equations is discussed in the following three possible cases for the value of μ. Without loss of generality, $c \neq 0$ is assumed.

Case 1: μ is not an eigenvalue of D. Since $\Lambda - \mu I$ is invertible, we have $x = (\Lambda - \mu I)^{-1} c$. Thus,

$$c^T (\Lambda - \mu I)^{-2} c = \rho_f^2, \tag{6.15}$$

which is a 6^{th} order polynomial equation and can be easily solved.

Case 2: μ is a distinct eigenvalue of D. Suppose that $\mu = \lambda_i$ where λ_i is a distinct eigenvalue of D. Note that this is possible only if $c_i = 0$. In

this case, $x_j = c_j/(\lambda_j - \lambda_i)$ for all $j \neq i$. It follows that

$$x_i^2 + \sum_{j \neq i} \frac{c_j^2}{(\lambda_j - \lambda_i)^2} = \rho_f^2,$$

which determines x_i provided that

$$\sum_{j \neq i} \frac{c_j^2}{(\lambda_j - \lambda_i)^2} \leqslant \rho_f^2.$$

Case 3: μ is an eigenvalue of D with multiplicity $k \geqslant 2$. Without loss of generality, assume that $\mu = \lambda_1 = \cdots = \lambda_k$. This is only possible if $c_1 = \cdots = c_k = 0$. In this case, $x_j = c_j/(\lambda_j - \lambda_1)$ for all $j \geqslant k+1$. We split x into the form $x = (y^T, \hat{y}^T)^T$, where $\hat{y}$ contains the $3-k$ known components. Let us write $n^T f = n^T U x = r^T y + \gamma$. Provided that $\hat{y}^T \hat{y} \leqslant \rho_f^2$, we may seek $y \in \mathbb{R}^k$ such that

$$y^T y = \rho_f^2 - \hat{y}^T \hat{y} \quad \text{and} \quad r^T y + \gamma \geqslant 0. \tag{6.16}$$

This is equivalent to the following convex quadratic minimization problem:

$$\sigma = \min\{y^T y : \ r^T y + \gamma \geqslant 0\}.$$

It is easily verified that the problem (6.16) admits a solution if $\sigma \leqslant \rho_f^2$, and has no solution if $\sigma > \rho_f^2$.

Example 6.3.5. We illustrate our approach by a planar fixture. Figure 6.9(a) shows a planar part of thickness 1/4 inches fixtured by four fingers. The part is made of AISI 1040 steel, with $E = 200 \times 10^9$Pa, $\sigma_s = 413 \times 10^6$Pa and

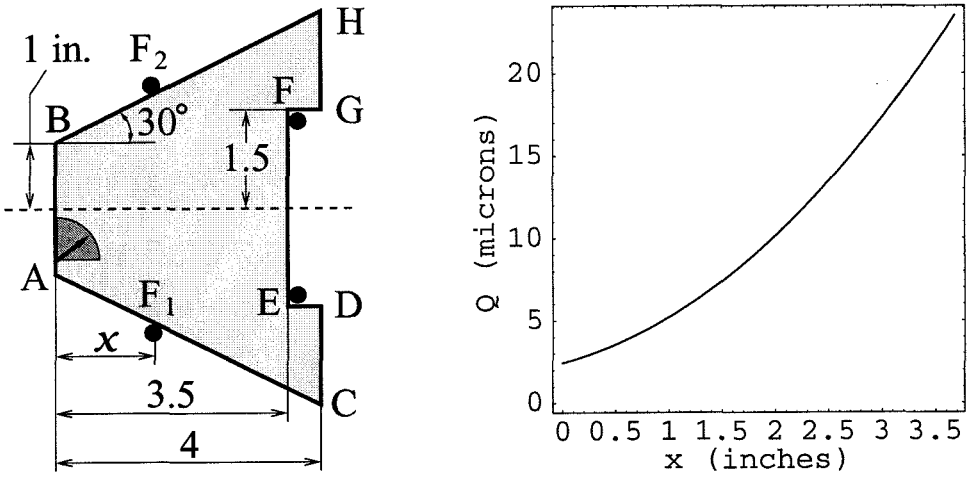

(a) A steel part fixture (b) Variation of the quality measure

Figure 6.9: Task primitive for milling operation.

$\nu = 0.3$. The machining tasks involve removing 1/8 of an inch using a side mill along the edges AB, CD and GH so that AB is accurately parallel to CD and GH. The cutting force is estimated at 341 Newtons [118], lying in a sector which moves along the edge being machined. The fingers have spherical tips of uniform radius 2 inches, and are placed on the edges AC, BH, and EF (each of EF's endpoints contact a finger). For demonstration we focus on the milling force acting on the edge AB, and consider the variation of the deflection quality measure Δ_W as the fingers F_1 and F_2, aligned vertically, move along the edges AC and BH. Preload the fixture, for all finger arrangements, such that the maximum shear stress near the contacts is 70% of the steel's yield stress. Using the Hertz contact model to compute the stiffness matrix (Chapter 4), we found that the fixture satisfies the contact maintainability condition for all cutting force positions and directions if the fingers F_1 and F_2 are placed such that $x \leqslant 3.68$ inches. As shown in Figure 6.9(b), when x decreases from this value, the deflection quality measure, defined using the vertices A and B as feature points, assumes a monotonically decreasing value, indicating improvement of fixture quality. Thus, of the fixtures we consider, the best one

is given by placing the fingers F_1 and F_2 at A and B, respectively, with $\Delta_W =$ 2.4 micro meters. This agrees with the intuition that the fixture arrangement best restrains the displacement of the edge AB.

6.4 Minimum-Deflection Fixtures of Polygons

This section applies the deflection quality measure to minimum-deflection fixturing of polygonal objects by three and four frictionless fingers. For simplicity we use the quality measure Q_{defl} as defined with respect to the velocity rms-norm and wrench rms-norm. The overlap-based compliance computation scheme, as applied to three- and four-finger polygonal fixtures in Section 5.4.1, will be used. But it should be noted that the deflection quality measure, formulated either in terms of Δ_W or Q_{defl}, is valid for all well-defined norms or pseudo-norms, and for fixtures by any number of fingers with compliance represented by any contact model that is based on the quasi-rigid body assumption.

With respect to the rms velocity and wrench norms, the quality measure Q_{defl} characterizes $\mathcal{B}$'s worst-case rms-deflection due to a unit rms-norm ball of wrenches, and can be computed from $Q_{defl} = \lambda_{\min}(\widetilde{K})$, where $\widetilde{K} = M^{-1/2}KM^{-1/2}$ is the scaled stiffness matrix. Given any weighting function $\nu(r)$ for a planar object, there exists a unique point, called the *centroid* of the object, such that when the body frame is based at this point, the 3×3 weighting matrix is diagonal: $M = \mathrm{diag}(1, 1, \rho_c^2)$, where $\rho_c = (\int_{\mathcal{B}} \nu(r)|r|^2 dV)^{1/2}$, called $\mathcal{B}$'s *radius of gyration*, is a purely kinematic quantity.

Recall that a planar fixture has a unique center of compliance, about which there are two translational stiffnesses $\sigma_1 \leqslant \sigma_2$ and a rotational stiffness μ. The parameters were computed for three- and four-finger polygonal fixtures in Sections 5.4.1 and 5.4.2. Since Q_{defl} is frame-invariant, we can conveniently

choose a body frame $\mathcal{F}_B$ that simplifies the computation of Q_{defl}. Let $\mathcal{F}_B$'s origin coincide with $\mathcal{B}$'s centroid. Let $p_c = (\xi, \eta)$ be the coordinates in $\mathcal{F}_B$ of the fixture's center of compliance. With a proper choice of $\mathcal{F}_B$'s orientation, the scaled stiffness matrix can be cast in the following form:

$$\widetilde{K} = \begin{pmatrix} \sigma_1 & 0 & -\sigma_1\widetilde{\eta} \\ 0 & \sigma_2 & \sigma_2\widetilde{\xi} \\ -\sigma_1\widetilde{\eta} & \sigma_2\widetilde{\xi} & \widetilde{\mu}^2 + \sigma_2\widetilde{\xi}^2 + \sigma_1\widetilde{\eta}^2 \end{pmatrix}, \tag{6.17}$$

where $\widetilde{\xi} = \xi/\rho_c$, $\widetilde{\eta} = \eta/\rho_c$, and $\widetilde{\mu} = \mu/\rho_c^2$. With this formulation of the stiffness matrix, we can proceed to consider minimum-deflection three- and four-finger fixtures.

6.4.1 Minimum-Deflection Three-Finger Fixtures

Recall from 5.4.1 that when a polygonal object is fixtured by three frictionless fingers, each finger must lie on a different edge of the object. Therefore, triplets of edges can be considered. Hereafter we focus on a particular admissible edge-triplet. Let the body frame $\mathcal{F}_B$ be chosen such that the scaled stiffness takes the form (6.17). Since the contact normals have constant directions for the edge-triplet, the scaled stiffness matrix $\widetilde{K}$ of all fixtures on the edge triplet can be written as (6.17) in the *same* frame $\mathcal{F}_B$. Using this formula, the deflection quality measure can be computed from the following lemma.

Lemma 6.4.1. *For three-finger stable equilibrium fixtures modelled by a general contact model, the deflection quality measure with respect to the rms velocity and wrench norms is approximately given by*

$$Q_{defl} = \frac{\mu}{\rho_c^2 + \rho^2},$$

where $\rho = (\xi^2 + \eta^2)^{1/2}$ *is the distance between the concurrency point and* $\mathcal{B}$*'s centroid.*

Proof. Decompose the scaled stiffness matrix into the form $\widetilde{K} = \widetilde{K}_1 + \widetilde{K}_2$, where

$$\widetilde{K}_1 = \begin{pmatrix} \sigma_1 & 0 & -\sigma_1\widetilde{\eta} \\ 0 & \sigma_2 & \sigma_2\widetilde{\xi} \\ -\sigma_1\widetilde{\eta} & \sigma_2\widetilde{\xi} & \sigma_2\widetilde{\xi}^2 + \sigma_1\widetilde{\eta}^2 \end{pmatrix},$$

and $\widetilde{K}_2 = \mathrm{diag}(0, 0, \widetilde{\mu})$. Recall from (5.11) that $\mu/l^2 \ll \sigma_i$. Since $\rho_c/l \sim 1$, we have $\widetilde{\mu} = \mu/\rho_c^2 \ll \sigma_i$. Therefore, $\widetilde{K}_2$ can be viewed as a *small perturbation* to $\widetilde{K}_1$. Now, $\widetilde{K}_1$ is positive semidefinite with 0 as a distinct eigenvalue and $(\widetilde{\eta}, -\widetilde{\xi}, 1)$ a corresponding eigenvector. Using Lemma A.3.1 (which computes perturbations to matrix eigenvalues), $\widetilde{\mu}/(\widetilde{\xi}^2 + \widetilde{\eta}^2 + 1) = \mu/(\rho_c^2 + \rho^2)$ is approximately an eigenvalue of $\widetilde{K}$.

Now, it can be shown that regardless of the values of $\widetilde{\xi}$ and $\widetilde{\eta}$, the nonzero eigenvalues of $\widetilde{K}_1$ are no less than σ_1, the smaller translational stiffness. According to Lemma A.3.1, these eigenvalues are also perturbed to give the remaining two eigenvalues of $\widetilde{K}$, and the perturbations are bounded by $\|\widetilde{K}_2\|$, which is much smaller than σ_1. It follows that $\mu/(\rho_c^2 + \rho^2)$ is actually the smallest eigenvalue of $\widetilde{K}$. □

Now consider minimum-deflection three-finger fixtures on a particular triplet of edges. Recall that the set of three-finger equilibrium fixtures can be parametrized by the concurrency point of the contact normals. The concurrency point, denoted p, lies inside a convex polygonal region, denoted S, formed by intersecting three strips whose bounding lines are perpendicular to an edge and pass through the edge's endpoints (Figure 5.3). For a general contact model, μ is a *constant* regardless of the concurrency point position as long as

fixtures with different positions of p have the same specified total preload f_T. In addition, ρ_c is also *constant* after a weighting function is chosen. Therefore, in the quality measure formula given in Lemma 6.4.1, ρ is the only variable that changes with p. It follows that Q_{defl} is maximized for the edge triplet when $\rho(p)$, the distance between the concurrency point and $\mathcal{B}$'s centroid, is minimized.

The problem of finding minimum-deflection fixture on a given edge-triplet reduces to minimization of $\rho^2(p)$ for all $p \in S$. Thus, in the optimal finger arrangement, the concurrency point is as close to the object's centroid as possible. It follows that the optimal finger arrangement can be identified graphically. First, find the region S as shown in Figure 5.3. Second, find the centroid of the object with respect to a given weighting function ν. If the centroid lies in S, then it is the optimal concurrency point. Otherwise the centroid lies outside S. Since S is a polygonal region, we can efficiently compute the closest point in S to the centroid. This point either lies on an edge of S or is a vertex of S.

Example 6.4.1. The minimum-deflection fixture of a triangle can be determined graphically, as shown in Figure 6.10 by solid circles. The region S, which is the set of concurrency point positions that form equilibrium fixtures, can first be determined. When the centroid lies inside this region, the optimal concurrency point coincides with the centroid as shown in Figure 6.10(a). When the centroid falls outside S, a perpendicular line can be drawn through the centroid to the closest boundary edge of S. The resulting intersection gives the optimal concurrency point, as shown in Figure 6.10(b). For comparison the maximum-stiffness fixtures in Example 5.5.1 are also shown in the figures by regular circles. While ρ is minimized for minimum-deflection, $\rho_{\max}$ is minimized for maximum-stiffness. This explains why the minimum-deflection fixtures are determined by the location of $\mathcal{B}$'s centroid, and the maximum-

stiffness fixtures by that of $\mathcal{B}$'s geometric center.

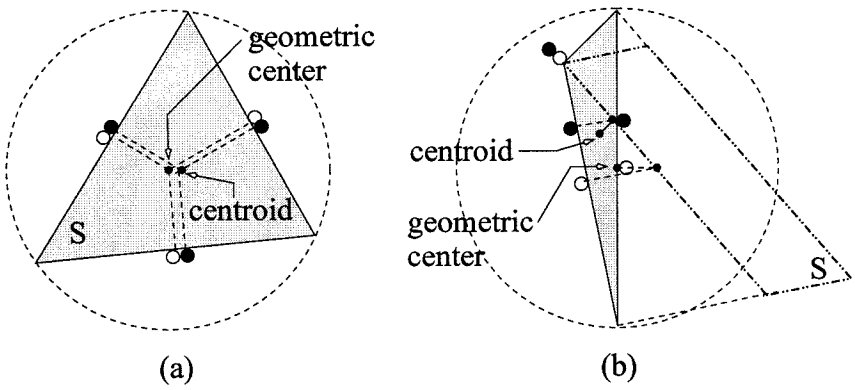

Figure 6.10: Minimum-deflection three-finger fixtures of two triangular objects, for which the centroid lies (a) inside S and (b) outside S.

We now discuss the characteristics of the global minimum-deflection fixture over all admissible edge-triplets of a polygon. While μ is a constant for a particular edge-triplet, it *varies* with different triplets. When f_T is specified, μ is influenced by the *shape* and *size* of the triangle determined by each edge triplet. Thus, the distance ρ is desired to be *small* for minimum-deflection, which is in contrast to $\rho_{\max}$ being preferred to be small for maximum-stiffness fixtures (Section 5.5.1). In addition, as is similar to maximum-stiffness fixtures, both the size parameter a, which is the radius of the triangle's circumscribing circle, and the shape parameter ζ, which is determined from the triangle's interior angles, are preferred to be *large* for achieving minimum-deflection. Therefore, in the globally optimal finger arrangement, the fingers *spread apart*, and the edges in the triplet are oriented *evenly*, while the concurrency point is as close to $\mathcal{B}$'s centroid as possible. The parameters ρ, a, and ζ *combine* to determine the fixture quality; a single parameter alone is *not* sufficient for global optimality. The following two examples will be used to illustrate these observations. Again, the limiting case of zero finger radii will be taken.

Example 6.4.2. Consider the minimum-deflection three-finger fixturing of the polygonal object of Example 5.5.2. Choose a weighting function $\nu(r) =$

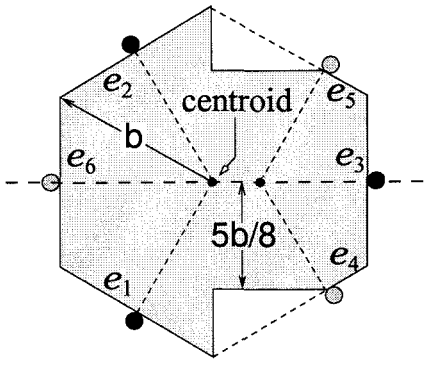

Figure 6.11: Minimum-deflection three-finger fixtures of a polygon.

$\frac{1}{6}\delta(r - r_j)$ where r_j are vertices of $\mathcal{B}$'s regular hexagonal convex hull. Then the centroid coincides with the center of symmetry of the hexagon, and the radius of gyration is $\rho_c = b$. We focus on the edge combinations (e_1, e_2, e_3) and (e_4, e_5, e_6), which determine two congruent triangles with $a\zeta = \frac{\sqrt{3}}{4}b$. The optimal concurrency point of the triplet (e_1, e_2, e_3) coincides with the centroid. Hence, $\rho = 0$, and for this fixture we obtain $Q_{defl} = \frac{\sqrt{3}}{2}(\frac{f_T}{b})$. For (e_3, e_4, e_5), the optimal concurrency point lies on the line of symmetry of $\mathcal{B}$ at a distance $\rho = \frac{\sqrt{3}}{6}b$ from the centroid. Therefore, it can be computed that $Q_{defl} = \frac{6\sqrt{3}}{13}(\frac{f_T}{b})$. Thus, while the triangles associated with the two edge-triplets have the same shape and size, the different distance of the optimal concurrency point from $\mathcal{B}$'s centroid makes the optimal fixture on (e_1, e_2, e_3) better than the optimal fixture on (e_4, e_5, e_6).

Example 6.4.3. Consider the minimum-deflection three-finger fixture of the quadrilateral shown in Figure 6.12(a), which was also used in Example 5.5.2. Choose a weighting function $\nu(r) = (1/4)\delta(r - r_j)$ where r_j are the object's vertices. Then $\rho_c = 0.4857b$, with the centroid having coordinates $(0.4625b, 0.2625b)$. For the admissible edge-triplets (e_1, e_2, e_3) and (e_1, e_2, e_4), the minimum-deflection finger locations are shown in the figure. The concurrency points of these fixtures both coincide with the centroid. However, the edge triplets have different geometry and size. For the fixture on (e_1, e_2, e_3),

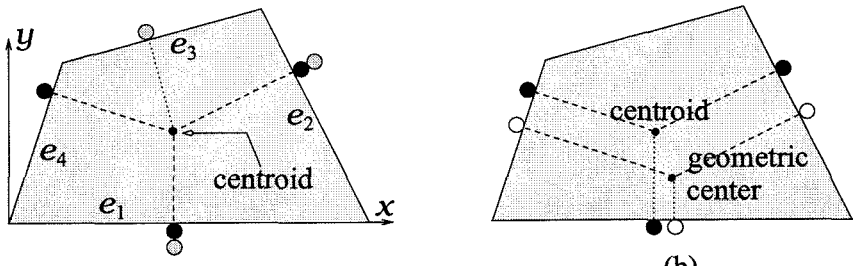

Figure 6.12: (a) Minimum-deflection three-finger fixtures of a quadrilateral, and (b) comparison of global minimum-deflection and maximum-stiffness fixtures.

$a\zeta = 0.1376b$, and therefore $Q_{defl} = 1.1665 f_T/b$. For the fixture on (e_1, e_2, e_4), $a\zeta = 0.1664b$, and $Q_{defl} = 1.4105 f_T/b$. It is concluded that the optimal finger arrangement on (e_1, e_2, e_4) is the global minimum-deflection fixture. For comparison the global minimum-deflection and maximum-stiffness fixtures are shown in Figure 6.12(b) in solid and regular circles, respectively.

6.4.2 Formulating the Minimum-Deflection Four-Finger Fixture Problem

Now consider minimum-deflection four-finger fixtures of polygons. Similar to the maximum-stiffness case, we first formulate the optimization problem, and then describe a technique for finding globally optimal fixtures. Finally, several examples will be presented for demonstration.

As discussed in Section 5.4.2, finding the optimal fixture of a polygon can be performed over all four-finger placements on triplets and quadruplets of edges. On a particular edge combination, the set of stable equilibrium fixtures is parametrized by the parameter vector s consisting of the moments of the unit contact normals about $\mathcal{F}_B$'s origin, and is characterized by Lemma 5.4.2. For simplicity $k_i = \text{const}$ is assumed when Lemma 5.4.2 is used to compute the fixture stiffness matrix. Then, the stiffness parameters $\sigma_1 \leqslant \sigma_2$ are *constant*

for all finger placements s on the edge combination. Consequently, with $\mathcal{F}_B$ based at the object's centroid and properly oriented, the scaled stiffness takes the form (6.17), in which $\widetilde{\mu}$, $\widetilde{\xi}$ and $\widetilde{\eta}$ depend on s. The deflection quality measure is given by $Q_{defl} = \lambda_{\min}(\widetilde{K}(s))$.

It is instructive to make some qualitative observations on the characteristics of the optimal fixture associated with a given edge combination. We first introduce the following lemma.

Lemma 6.4.2. *On a given edge combination, the stiffness quality measure has the following upper bound:*

$$Q_{defl}(s) \leqslant \min\{\sigma_1, \frac{\mu(s)}{\rho_c^2 + \rho(s)^2}\},$$

where ρ_c is $\mathcal{B}$'s radius of gyration and $\rho = (\xi^2 + \eta^2)^{1/2}$ the distance between the fixture's center of compliance and $\mathcal{B}$'s centroid.

Proof. For any $x = (x_1, x_2, x_3) \in \mathbb{R}^3$, we have $x^T\widetilde{K}x = \sigma_1(x_1 - \widetilde{\eta}x_3)^2 + \sigma_2(x_2 + \widetilde{\xi}x_3)^2 + \widetilde{\mu}x_3^2$, and

$$Q_{defl}(s) = \lambda_{\min}(\widetilde{K}(s)) = \min_{y\in\mathbb{R}^3} \frac{y^T\widetilde{K}y}{y^Ty} \leqslant \frac{x^T\widetilde{K}x}{x^Tx}.$$

Taking $x = (\widetilde{\eta}, -\widetilde{\xi}, 1)$ and $x = (1, 1, 0)$, and using the formulas $\widetilde{\xi} = \xi/\rho_c$, $\widetilde{\eta} = \eta/\rho_c$ and $\widetilde{\mu} = \mu/\rho_c^2$ complete the proof. □

Based on this lemma, we can first observe that Q_{defl} can *never* exceed the constant σ_1. Since σ_1 is the smaller eigenvalue of $K_{11} = \sum_{i=1}^4 k_i N_i N_i^T$, the contact normals are preferred to be *evenly oriented* to increase σ_1. In particular, if the stiffness constants are uniform, i.e., $k_i = k$, then $\sigma_1 \leqslant 2k$, and $\sigma_1 = 2k$ precisely when the contact normals are 90° apart. Second, recall

that $\mu(s) = \sum_{i=1}^{4} k_i \bar{s}_i(s)^2$, where $\bar{s}_i(s)$ is the moment of N_i about the center of compliance. Thus, μ, and hence the bound in Lemma 6.4.2 increase monotonically with $|\bar{s}_i|$. This indicates that the fingers should *spread apart* with respect to the center of compliance, so as to make $|\bar{s}_i|$ large. Finally, as ρ, the distance between the fixture's center of compliance and $\mathcal{B}$'s centroid, increases, the upper bound decreases monotonically. Thus, ρ should necessarily be as *small* as possible, and most desirably, should be zero. The optimal fixture is therefore determined by the trade-off among these three factors.

6.4.3 Computation of Global Minimum-Deflection Four-Finger Fixtures

From the characterization of four-finger stable equilibrium fixtures, the maximization of $Q_{defl}(s)$ can be performed over a collection of bounded, convex polytopes. Let $\mathcal{D}$ be one of such polytopes. Then, each $s \in \mathcal{D}$ represents a stable equilibrium fixture. We now present a procedure for maximizing $Q_{defl}(s) = \lambda_{\min}(\widetilde{K}(s))$ over $\mathcal{D}$. For a parameter $t \in (0,1)$ define the following scalar function:

$$\psi(t) = \max_{s \in \mathcal{D}} \zeta(t,s) - (1-t)\sigma_1,$$

where $\zeta(t,s) = \widetilde{\mu}(s) + (1 - \frac{1}{1-\alpha(1-t)})\sigma_2 \widetilde{\xi}^2(s) + (1 - \frac{1}{t})\sigma_1 \widetilde{\eta}^2(s)$. The following proposition, which is proved in Appendix B.4, indicates that the scalar function ψ can be used to characterize the global maximum of $\lambda_{\min}(\widetilde{K}(s))$.

Proposition 6.4.3. *The scalar function ψ is strictly monotonic increasing in the interval $(0,1)$. Moreover, maximizing $\lambda_{\min}(\widetilde{K})$ is equivalent to finding the zero of ψ, if any. Specifically, either of the following two cases must be true.*

(1) There exists a unique scalar $t^* \in (0,1)$ *such that* $\psi(t^*) = 0$ *if and only if* t^* *satisfies the condition* $\max_{s\in\mathcal{D}} \lambda_{\min}(\widetilde{K}(s)) = (1-t^*)\sigma_1$. *In this case,* $s^* \in \mathcal{D}$ *maximizes* $\zeta(t^*, s)$, *regarded as a function of* s, *if and only if it maximizes* $\lambda_{\min}(\widetilde{K}(s))$.

(2) for the function ψ *in the interval* $(0,1)$ *if and only if* $\max_{s\in\mathcal{D}} \lambda_{\min}(\widetilde{K}(s)) = \sigma_1$. *In this case, for any fixed* $t \in (0,1)$, *any global maximizer* s^* *of* $\zeta(t,s)$ *satisfies the condition* $(1-t)\sigma_1 \leqslant \lambda_{\min}(\widetilde{K}(s^*)) \leqslant \sigma_1$. *Hence, a global maximizer of* $\lambda_{\min}(\widetilde{K}(s))$ *can be found by letting* $t \to 0$.

Thus, to find the optimal finger arrangement over the region $\mathcal{D}$, we may equivalently seek the zero of the scalar function ψ. This function is evaluated at a given value of t by maximizing the function $\zeta(t,s)$ over all $s \in \mathcal{D}$. Since $\widetilde{\xi}(s)$, $\widetilde{\eta}(s)$ are linear and $\widetilde{\mu}(s)$ is quadratic, the function $\zeta(t,s)$ for a fixed t is a generally indefinite quadratic function. Thus, to find its maximum we need to solve an *indefinite quadratic program.* As discussed in Section 5.5.3, while indefinite quadratic programming is difficult for problems of large size, it can be efficiently solved for the current fixture optimization problem since there are only four independent variables. The significance of this approach is that it guarantees to find the *global* maximum of $\lambda_{\min}(\widetilde{K}(s))$, a non-convex and non-differentiable function of s, at a reasonable computational cost.

6.4.4 Examples of Minimum-Deflection Four-Finger Fixtures

A few examples will now be presented for demonstration. For simplicity, it is assumed that the fingers have zero radii and the elasticity coefficients are uniform constants: $k_i = k$.

Example 6.4.4. Consider a rectangle shown in Figure 6.13. Choose a weighting function $\nu(r) = (1/4)\delta(r - r_j)$, where r_j are the rectangle's vertices. Con-

sider a family of symmetric finger placements where the fingers on the vertical edges are above or below the x-axis by a distance s_1, and the fingers on the horizontal edges are at a distance s_2 from the y-axis. Corresponding to such a symmetric finger arrangement, the fixture's center of compliance coincides with $\mathcal{B}$'s centroid, which for the choice of ν is precisely $\mathcal{B}$'s center of symmetry. The scaled stiffness matrix takes the form $\widetilde{K} = 2k\ \mathrm{diag}\big(1, 1, (s_1^2+s_2^2)/(a^2+b^2)\big)$. Hence, as $s_1 = a$ and $s_2 = b$, the quality measure is maximized at $Q_{defl} = 2k$. In this optimal fixture, the fingers spread apart and are placed at the endpoints of the edges. Comparing with Example 5.5.4, we see that the global minimum-deflection and maximum-stiffness fixtures are given by the same finger arrangement.

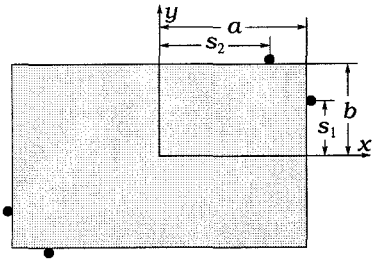

Figure 6.13: Four-finger minimum-deflection fixtures of a rectangle.

Example 6.4.5. This example considers four-finger minimum-deflection fixtures of an isosceles triangle as shown in Figure 6.14. Choose a weighting function $\nu(r) = (1/3)\delta(r - r_j)$ where r_j are the triangle's vertices. Then $\rho_c^2 = 2b^2(3 + \cot^2\alpha)/9$, and the object's centroid with respect to ν is at the geometric centroid of the triangle, which lies on the line of symmetry at a height $b\cot\alpha/3$ above the base edge. Choosing a body frame as shown in the figure, we consider the following family of symmetric finger arrangements. The fingers on the base edge are at a distance s from the y-axis. The fingers on the triangle's two sides are symmetric about the y-axis, and their corresponding contact normals intersect at the centroid. The center of compliance

of the resulting fixture coincides with the centroid, and the stiffness matrix is diagonal: $K = k\ \mathrm{diag}\big(2\cos^2\alpha, 2(1+\sin^2\alpha), 2s^2\big)$. The scaled stiffness matrix hence takes the diagonal form $\widetilde{K} = \mathrm{diag}\big(2k\cos^2\alpha, 2k(1+\sin^2\alpha), \widetilde{\mu}(s)\big)$, where $\widetilde{\mu}(s) = 9ks^2/(3b^2 + b^2\cot^2\alpha)$. The parameter $\widetilde{\mu}$ achieves maximum at $s = b$ with $\widetilde{\mu}(b) = 9k/(3+\cot^2\alpha)$, i.e., the fingers contact the base edge at the endpoints. It follows that when $\widetilde{\mu} \geqslant 2\cos^2\alpha$, or $\alpha \geqslant 30^\circ$, this finger placement is optimal, with $Q_{defl} = \lambda_{\min}(\widetilde{K}) = 2k\cos^2\alpha$. Again, it is seen that the grasp quality improves as s increases, i.e., the fingers spread apart.

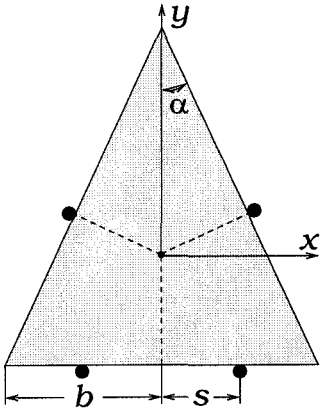

Figure 6.14: Four-finger minimum-deflection fixtures of an isosceles triangle.

Example 6.4.6. This example demonstrates fixturing applications where no symmetry of objects is available to allow a closed-form optimization analysis and therefore the numerical procedure outlined in Proposition 6.4.3 must be invoked. For the quadrilateral that was used in Example 6.4.3, when choosing again a weighting function $\nu(r) = (1/4)\delta(r - r_j)$ where r_j are the $\mathcal{B}$'s vertices, the centroid is located at $(0.4625b, 0.2625b)$ with $\rho_c = 0.4857b$. According to Proposition 6.4.3, the optimal finger arrangement can be numerically found for each edge combination. The globally optimal fixture thus determined is shown in Figure 6.15 in solid circles, and can be compared with the global maximum-stiffness fixture obtained in Example 5.5.6 shown with regular circles. For this

minimum-deflection fixture, $\sigma_1 = 1.6838k$ and $\sigma_2 = 2.3162k$, and $Q_{defl} = 1.6838k$. It follows that Q_{defl} achieves the upper bound given in Lemma 6.4.2.

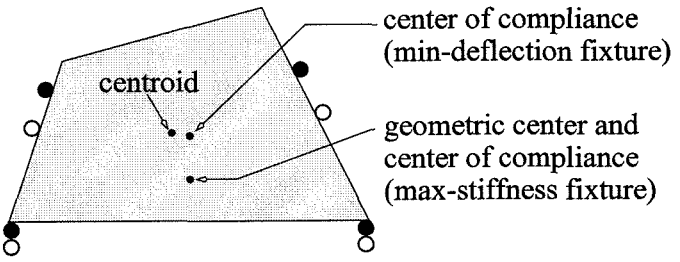

Figure 6.15: Four-finger minimum-deflection fixtures of a quadrilateral.

Summary:

This chapter defined the deflection quality measure as the worst-case deflection of a fixtured workpiece induced by any wrench that lies in a task wrench set. The deflection quality measure has the following properties. First, the quality measure, defined in terms of frame-invariant rigid body velocity and wrench norms, is frame-invariant. Second, the quality measure applies to two- and three-dimensional compliant fixtures modelled by general compliance models and employing any number of fingers. Finally, the quality measure directly characterizes workpiece deflections, and is therefore practically useful in monitoring manufacturing tolerances. To allow efficient computation of the quality measure and verification of contact maintainability, task wrench sets were modelled in terms of a collection of simple primitive wrench sets that represent basic manufacturing operations. The utility of the deflection quality measure was illustrated by its application to minimum-deflection fixtures of polygonal objects by three and four fingers. In each case the qualitative properties of the optimal fixture were characterized, and efficient algorithms developed for graphically or numerically finding the optimal fixture. The promise of the deflection quality measure is demonstrated by the intuitively effective minimum-deflection fixtures in the examples. It was also observed that the

definition of the deflection quality measure makes extensive use of velocity and wrench norms, which are special cases of kinematic metric functions. In the next two chapters the well-definedness of metric functions will be addressed, and frame-invariant norms will be developed.

Chapter 7

Objective and Frame-Invariant Kinematic Metric Functions for Rigid Bodies

7.1 Introduction

This chapter addresses the frame-invariance issue by considering objective rigid body kinematic metric functions. As discussed by Marsden and Hughes [99], objectivity is a general principle in mechanics. In particular, this principle has been used to characterize well-defined constitutive laws [51, 80, 99, 140, 160, 167]. The application of the objectivity principle in the context of rigid body kinematic metric functions allows accurate characterization of well-definedness conditions for such functions, and offers physical insight into left-, right- and bi-invariant functions on the space $SE(3)$.

7.1.1 A Motivating Example

To motivate the investigation of kinematic metric functions, and to observe the undesirable consequences of lack of frame-invariance, consider the following example where two candidate fixtures are to be compared. As shown in

Figure 7.1, a planar object of right triangular shape is compliantly fixtured by two candidate fixtures, and is subjected to a pure torque due to a drilling operation. The overall displacement caused by this torque is small and can be approximated by an instantaneous rigid displacement (or rigid body velocity). In each candidate fixture, the displacement is approximately an instantaneous rotation, which is of magnitude $0 < \theta \ll 1$ and centered at the common intersection point of the normal lines to the triangle's edges at the contacts. We wish to choose the fixture that allows the *smaller* displacement.

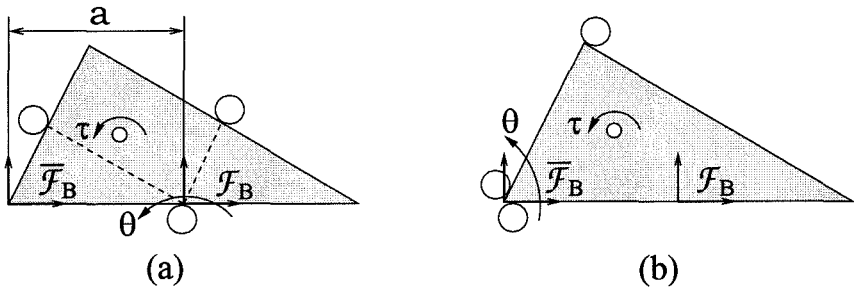

Figure 7.1: Two candidate fixtures: (a) Fixture I, and (b) Fixture II.

A notion of "lengths" is needed for comparison of two instantaneous displacements, . Using a body reference frame, a planar rigid body velocity can be written as a vector $\dot{q} = (v_x, v_y, \theta)$, where (v_x, v_y) is the velocity of the origin, and θ the angular velocity, relative to some stationary reference frame. A commonly used "length" formula is given by

$$\|\dot{q}\| = \sqrt{v_x^2 + v_y^2 + (\theta l)^2}, \tag{7.1}$$

where l is a characteristic object length that is used to make the rotational and translational velocities comparable.

Two candidate choices of body frame, $\mathcal{F}_B$ and $\bar{\mathcal{F}}_B$, are shown in the figure. With respect to $\mathcal{F}_B$, the body velocities for the two fixtures are given by $\dot{q}_1 = (0, 0, \theta)$ with "length" $\|\dot{q}_1\| = \theta l$, and $\dot{q}_2 = (0, \theta a, \theta)$ with "length" $\|\dot{q}_2\| =$

$\theta\sqrt{l^2+a^2}$, respectively. Since $\|\dot{q}_1\| < \|\dot{q}_2\|$, one would conclude that Fixture I is better.

However, with respect to $\bar{\mathcal{F}}_B$, the two instantaneous displacements are represented as $\dot{\bar{q}}_1 = (0, -\theta a, \theta)$ and $\dot{\bar{q}}_2 = (0, 0, \theta)$, respectively. Now, $\|\dot{\bar{q}}_1\| = \theta\sqrt{l^2+a^2}$ and $\|\dot{\bar{q}}_2\| = \theta l$. Thus $\|\dot{\bar{q}}_1\| > \|\dot{\bar{q}}_2\|$, which indicates that Fixture II is better! Formula (7.1) is therefore not well-defined: its dependence on choice of reference frame leads to conflicting conclusions.

To illustrate well-defined measurement of "lengths", consider the following "length" formula:

$$\|\dot{q}\| = \max\{\sqrt{(v_x - \theta y)^2 + (v_y + \theta x)^2} : \ (x, y) \in \mathcal{B}\}, \tag{7.2}$$

where $\mathcal{B}$ also denotes the region of $\mathbb{R}^2$ occupied by the body with respect to the given body frame. This formula can be interpreted as the maximal displacement of any particle in the body during an infinitesimal motion. Clearly, $\|\dot{q}\|$, as the maximal velocity of the body's particles, is frame-invariant. Applying this formula to compare the two instantaneous displacements yields $\|\dot{q}_1\| = \|\dot{\bar{q}}_1\| = \theta a$ and $\|\dot{q}_2\| = \|\dot{\bar{q}}_2\| = 2\theta a$. Therefore, with respect to either frame, one arrives at the following consistent conclusion: Fixture I allows a smaller maximum displacement and should hence be considered a better design. This indicates that Formula (7.2) is well-defined.

7.1.2 Kinematic Metric Functions

The above motivating example considered "lengths" of instantaneous rigid body displacements. Such lengths can be formalized as one of several types of kinematic metric functions, whose objectivity (or frame-invariance) is the main focus of this chapter.

A *kinematic metric function* is a real-valued function of configurations, tangent vectors or covectors; or more formally, it is a real-valued function on the configuration space or its vector (i.e., tangent and cotangent) bundles. The following types of metric functions are of practical interest. A *distance metric* on the c-space, formalizing the "distance" between two rigid body locations, is a positive definite function that maps two configurations to a real number. A *norm* or *inner product* on the tangent bundle or cotangent bundle assigns a norm or inner product to the tangent or cotangent space at each configuration. It is well-known that tangent vectors formalize rigid body velocities or instantaneous motions, and covectors formalize generalized forces or wrenches. Thus, a norm on the tangent or cotangent bundle formalizes the "lengths", and an inner product formalizes the "lengths" as well as "angles" of rigid body velocities or wrenches. While our focus will be on these types of kinematic metric functions, our formulation applies to functions that are not distances, norms or inner products. For example, the *magnitude* and *pitch* (in the screw coordinates) of a velocity or wrench may be regarded as kinematic metric functions as well.

7.1.3 Objectivity Illustrated

As illustrated by the motivating example, kinematic metric functions must be *well-defined* so as to give consistent results. When frames are used to describe rigid body kinematics, the well-definedness condition is manifested in terms of *frame-invariance*. However, there is a more fundamental interpretation of this condition, which is characterized by the notion of *objectivity*.

The idea of objectivity can be illustrated using norms on the tangent bundle of the c-space. Consider the two instantaneous motions of a triangular object shown in Figure 7.2. These motions are *congruent* in the sense that they can be made coincident by a rigid transformation, and may also be in-

terpreted as the *same* instantaneous motion as it appears to the observers shown in Figure 7.3. Since these two motions should clearly have the same size, a well-defined tangent vector norm should have the same value for these two motions. Two tangent vectors, such as these two instantaneous motions, are said to be *equivalent* if they can be brought into coincidence by making their base configurations coincide. A tangent vector norm is *objective* if it evaluates to the *same* value at equivalent tangent vectors. It follows that the notion of objectivity formalizes the natural requirement that *kinematic metric measurement be observer-indifferent.* It will be shown in Section 7.8 that the frame-invariant formula (7.2) is indeed an objective tangent vector norm, while the frame dependent formula (7.1) is not.

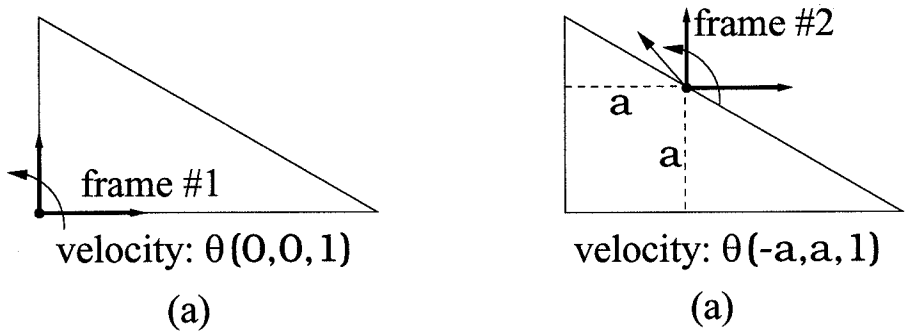

Figure 7.2: Two equivalent instantaneous motions.

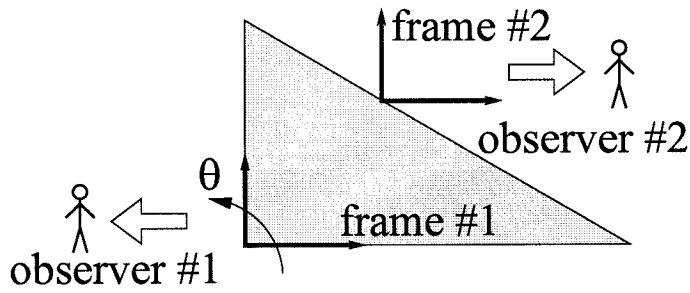

Figure 7.3: Two observers seeing the same motion.

7.1.4 Overview of the Approach and Resulting Findings

To facilitate the understanding of the formal notions developed in this chapter, we present an overview of our approach and the resulting findings. The approach is based on the intrinsically defined configuration space of a rigid body, which is addressed in Section 7.3 following a brief review of metric functions in Section 7.2. Key to the intrinsic c-space definition is the *differentiation* between three-dimensional Euclidean space, denoted $\mathbb{E}^3$, of axiomatically defined points, and three-dimensional Cartesian space, denoted $\mathbb{R}^3$, of triples of real numbers. The distinctions between $\mathbb{E}^3$ and $\mathbb{R}^3$ are discussed in Section 7.3.2, where it is noted that $\mathbb{E}^3$ is defined by axioms and involves *no* use of coordinate frames. However, as an *extra* structure, a coordinate frame can be embedded in $\mathbb{E}^3$ to give each point in $\mathbb{E}^3$ a set of coordinates (Section 7.4.1), and thus represent $\mathbb{E}^3$ by $\mathbb{R}^3$. Based on the axiomatic Euclidean space definition, Section 7.3.2 defines the *configuration* of a rigid body, denoted $\mathcal{B}$, as a map that places $\mathcal{B}$ in $\mathbb{E}^3$, and the *configuration space*, denoted $\mathcal{C}$, as the collection of such maps. This c-space definition is *intrinsic* in that it involves *no* coordinate frames. It is also *unambiguous* in that a given physical location of $\mathcal{B}$ corresponds to a *unique* configuration. In other words, there is only a *single* configuration space for a given rigid body.

While $\mathcal{C}$ is different from $SE(3)$, the conventional representation of the c-space of a rigid body, it can be represented by $SE(3)$ using a reference configuration and a coordinate frame embedded in $\mathbb{E}^3$. This representation is addressed in Section 7.4. The middle ground between $\mathcal{C}$ and $SE(3)$ is the set of rigid transformations on $\mathbb{E}^3$, which is denoted $\widetilde{SE}(3)$ and is introduced in Section 7.3.2. Based on the representation of $\mathbb{E}^3$ by $\mathbb{R}^3$ via an embedded frame, $\widetilde{SE}(3)$ can be represented by $SE(3)$ (Section 7.4.2). Since $\mathcal{C}$ can be represented by $\widetilde{SE}(3)$ using a *reference configuration* (Section 7.4.3), one can eventually represent $\mathcal{C}$ by $SE(3)$, as discussed in Section 7.4.4. While the conventional

representation of $\mathcal{C}$ by $SE(3)$ using body and world frames (Section 7.8.1) offers convenience in practical applications, the representation scheme developed in this chapter allows conceptual clarity in dealing with objective metric functions. The diagram shown in Figure 7.4 illustrates how the sets involved in Section 7.3 are inter-related.

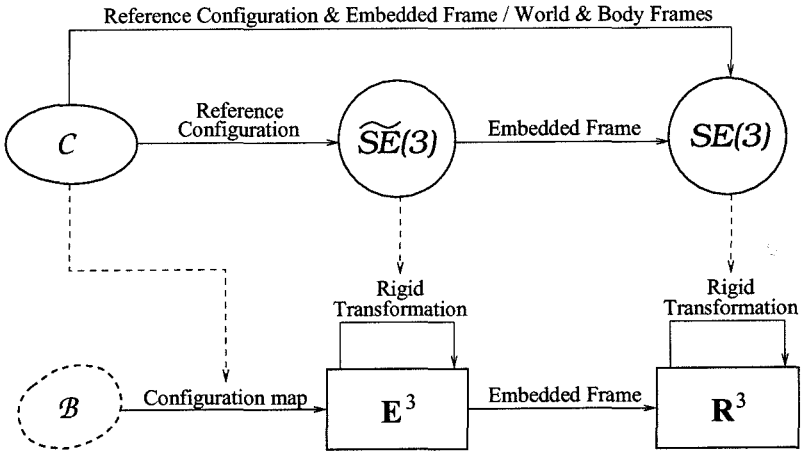

Figure 7.4: C-space definition and representation diagram.

The notion of objectivity is introduced in Section 7.6 based on the intrinsic c-space definition. While $\mathcal{C}$ is the configuration space of a rigid body, Euclidean space $\mathbb{E}^3$ can be regarded as the "configuration space" of a particle. This simple analogy suggests that we first consider the notion of objectivity in $\mathbb{E}^3$ (Section 7.5), and then use this case to motivate the notion of objectivity in $\mathcal{C}$. In both cases, the notions of *equivalent curves, tangent vectors and covectors* are used to define the notion of *objectivity*, which formalizes the natural requirement that metric functions be *indifferent to observers* who perform metric measurements (Sections 7.5.1 and 7.6.3).

A metric functions on $\mathcal{C}$ (or $\mathbb{E}^3$) can be represented as a family of metric functions on $SE(3)$ (or $\mathbb{R}^3$), which are generally *different* with respect to different choices of reference configuration and embedded frame. This is addressed in Section 7.7 (or 7.5), and is illustrated in Figure 7.5, which visualizes metric

functions as "rulers". The "rulers" on $SE(3)$ (or $\mathbb{R}^3$) have certain properties when the "ruler" on $\mathcal{C}$ (or $\mathbb{E}^3$) is objective. Section 7.5 shows that if a metric function on $\mathbb{E}^3$ is objective, then its representations, or the "rulers" in Figure 7.5, on $\mathbb{R}^3$ are *identical*. On the other hand, when a metric function on $\mathcal{C}$ is objective, the corresponding metric functions, or the "rulers" shown in Figure 7.5, on $SE(3)$ are *left invariant*, and are inter-related via pull-backs by right translations. These inter-related left invariant functions are in general *not* right invariant. However, when they are indeed right invariant, these generally different functions become a *unique* bi-invariant function regardless of choices of reference configuration and embedded frame. That is, the "rulers" on $SE(3)$, as shown in Figure 7.5, are *identical* if they are bi-invariant. But it is important to note that *bi-invariance is sufficient, but not necessary, for objectivity.*

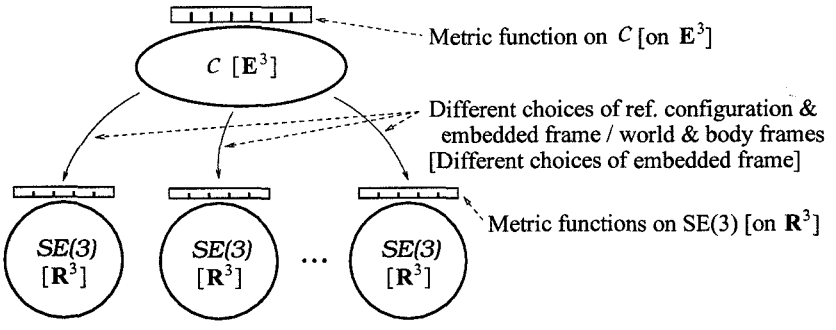

Figure 7.5: A metric function on $\mathcal{C}$ (or $\mathbb{E}^3$) represented by metric functions on $SE(3)$ (or $\mathbb{R}^3$).

To facilitate practical applications of the objectivity notion, Section 7.8 considers objective functions in the framework of the conventional approach where the rigid body's configuration is specified in terms of the location of a body frame relative to a world frame. The notion of frame-invariance is clarified by giving it an accurate definition, and show that an objective function is represented by metric functions on $SE(3)$ which are inter-related precisely by the frame-invariance condition. In other words, frame-invariant "rulers" on

$SE(3)$ in Figure 7.5 are equivalent to an objective "ruler" on $\mathcal{C}$.

7.2 Metric Functions on Manifolds

This section briefly reviews the notion of metric functions on manifolds. Recall from Section 3.1 that a smooth manifold is a generalization of smooth curves and surfaces in $\mathbb{R}^3$, on which tangent and cotangent bundles are also defined. We begin with the notion of diffeomorphisms on manifolds.

Let $f\colon M \to N$ be a map between smooth manifolds M and N, and let (ϕ, U) and (ψ, V) be charts for M and N, respectively. The *local expression* of f with respect to the two charts is the map $f_{loc} = \psi \circ f \circ \phi^{-1}\colon \phi(U) \to \psi(U)$. By definition f is *smooth* if all of its local expressions are smooth. f is said to be a *diffeomorphism* if it is a smooth bijection with a smooth inverse.

Let $f\colon M \to N$ be smooth. The *tangent map of f at $x \in M$* is a map $T_x f\colon T_x M \to T_{f(x)} N$ given by $T_x f(\dot{c}(0)) = (f \circ c)'(0)$ for any tangent vector $\dot{c}(0) \in T_x M$. The *tangent map of f* is a map $Tf\colon TM \to TN$ that is given by $T_x f$ when restricted to $T_x M$ for each $x \in M$. By definition of the tangent map, if (ϕ, U) is a chart around x, the coordinates of $\dot{c}(0) \in T_x M$ are given by $T\phi(\dot{c}(0))$. For smooth functions f and g, the *chain rule* holds: $T(g \circ f) = Tg \circ Tf$. Therefore, if f is a diffeomorphism, then Tf is bijective and $(Tf)^{-1} = T(f^{-1})$.

Given a smooth map $f\colon M \to N$, the *transpose* of the tangent map $T_x f$, where $x \in M$, is a linear map $(T_x f)^*\colon T^*_{f(x)} N \to T^*_x M$ defined by $(T_x f)^*(\beta) = \beta \circ T_x f$. When f is a diffeomorphism, the *cotangent* of f is defined as a map $T^*f\colon T^*N \to T^*M$ whose restriction to $T^*_y N$ is given by $T^*_y f = (T_{f^{-1}(y)} f)^*$. Thus one can simply write $T^*f(\beta) = \beta \circ Tf$ for any $\beta \in T^*N$. Clearly, T^*f is bijective and $(T^*f)^{-1} = T^*(f^{-1})$. Moreover, it can be shown that $T^*(g \circ f) = T^*f \circ T^*g$ where $g\colon N \to P$ is smooth. If (ϕ, U) is a chart around x, the

coordinates of $\alpha \in T_x^*M$ are given by $T^*\phi^{-1}(\alpha) = \alpha \circ T\phi^{-1}$, a linear functional on $\mathbb{R}^n$.

The following definition introduces the important notion of metric functions on a manifold. In the definition the superscripts s, k and l denote Cartesian products of sets.

Definition 7.2.1 (Metric functions on a manifold). Let M be a smooth manifold. A *metric function* on M is a real-valued function Θ on M of the form $\Theta\colon M^s \to \mathbb{R}$, or a real-valued function Φ on the vector (i.e., tangent and cotangent) bundles of M: for each $x \in M$, Φ assigns a function Φ_x of the form $\Phi_x\colon (T_xM)^k \times (T_x^*M)^l \to \mathbb{R}$. In particular, if Φ_x is linear in each of its arguments for each x, Φ is called a *multilinear function.*

In the following we review pull-backs and push-forwards of the above two types of metric functions, as well as pull-backs and push-forwards of smooth functions that map a manifold into itself. In Definitions 7.2.2 and 7.2.3, M and N are assumed to be smooth manifolds, and $f\colon M \to N$ and $g\colon N \to M$ are assumed to be diffeomorphisms[1].

Definition 7.2.2 (Pull-backs and push-forwards of metric functions). Let Θ and Φ be metric functions defined in Definition 7.2.1. The *pull-back* of the function Θ by g is a real-valued function on N defined by $g^*\Theta(y_1, \ldots, y_s) = \Theta(g(y_1), \ldots, g(y_s))$ for $(y_1, \ldots, y_s) \in N^s$. The *push-forward* of Θ by f is a map $f_*\Theta\colon N^s \to \mathbb{R}$ given by $f_*\Theta = (f^{-1})^*\Theta$. The *pull-back* of Φ by g, denoted by $g^*\Phi$, is a real-valued function on the vector bundles of N defined, for each

[1] A diffeomorphism is actually not required to define the pull-back of a real-valued function on a manifold or its tangent bundle. However, only pull-backs defined by a diffeomorphism will be considered in this chapter.

$y \in N$, by

$$g^*\Phi_y(\mathbf{u}_1, \ldots, \mathbf{u}_k, \boldsymbol{\beta}_1, \ldots, \boldsymbol{\beta}_l) \\ = \Phi_{g(y)}(Tg(\mathbf{u}_1), \ldots, Tg(\mathbf{u}_k), T^*g^{-1}(\boldsymbol{\beta}_1), \ldots, T^*g^{-1}(\boldsymbol{\beta}_l))$$

where $(\mathbf{u}_1, \ldots, \mathbf{u}_k) \in (T_yN)^k$ and $(\boldsymbol{\beta}_1, \ldots, \boldsymbol{\beta}_l) \in (T_y^*N)^l$. The *push-forward* of Φ by f is defined by $f_*\Phi = (f^{-1})^*\Phi$.

In addition to metric functions, the pull-back and push-forward maps can be defined for a smooth function that maps a manifold into itself.

Definition 7.2.3 (Another Type of pull-backs and push-forwards). The *pull-back* of a smooth function $\varphi\colon M \to M$ by g is a map $g^*\varphi\colon N \to N$ defined by $g^*\varphi = g^{-1} \circ \varphi \circ g$. The *push-forward* of φ by f is a map $f_*\varphi\colon N \to N$ given by $f_*\varphi = (f^{-1})^*\varphi = f \circ \varphi \circ f^{-1}$.

By the definitions of pull-back and push-forward maps, the following lemma can be easily proved.

Lemma 7.2.1. *Let $f\colon M \to N$ and $g\colon N \to P$ be diffeomorphisms between manifolds. Let $\bar{\Psi}$ be a metric function on M or a smooth function mapping M into itself, and let Ψ be a similar function whose domain is associated with P. Then,*

$$(g \circ f)^*\Psi = f^*g^*\Psi \quad \textit{and} \quad (g \circ f)_*\bar{\Psi} = g_*f_*\bar{\Psi}.$$

Remark 7.2.1. Pull-back or push-forward maps can be used as *representations* of functions. Let $f\colon M \to N$ be a diffeomorphism, where M is an *abstract* manifold and N a subset of $\mathbb{R}^n$. While M is not a subset of $\mathbb{R}^n$ and a function defined on M may be difficult for direct calculations, the push-

forward by f of the function can be more manipulable. This is illustrated by the metric functions in the following simple example.

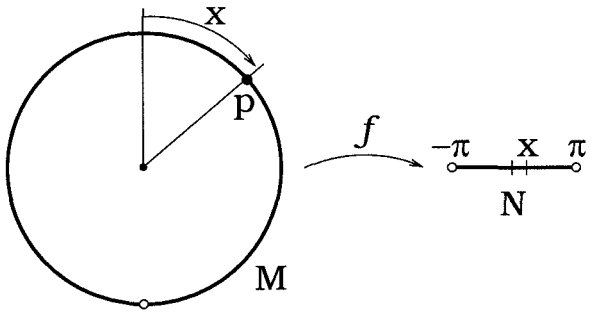

Figure 7.6: A diffeomorphism f: $M \to N$.

Example 7.2.1. Figure 7.6 shows a manifold M, which is a unit circle with its south pole removed. Let s be a non-negative function such that $s(p_1, p_2)$ is the length of the arc between the points p_1 and p_2 in M. Define $\bar{\Theta}$: $M \times M \to \mathbb{R}$ by $\bar{\Theta}(p_1, p_2) = s(p_1, p_2)$, and define $\bar{\Phi}$: $TM \to \mathbb{R}$ by $\bar{\Phi}_p(\dot{c}(0)) = |\frac{d}{dt}|_{t=0} s(p, c(t))|$ for a tangent vector $\dot{c}(0) \in T_pM$ which is the velocity of a curve $c(t)$ such that $c(0) = p$. As can be shown, $\bar{\Theta}$ is a distance on M, and $\bar{\Phi}$ a norm on TM, respectively. Now consider the representation of these metric functions on the open interval $N = (-\pi, \pi)$ via the diffeomorphism f: $M \to N$ defined by $f(p) = x$, where x is the signed arc length, positive if clockwise, from the north pole to p. Let $\Theta = f_* \bar{\Theta}$ and $\Phi = f_* \bar{\Phi}$, which are defined on N and TN. For $x, x_1, x_2 \in N$ and $v \in T_xN \cong \mathbb{R}$, one has $\Theta(x_1, x_2) = \bar{\Theta}(f^{-1}(x_1), f^{-1}(x_2)) = |x_1 - x_2|$, and $\Phi_x(v) = \bar{\Phi}_{f^{-1}(x)}(Tf^{-1}(v)) = |v|$.

Using the notion of pull-back maps, we can introduce a notion of invariance of metric functions characterized by the following definition and lemma.

Definition 7.2.4 (f-invariance). Let M be a smooth manifold and f: $M \to M$ be a smooth function. A metric function Ψ on M, of the types given in Definition 7.2.1, is said to be *f-invariant* if $f^*\Psi = \Psi$.

Lemma 7.2.2. *Let $f\colon M \to M$ be a smooth function and $g\colon M \to N$ a diffeomorphism, where M and N are smooth manifolds. A metric function Ψ is f-invariant if and only if $g_*\Psi$, a metric function on N, is g_*f-invariant. That is, $f^*\Psi = \Psi$ if and only if $(g_*f)^*(g_*\Psi) = g_*\Psi$.*

We will be particularly interested in invariant functions on Lie groups, which are briefly reviewed here. A *Lie group* is a group G (with identity element denoted by e) which is also a smooth manifold and for which the group operations $(g,h) \mapsto gh$ and $g \mapsto g^{-1}$ are smooth. For every $g \in G$, define $L_g\colon G \to G$, called a *left translation*, and $R_g\colon G \to G$, a *right translation*, by $L_g(h) = gh$ and $R_g(h) = hg$ for $h \in G$, respectively. Note that L_g and R_g are both diffeomorphisms, with inverses given by $(L_g)^{-1} = L_{g^{-1}}$ and $(R_g)^{-1} = R_{g^{-1}}$, respectively. Moreover, left and right translations commute: $L_g \circ R_h = R_h \circ L_g$. Define the *inner automorphism* of G associated with g, denoted $I_g\colon G \to G$, by $I_g = L_g \circ R_{g^{-1}} = R_{g^{-1}} \circ L_g$. The tangent map $Ad_g = T_eI_g$, an isomorphism on T_eG, is called the *adjoint* associated with g.

Definition 7.2.5 (Invariance on a Lie group). A metric function Ψ on a Lie group G is said to be *left invariant* if Ψ is L_g-invariant, i.e., $L_g^*\Psi = \Psi$, for all $g \in G$. It is *right invariant* if $R_g^*\Psi = \Psi$ for all $g \in G$. If Ψ is both left and right invariant, it is said to be *bi-invariant.*

It is well-known that the space $SE(3)$ is a Lie group. Therefore, the notions of left and right invariance are relevant. It is one of the goals of this chapter to seek physical implications of these invariance properties, and clarify their relationship to well-defined requirements of kinematic metric functions.

7.3 Configuration Space of a Rigid Body

This section defines the configuration space (c-space) of a rigid body in an intrinsic, frame-free manner and considers its representation as $SE(3)$. For

this purpose, a motivational discussion on such an intrinsic c-space definition is of interest.

7.3.1 Motivation for an Intrinsic Definition

Traditionally, the configuration of a rigid body is specified as the location of a body frame relative to a stationary world frame, and the configuration space is defined as the set of all possible body frame locations. This c-space definition, while convenient for practical calculations, suffers from a major ambiguity.

The ambiguity lies in the frame dependence of configuration specification. With respect to different choices of reference frames, a given physical location of the body corresponds to *different* relative body frame locations, and a rigid body velocity or wrench corresponds to *different* tangent vectors or covectors associated with the frame choices. Thus, there are infinitely many copies of "configuration spaces". This ambiguity causes much confusion when one considers, for example, the "distance" between the body's locations, or the "length" of rigid body velocities or wrenches. The common approach that uses a single distance metric or norm for all "c-space" copies leads to inconsistent results, as demonstrated by formula (7.1). To obtain consistent results, *different* distance metrics or norms associated with the different "c-space" copies must be used. Then, how should one choose these metrics or norms? One may choose a particular distance metric or norm associated with a particular copy of "configuration space", and determine distance metrics or norms associated with other "c-space" copies in such a way that the results are consistent. However, which "c-space" copy should one start from? Since there is no natural way of choosing reference frames, there is no natural way of choosing this preferred copy of "configuration space"! In such a situation, it becomes very difficult to gain a clear understanding of the conditions that guarantee well-defined notions of "distances" and "lengths".

Fortunately, the ambiguity in the conventional c-space definition can be eliminated by using an intrinsic c-space definition considered in the remainder of this section. According to such an intrinsic definition, there is a *unique* copy of configuration space associated with a given rigid body. That is, each physical location of the body corresponds to a *single* configuration, and each instantaneous motion or wrench corresponds to a *single* tangent or cotangent vector.

7.3.2 The Configuration Space of a Rigid Body: An Intrinsic Definition

This subsection considers an intrinsic definition of the configuration space of a rigid body. This definition, involving no reference frames, explores the distinction between Euclidean space and Cartesian space. Frame-free definitions of Euclidean space have been used in continuum mechanics theory, for example, by Noll [117].

Three-dimensional *Euclidean space*, denoted by $\mathbb{E}^3$, is a geometric model for the physical space. It is defined in terms of three systems of geometric objects: *points*, *(straight) lines* and *planes* which are related by the axioms of incidence, order, congruence, and parallels as summarized in Appendix C. For the purposes of this chapter, it suffices to recognize that the axiomatic definition of Euclidean space does *not* involve any coordinate frames, and in consequence Euclidean space $\mathbb{E}^3$ must be *distinguished* from Cartesian space $\mathbb{R}^3$. For example, a point in $\mathbb{E}^3$ is *not* a triple of real numbers, and a straight line in $\mathbb{E}^3$ is *not* a linear algebraic equation. As remarked by Boothby [14], Euclid and other great geometers before the seventeenth century defined and studied Euclidean space only axiomatically; without the tool of analytical geometry, which was yet to be invented by Fermat and Descartes, they clearly did not think of $\mathbb{E}^3$ as triples of real numbers. While each point of $\mathbb{E}^3$ can be

assigned a set of coordinates as discussed in Section 7.4.1, this representation of $\mathbb{E}^3$ by $\mathbb{R}^3$ is only achieved by embedding a coordinate frame in $\mathbb{E}^3$ and is hence unnatural.

In addition to distinguishing $\mathbb{E}^3$ from $\mathbb{R}^3$, one also needs to distinguish $\widetilde{SE}(3)$, the set of rigid transformations on $\mathbb{E}^3$ defined as follows, from $SE(3)$, the set of rigid transformations on $\mathbb{R}^3$.

Definition 7.3.1 (Rigid transformations of $\mathbb{E}^3$). Let $U \subset \mathbb{E}^3$ contain at least four points not in a plane[2]. A map $\widetilde{g}\colon U \to \mathbb{E}^3$ is called a *rigid transformation of* U if it preserves distance and orientation[3]. If $U = \mathbb{E}^3$, then $\widetilde{g}$ is said to be a *rigid transformation of* $\mathbb{E}^3$. The set of all rigid transformations on $\mathbb{E}^3$ is denoted by $\widetilde{SE}(3)$.

It can be shown that a rigid transformation of a subset of $\mathbb{E}^3$ containing at least four non-coplanar points can be uniquely extended to a rigid transformation of $\mathbb{E}^3$. Thus, one can naturally identify these two rigid transformations, and thereby naturally identify the set of all rigid transformations of a subset of $\mathbb{E}^3$ with $\widetilde{SE}(3)$.

The spaces $\mathbb{E}^3$ and $\widetilde{SE}(3)$ can be used to define the configuration space of a rigid body as follows.

Definition 7.3.2 (Rigid bodies and their configuration spaces). A set $\mathcal{B}$ consisting of at least four elements is said to be a *rigid body* if there is a nonempty set of mappings, denoted $\mathcal{C}$, with the following properties.

(1) Each map $\chi \in \mathcal{C}$ is a bijection from $\mathcal{B}$ onto a closed subset of $\mathbb{E}^3$ such that $\chi(\mathcal{B})$ is not contained in a plane;

[2] A set of three non-collinear points of $\mathbb{E}^3$ is not sufficient to determine whether a distance-preserving transformation is orientation-preserving or orientation-reversing. But if this transformation is *known* to be orientation-preserving, then it can be uniquely determined by the three-point set.

[3] It suffices to understand the distance and orientation in the context of elementary solid geometry. These notions, along with distance- and orientation-preserving maps, are formally defined in Appendix C.

(2) Given any $\chi_1, \chi_2 \in \mathcal{C}$, the *transition map* $\chi_2 \circ \chi_1^{-1} \colon \chi_1(\mathcal{B}) \to \chi_2(\mathcal{B})$ is a rigid transformation of $\chi_1(\mathcal{B}) \subset \mathbb{E}^3$, i.e., $\chi_2 \circ \chi_1^{-1} \in \widetilde{SE}(3)$.

The elements of $\mathcal{B}$ are called *particles* or *points*. Each map $\chi \in \mathcal{C}$ is called a *configuration* of the body, and $\mathcal{C}$ is called the *configuration space* of $\mathcal{B}$.

Remark 7.3.1. Intuitively, a configuration $\chi \in \mathcal{C}$ may be thought of as a *placement* of the rigid body at some location in $\mathbb{E}^3$, and a transition map $\chi_2 \circ \chi_1^{-1} \in \widetilde{SE}(3)$, where $\chi_1, \chi_2 \in \mathcal{C}$, may be regarded as a *(rigid) displacement* of the body, as shown in Figure 7.7. Thus, a rigid body is a set of particles that move in $\mathbb{E}^3$ in such a way that distance and orientation are preserved.

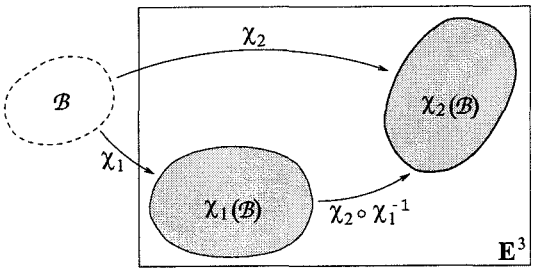

Figure 7.7: Placement and displacement of a rigid body.

Definition 7.3.2 is *intrinsic* in that it does *not* involve any coordinate frames. A rigid body and its configuration space are defined using maps involving an abstract set $\mathcal{B}$ and Euclidean space $\mathbb{E}^3$, which is axiomatically defined and involves no coordinate frames. Also, note that this definition does *not* use any reference configuration[4]; in this sense all configurations are of equal significance. Given a rigid body, there is *one and only one* copy of configuration space (a set of mappings), which will allow an unambiguous understanding of rigid body kinematics.

[4]As will be discussed in Section 7.4.3, an arbitrary *reference configuration* can be chosen so that any configuration may be identified with the displacement (Remark 7.3.1) from the reference configuration to that configuration.

7.4 Representation of the Configuration Space

The configuration space, defined in Definition 7.3.2 in an intrinsic and frame-free fashion, affords conceptual clarity and will later allow the clarification of the notion of objectivity (Section 7.6). However, this abstract entity is obviously not amenable to practical calculations. Fortunately, $\mathcal{C}$ can be represented by $SE(3)$, the set of rigid transformations of $\mathbb{R}^3$, and hence matrix algebra can be used for symbolic and numerical calculations.

The representation of $\mathcal{C}$ by $SE(3)$ is the subject of this section. The idea is to use $\widetilde{SE}(3)$, the set of rigid transformations of $\mathbb{E}^3$, as an intermediate set bridging $\mathcal{C}$ and $SE(3)$. It will be shown that while $\widetilde{SE}(3)$ can be represented by $SE(3)$, the set $\mathcal{C}$ can be represented by $\widetilde{SE}(3)$. Thus, concatenating the two representations allows the representation of $\mathcal{C}$ by $SE(3)$. We start with the representation of $\mathbb{E}^3$ by $\mathbb{R}^3$, which will lead to that of $\widetilde{SE}(3)$ by $SE(3)$.

7.4.1 Representation of $\mathbb{E}^3$ by $\mathbb{R}^3$

Euclidean space $\mathbb{E}^3$ can be represented by Cartesian space $\mathbb{R}^3$ in terms of a coordinate frame embedded in $\mathbb{E}^3$. Because there are many choices of embedded frames, the following notational convention is introduced.

Notational Convention. Choose a *nominal* embedded frame and denote it by $\mathcal{F}_X$. An arbitrary embedded frame is denoted by $\mathcal{F}_X^b$, where the superscript b always means that $\mathcal{F}_X^b$ is displaced from $\mathcal{F}_X$ by $b \in SE(3)$.

Note that $\mathcal{F}_X^e = \mathcal{F}_X$, where e is the identity element of $SE(3)$. Since each point in $\mathbb{E}^3$ has a unique set of coordinates with respect to an embedded frame, a corresponding map from $\mathbb{E}^3$ to $\mathbb{R}^3$ can be defined as follows.

Definition 7.4.1 (Coordinate maps). The *coordinate map* associated with an embedded frame $\mathcal{F}_X^b$ is a bijection $X^b\colon \mathbb{E}^3 \to \mathbb{R}^3$, such that the coordinates

of each $p \in \mathbb{E}^3$ in $\mathcal{F}_X^b$ are given by $X^b(p) \in \mathbb{R}^3$. In particular, the notation $X \triangleq X^e$ will be used for the coordinate map associated with the nominal embedded frame $\mathcal{F}_X$.

Remark 7.4.1. Because the map X^b gives a one-to-one correspondence between the elements of $\mathbb{E}^3$ and $\mathbb{R}^3$, Euclidean space $\mathbb{E}^3$ is trivially a smooth manifold with a global chart $(X^b, \mathbb{E}^3)$, and X^b is a diffeomorphism by design.

Remark 7.4.2. $\mathbb{E}^3$ and $\mathbb{R}^3$ may be identified via the map X^b, and for this reason, $\mathbb{R}^3$ is sometimes simply referred to as the "Euclidean space". However, this identification involves an embedded frame, whose choice is arbitrary and cannot be naturally given. To avoid confusion, this unnatural identification will not be used.

Now consider the relationship between the coordinate maps X^b and X. Suppose that $x \in \mathbb{R}^3$ is the coordinates of some point $p \in \mathbb{E}^3$ with respect to the nominal frame $\mathcal{F}_X$, then the coordinates of p in the frame $\mathcal{F}_X^b$ are given by $X^b \circ X^{-1}(x) = b^{-1}x$. The arbitrariness of x yields

Lemma 7.4.1. *The coordinate maps X and X^b, which are associated with the embedded frames $\mathcal{F}_X$ and $\mathcal{F}_X^b$, are related by $X^b \circ X^{-1} = b^{-1}$, or $X \circ (X^b)^{-1} = b$.*

7.4.2 Representation of $\widetilde{SE}(3)$ by $SE(3)$

There is a close relationship between the rigid transformation groups $\widetilde{SE}(3)$ and $SE(3)$, which will allow the use of $SE(3)$ to represent the c-space $\mathcal{C}$.

Given an embedded frame $\mathcal{F}_X^b$, the associated coordinate map X^b is a diffeomorphism of $\mathbb{E}^3$ onto $\mathbb{R}^3$. For any rigid transformation $\widetilde{g} \in \widetilde{SE}(3)$, the push-forward $X_*^b\widetilde{g}$, as defined in Definition 7.2.3, maps $\mathbb{R}^3$ into itself. Moreover, it can be shown that $X_*^b\widetilde{g}$ is actually a rigid transformation of $\mathbb{R}^3$. Hence $X_*^b\widetilde{g}$ can be regarded as a *representation* of $\widetilde{g}$ and the following definition can be given.

Definition 7.4.2 (Rigid transformation representation maps). The *rigid transformation representation map* corresponding to the embedded frame $\mathcal{F}_X^b$ is a mapping $F^b\colon \widetilde{SE}(3) \to SE(3)$ defined by $F^b(\widetilde{g}) = X_*^b\widetilde{g} = X^b \circ \widetilde{g} \circ (X^b)^{-1}$ for $\widetilde{g} \in \widetilde{SE}(3)$. The notation $F \triangleq F^e$ will be used.

Remark 7.4.3. The sets $\widetilde{SE}(3)$ and $SE(3)$ may be identified via the map F^b. In fact, $SE(3)$ is often simply referred to as *the* special Euclidean group. However, similar to the case of $\mathbb{E}^3$ and $\mathbb{R}^3$, this identification is unnatural since it involves an arbitrary choice of embedded frame. Each choice of embedded frame leads to a *different* copy of $SE(3)$, and there is *no* natural way of choosing a particular copy and identifying it with $\widetilde{SE}(3)$.

The rigid transformation representation map F^b can be interpreted as follows. Consider $\widetilde{g} \in \widetilde{SE}(3)$, which corresponds to $g = F^b(\widetilde{g}) \in SE(3)$. The coordinates of any $p \in \mathbb{E}^3$ are given by $X^b(p)$, and those of $\widetilde{g}(p)$ by $X^b(\widetilde{g}(p))$, in the embedded frame $\mathcal{F}_X^b$. These coordinates are related by $X^b(\widetilde{g}(p)) = \big(X^b \circ \widetilde{g} \circ (X^b)^{-1}\big)(X^b(p)) = g(X^b(p))$. Therefore, as illustrated in Figure 7.8, g is the displacement of $\mathcal{F}_X^b$ if $\mathcal{F}_X^b$ moves along with $\mathbb{E}^3$ according to $\widetilde{g}$.

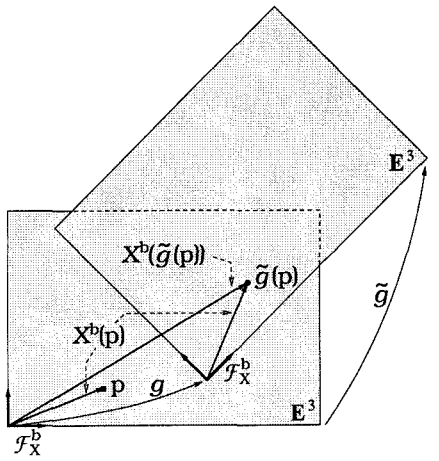

Figure 7.8: Geometric interpretation of $g = X^b \circ \widetilde{g} \circ (X^b)^{-1}$.

Rigid transformation representation maps corresponding to different choices

of embedded frame are related by the following lemma.

Lemma 7.4.2. *The rigid transformation representation maps F and F^b corresponding to the embedded frames $\mathcal{F}_X$ and $\mathcal{F}_X^b$ have the following relationship: $F^b \circ F^{-1} = I_b^{-1}$, or $F \circ F^{b^{-1}} = I_b$, where $I_b = L_b \circ R_{b^{-1}}$.*

Proof. Lemma 7.4.1, which relates the maps X^b and X, implies that for any $g \in SE(3)$, $F^b \circ F^{-1}(g) = F^b(X^{-1} \circ g \circ X) = X^b \circ X^{-1} \circ g \circ X \circ (X^b)^{-1} = b^{-1}gb = I_b^{-1}(g)$. Using the arbitrariness of g completes the proof. □

Similar to $SE(3)$, it can be shown that $\widetilde{SE}(3)$ is a Lie group, on which two systems of diffeomorphisms—left translations and right translations—naturally arise. The following lemma relates such maps to left and right translations on $SE(3)$.

Lemma 7.4.3. *Given an embedded frame $\mathcal{F}_X^b$, left and right translations on $\widetilde{SE}(3)$ are represented by left and right translations on $SE(3)$, respectively. Specifically, for $\widetilde{g} \in \widetilde{SE}(3)$, we have $F_*^b \widetilde{L}_{\widetilde{g}} = L_{F^b(\widetilde{g})}$ and $F_*^b \widetilde{R}_{\widetilde{g}} = R_{F^b(\widetilde{g})}$.*

Proof. For any $h \in SE(3)$, Definition 7.4.2 implies that

$$\begin{aligned} F_*^b \widetilde{L}_{\widetilde{g}}(h) &= F^b \circ \widetilde{L}_{\widetilde{g}} \circ (F^b)^{-1}(h) = F^b(\widetilde{L}_{\widetilde{g}}((X^b)^{-1} \circ h \circ X^b)) \\ &= F^b(\widetilde{g} \circ (X^b)^{-1} \circ h \circ X^b) = X^b \circ \widetilde{g} \circ (X^b)^{-1} \circ h = F^b(\widetilde{g})h = L_{F^b(\widetilde{g})}(h). \end{aligned}$$

The case of right translation is similar. The arbitrariness of h and Lemma 7.4.2 lead to the desired conclusion. □

7.4.3 Representation of $\mathcal{C}$ by $\widetilde{SE}(3)$

The representation of $\mathcal{C}$ by $\widetilde{SE}(3)$ is achieved by use of a *reference configuration*: any configuration can be represented by a rigid displacement (i.e., the transition map) from the reference configuration to that configuration. Since

there are an infinite number of reference configurations, we introduce a notational convention, which is followed by the definition of maps representing $\mathcal{C}$ by $\widetilde{SE}(3)$.

Notational Convention. Choose a *nominal* reference configuration $\chi_0 \in \mathcal{C}$. Denote by $\chi_{\widetilde{a}}$ an arbitrary reference configuration, where the subscript $\widetilde{a}$ always indicates that $\chi_{\widetilde{a}}$ is determined by $\chi_{\widetilde{a}} \circ \chi_0^{-1} = \widetilde{a} \in \widetilde{SE}(3)$. That is, $\chi_{\widetilde{a}}$ is displaced from χ_0 by $\widetilde{a}$.

Definition 7.4.3 (Intermediate c-space representation maps). Corresponding to an arbitrary reference configuration $\chi_{\widetilde{a}} \in \mathcal{C}$, the *intermediate c-space representation map* is a mapping $J^{\widetilde{a}} \colon \mathcal{C} \to \widetilde{SE}(3)$ defined by $J^{\widetilde{a}}(\chi) = \chi \circ \chi_{\widetilde{a}}^{-1}$ for any $\chi \in \mathcal{C}$. In particular, we write $J \triangleq J^{\widetilde{e}}$, which corresponds to χ_0.

In other words, $J^{\widetilde{a}}(\chi)$, a rigid transformation of $\mathbb{E}^3$, is the displacement of the rigid body $\mathcal{B}$ from $\chi_{\widetilde{a}}(\mathcal{B})$ to $\chi(\mathcal{B})$. Since the map $J^{\widetilde{a}}$ is bijective and establishes a one-to-one relationship between the sets $\mathcal{C}$ and $\widetilde{SE}(3)$, the c-space $\mathcal{C}$ can be represented by $\widetilde{SE}(3)$. However, it is important to note that this representation depends on the choice of reference configuration. Therefore, $\mathcal{C}$ and $\widetilde{SE}(3)$ *cannot* be naturally identified. The effect of choices of reference configuration is given by the following lemma.

Lemma 7.4.4. *The intermediate c-space representation maps corresponding to different reference configurations are related by* $J^{\widetilde{a}} \circ J^{-1} = \widetilde{R}_{\widetilde{a}}^{-1}$, *or* $J \circ (J^{\widetilde{a}})^{-1} = \widetilde{R}_{\widetilde{a}}$.

Proof. For any $\widetilde{g} \in \widetilde{SE}(3)$, we have

$$J^{\widetilde{a}} \circ J^{-1}(\widetilde{g}) = J^{\widetilde{a}}(\widetilde{g} \circ \chi_0) = \widetilde{g} \circ \chi_0 \circ \chi_{\widetilde{a}}^{-1} = \widetilde{g} \circ \widetilde{a}^{-1} = \widetilde{R}_{\widetilde{a}}^{-1}(\widetilde{g}),$$

where $\widetilde{R}_{\widetilde{a}}$ is a right translation on $\widetilde{SE}(3)$ by $\widetilde{a}$. Since $\widetilde{g}$ is arbitrary, the desired relationship follows. □

7.4.4 Representation of $\mathcal{C}$ by $SE(3)$

We have derived the representation of $\mathcal{C}$ by $\widetilde{SE}(3)$, and that of $\widetilde{SE}(3)$ by $SE(3)$. By concatenating the two representations, $\mathcal{C}$ can be represented by $SE(3)$ as follows. This approach, illustrated by the diagram shown in Figure 7.9, clarifies all of the assumptions regarding embedded frames and reference configurations.

Definition 7.4.4 (C-space representation maps). The *c-space representation map* corresponding to a reference configuration $\chi_{\widetilde{a}}$ and an embedded frame $\mathcal{F}_X^b$ is a map $\Gamma^{\widetilde{a},b}\colon \mathcal{C} \to SE(3)$ defined by $\Gamma^{\widetilde{a},b} = F^b \circ J^{\widetilde{a}}$, where $J^{\widetilde{a}}$ and F^b are defined in Definitions 7.4.2 and 7.4.3. In particular, $\Gamma \triangleq \Gamma^{\widetilde{e},e} = F \circ J$ corresponds to the nominal reference configuration χ_0 and embedded frame $\mathcal{F}_X$.

Remark 7.4.4. A c-space representation map establishes a one-to-one correspondence[5] between $\mathcal{C}$ and $SE(3)$, which can be used to identify the two sets. However, this identification is *unnatural* in that it involves an arbitrary choice of reference configuration and embedded frame. Thus, if used without caution it may hamper the clarification of objective functions.

The one-to-one correspondence between $\mathcal{C}$ and $SE(3)$ implies that $\mathcal{C}$ is a smooth manifold. Therefore, the notions of tangent vectors and covectors to $\mathcal{C}$ are well-defined, which can be used to formalize the intuitive notions of rigid body velocities and wrenches. The following lemma characterizes the effect of

[5]While a one-to-one correspondence between $\mathcal{C}$ and $SE(3)$ can be equivalently established using world and body frames (Section 7.8), the use of a reference configuration and an embedded frame is more conducive to clarifying the notion of objectivity.

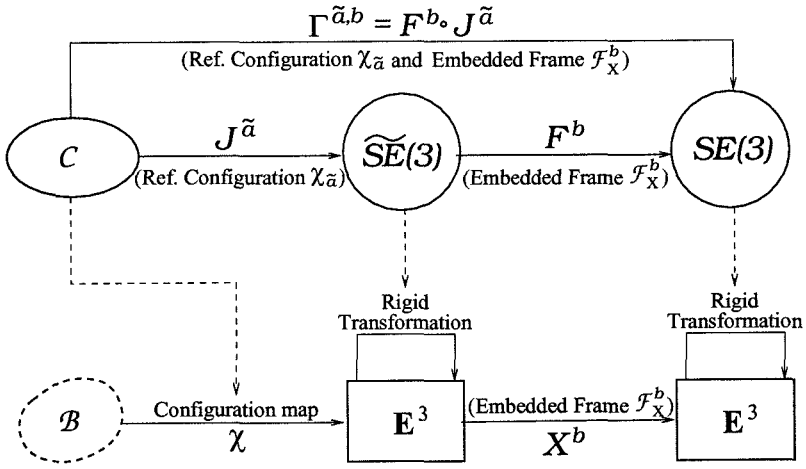

Figure 7.9: C-space definition and representation diagram.

choices of reference configuration and embedded frame on the representation of $\mathcal{C}$ by $SE(3)$.

Lemma 7.4.5. *The relationship between the c-space representation maps* $\Gamma^{\widetilde{a},b}$ *and* Γ *is given by* $\Gamma^{\widetilde{a},b} \circ \Gamma^{-1} = L_{b^{-1}} \circ R_{(F(\widetilde{a}))^{-1}b} = R_{(F(\widetilde{a}))^{-1}b} \circ L_{b^{-1}}$.

Proof. By Lemmas 7.4.2, 7.4.3 and 7.4.4,

$$\begin{aligned}\Gamma^{\widetilde{a},b} \circ \Gamma^{-1} &= F^b \circ J^{\widetilde{a}} \circ J^{-1} \circ F^{-1} = F^b \circ \widetilde{R}_{\widetilde{a}}^{-1} \circ F^{-1} \\ &= (F^b \circ F^{-1}) \circ (F \circ \widetilde{R}_{\widetilde{a}}^{-1} \circ F^{-1}) = I_b^{-1} \circ (F_* \widetilde{R}_{\widetilde{a}}^{-1}) = I_b^{-1} \circ R_{F(\widetilde{a})}^{-1}.\end{aligned}$$

Using $I_b = L_b \circ R_{b^{-1}}$ completes the proof. □

This lemma indicates that if a physical location of $\mathcal{B}$ is represented by $g \in SE(3)$ with respect to the reference configuration χ_0 and embedded frame $\mathcal{F}_X$, then it is represented by $b^{-1} g a^{-1} b \in SE(3)$ with respect to the reference configuration $\chi_{\widetilde{a}}$ and embedded frame $\mathcal{F}_X^b$, where $a = F(\widetilde{a})$ is the representation of $\widetilde{a} \in \widetilde{SE}(3)$ via the embedded frame $\mathcal{F}_X$.

7.5 Objective Metric Functions on $\mathbb{E}^3$

This section discusses the notion of objectivity in Euclidean space $\mathbb{E}^3$. While this will lead to some well-known facts in $\mathbb{R}^3$, it motivates the consideration of objective metric functions on $\mathcal{C}$, the intrinsically defined configuration space of a rigid body, in an analogous manner.

7.5.1 Formal Definition of Objectivity in $\mathbb{E}^3$

Euclidean space $\mathbb{E}^3$ can be regarded as the "configuration space" of a particle. A point in $\mathbb{E}^3$ can be thought of as the position of the particle; a tangent vector to $\mathbb{E}^3$ can be considered as the velocity of the particle; a covector is a force acting on the particle. First consider the notion of equivalent curves in $\mathbb{E}^3$.

Definition 7.5.1 (Equivalent curves in $\mathbb{E}^3$). Let $\widetilde{\gamma}_1$ and $\widetilde{\gamma}_2$ be two curves in Euclidean space $\mathbb{E}^3$ parametrized by the same parameter $t \in I$, where I is an open interval $(-\epsilon, \epsilon)$ $(\epsilon > 0)$ or closed interval $[0, 1]$. If there exists a rigid transformation $\widetilde{g} \in \widetilde{SE}(3)$ such that $\widetilde{\gamma}_2(t) = \widetilde{g}(\widetilde{\gamma}_1(t))$ for all $t \in I$, then $\widetilde{\gamma}_2$ is said to be *equivalent* to $\widetilde{\gamma}_1$ with respect to $\widetilde{g}$.

Clearly, equivalence of curves is an equivalence relation, which has some interesting interpretations. Two equivalent curves can be thought of as the *congruent* trajectories of two moving particles; that is, the trajectories can be made coincident by a rigid transformation. Alternatively, the two equivalent curves can be interpreted as the trajectory of *one* particle as viewed by *different observers* whose locations differ by a rigid displacement. This is illustrated by the equivalent curves shown in Figure 7.10.

Given a pair of points in $\mathbb{E}^3$, one can always find a curve with these points as endpoints. This observation and the notion of equivalent curves lead to the definition of equivalent pairs of points, which is illustrated in Figure 7.10(a).

Definition 7.5.2 (Equivalent pairs of points in $\mathbb{E}^3$). Two pairs of points $p_1, q_1 \in \mathbb{E}^3$ and $p_2, q_2 \in \mathbb{E}^3$ are said to be *equivalent* if there are two equivalent curves $\widetilde{\gamma}_1, \widetilde{\gamma}_2 \colon [0,1] \to \mathbb{E}^3$ such that $\widetilde{\gamma}_i(0) = p_i$, $\widetilde{\gamma}_i(1) = q_i$ for $i = 1, 2$.

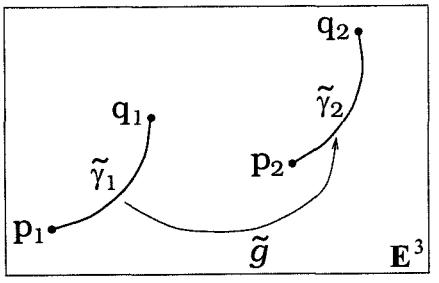

(a) Equivalent pairs of points

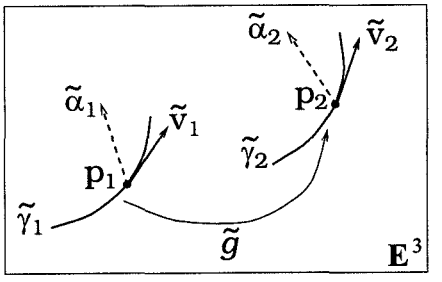

(b) Equivalent tangent and cotangent vectors

Figure 7.10: Equivalent relations in $\mathbb{E}^3$.

Based on equivalence of curves one can also define equivalent tangent and cotangent vectors to $\mathbb{E}^3$, as illustrated in Figure 7.10(b).

Definition 7.5.3 (Equivalent tangent vectors to $\mathbb{E}^3$). A tangent vector $\widetilde{v}_2 \in T_{p_2}\mathbb{E}^3$ is *equivalent* to another tangent vector $\widetilde{v}_1 \in T_{p_1}\mathbb{E}^3$ with respect to $\widetilde{g} \in \widetilde{SE}(3)$ if there are two curves $\widetilde{\gamma}_1, \widetilde{\gamma}_2 \colon (-\epsilon, \epsilon) \to \mathbb{E}^3$, where $\widetilde{\gamma}_2$ is equivalent to $\widetilde{\gamma}_1$ with respect to $\widetilde{g}$, such that $\widetilde{\gamma}_i(0) = p_i$ and $\dot{\widetilde{\gamma}}_i(0) = \widetilde{v}_i$.

Definition 7.5.4 (Equivalent covectors to $\mathbb{E}^3$). A covector $\widetilde{\alpha}_2 \in T^*_{p_2}\mathbb{E}^3$ is *equivalent* to another covector $\widetilde{\alpha}_1 \in T^*_{p_1}\mathbb{E}^3$ if there exists $\widetilde{g} \in \widetilde{SE}(3)$, with $\widetilde{g}(p_1) = p_2$, such that $\widetilde{\alpha}_2(\widetilde{v}_2) = \widetilde{\alpha}_1(\widetilde{v}_1)$ whenever $\widetilde{v}_2 \in T_{p_2}\mathbb{E}^3$ is equivalent to $\widetilde{v}_1 \in T_{p_1}\mathbb{E}^3$ with respect to $\widetilde{g}$.

Two equivalent pairs of points can be thought of as the positions, as they appear to different observers, of a moving particle at two time instants. Similarly, two equivalent tangent or cotangent vectors can be viewed as the velocity of a particle, or a force acting on the particle, recorded by two different observers whose locations differ by a rigid displacement. When a metric function

is evaluated at two equivalent quantities, it is expected to yield the same value. This idea leads to the following definition.

Definition 7.5.5 (Objective metric functions on $\mathbb{E}^3$). A real-valued function $\widetilde{\Theta}$ on $\mathbb{E}^3 \times \cdots \times \mathbb{E}^3$ (s copies) is said to be *objective* if $\widetilde{\Theta}(p_1, \ldots, p_s) = \widetilde{\Theta}(q_1, \ldots, q_s)$ whenever $p_i, p_j \in \mathbb{E}^3$ and $q_i, q_j \in \mathbb{E}^3$ are equivalent pairs of points for all $1 \leqslant i, j \leqslant s$. A real-valued function $\widetilde{\Phi}$ on the vector bundles of $\mathbb{E}^3$ is *objective* if $\widetilde{\Phi}_p(\widetilde{v}_1, \ldots, \widetilde{v}_k, \widetilde{\alpha}_1, \ldots, \widetilde{\alpha}_l) = \widetilde{\Phi}_q(\widetilde{u}_1, \ldots, \widetilde{u}_k, \widetilde{\beta}_1, \ldots, \widetilde{\beta}_l)$ whenever $\widetilde{v}_i \in T_p\mathbb{E}^3$ and $\widetilde{u}_i \in T_q\mathbb{E}^3$, and $\widetilde{\alpha}_j \in T_p^*\mathbb{E}^3$ and $\widetilde{\beta}_j \in T_q^*\mathbb{E}^3$ are equivalent, respectively, for all $1 \leqslant i \leqslant k$ and $1 \leqslant j \leqslant l$.

The notion of objectivity is a natural requirement; a well-defined metric function on $\mathbb{E}^3$ must be *observer-indifferent.* To characterize an objective metric function, the following lemmas will be needed which characterize equivalent quantities relevant to $\mathbb{E}^3$. The proofs are omitted.

Lemma 7.5.1. *Two pairs of points $p_1, q_1 \in \mathbb{E}^3$ and $p_2, q_2 \in \mathbb{E}^3$ are equivalent if and only if there is a rigid transformation $\widetilde{g} \in \widetilde{SE}(3)$ such that $p_2 = \widetilde{g}(p_1)$ and $q_2 = \widetilde{g}(q_1)$.*

Lemma 7.5.2. *A tangent vector $\widetilde{v}_2 \in T_{p_2}\mathbb{E}^3$ is equivalent to another tangent vector $\widetilde{v}_1 \in T_{p_1}\mathbb{E}^3$ with respect to $\widetilde{g} \in \widetilde{SE}(3)$ if and only if $p_2 = \widetilde{g}(p_1)$ and $\widetilde{v}_2 = T_{p_1}\widetilde{g}(\widetilde{v}_1)$. Two covectors $\widetilde{\alpha}_1 \in T_{p_1}^*\mathbb{E}^3$ and $\widetilde{\alpha}_2 \in T_{p_2}^*\mathbb{E}^3$ are equivalent if and only if there exists $\widetilde{g} \in \widetilde{SE}(3)$ such that $p_2 = \widetilde{g}(p_1)$ and $\widetilde{\alpha}_2 = T_{p_1}^*\widetilde{g}^{-1}(\widetilde{\alpha}_1)$.*

Lemmas 7.5.1 and 7.5.2 can used to show the following necessary and sufficient condition for objectivity.

Proposition 7.5.3. *A metric function $\widetilde{\Psi}$ on $\mathbb{E}^3$ is objective if and only if it is invariant to all rigid transformations. That is, $\widetilde{g}^*\widetilde{\Psi} = \widetilde{\Psi}$ for all $\widetilde{g} \in \widetilde{SE}(3)$.*

Proof. Let $\widetilde{g} \in \widetilde{SE}(3)$ be arbitrary. First suppose that $\widetilde{\Psi}$ is a real-valued function on $\mathbb{E}^3$. By Definition 7.5.5 and Lemma 7.5.1, $\widetilde{\Psi}$ is objective if and

only if

$$\widetilde{\Psi}(p_1,\ldots,p_s) = \widetilde{\Psi}(\widetilde{g}(p_1),\ldots,\widetilde{g}(p_s)) = \widetilde{g}^*\widetilde{\Psi}(p_1,\ldots,p_s)$$

for all $p_1,\ldots,p_s \in \mathbb{E}^3$. Hence, $\widetilde{g}^*\widetilde{\Psi} = \widetilde{\Psi}$.

Now suppose that $\widetilde{\Psi}$ is a real-valued function on the vector bundles of $\mathbb{E}^3$. Definition 7.5.5 and Lemma 7.5.2 imply that

$$\begin{aligned}
&\widetilde{\Psi}_p(\widetilde{v}_1,\ldots,\widetilde{v}_k,\widetilde{\alpha}_1,\ldots,\widetilde{\alpha}_l) \\
&\quad = \widetilde{\Psi}_{\widetilde{g}(p)}(T\widetilde{g}(\widetilde{v}_1),\ldots,T\widetilde{g}(\widetilde{v}_k),T^*\widetilde{g}^{-1}(\widetilde{\alpha}_1),\ldots,T^*\widetilde{g}^{-1}(\widetilde{\alpha}_l)) \\
&\quad = \widetilde{g}^*\widetilde{\Phi}_p(\widetilde{v}_1,\ldots,\widetilde{v}_k,\widetilde{\alpha}_1,\ldots,\widetilde{\alpha}_l)
\end{aligned}$$

for all $p \in \mathbb{E}^3$, $\widetilde{v}_i \in T_p\mathbb{E}^3$ and $\widetilde{\alpha}_j \in T_p^*\mathbb{E}^3$. This again leads to $\widetilde{g}^*\widetilde{\Psi} = \widetilde{\Psi}$. □

7.5.2 Objectivity in $\mathbb{E}^3$ versus Frame-Invariance in $\mathbb{R}^3$

Objective functions on $\mathbb{E}^3$ can be represented by metric functions on $\mathbb{R}^3$ by seeking an interpretation of Proposition 7.5.3, when $\mathbb{E}^3$ is represented by $\mathbb{R}^3$ via an embedded frame. Let X and X^b be the coordinate maps associated with the embedded frames $\mathcal{F}_X$ and $\mathcal{F}_X^b$, respectively. Let $\widetilde{\Psi}$ be an objective metric function on $\mathbb{E}^3$ as defined in Definition 7.5.5. Then, $\Psi = X_*\widetilde{\Psi}$ and $\Psi^b = X_*^b\widetilde{\Psi}$, the push-forwards by X and X^b of $\widetilde{\Psi}$, are metric functions on $\mathbb{R}^3$ with the following properties.

Proposition 7.5.4. *The function $\widetilde{\Psi}$ is objective if and only if $g_*\Psi = \Psi$ for all $g \in SE(3)$, i.e., Ψ is invariant to all rigid transformations of $\mathbb{R}^3$. Moreover, $\Psi^b = \Psi$ for all $b \in SE(3)$, and hence the objective function $\widetilde{\Psi}$ corresponds to a* unique *metric function on $\mathbb{R}^3$ regardless of the choice of embedded frame.*

Proof. First consider the function Ψ. Given any $\widetilde{g} \in \widetilde{SE}(3)$, Lemma 7.2.2 indicates that $\widetilde{\Psi}$ is $\widetilde{g}$-invariant if and only if Ψ is invariant to $X_*\widetilde{g} = F(\widetilde{g})$, a rigid transformation on $\mathbb{R}^3$. Since F, the rigid transformation representation map associated with $\mathcal{F}_X$, is a bijection, $\widetilde{\Psi}$ is invariant to all rigid transformations on $\mathbb{E}^3$ if and only if Ψ is so to all rigid transformations on $\mathbb{R}^3$.

By Lemmas 7.2.1 and 7.4.1, the function Ψ^b is related to Ψ as follows.

$$\Psi^b = (X^b \circ X^{-1})_*(X_*\widetilde{\Psi}) = (b^{-1})_*\Psi = \Psi,$$

where we have used the fact that Ψ is invariant to all rigid transformations on $\mathbb{R}^3$. □

It is instructive to consider the relationship between objectivity in $\mathbb{E}^3$ and bi-invariance in $\mathbb{R}^3$. For this purpose, recall that $\mathbb{R}^3$ is an additive commutative Lie group. Given any $x \in \mathbb{R}^3$, left and right translations by x are defined by $L_x(y) = R_x(y) = x + y$ for $y \in \mathbb{R}^3$. The set of all pure translations of $\mathbb{R}^3$ is a subset of $SE(3)$. Hence if a metric function on $\mathbb{R}^3$ is invariant to all rigid transformations, it is necessarily pure-translation invariant, i.e., bi-invariant. Since the converse is not true, the following remark can be made.

Remark 7.5.1. The bi-invariance of a metric function on $\mathbb{R}^3$ is necessary, but *not* sufficient to determine an objective metric function on $\mathbb{E}^3$.

The notion of objectivity in $\mathbb{E}^3$ can be illustrated by two examples. For a function Θ on $\mathbb{R}^3$ and a function Φ on the vector bundles of $\mathbb{R}^3$, invariance to rigid transformations can be written as

$$\Theta(x_1, \ldots, x_s) = \Theta(g(x_1), \ldots, g(x_s)),$$

$$\Phi_x(v_1, \ldots, v_k, \alpha_1, \ldots, \alpha_l) = \Phi_{g(x)}(Rv_1, \ldots, Rv_k, R\alpha_1, \ldots, R\alpha_l)$$

for $x_1, \ldots, x_s \in \mathbb{R}^3$, $v_1, \ldots, v_k \in T_x\mathbb{R}^3$, $\alpha_1, \ldots, \alpha_l \in T_x^*\mathbb{R}^3$, and $g = (d, R) \in SE(3)$. In the examples $\Phi_x = \Phi_y$ is taken for all $x, y \in \mathbb{R}^3$, since tangent and cotangent spaces to different points of $\mathbb{R}^3$ can all be naturally identified with $\mathbb{R}^3$.

Example 7.5.1. The standard distance metric on $\mathbb{R}^3$ defined by

$$d(x, y) = \Big(\sum_{i=1}^{3} (x_i - y_i)^2 \Big)^{\frac{1}{2}},$$

where $x = (x_1, x_2, x_3) \in \mathbb{R}^3$ and $y = (y_1, y_2, y_3) \in \mathbb{R}^3$, is invariant to all rigid transformations, and hence represents an objective function on $\mathbb{E}^3$ given by $\widetilde{d} = (X^b)^* d$. In fact it can be shown that $\widetilde{d}$ is a distance metric on $\mathbb{E}^3$.

Example 7.5.2. The standard norm and inner product on $T\mathbb{R}^3$ are defined by

$$|v| = \sqrt{(v, v)} \quad \text{and} \quad (u, v) = \sum_{i=1}^{3} u_i v_i$$

for $v = (v_1, v_2, v_3) \in T_x\mathbb{R}^3$ and $u = (u_1, u_2, u_3) \in T_x\mathbb{R}^3$. Since they are rigid-transformation invariant, $|\cdot|_{\mathbb{E}} = (X^b)^* |\cdot|$ and $(\cdot, \cdot)_{\mathbb{E}} = (X^b)^* (\cdot, \cdot)$ are objective, which as can be shown are an objective norm and an objective inner product on $T\mathbb{E}^3$, respectively. On the other hand, the following norm on $T\mathbb{R}^3$ defined by

$$|v|_\infty = \max_{i=1,2,3} |v_i|$$

is invariant to all pure translations and is hence bi-invariant. However, since this norm is not rotation invariant, $(X^b)^* |\cdot|_\infty$ is *not* objective.

7.6 Objective Metric Functions on the Configuration Space of a Rigid Body

Using objectivity in $\mathbb{E}^3$ as a motivation, and based on the intrinsic c-space definition, we are now in a position to consider the notion of objectivity for the configuration space of a rigid body. It will be seen that objectivity in $\mathcal{C}$, which is conceptually analogous to objectivity in $\mathbb{E}^3$, offers deep physical insight into left invariance, right invariance and bi-invariance in $SE(3)$. Similar to the case of $\mathbb{E}^3$, we first consider the notion of equivalent curves, which are defined in terms of c-space repositionings.

7.6.1 C-Space Repositionings

In defining equivalence of curves in $\mathbb{E}^3$, one curve was said to be equivalent to another if they could be brought into coincidence by a rigid transformation of $\mathbb{E}^3$. In the case of the c-space of a rigid body, this role will be played by c-space repositionings defined as follows.

Definition 7.6.1 (C-space repositionings). Given any $\widetilde{g} \in \widetilde{SE}(3)$, the *c-space repositioning* by $\widetilde{g}$ is a map $\Upsilon_{\widetilde{g}} \colon \mathcal{C} \to \mathcal{C}$ defined by $\Upsilon_{\widetilde{g}}(\chi) = \widetilde{g} \circ \chi$ for $\chi \in \mathcal{C}$.

The term "repositioning" is motivated by the interpretation of a configuration χ as a placement of the body in $\mathbb{E}^3$, since $\Upsilon_{\widetilde{g}}(\chi)$ just places $\mathcal{B}$ at a different location by rigidly displacing $\mathcal{B}$ from χ by $\widetilde{g}$. Clearly, a c-space repositioning is a diffeomorphism, whose inverse is given by $\Upsilon_{\widetilde{g}}^{-1} = \Upsilon_{\widetilde{g}^{-1}}$.

In Definition 7.4.4, a c-space representation map $\Gamma^{\widetilde{a},b} \colon \mathcal{C} \to SE(3)$ was defined corresponding to a reference configuration $\chi_{\widetilde{a}}$ and an embedded frame $\mathcal{F}_X^b$. Via the map $\Gamma^{\widetilde{a},b}$, a c-space repositioning $\Upsilon_{\widetilde{g}}$ induces a map $(\Gamma^{\widetilde{a},b})_* \Upsilon_{\widetilde{g}}$, which maps $SE(3)$ onto itself and can be calculated using the following lemma.

Lemma 7.6.1. *By use of the c-space representation map $\Gamma^{\widetilde{a},b}$, a c-space repositioning $\Upsilon_{\widetilde{g}}$ induces a left translation on $SE(3)$. Specifically, $(\Gamma^{\widetilde{a},b})_*\Upsilon_{\widetilde{g}} = L_{F^b(\widetilde{g})}$, where F^b is the rigid transformation representation map associated with $\mathcal{F}_X^b$.*

Proof. First consider $(J^{\widetilde{a}})_*\Upsilon_{\widetilde{g}}\colon \widetilde{SE}(3) \to \widetilde{SE}(3)$, where $J^{\widetilde{a}}\colon \mathcal{C} \to \widetilde{SE}(3)$ is the intermediate rigid transformation representation map associated with $\chi_{\widetilde{a}}$. For any $\widetilde{h} \in \widetilde{SE}(3)$,

$$\begin{aligned}(J^{\widetilde{a}})_*\Upsilon_{\widetilde{g}}(\widetilde{h}) &= J^{\widetilde{a}} \circ \Upsilon_{\widetilde{g}} \circ (J^{\widetilde{a}})^{-1}(\widetilde{h}) = J^{\widetilde{a}} \circ \Upsilon_{\widetilde{g}}(\widetilde{h} \circ \chi_{\widetilde{a}}) \\ &= J^{\widetilde{a}}(\widetilde{g} \circ \widetilde{h} \circ \chi_{\widetilde{a}}) = \widetilde{g} \circ \widetilde{h} = \widetilde{L}_{\widetilde{g}}(\widetilde{h}),\end{aligned}$$

which implies that $(J^{\widetilde{a}})_*\Upsilon_{\widetilde{g}} = \widetilde{L}_{\widetilde{g}}$. Since $\Gamma^{\widetilde{a},b} = F^b \circ J^{\widetilde{a}}$, Lemma 7.2.1 gives

$$(\Gamma^{\widetilde{a},b})_*\Upsilon_{\widetilde{g}} = (F^b \circ J^{\widetilde{a}})_*\Upsilon_{\widetilde{g}} = F^b_*(J^{\widetilde{a}})_*\Upsilon_{\widetilde{g}} = F^b_*\widetilde{L}_{\widetilde{g}}.$$

By Lemma 7.4.3, $F^b_*\widetilde{L}_{\widetilde{g}} = L_{F^b(\widetilde{g})}$, which completes the proof. □

Since $\widetilde{a}$ does not appear in the right side of the formula in Lemma 7.6.1 and F^b is a bijection, the following observation can be made.

Remark 7.6.1. A c-space repositioning of the body induces a left translation on $SE(3)$, and *vice versa*. Moreover, there is a *one-to-one* correspondence between the set of c-space repositionings and the set of left translations on $SE(3)$. This correspondence is not influenced by the choice of reference configuration but does depend on the choice of embedded frame.

7.6.2 Equivalence Relations Relevant to the C-Space

While a curve in $\mathbb{E}^3$ can be thought of as the motion of a particle, a curve in $\mathcal{C}$ can be interpreted as a rigid body motion. When acting on a curve in $\mathbb{E}^3$, a rigid transformation of $\mathbb{E}^3$ rigidly displaces the curve. Analogously, a c-space repositioning can play the role of "rigidly displacing" a c-space curve. These simple analogous features of the two spaces motivate the notion of equivalent c-space curves defined as follows.

Definition 7.6.2 (Equivalent curves in $\mathcal{C}$). Let $\bar{c}_1 : I \to \mathcal{C}$ and $\bar{c}_2 : I \to \mathcal{C}$, where I is an open interval $(-\epsilon, \epsilon)$ $(\epsilon > 0)$ or closed interval $[0, 1]$, be two c-space curves. If there exists some $\widetilde{g} \in \widetilde{SE}(3)$ such that $\bar{c}_2(t) = \Upsilon_{\widetilde{g}}(\bar{c}_1(t)) = \widetilde{g} \circ \bar{c}_1(t)$ for all $t \in I$, then $\bar{c}_2$ is said to be *equivalent* to $\bar{c}_1$ with respect to the c-space repositioning by $\widetilde{g}$.

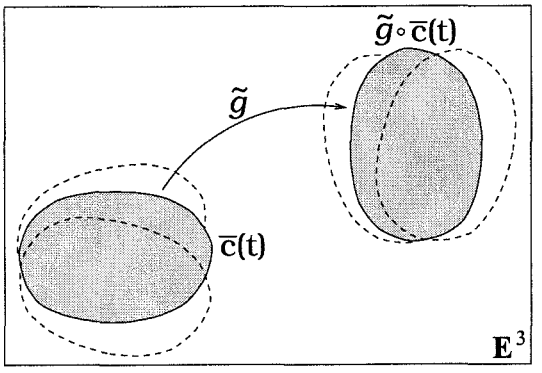

Figure 7.11: Equivalent curves in c-space.

Equivalence of c-space curves is clearly an equivalence relation. From a geometric viewpoint, two equivalent curves can be interpreted as being *congruent*; that is, the two curves can be brought into coincidence by a rigid displacement, as shown in Figure 7.11. Hence, these two equivalent curves can be thought of as the motions, which differ only by a rigid displacement, of two identical rigid bodies; or alternatively, the two curves can be regarded as the motion of *one* rigid body viewed by two observers whose locations differ by

a rigid displacement. These interpretations motivate us to define the following equivalence relations.

Definition 7.6.3 (Equivalent configuration pairs). Two pairs of configurations $\chi_1, \kappa_1 \in \mathcal{C}$ and $\chi_2, \kappa_2 \in \mathcal{C}$ are said to be *equivalent* if there are two equivalent curves $\bar{c}_1, \bar{c}_2 \colon [0,1] \to \mathcal{C}$ such that $\bar{c}_i(0) = \chi_i$, $\bar{c}_i(1) = \kappa_i$ for $i = 1, 2$.

Two equivalent pairs of configurations can be considered either as the initial and terminal configurations of some motion of a rigid body when viewed by different observers, or as the respective initial and terminal configurations of two rigid body motions that differ only by a rigid displacement.

Definition 7.6.4 (Equivalent tangent vectors to $\mathcal{C}$). Given tangent vectors $\overline{\mathbf{v}}_1 \in T_{\chi_1}\mathcal{C}$ and $\overline{\mathbf{v}}_2 \in T_{\chi_2}\mathcal{C}$, we say that $\overline{\mathbf{v}}_2$ is *equivalent* to $\overline{\mathbf{v}}_1$ with respect to $\widetilde{g} \in \widetilde{SE}(3)$ if there are two curves $\bar{c}_1, \bar{c}_2 \colon (-\epsilon, \epsilon) \to \mathcal{C}$, where $\bar{c}_2$ is equivalent to $\bar{c}_1$ with respect to $\widetilde{g}$, such that $\bar{c}_1(0) = \chi_1$ and $\dot{\bar{c}}_1(0) = \overline{\mathbf{v}}_1$, and $\bar{c}_2(0) = \chi_2$ and $\dot{\bar{c}}_2(0) = \overline{\mathbf{v}}_2$.

A tangent vector to $\mathcal{C}$ represents an instantaneous motion of the rigid body. Therefore, two tangent vectors being equivalent means two instantaneous motions that differ only by a rigid displacement. Alternatively, two equivalent tangent vectors can be interpreted as some instantaneous motion of the rigid body recorded by two observers. Figure 7.12(a) shows two equivalent planar motions with instantaneous centers of rotation at p and $\widetilde{g}(p)$, respectively.

Definition 7.6.5 (Equivalent covectors to $\mathcal{C}$). A covector $\overline{\boldsymbol{\alpha}}_2 \in T^*_{\chi_2}\mathcal{C}$ is said to be *equivalent* to another covector $\overline{\boldsymbol{\alpha}}_1 \in T^*_{\chi_1}\mathcal{C}$ with respect to a c-space repositioning by $\widetilde{g} \in \widetilde{SE}(3)$, if $\chi_2 = \Upsilon_{\widetilde{g}}(\chi_1)$ and $\overline{\boldsymbol{\alpha}}_2(\overline{\mathbf{v}}_2) = \overline{\boldsymbol{\alpha}}_1(\overline{\mathbf{v}}_1)$ whenever $\overline{\mathbf{v}}_2 \in T_{\chi_2}\mathcal{C}$ is equivalent to $\overline{\mathbf{v}}_1 \in T_{\chi_1}\mathcal{C}$ with respect to $\widetilde{g}$.

The physical intuition for equivalent covectors is illustrated in Figure 7.12(b). Recall that a covector can be interpreted as a wrench that consists of a force

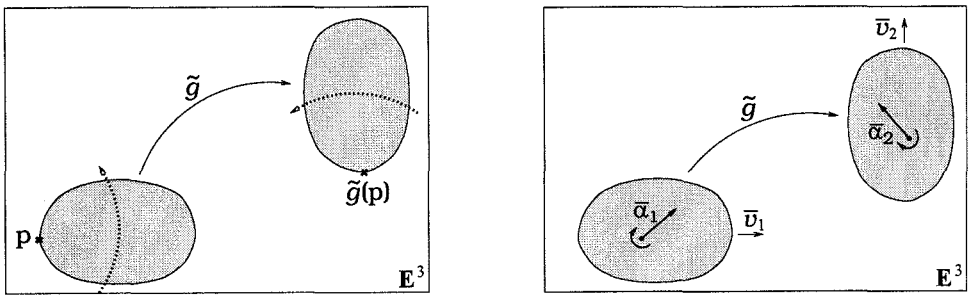

(a) Equivalent tangent vectors (b) Equivalent covectors

Figure 7.12: Equivalent tangent and cotangent vectors.

and a torque. Consider two covectors $\overline{\boldsymbol{\alpha}}_1 \in T^*_{\chi_1}\mathcal{C}$ and $\overline{\boldsymbol{\alpha}}_2 \in T^*_{\chi_2}\mathcal{C}$, which determine two wrenches physically acting on the body. If $\overline{\boldsymbol{\alpha}}_2$ is equivalent to $\overline{\boldsymbol{\alpha}}_1$ with respect to $\widetilde{g}$, then as the body undergoes the rigid displacement $\widetilde{g}$, the two wrenches become coincident. Clearly, these two wrenches do the same amount of work when acting on two equivalent rigid body velocities that can be brought into coincidence by the rigid displacement $\widetilde{g}$.

We conclude this discussion by giving two lemmas that characterize equivalent configurations as well as equivalent tangent and cotangent vectors.

Lemma 7.6.2. *Two pairs of configurations $\chi_1, \kappa_1 \in \mathcal{C}$ and $\chi_2, \kappa_2 \in \mathcal{C}$ are equivalent if and only if there is a c-space repositioning $\Upsilon_{\widetilde{g}}$ with $\widetilde{g} \in \widetilde{SE}(3)$ such that $\chi_2 = \Upsilon_{\widetilde{g}}(\chi_1)$ and $\kappa_2 = \Upsilon_{\widetilde{g}}(\kappa_1)$.*

Proof. The condition is obviously necessary. To show its sufficiency, consider $\widetilde{g} \in \widetilde{SE}(3)$ such that $\chi_2 = \Upsilon_{\widetilde{g}}(\chi_1)$ and $\kappa_2 = \Upsilon_{\widetilde{g}}(\kappa_1)$. Using the c-space representation map Γ (Definition 7.4.4) gives $g_i = \Gamma(\chi_i) \in SE(3)$ and $h_i = \Gamma(\kappa_i) \in SE(3)$. Invoking Lemma 7.6.1 with $b = e$ leads to

$$g_2 = \Gamma \circ \Upsilon_{\widetilde{g}}(\chi_1) = (\Gamma \circ \Upsilon_{\widetilde{g}} \circ \Gamma^{-1})(\Gamma(\chi_1)) = \Gamma_* \Upsilon_{\widetilde{g}}(\Gamma(\chi_1)) = L_{F(\widetilde{g})}(g_1).$$

Similarly, it can be shown that $h_2 = L_{F(\widetilde{g})}(h_1)$. Let $c_1, c_2 \colon [0,1] \to SE(3)$ be two curves in $SE(3)$ such that $c_1(0) = g_1$ and $c_1(1) = h_1$, and $c_2(t) =$

$L_{F(\widetilde{g})}(c_1(t))$. Then $c_2(0) = g_2$ and $c_2(1) = h_2$. Define two c-space curves by $\overline{c}_i = \Gamma^{-1}(c_i(t))$. Then,

$$\begin{aligned}\overline{c}_2(t) &= \Gamma^{-1}(c_2(t)) = \Gamma^{-1}(L_{F(\widetilde{g})}(c_1(t))) \\ &= \big(\Gamma^{-1} \circ L_{F(\widetilde{g})} \circ \Gamma\big)\big(\Gamma^{-1}(c_1(t))\big) = \Gamma^* L_{F(\widetilde{g})}(\overline{c}_1(t)) = \Upsilon_{\widetilde{g}}(\overline{c}_1(t)).\end{aligned}$$

Therefore $\overline{c}_1$ and $\overline{c}_2$ are equivalent curves with $\overline{c}_i(0) = \chi_i$ and $\overline{c}_i(1) = \kappa_i$. □

Lemma 7.6.3. *Given two tangent vectors $\overline{\mathbf{v}}_1 \in T_{\chi_1}\mathcal{C}$ and $\overline{\mathbf{v}}_2 \in T_{\chi_2}\mathcal{C}$, we have $\overline{\mathbf{v}}_2$ equivalent to $\overline{\mathbf{v}}_1$ with respect to $\widetilde{g} \in \widetilde{SE}(3)$ if and only if $\Upsilon_{\widetilde{g}}(\chi_1) = \chi_2$ and $\overline{\mathbf{v}}_2 = T_{\chi_1}\Upsilon_{\widetilde{g}}(\overline{\mathbf{v}}_1)$. Two covectors $\overline{\boldsymbol{\alpha}}_1 \in T^*_{\chi_1}\mathcal{C}$ and $\overline{\boldsymbol{\alpha}}_2 \in T^*_{\chi_2}\mathcal{C}$ are equivalent if and only if there is $\widetilde{g} \in \widetilde{SE}(3)$ such that $\chi_2 = \Upsilon_{\widetilde{g}}(\chi_1)$ and $\overline{\boldsymbol{\alpha}}_2 = T^*_{\chi_1}\Upsilon^{-1}_{\widetilde{g}}(\overline{\boldsymbol{\alpha}}_1)$.*

Proof. We only show the sufficiency of the condition for equivalent tangent vectors (the covector equivalence condition immediately follows from this). Suppose that $\widetilde{g} \in \widetilde{SE}(3)$ is such that $\Upsilon_{\widetilde{g}}(\chi_1) = \chi_2$ and $\overline{\mathbf{v}}_2 = T_{\chi_1}\Upsilon_{\widetilde{g}}(\overline{\mathbf{v}}_1)$. Let c_1, $c_2 \colon (-\epsilon, \epsilon) \to SE(3)$ be curves in $SE(3)$ such that $c_1(0) = \Gamma(\chi_1)$ and $\dot{c}_1(0) = T\Gamma(\overline{\mathbf{v}}_1)$, and $c_2(t) = L_{F(\widetilde{g})}(c_1(t))$. Then,

$$\begin{aligned}T\Gamma(\overline{\mathbf{v}}_2) &= T\Gamma(T\Upsilon_{\widetilde{g}}(\overline{\mathbf{v}}_1)) = T\big(\Gamma \circ \Upsilon_{\widetilde{g}} \circ \Gamma^{-1}\big)\big(T\Gamma(\overline{\mathbf{v}}_1)\big)\big) \\ &= T\big(\Gamma_* \Upsilon_{\widetilde{g}}\big)(\dot{c}_1(0)) = TL_{F(\widetilde{g})}(\dot{c}_1(0)) = \dot{c}_2(0),\end{aligned}$$

where Lemma 7.6.1 has been invoked. Therefore, $\overline{c}_i(t) = \Gamma^{-1}(c_i(t))$ are the desired equivalent curves. □

7.6.3 Formal Definition of Objectivity in $\mathcal{C}$

The notion of objectivity in Euclidean space $\mathbb{E}^3$ can now be extended to the configuration space $\mathcal{C}$ of a rigid body. Analogous to the case of $\mathbb{E}^3$, the key role in c-space objectivity is played by the equivalence relations of configurations,

tangent vectors and covectors. Two equivalent pairs of configurations can be interpreted as the initial and final configurations, as they appear to different observers, of a rigid body motion. Two equivalent tangent or cotangent vectors can be thought of as an instantaneous motion of the rigid body, or a wrench acting on the body, as viewed by different observers. Clearly, for a metric function on $\mathcal{C}$ to be well-defined, it should yield the same value when evaluated at these equivalent quantities. This leads to the following definition.

Definition 7.6.6 (Objective metric functions on the c-space). A real-valued function $\overline{\Theta}$ on $\mathcal{C}\times\cdots\times\mathcal{C}$ (s copies) is said to be *objective* if $\overline{\Theta}(\chi_1,\ldots,\chi_s) = \overline{\Theta}(\kappa_1,\ldots,\kappa_s)$ whenever $\chi_i,\chi_j \in \mathcal{C}$ and $\kappa_i,\kappa_j \in \mathcal{C}$ are equivalent pairs of configurations for all $1 \leqslant i,j \leqslant s$. Meanwhile, a real-valued function $\overline{\Phi}$ on the vector bundles of $\mathcal{C}$ is said to be *objective* if $\overline{\Phi}_\chi(\overline{\mathbf{v}}_1,\ldots,\overline{\mathbf{v}}_k,\overline{\boldsymbol{\alpha}}_1,\ldots,\overline{\boldsymbol{\alpha}}_l) = \overline{\Phi}_\kappa(\overline{\mathbf{u}}_1,\ldots,\overline{\mathbf{u}}_k,\overline{\boldsymbol{\beta}}_1,\ldots,\overline{\boldsymbol{\beta}}_l)$ whenever $\overline{\mathbf{v}}_i \in T_\chi\mathcal{C}$ and $\overline{\mathbf{u}}_i \in T_\kappa\mathcal{C}$ are equivalent for all $1 \leqslant i \leqslant k$, and $\overline{\boldsymbol{\alpha}}_j \in T^*_\chi\mathcal{C}$ and $\overline{\boldsymbol{\beta}}_j \in T^*_\kappa\mathcal{C}$ are equivalent for all $1 \leqslant j \leqslant l$.

Remark 7.6.2. Because of its importance, the essence of objectivity is reiterated: a well-defined kinematic metric function should give measurement results that are *indifferent* to observers. That is, different observers should make *consistent* measurements.

The characterizations of the c-space equivalence relations given in Section 7.6.2 can be used to characterize objective metric functions as follows.

Proposition 7.6.4. *A kinematic metric function $\overline{\Psi}$ of the types given in Definition 7.6.6 is objective if and only if it is invariant to all c-space repositionings. That is, $\Upsilon^*_{\widetilde{g}}\overline{\Psi} = \overline{\Psi}$ for all $\widetilde{g} \in \widetilde{SE}(3)$.*

Proof. Suppose that $\overline{\Psi}$ is a real-valued function on $\mathcal{C}$. By Lemma 7.6.2, $\overline{\Psi}$ is objective if and only if

$$\overline{\Psi}(\chi_1,\ldots,\chi_s) = \overline{\Psi}(\Upsilon_{\widetilde{g}}(\chi_1),\ldots,\Upsilon_{\widetilde{g}}(\chi_s)) = \Upsilon^*_{\widetilde{g}}\overline{\Psi}(\chi_1,\ldots,\chi_s)$$

for all $\chi_1, \ldots, \chi_s \in \mathcal{C}$. If $\overline{\Psi}$ is a real-valued function on the vector bundles of $\mathcal{C}$, then Lemma 7.6.3 implies that

$$\begin{aligned}
&\overline{\Psi}_\chi(\overline{\mathbf{v}}_1, \ldots, \overline{\mathbf{v}}_k, \overline{\boldsymbol{\alpha}}_1, \ldots, \overline{\boldsymbol{\alpha}}_l) \\
&\quad = \overline{\Psi}_{\Upsilon_{\widetilde{g}}(p)}(T\Upsilon_{\widetilde{g}}(\overline{\mathbf{v}}_1), \ldots, T\Upsilon_{\widetilde{g}}(\overline{\mathbf{v}}_k), T^*\Upsilon_{\widetilde{g}}^{-1}(\overline{\boldsymbol{\alpha}}_1), \ldots, T^*\Upsilon_{\widetilde{g}}^{-1}(\overline{\boldsymbol{\alpha}}_l)) \\
&\quad = \Upsilon_{\widetilde{g}}^*\overline{\Psi}_p(\overline{\mathbf{v}}_1, \ldots, \overline{\mathbf{v}}_k, \overline{\boldsymbol{\alpha}}_1, \ldots, \overline{\boldsymbol{\alpha}}_l)
\end{aligned}$$

for all $\chi \in \mathcal{C}$, $\overline{\mathbf{v}}_i \in T_\chi\mathcal{C}$ and $\overline{\boldsymbol{\alpha}}_j \in T_\chi^*\mathcal{C}$. It follows that in either case $\overline{\Psi}$ is objective if and only if $\Upsilon_{\widetilde{g}}^*\overline{\Psi} = \overline{\Psi}$ for all $\widetilde{g} \in \widetilde{SE}(3)$. □

Example 7.6.1. For demonstration, consider the following objective function on the tangent bundle of $\mathcal{C}$. Let a c-space curve $\overline{c}(t)$ determine a tangent vector $\dot{\overline{c}}(0) \in T_\chi\mathcal{C}$. The corresponding trajectory of a particle $\wp \in \mathcal{B}$ is given by a curve $\widetilde{\gamma}_\wp(t) \triangleq \overline{c}_t(\wp)$ in $\mathbb{E}^3$, where the notation $\overline{c}_t = \overline{c}(t)$ is used. Define a map $K_\wp\colon T\mathcal{C} \to T\mathbb{E}^3$ by $K_\wp(\dot{\overline{c}}(0)) = \dot{\widetilde{\gamma}}_\wp(0) = \frac{d}{dt}\big|_{t=0}\overline{c}_t(\wp)$, which gives the corresponding velocity of $\wp$. Define a real-valued function $\overline{\Phi}$ on the tangent bundle of $\mathcal{C}$ by

$$\overline{\Phi}_\chi(\dot{\overline{c}}(0)) = \max_{\wp \in \mathcal{B}} \left| K_\wp(\dot{\overline{c}}(0)) \right|.$$

where $|\cdot|_{\mathbb{E}}$ is the standard norm on $T\mathbb{E}^3$ (Example 7.5.2). Intuitively, $\overline{\Phi}_\chi(\dot{\overline{c}}(0))$ is the maximal speed of $\mathcal{B}$'s particles. We now show that $\overline{\Phi}$ is objective. For any $\widetilde{g} \in \widetilde{SE}(3)$, the definition of the map $K_\wp$ implies that

$$K_\wp\big(T\Upsilon(\dot{\overline{c}}(0))\big) = \frac{d}{dt}\bigg|_{t=0} \widetilde{g} \circ \overline{c}_t(\wp) = T\widetilde{g}\left(\frac{d}{dt}\bigg|_{t=0} \overline{c}_t(\wp)\right) = T\widetilde{g}\left(K_\wp(\dot{\overline{c}}(0))\right).$$

Hence, the objectivity of the norm $|\cdot|_{\mathbb{E}}$ on $T\mathbb{E}^3$ yields

$$\Upsilon^*_{\widetilde{g}}\overline{\Phi}_\chi(\dot{\widetilde{c}}(0)) = \Phi_{\widetilde{g}\circ\chi}\big(T\Upsilon(\dot{\widetilde{c}}(0))\big) = \max_{\wp\in\mathcal{B}}\big|T\widetilde{g}\big(K_\wp(\dot{\widetilde{c}}(0))\big)\big| = \max_{\wp\in\mathcal{B}}\big|K_\wp(\dot{\widetilde{c}}(0))\big|\,.$$

It follows that $\Upsilon^*_{\widetilde{g}}\overline{\Phi} = \overline{\Phi}$, and that $\overline{\Phi}$ is indeed objective. Both the function $\overline{\Phi}$ and Formula (7.2), which applies to planar instantaneous motions, give the maximum magnitude of the instantaneous displacements of $\mathcal{B}$'s particles. Therefore, this example is a (complicated) generalization of Formula (7.2) to the three-dimensional case.

While the notion of objectivity captures the fundamental requirement for kinematic metric functions to be well-defined, this example shows that the direct manipulation of objective functions is cumbersome and inconvenient for practical applications. It is therefore highly desirable to develop a practical method for defining objective functions. The fact that the function $\overline{\Phi}$ in this example and the frame-invariant formula (7.2) have the same physical meaning suggests a strong relationship between objectivity and frame-invariance. This relationship, when clarified in Section 7.8 in the context of the conventional rigid body kinematic description, will lead to a practical treatment of objective functions.

7.7 Objectivity in $\mathcal{C}$ versus Invariance in $SE(3)$

This section considers the relationship of objectivity in $\mathcal{C}$ to invariance in $SE(3)$. This allows the clarification of some long-standing confusion about invariance properties relevant to $SE(3)$, and is crucial for the clarification of frame-invariance in Section 7.8.

Let $\overline{\Psi}$ be an objective metric function on $\mathcal{C}$. This function induces $\Psi^{\widetilde{a},b} = (\Gamma^{\widetilde{a},b})_*\overline{\Psi}$, a metric function on $SE(3)$. Recall that $\Gamma^{\widetilde{a},b}\colon \mathcal{C} \to SE(3)$ is the

c-space representation map (Definition 7.4.4) corresponding to the choice of reference configuration $\chi_{\widetilde{a}}$ and embedded frame $\mathcal{F}_X^b$. The notation $\Psi \triangleq \Psi^{\widetilde{e},e} = \Gamma_*\overline{\Psi}$ is used, where the map $\Gamma = \Gamma^{\widetilde{e},e}$ corresponds to the nominal reference configuration χ_0 and embedded frame $\mathcal{F}_X$. The following proposition characterizes the invariance properties of $\Psi^{\widetilde{a},b}$ and how these functions are inter-related.

Proposition 7.7.1. *A metric function $\overline{\Psi}$ on the c-space $\mathcal{C}$ is objective if and only if $\Psi^{\widetilde{a},b} = (\Gamma^{\widetilde{a},b})_*\overline{\Psi}$, a metric function on $SE(3)$, is left invariant. The induced function $\Psi^{\widetilde{a},b}$ can be characterized as follows.*

(1) $\Psi^{\widetilde{a},b}$ is left invariant but need not be right invariant.

(2) $\Psi^{\widetilde{a},b} = R^*_{b^{-1}F(\widetilde{a})}\Psi$. That is, $\Psi^{\widetilde{a},b}$ is in general different for different choices of reference configuration and embedded frame (i.e., different $\widetilde{a} \in \widetilde{SE}(3)$ and $b \in SE(3)$).

(3) If $\Psi^{\widetilde{a},b}$ is right invariant for any $\widetilde{a}$ and b, then it is a unique bi-invariant function independent of $\widetilde{a}$ and b.

Proof. By Proposition 7.6.4, $\overline{\Psi}$ is objective if and only if $\Upsilon^*_{\widetilde{g}}\overline{\Psi} = \overline{\Psi}$ for all $\widetilde{g} \in \widetilde{SE}(3)$. By Lemma 7.2.2, this is equivalent to the condition that

$$\underbrace{((\Gamma^{\widetilde{a},b})_*\Upsilon_{\widetilde{g}})^*}_{L_{F^b(\widetilde{g})}}\underbrace{(\Gamma^{\widetilde{a},b})_*\overline{\Psi}}_{\Psi^{\widetilde{a},b}} = \underbrace{(\Gamma^{\widetilde{a},b})_*\overline{\Psi}}_{\Psi^{\widetilde{a},b}},$$

i.e., using Lemma 7.6.1 yields $L^*_{F^b(\widetilde{g})}\Psi^{\widetilde{a},b} = \Psi^{\widetilde{a},b}$. Since F^b is bijective, $\overline{\Psi}$ is objective if and only $\Psi^{\widetilde{a},b}$ is a left invariant metric function on $SE(3)$. However, as is not implied by the objectivity of $\overline{\Psi}$, the function $\Psi^{\widetilde{a},b}$ is not necessarily right invariant.

To find the relationship between $\Psi^{\widetilde{a},b}$ and Ψ, we use Lemmas 7.2.1, 7.4.2,

and 7.4.5 to obtain

$$\Psi^{\tilde{a},b} = ((\Gamma^{\tilde{a},b} \circ \Gamma^{-1}) \circ \Gamma)_* \overline{\Psi} = (\underbrace{\Gamma^{\tilde{a},b} \circ \Gamma^{-1}}_{R_{(F(\tilde{a}))^{-1}b} \circ L_{b^{-1}}})_* \underbrace{\Gamma_* \overline{\Psi}}_{\Psi}$$
$$= (R_{(F(\tilde{a}))^{-1}b})_* (L_{b^{-1}})_* \Psi = R^*_{b^{-1}F(\tilde{a})} \Psi,$$

where the final equation resulted from the left invariance of Ψ. If Ψ is further right invariant and hence bi-invariant, then this equation implies that $\Psi^{\tilde{a},b} = \Psi$. Thus, the objective function $\overline{\Psi}$ corresponds to a unique bi-invariant function. □

Remark 7.7.1. An objective function $\overline{\Psi}$ thus corresponds to *a family of generally distinct left invariant functions*, which can be indexed by the choices of embedded frame and reference configuration, and which are *not* necessarily right invariant. Hence, bi-invariance is sufficient, but *not* necessary for objectivity in $\mathcal{C}$. This compares interestingly with the necessity and insufficiency of bi-invariance for objectivity in $\mathbb{E}^3$ (Remark 7.5.1).

Remark 7.7.2. While left invariant functions are often used in the literature (e.g., [150]), little justification has been given to the preference of left invariance over right invariance. Proposition 7.7.1 convincingly justifies this preference: left invariance represents the fundamental requirement of objectivity. Therefore, a function that is right invariant but not left invariant should actually be avoided.

The representation of an objective function on $\mathcal{C}$ by left invariant functions on $SE(3)$ offers a practical means for working with the abstract notions of configuration space and objectivity. Since a metric function on $\mathcal{C}$ can be recovered from its representation corresponding to a given choice of reference configuration and embedded frame via the relationship $\overline{\Psi} = (\Gamma^{\tilde{a},b})^* \Psi^{\tilde{a},b}$, one can focus on the representation functions $\Psi^{\tilde{a},b}$. As long as these functions

are left invariant and are inter-related by $\Psi^{\widetilde{a},b} = R^*_{b^{-1}F(\widetilde{a})}\Psi$, Proposition 7.7.1 ensures that $\overline{\Psi}$ is objective. Section 7.8 will interpret such representation metric functions on $SE(3)$ in the framework of the conventional rigid body kinematics approach which uses world and body frames. It will be seen that the notion of frame-invariance resulting from the discussion allows one to write abstract objective functions in terms of intuitive frame-invariant functions.

7.8 Frame-Invariant Metric Functions

Objective metric functions on $\mathcal{C}$ accurately characterize the natural requirement of observer-indifference, and can be represented as a family of left invariant functions on $SE(3)$. To facilitate practical kinematic metric calculations, these left invariant functions will now be considered in the framework of the conventional approach that specifies the location of a rigid body in terms a world frame and a body frame. The goal of this section is to develop a representation of objective functions in this framework and understand the influence of frame changes on such a representation.

7.8.1 Representation of the C-Space Based on the Conventional Approach

Section 7.4 represented $\mathcal{C}$ by $SE(3)$ in terms of a reference configuration and embedded frame. This approach is conducive to relating objectivity to invariance properties in $SE(3)$, but is not convenient for practical use. To provide a practical tool for developing objective metric functions, it is useful to consider the c-space in terms of the conventional approach, which represents $\mathcal{B}$'s configuration as the location of a body frame relative to a world frame. Recall that a world frame is a stationary coordinate frame in $\mathbb{E}^3$, and a body frame is a coordinate frame fixed to the rigid body in the sense that a particle $\wp \in \mathcal{B}$ has

the same coordinates in this frame for all configurations of $\mathcal{B}$. Since the choice of world and body frames is not unique, the following notational convention will be convenient.

Notational Convention. Choose a *nominal* world frame, denoted by $\mathcal{F}_W$ and a *nominal* body frame, denoted by $\mathcal{F}_B$. Denote an arbitrary world frame by $\mathcal{F}_W^b$ and an arbitrary body frame by $\mathcal{F}_B^a$, where the superscripts always indicate that $\mathcal{F}_W^b$ is displaced frame $\mathcal{F}_W$ by $b \in SE(3)$, and that $\mathcal{F}_B^a$ is displaced from $\mathcal{F}_B$ by $a \in SE(3)$.

For a given choice of world and body frames, one wishes to represent an objective function by an appropriate left invariant function. In addition, when the world and body frames are changed, the left invariant function should transform accordingly. For this purpose, one needs to interpret locations of a body frame relative to a world frame in terms of the formal approach given in Section 7.4.4, where $\mathcal{C}$ was represented by $SE(3)$ using a reference configuration and an embedded frame.

As shown in Figure 7.13, choose the nominal embedded frame $\mathcal{F}_X$ to be coincident with the nominal world frame $\mathcal{F}_W$, and choose the nominal reference configuration χ_0 such that $\mathcal{F}_B$ and $\mathcal{F}_W$ coincide when $\mathcal{B}$'s configuration is χ_0. It follows from Sections 7.4.2 and 7.4.4 that corresponding to a configuration $\chi \in \mathcal{C}$, the location of $\mathcal{F}_B$ relative to $\mathcal{F}_W$ is given by $\Gamma(\chi)$, where $\Gamma\colon \mathcal{C} \to SE(3)$ is the c-space representation map associated with χ_0 and $\mathcal{F}_X$.

When different world and body frames are used, a given configuration of $\mathcal{B}$ corresponds to different relative frame locations. With respect to the frames $\mathcal{F}_W^b$ and $\mathcal{F}_B^a$, suppose that we choose a reference configuration $\chi_{\widetilde{h}} \in \mathcal{C}$ given by $\chi_{\widetilde{h}} \circ \chi_0^{-1} = \widetilde{h} \in \widetilde{SE}(3)$ and an embedded frame $\mathcal{F}_X^c$ displaced from $\mathcal{F}_X$ by $c \in SE(3)$. Let $\Gamma^{\widetilde{h},c}\colon \mathcal{C} \to SE(3)$ be the corresponding c-space representation map. It is desired to choose $\widetilde{h}$ and c in such a way that $\Gamma^{\widetilde{h},c}(\chi)$ is the location of $\mathcal{F}_B^a$ relative to $\mathcal{F}_W^b$ when $\mathcal{B}$'s configuration is χ.

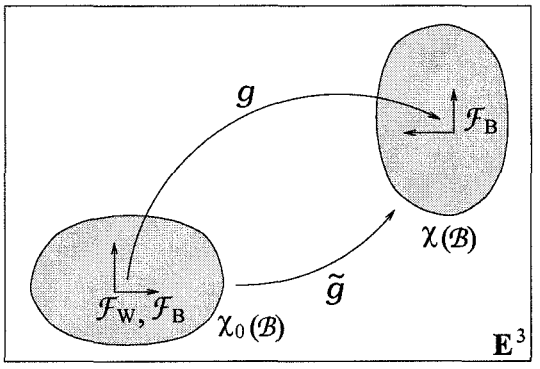

Figure 7.13: A configuration in terms of the location of $\mathcal{F}_B$ relative to $\mathcal{F}_W$.

It can be verified that the desired reference configuration and embedded frame are given by the following proposition, as illustrated in Figure 7.14, where it is assumed that either the world or the body frame remains unchanged. There is no loss of generality in this assumption, since any change of both frames can be considered, for example, as a change of world frame followed by a change of body frame.

Proposition 7.8.1. *Given the nominal frames $\mathcal{F}_W$ and $\mathcal{F}_B$ with corresponding nominal reference configuration χ_0 and embedded frame $\mathcal{F}_X$, consider changing the world frame to $\mathcal{F}_W^b$, or the body frame to $\mathcal{F}_B^a$, respectively. The reference configuration $\chi_{\tilde{h}}$ and embedded frame $\mathcal{F}_X^c$ should be chosen as follows so that $\Gamma^{\tilde{h},c}(\chi)$ is exactly the location of the body frame relative to the world frame as $\mathcal{B}$'s configuration is χ.*

(1) World frame changes to $\mathcal{F}_W^b$ with body frame $\mathcal{F}_B$ unchanged*:* $\tilde{h} = F^{-1}(b)$ *and* $c = b$. *The corresponding c-space representation maps are related by* $\Gamma^{\tilde{h},b} \circ \Gamma^{-1} = L_b^{-1}$.

(2) Body frame changes to $\mathcal{F}_B^a$ with world frame $\mathcal{F}_W$ unchanged*:* $\tilde{h} = F^{-1}(a^{-1})$ *and* $c = e$. *The corresponding c-space representation maps are related by* $\Gamma^{\tilde{h},e} \circ \Gamma^{-1} = R_a$.

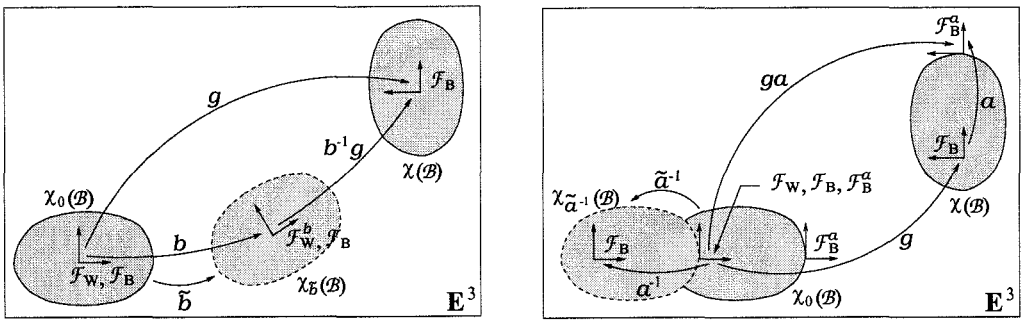

(a) Change of world frame ($\widetilde{b} = F^{-1}(b)$)

(b) Change of body frame ($\widetilde{a} = F^{-1}(a)$)

Figure 7.14: Change of world or body frame.

Remark 7.8.1. By Proposition 7.8.1, the embedded frame is always chosen to coincide with the given world frame. However, even though an embedded frame and a world frame are both stationary in $\mathbb{E}^3$, they play *different* roles. This is highlighted by the fact that a change of world frame usually involves changes in *both* embedded frame and reference configuration.

Let $g \in SE(3)$, and $\mathbf{v} \in TSE(3)$ and $\boldsymbol{\alpha} \in T^*SE(3)$ represent a configuration in $\mathcal{C}$, and a tangent vector and a covector to $\mathcal{C}$ with respect to the nominal frames $\mathcal{F}_W$ and $\mathcal{F}_B$. As the frames are changed to $\mathcal{F}^b_W$ and $\mathcal{F}^a_B$, these quantities transform to $g^{\{b,a\}}$, $\mathbf{v}^{\{b,a\}}$ and $\boldsymbol{\alpha}^{\{b,a\}}$, which can be obtained from Proposition 7.8.1 as follows.

Corollary 7.8.2. *As the world frame changes from $\mathcal{F}_W$ to $\mathcal{F}^b_W$ while $\mathcal{F}_B$ remains the body frame, g, $\mathbf{v}$, and $\boldsymbol{\alpha}$ transform to $g^{\{b,e\}} = L_b^{-1}(g)$, $\mathbf{v}^{\{b,e\}} = TL_b^{-1}(\mathbf{v})$, and $\boldsymbol{\alpha}^{\{b,e\}} = T^*L_b(\boldsymbol{\alpha})$, respectively. As $\mathcal{F}_W$ remains to be the world frame while $\mathcal{F}_B$ changes to $\mathcal{F}^a_B$, the quantities transform to $g^{\{e,a\}} = R_a(g)$, $\mathbf{v}^{\{e,a\}} = TR_a(\mathbf{v})$, and $\boldsymbol{\alpha}^{\{e,a\}} = T^*R_a^{-1}(\boldsymbol{\alpha})$.*

7.8.2 Frame-Invariance in $SE(3)$

According to Proposition 7.8.1, each choice of world and body frames corresponds to a c-space representation map relating $\mathcal{C}$ to $SE(3)$. Consequently,

an objective metric function on $\mathcal{C}$ induces a left invariant metric function on $SE(3)$ corresponding to the given choice of frames. By examining the dependence of such left invariant functions on frame choices, we introduce the notion of frame-invariance, and show that frame-invariance is an equivalent condition for objectivity.

Corresponding to the world frame $\mathcal{F}_W^b$ and body frame $\mathcal{F}_B^a$, let $\Psi^{\{b,a\}}$ be a metric function on $SE(3)$. For convenience denote $\Psi^{\{e,e\}}$ by Ψ. Hence, there is a family of metric functions on $SE(3)$, each of which corresponds to a particular frame choice. The following lemma characterizes the condition under which these functions determine an objective function by $\overline{\Psi} = (\Gamma^{\widetilde{h},c})^*\Psi^{\{b,a\}}$, where $\Gamma^{\widetilde{h},c}$ is the c-space representation map corresponding to $\mathcal{F}_W^b$ and $\mathcal{F}_B^a$, with $\widetilde{h}$ and c determined from Proposition 7.8.1.

Lemma 7.8.3. *The function $\Psi^{\{b,a\}}$ determines an objective function on $\mathcal{C}$ if and only if it satisfies the condition $\Psi^{\{b,a\}} = R_{a*}\Psi$. In words, $\Psi^{\{b,a\}}$ is independent of the choice of world frame, which implies that the function is left invariant, and transforms by a right translation in response to change of body frame.*

Proof. First suppose that $\overline{\Psi} = \Gamma^*\Psi$ is objective. Thus, Ψ is left invariant. When the world frame is changed to $\mathcal{F}_W^b$ while $\mathcal{F}_B$ remains the same, $\Psi^{\{b,e\}} = (L_b^{-1})_*\Psi = \Psi$ by Proposition 7.8.1. When the body frame changes to $\mathcal{F}_B^a$ with the world frame $\mathcal{F}_W$ kept unchanged, using Proposition 7.8.1 yields $\Psi^{\{e,a\}} = R_{a*}\Psi$. The necessity of the condition is proved by combining these two cases. Conversely, suppose that $\Psi^{\{b,a\}} = R_{a*}\Psi$. The arbitrariness of b and the relation $\Psi^{\{b,e\}} = (L_b^{-1})_*\Psi = \Psi$ imply that Ψ, and hence $\Psi^{\{b,a\}}$, are left invariant. Moreover, since a is arbitrary, $\Psi^{\{b,a\}}$ gives a family of left invariant functions inter-related by arbitrary right translations. Hence, it follows from Proposition 7.7.1 that $\overline{\Psi}$ is objective. □

Note that in this lemma the left invariance of each function $\Psi^{\{b,a\}}$ is *not* a

prerequisite condition, but a *consequence* that follows from the more general condition $\Psi^{\{b,a\}} = R_{a*}\Psi$. The lemma along with Corollary 7.8.2 suggests the introduction of the following notion of frame-invariance.

Definition 7.8.1 (Frame-invariance). Corresponding to the world and body frames $\mathcal{F}_W^b$ and $\mathcal{F}_B^a$, let $\Theta^{\{b,a\}}$ be a family of real-valued functions on $SE(3)$, and $\Phi^{\{b,a\}}$ a family of real-valued functions on the vector bundles of $SE(3)$. Let arbitrary configurations in $\mathcal{C}$, tangent vectors and covectors to $\mathcal{C}$ be correspondingly represented by $g^{\{b,a\}}$ or $g_i^{\{b,a\}}$, $\mathbf{v}_i^{\{b,a\}}$, and $\boldsymbol{\alpha}_i^{\{b,a\}}$, respectively. The functions $\Theta^{\{b,a\}}$ and $\Phi^{\{b,a\}}$ are said to be *weakly frame-invariant* if they satisfy the conditions $\Theta^{\{b,a\}}(g_1^{\{b,a\}}, \ldots, g_s^{\{b,a\}}) = \Theta(g_1, \ldots, g_s)$ and $\Phi^{\{b,a\}}_{g^{\{b,a\}}}(\mathbf{v}_1^{\{b,a\}}, \ldots, \mathbf{v}_k^{\{b,a\}}, \boldsymbol{\alpha}_1^{\{b,a\}}, \ldots, \boldsymbol{\alpha}_l^{\{b,a\}}) = \Phi_g(\mathbf{v}_1, \ldots, \mathbf{v}_k, \boldsymbol{\alpha}_1, \ldots, \boldsymbol{\alpha}_l)$, where the superscript $\{e,e\}$ is dropped for brevity. The functions $\Theta^{\{b,a\}}$ and $\Phi^{\{b,a\}}$ are said to be *frame-invariant* if they are weakly frame-invariant and satisfy the conditions $\Theta^{\{b,a\}} = \Theta^{\{e,a\}}$ and $\Phi^{\{b,a\}} = \Phi^{\{e,a\}}$, i.e., the functions are independent of the choice of world frame.

The notion of weak frame-invariance allows $\Psi^{\{b,a\}}$ to determine a metric function on $\mathcal{C}$, which may or may not be objective, in a *consistent* manner. The weakly frame-invariant function $\Psi^{\{b,a\}}$ determines the *same* metric function on $\mathcal{C}$ for different b and a, i.e., different choices of frames. In other words, if $\Psi^{\{b,a\}}$ is not weakly frame-invariant, it will determine *different* functions on $\mathcal{C}$ corresponding to different frame choices and lead to a contradiction. The notion of frame-invariance guarantees not only the consistent determination of a metric function on $\mathcal{C}$, but also the objectivity of the function. This is established in the following proposition, which can be verified from Corollary 7.8.2 and Lemma 7.8.3.

Proposition 7.8.4. *Let $\Psi^{\{b,a\}}$ be a real-valued function on $SE(3)$ or its vector bundles corresponding to arbitrary world and body frames $\mathcal{F}_W^b$ and $\mathcal{F}_B^a$. Then*

$\Psi^{\{b,a\}}$ determines an objective metric function $\overline{\Psi} = (\Gamma^{\tilde{h},c})^*\Psi^{\{b,a\}}$ on $\mathcal{C}$ if and only if it is frame-invariant.

Thus, frame-invariance is equivalent to objectivity, and can be interpreted as follows. A frame-invariant metric function on $SE(3)$ must be *independent* of the choice of world frame. This is equivalent to saying that the function is *left invariant* and is implied by the *observer-indifference* condition in the objectivity notion. The frame-invariant metric function must also *consistently* depend on the choice of body frame in such a way that it evaluates to the same value when the representations of configurations, tangent vectors and covectors are appropriately transformed in accordance with the frame change. The consistent dependence condition ensures the consistent determination of the metric function on $\mathcal{C}$, as mentioned in the previous discussion of weak frame invariance.

Objective metric functions are most conveniently written in terms of frame-invariant functions. While frame-invariant functions are merely a convenient *representation* of objective functions and do *not* actually *define* objective functions[6], the notion of frame-invariance offers considerable intuition and convenience in developing well-defined, physically meaningful kinematic metric functions.

We now present some examples of frame-invariant distance metrics. More examples on frame-invariant norms and inner products (Riemannian metrics) can be found in Chapter 8. Recall that given a set S, a function $\rho\colon S \times S \to \mathbb{R}$ is said to be a *distance (metric)* if it satisfies: $\rho(x,y) = \rho(y,x)$ (symmetry); $\rho(x,y) \geqslant 0$ and $\rho(x,y) = 0$ if and only if $x = y$ (positive definiteness); and $\rho(x,y) \leqslant \rho(x,z) + \rho(z,y)$ (triangle inequality) for all $x, y, z \in S$. A distance

[6]We carefully *avoid* saying that an objective function is *defined* as the pull-back of a frame-invariant function Ψ by a diffeomorphism from $\mathcal{C}$ onto $SE(3)$, since such a definition generally depends on the choice of diffeomorphism. This is similar to the situation where a metric function on a manifold in general *cannot* be defined, in a parametrization-invariant manner, based on some parametrization of the manifold.

metric on $SE(3)$ allows us to measure the distance between two configurations, and its frame-invariance ensures that the measurement is made in a well-defined manner. Some frame-invariant distances have been proposed in the robotics literature, however, the notion of objectivity clarifies the fundamental implication of frame-invariance.

Example 7.8.1 (Frame-Invariant Distance Metrics). The real-valued function [85] $\rho\colon SE(3) \times SE(3) \to \mathbb{R}$ given by

$$\rho(g_1, g_2) = \max_{r \in \mathcal{B}} |g_1 r - g_2 r|$$

is a frame-invariant distance metric, where $|\cdot|$ is the standard norm on $\mathbb{R}^3$. This distance can be interpreted as the *maximum* of the distances between the corresponding positions of $\mathcal{B}$'s particles. Alternatively, instead of the maximal distance, one may consider the *average* of the distances between the corresponding positions of $\mathcal{B}$'s particles [73]:

$$\rho(g_1, g_2) = \int_{\mathcal{B}} |g_1 r - g_2 r| dV,$$

This is again a frame-invariant distance metric. Other approaches to defining distance metrics will be discussed in Chapter 8.

7.8.3 Representing Frame-Invariance in Body Coordinates

There is a simple representation of frame-invariance in terms of body coordinates. This representation can be used as a practical tool for developing frame-invariant, and hence objective, functions of rigid body velocities and

wrenches.

In the world and body frames $\mathcal{F}_W$ and $\mathcal{F}_B$, let $\chi \in \mathcal{C}$, $\overline{\mathbf{v}} \in T_\chi\mathcal{C}$ and $\overline{\boldsymbol{\alpha}} \in T^*_\chi\mathcal{C}$ be represented by $g \in SE(3)$, $\mathbf{v} \in T_gSE(3)$ and $\boldsymbol{\alpha} \in T^*_gSE(3)$, respectively. Recall from Section 3.2.1 that the tangent vector $\mathbf{v} \in T_gSE(3)$ can be further represented as a body velocity $\widehat{\dot{q}} = TL_{g^{-1}}(\mathbf{v}) = g^{-1}\mathbf{v} \in T_eSE(3)$ with coordinates $\dot{q} = (\widehat{\dot{q}})^\vee = \left(\begin{smallmatrix} v \\ \omega \end{smallmatrix}\right) \in \mathbb{R}^6$. Here the "vee" operator has been used, which maps $\left(\begin{smallmatrix} \widehat{\omega} & v \\ 0 & 0 \end{smallmatrix}\right) \in T_eSE(3)$ to $\left(\begin{smallmatrix} v \\ \omega \end{smallmatrix}\right) \in \mathbb{R}^6$, and the "hat" operator, which is the inverse of the "vee". Meanwhile, the covector $\boldsymbol{\alpha}$ can be further represented as a body wrench $\widehat{\boldsymbol{w}} = T^*L^{-1}_{g^{-1}}(\boldsymbol{\alpha}) = T^*L_g(\boldsymbol{\alpha}) \in T^*_eSE(3)$ with coordinates $\boldsymbol{w} = (\widehat{\boldsymbol{w}})^\vee = \left(\begin{smallmatrix} f \\ \tau \end{smallmatrix}\right) \in \mathbb{R}^6$. Note that given $\boldsymbol{\alpha} \in T^*_eSE(3)$, the "vee" operator for covectors is defined by $\check{\boldsymbol{\alpha}}(\check{\mathbf{v}}) = \boldsymbol{\alpha}(\mathbf{v})$ for all $\mathbf{v} \in T_eSE(3)$. The covector "hat" operator is the inverse of the covector "vee" operator.

Also recall from Section 3.2.1 that body velocities and wrenches depend on the choice of body frame but are not affected by the choice of world frame. With respect to the world and body frames $\mathcal{F}^b_W$ and $\mathcal{F}^a_B$, $\overline{\mathbf{v}} \in T_\chi\mathcal{C}$ corresponds to a body velocity $\dot{q}^a$ and $\overline{\boldsymbol{\alpha}} \in T^*_\chi\mathcal{C}$ to a body wrench $\boldsymbol{w}^a$. The transformation formulas, as given in (3.7), are reproduced here for convenience:

$$\dot{q}^a = \mathrm{Ad}_a^{-1}\,\dot{q} \quad \text{and} \quad \boldsymbol{w}^a = \mathrm{Ad}_a^T\,\boldsymbol{w}. \tag{7.3}$$

We now use body coordinates to represent frame-invariant metric functions of tangent vectors and covectors. With respect to the world frame $\mathcal{F}_W$ and body frame $\mathcal{F}_B$, a frame-invariant metric function Φ on $SE(3)$ can be represented by a function $\phi\colon \mathbb{R}^6 \to \mathbb{R}$ using body velocities and wrenches as follows:

$$\Phi_g(\mathbf{v}_1, \ldots, \mathbf{v}_k, \boldsymbol{\alpha}_1, \ldots, \boldsymbol{\alpha}_l) = \phi(\dot{q}_1, \ldots, \dot{q}_k, \boldsymbol{w}_1, \ldots, \boldsymbol{w}_l),$$

where $\dot{q}_i$ and $\boldsymbol{w}_j$ are body coordinates corresponding to tangent vectors $\mathbf{v}_i \in T_g SE(3)$ and $\boldsymbol{\alpha}_j \in T_g^* SE(3)$ with respect to $\mathcal{F}_W$ and $\mathcal{F}_B$. With respect to the world frame $\mathcal{F}_W^b$ and body frame $\mathcal{F}_B^a$, the frame-invariant function Φ transforms to $\Phi^{\{b,a\}} = \Phi^{\{e,a\}}$, which is independent of the choice of world frame. To represent the same tangent vectors and covectors to $\mathcal{C}$, $\mathbf{v}_i$ and $\boldsymbol{\alpha}_j$ transform to $\mathbf{v}_i^{\{b,a\}}$ and $\boldsymbol{\alpha}_j^{\{b,a\}}$, which correspond to body velocities and wrenches $\dot{q}_i^a$ and $\boldsymbol{w}_j^a$, respectively, as given in (7.3). Since $\Phi^{\{b,a\}}$ and the body coordinates are both independent of world frame choices, ϕ transforms to ϕ^a, which depends only on the choice of world frame and satisfies

$$\Phi_g^{\{b,a\}}(\mathbf{v}_1^{\{b,a\}}, \ldots, \mathbf{v}_k^{\{b,a\}}, \boldsymbol{\alpha}_1^{\{b,a\}}, \ldots, \boldsymbol{\alpha}_l^{\{b,a\}}) = \phi^a(\dot{q}_1^a, \ldots, \dot{q}_k^a, \boldsymbol{w}_1^a, \ldots, \boldsymbol{w}_l^a).$$

The above equations involving ϕ and ϕ^a lead to the following necessary and sufficient condition for frame-invariance:

Proposition 7.8.5. *With respect to $\mathcal{F}_W$ and $\mathcal{F}_B$, let ϕ be a real-valued function of body velocities and wrenches. With respect to the body frame $\mathcal{F}_B^a$, if the function ϕ obeys the change-of-frame formula $\phi^a(\dot{q}_1^a, \ldots, \dot{q}_k^a, \boldsymbol{w}_1^a, \ldots, \boldsymbol{w}_l^a) = \phi(\dot{q}_1, \ldots, \dot{q}_k, \boldsymbol{w}_1, \ldots, \boldsymbol{w}_l)$, where $\dot{q}_i^a = Ad_a^{-1}\dot{q}_i$ and $\boldsymbol{w}_j^a = Ad_a^T \boldsymbol{w}_j$, then it defines a frame-invariant function.*

This proposition provides a simple and practical representation of frame-invariant functions on the vector bundles of $SE(3)$, which in turn define objective functions on the vector bundles of $\mathcal{C}$. While body coordinates have been used, it is interesting to consider whether the dual representation by spatial coordinates is appropriate to be used to represent frame-invariant functions. From Section 3.2.2, a tangent vector $\mathbf{v} \in T_g SE(3)$ can be represented as $\mathbf{v}g^{-1}$, called the *spatial velocity*, and a covector can be represented as a *spatial wrench*. A function defined in terms of spatial velocities and wrenches are au-

tomatically right invariant. However, since right invariant functions in general do not lead to objective functions, the following important observation can readily be made.

Remark 7.8.2. The spatial representations of tangent and cotangent vectors are in general *not* appropriate to be used to define a well-defined, physically meaningful real-valued function. Unless the function is bi-invariant, it is *not* frame-invariant, and does *not* determine an objective function.

Summary:

This chapter introduced the notion of objectivity using an intrinsic definition of the configuration space of a rigid body. This notion formalizes the natural requirement of metric functions that metric measurements be made in a way indifferent to observers. Based on the notion of objectivity, the invariance properties in $SE(3)$ have been clarified. An objective function on $\mathcal{C}$ or its vector bundles corresponds to a family of left invariant functions, which are inter-related via pull-backs by right translations, on $SE(3)$ or its vector bundles. It was clarified that left invariance is necessary but not sufficient, bi-invariance is sufficient but not necessary, while frame-invariance is sufficient and necessary for objectivity. The equivalence between objectivity and frame-invariance can be used as a general framework for developing well-defined metric functions. Chapter 8 uses this framework to develop frame-invariant norms of rigid body velocities and wrenches. It will be shown that while there is a lack of bi-invariance in $SE(3)$, there are frame-invariant norms that have interesting physical interpretations and can be attractive to practical applications.

Chapter 8

Frame-Invariant Norms and Pseudo-Norms of Rigid Body Velocities and Wrenches

8.1 Introduction

It is of great practical interest to define norms and inner products of tangent vectors and covectors to the configuration space of a rigid body. A tangent vector norm allows to measure the "length" of rigid body velocities, or instantaneous displacements that approximate small rigid body displacements. The notion of velocity "lengths" is needed in many practical applications. For example, it can be used to indicate how far a fixtured quasi-rigid workpiece is displaced from its initial location due to a manufacturing operation, and is hence a measure of the workpiece's deflection. This interpretation of velocity norm was the basis for the minimum-deflection fixturing approach in Chapter 6. Dual to velocity norms, wrench norms are used to measure the "length" of wrenches. Such a notion is necessary for determining the size of a work load applied to a rigid or quasi-rigid object. It also allows for the definition of balls in the wrench space, whose usefulness for defining quality measures was also

demonstrated in Chapter 6.

While they are practically important, well-defined velocity and wrench norms have not been available to engineers. Traditionally, the Euclidean norm on $\mathbb{R}^6$ has been employed to define velocity and wrench norms. For example, the Euclidean wrench norm has been widely used in defining quality measures for rigid grasps, for example, by Kirkpatrick, Mishra and Yap [79], Ferrari and Canny [41], and Teichmann [151]. Whether there exist frame-invariant velocity and wrench norms has largely been an open problem.

The frame-dependence problem can partially be attributed to the lack of bi-invariance in $SE(3)$. It is well-known that there exist no bi-invariant Riemannian metrics on $SE(3)$ [92]. Because of this fact, it was perceived that there are no frame-invariant Riemannian metrics. Since norms are commonly induced from Riemannian metrics, it was also perceived that there are no frame-invariant norms of rigid body velocities and wrenches.

Fortunately, as has been shown in Chapter 7, bi-invariance is not a necessary condition for velocity and wrench norms to be well-defined. As has been clarified, bi-invariance is sufficient, but not necessary, for frame-invariance. Therefore, despite the lack of bi-invariance on $SE(3)$, frame-invariant norms of tangent vectors and covectors can exist. Seeking such norms is the subject of this chapter.

Body velocities and wrenches will be conveniently used in this chapter, which is organized as follows. Following Section 8.2, which briefly reviews the notion of norms, Section 8.3 shows that there indeed exist no bi-invariant velocity and wrench norms. Thus, well-defined velocity and wrench norms are expected to be frame-invariant but not bi-invariant. Section 8.4 proposes several frame-invariant velocity norms with interesting physical meanings. The root-mean-square velocity norm, which was used in Chapter 6, can be induced from a Riemannian metric as in common practice, but the other norms pre-

sented in the section are not inducible from Riemannian metrics. Sections 8.5 and 8.6 consider frame-invariant wrench norms. These norms are defined based on frame-invariant velocity norms, and have interesting physical interpretations. In addition, closed-form formulas or efficient algorithms will be provided for the root-mean-square norm in the general three-dimensional case, and the average wrench norm in the case of polygonal objects.

8.2 Norms and Inner Products on Linear Vector Spaces and Vector Bundles

This section briefly reviews the notions of distance metrics on sets, as well as norms and inner products on vector spaces and vector bundles. Let V be a real vector space. A mapping $\|\cdot\| : V \to \mathbb{R}$ is said to be a *pseudo-norm* if it satisfies the following properties for all $x, y \in V$ and $a \in \mathbb{R}$: $\|x\| \geqslant 0$ (non-negativity); $\|ax\| = |a|\|x\|$ (homogeneity); and $\|x + y\| \leqslant \|x\| + \|y\|$ (triangle inequality). If in addition $\|x\| = 0$ implies that $x = 0$ (nonsingularity), $\|\cdot\| : V \to \mathbb{R}$ is said to be a *norm*. A *pseudo inner product* is a mapping $\langle \cdot, \cdot \rangle : V \times V \to \mathbb{R}$ with the following properties for all $x, y, z \in V$ and $a, b \in \mathbb{R}$: $\langle x, x \rangle \geqslant 0$ (positive semi-definiteness); $\langle x, y \rangle = \langle y, x \rangle$ (symmetry); $\langle ax + by, z \rangle = a \langle x, z \rangle + b \langle y, z \rangle$ and $\langle x, ay + bz \rangle = a \langle x, y \rangle + b \langle x, z \rangle$ (bilinearity). If in addition $\langle x, x \rangle = 0$ implies that $x = 0$ (nonsingularity), then $\langle \cdot, \cdot \rangle : V \times V \to \mathbb{R}$ is an *inner product*. Note that a (pseudo) inner product induces a (pseudo) norm by $\|x\| = \langle x, x \rangle^{1/2}$.

The notions of norms and inner products can be easily extended to the tangent and cotangent bundles of a manifold M. A *norm* (or pseudo-norm) on TM (or T^*M) is a real-valued map $\|\cdot\|$ that assigns a norm (or pseudo-norm) $\|\cdot\|_x$ (the subscript "x" is usually omitted for brevity) for each tangent space T_xM (or each cotangent space T_x^*M). Similarly, an *inner product* (or pseudo-inner product) on the tangent (or cotangent) bundle assigns an inner

product (or pseudo-inner product) to each tangent (or cotangent) space. Note that an inner product on TM, which is called a *Riemannian metric* for the manifold M, allows the measurement of the "length" of a curve in M.

It can be verified that given a diffeomorphism $f\colon N \to M$ between smooth manifolds, and a real-valued function Ψ on M (or TM or T^*M) with an appropriate number of arguments, Ψ is a norm or inner product (or pseudo-norm or pseudo inner product) on TM or T^*M if and only if $f^*\Psi$ is a norm or inner product (or pseudo-norm or pseudo inner product) on TN or T^*N. Thus, a frame-invariant norm on $TSE(3)$ is necessary and sufficient to determine an objective norm on $\mathcal{C}$, and this is also true for pseudo-norms, pseudo inner products and inner products. Thus we will focus on frame-invariance to ultimately guarantee objectivity.

8.3 Lack of Bi-Invariant Norms

Section 7.8 indicated that if a velocity norm is bi-invariant, it will be frame-invariant. Since there are no bi-invariant Riemannian metrics on $SE(3)$, there are no bi-invariant norms that can be induced from a Riemannian metric. It is then interesting to know whether there are bi-invariant norms that cannot be induced from Riemannian metrics. The following proposition indicates that such norms do not exist.

Proposition 8.3.1. *There exist no bi-invariant norms on $TSE(3)$, inducible or not inducible from a Riemannian metric.*

Proof. Consider a left invariant norm Φ, which is determined by Φ_e by $\Phi_g = L_{g*}\Phi_e$ for any $g \in SE(3)$. Let

$$\Phi_e(\widehat{\dot{q}}) = \phi(\dot{q}) = \phi(v, \omega)$$

for $\widehat{\dot{q}} \in T_e SE(3)$ where $\dot{q} = \binom{v}{\omega} \in \mathbb{R}^6$. Now suppose that Φ is also right invariant. Then for any $a = (d, R) \in SE(3)$,

$$\Phi_e(\widehat{\dot{q}}) = R_a^* \Phi_e(\widehat{\dot{q}}) = \Phi_a(\widehat{\dot{q}}a) = \Phi_e(a^{-1}\widehat{\dot{q}}a).$$

In coordinate form, this can be written as $\phi(\dot{q}) = \phi(\mathrm{Ad}_a^{-1}\,\dot{q})$. Using (8.1) to expand the right-hand side of this equation yields

$$\phi(v, \omega) = \phi(R^T(v + \omega \times d),\ R^T\omega)$$

for all $d \in \mathbb{R}^3$ and 3×3 proper orthogonal matrices R. If $\omega = 0$, $\phi(v, 0)$ must be a norm of $v \in \mathbb{R}^3$, hence $\phi(v, 0) = |v|$. When $\omega \neq 0$, choosing $d = \omega \times v/|\omega|^2$ yields $v + \omega \times d = (\omega^T v)\omega/|\omega|^2$. Hence

$$\phi(v, \omega) = \phi\Big(|\omega|\Big(\frac{\omega^T v}{|\omega|^2}\Big)\Big(R^T \frac{\omega}{|\omega|}\Big),\ |\omega|\Big(R^T \frac{\omega}{|\omega|}\Big)\Big) = \phi(h|\omega|u,\ |\omega|u),$$

where $h = \frac{\omega^T v}{|\omega|^2}$ is the pitch associated with $\dot{q}$, and $u \in \mathbb{R}^3$ is an arbitrary unit vector since R is arbitrary. It follows that if $\omega \neq 0$, the function ϕ depends only on the magnitude of the angular velocity and the pitch h. There must be some function $f\colon \mathbb{R} \times \mathbb{R}_+ \to \mathbb{R}$ such that

$$\phi(v, \omega) = \begin{cases} |v| & \text{if } \omega = 0, \\ f(h, |\omega|) & \text{if } \omega \neq 0. \end{cases}$$

The homogeneity of a norm implies that for $c \in \mathbb{R}$,

$$f(h, |c\omega|) = |c| f(h, |\omega|),$$

where the fact that $\dot{q}$ and $c\dot{q}$ have the same pitch h has been used. Therefore, f must be positively linear in its second argument. This requirement implies that f must take the form

$$f(h, |\omega|) = \sigma(h)|\omega|,$$

for some positive function σ. Choose $\dot{q}_1 = \binom{v_1}{\omega_1}$ and $\dot{q}_2 = \binom{v_2}{\omega_2}$ such that $v_1 = v_2 = v$ and $\omega_1 = -\omega_2 = \omega$, where v and ω are nonzero and are related by $\omega^T v = 0$. Since $h_i = v_i^T \omega_i / |\omega_i|^2 = 0$ and $\omega_1 + \omega_2 = 0$, the triangle inequality $\Phi_e(\widehat{\dot{q}}_1 + \widehat{\dot{q}}_2) \leqslant \Phi_e(\widehat{\dot{q}}_1) + \Phi_e(\widehat{\dot{q}}_2)$ implies that

$$|v| \leqslant \sigma(0)|\omega|.$$

Since $|\omega|$ can be arbitrarily small while $\|v\|$ is fixed, this inequality is not always satisfied, a contradiction. This implies that there are no bi-invariant norms on $TSE(3)$. □

The proposition yields the following corollary on the lack of bi-invariant wrench norms.

Corollary 8.3.2. *There exist no bi-invariant norms or inner products on* $T^*SE(3)$.

Proof. The tangent space $T_gSE(3)$ and cotangent space $T_g^*SE(3)$ at any $g \in SE(3)$ are finite dimensional vector spaces, and $T_g^*SE(3)$ is the dual space

of $T_gSE(3)$. Let $T_g^{**}SE(3)$ be the dual space of $T_g^*SE(3)$. Then since the spaces are finite dimensional, any $\boldsymbol{\lambda} \in T_g^{**}SE(3)$ can be identified with a unique tangent vector $\mathbf{v} \in T_gSE(3)$ by the relationship $\boldsymbol{\lambda}(\boldsymbol{\alpha}) = \boldsymbol{\alpha}(\mathbf{v})$ for any $\boldsymbol{\alpha} \in T_g^*SE(3)$. Suppose that Φ is a bi-invariant norm on $T^*SE(3)$. Then Φ induces a norm, denoted Ψ, on $T_g^{**}SE(3)$ by

$$\Psi_g(\boldsymbol{\lambda}) = \sup\left\{\frac{\boldsymbol{\lambda}(\boldsymbol{\alpha})}{\Phi_g(\boldsymbol{\alpha})} : \boldsymbol{\alpha} \in T_g^*SE(3)\right\}.$$

With $T_g^{**}SE(3)$ identified with $T_gSE(3)$, Ψ is a norm on $TSE(3)$. It can be verified that the function Θ on $TSE(3) \times T^*SE(3)$ defined by $\Theta_g(\mathbf{v}, \boldsymbol{\alpha}) = \boldsymbol{\alpha}(\mathbf{v})$ is bi-invariant. Now Φ is bi-invariant by assumption. It can be shown that Ψ, defined via two bi-invariant functions, is also bi-invariant. Thus, there is a bi-invariant norm on $TSE(3)$, a contradiction to Proposition 8.3.1. Therefore, there are no bi-invariant norms on $T^*SE(3)$. Now suppose that there is a bi-invariant inner product on $T^*SE(3)$. Then this inner product induces a bi-invariant norm on $T^*SE(3)$, a contradiction. Hence, there are no bi-invariant inner products on $T^*SE(3)$. □

The fact that there are no bi-invariant norms on $TSE(3)$ and $T^*SE(3)$ implies that *no objective tangent vector or covector norms can be represented on* $TSE(3)$ *or* $T^*SE(3)$ *as a single function.* In other words, with respect to different choices of reference frames, the norms on $TSE(3)$ and $T^*SE(3)$ need to transform according the frame-invariance conditions given in Definition 7.8.1 or Proposition 7.8.5 in terms of body coordinates.

8.4 Frame-Invariant Velocity Norms

Section 8.3 showed that there exist no bi-invariant norms of rigid body velocities and wrenches. Therefore, well-defined norms are expected to be frame-

invariant but not bi-invariant. According to Chapter 7, so long as the norms are frame-invariant, the "length" measurements of rigid body velocities and wrenches can still be performed in a observer-indifferent manner and are therefore well-defined.

For convenience in verifying the frame-invariance of the norms that will be proposed, expand the body velocity transformation formula (3.7) as follows. In a new body frame $\bar{\mathcal{F}}_B$ displaced by $a = \left(\begin{smallmatrix} R & d \\ 0 & 1 \end{smallmatrix}\right)$ from the original body frame $\mathcal{F}_B$, a body velocity $\dot{q} = (v, \omega)$ transforms to $\dot{\bar{q}} = (\bar{v}, \bar{\omega}) = \mathrm{Ad}_a^{-1}\, \dot{q}$, i.e.,

$$\bar{v} = R^T(v + \omega \times d) \quad \text{and} \quad \bar{\omega} = R^T\omega. \tag{8.1}$$

Meanwhile, the coordinates of a point in the object in the new and old body frames are related by $\left(\begin{smallmatrix} \bar{r} \\ 1 \end{smallmatrix}\right) = a^{-1} \left(\begin{smallmatrix} r \\ 1 \end{smallmatrix}\right)$, or

$$\bar{r} = R^T(r - d). \tag{8.2}$$

It follows that the region in $\mathbb{R}^3$ occupied by $\mathcal{B}$ with respect to the frame $\mathcal{F}_B$, also denoted $\mathcal{B}$, transforms to $\bar{\mathcal{B}} = \{R^T(r - d) : r \in \mathcal{B}\}$.

Weighting functions defined on $\mathcal{B}$ will be used extensively. For the purposes of this chapter, the following class of weighting functions will be used. In the following definition, δ denotes the Dirac delta function.

Definition 8.4.1 (Weighting Functions). A function $\nu \colon \mathcal{B} \to \mathbb{R}$ is said to be a *weighting function* if it is of the form $\nu = \nu_a + \nu_b$ (explained below), is *normalized* such that $\int_{\mathcal{B}} \nu(r) dV = 1$, and is *frame-invariant*, i.e., in a new body frame $\bar{\mathcal{F}}_B$, ν transforms to $\bar{\nu}$ such that $\nu(r) = \bar{\nu}(\bar{r})$ while r transforms to $\bar{r}$. The function $\nu_a \colon U \to \mathbb{R}$ is *piecewise continuous* and *non-negative*, where $U \subset \mathcal{B}$ has *non-zero* volume. The function $\nu_b \colon \mathcal{B} \to \mathbb{R}$ is of the discrete form

$\nu_b(r) = \sum_{i=1}^{p} w_i \delta(r - r_i)$ where $w_i > 0$ and $r_i \in \mathcal{B}$ for all $i = 1, \ldots, p$. We say that $\nu = \nu_a + \nu_b$ is *positive definite* if $\int_{\mathcal{B}} \nu_a(r) dV > 0$, or ν_b is nonzero at no less than three non-collinear points.

First consider a velocity norm that is induced from a Riemannian metric. For arbitrary body velocities $\dot{q}_i = \binom{v_i}{\omega_i}$ specified in $\mathcal{F}_B$, define a real-valued function by the following weighted average

$$\langle \dot{q}_1, \dot{q}_2 \rangle = \int_{\mathcal{B}} \nu(r)(v_1 + \omega_1 \times r)^T (v_2 + \omega_2 \times r) dV, \tag{8.3}$$

where $\nu \colon \mathcal{B} \to \mathbb{R}$ is a weighting function. The properties of this function are characterized as follows.

Proposition 8.4.1. *The function $\langle \dot{q}_1, \dot{q}_2 \rangle$ is frame-invariant. If ν is positive definite, then $\langle \dot{q}_1, \dot{q}_2 \rangle$ is a Riemannian metric on $SE(3)$. Otherwise it is a pseudo-Riemannian metric on $SE(3)$. In either case, it can be computed from the quadratic form $\langle \dot{q}_1, \dot{q}_2 \rangle = \dot{q}_1^T M \dot{q}_2$, where $M = \int_{\mathcal{B}} \nu(r) \begin{pmatrix} I & -\hat{r} \\ \hat{r} & -\hat{r}^2 \end{pmatrix} dV$ is the weighting matrix associated with ν.*

Proof. According to formulas (8.1) and (8.2), with respect to a new body frame $\bar{\mathcal{F}}_B$, $\bar{v}_i + \bar{\omega}_i \times r = R^T(\bar{v}_i + \bar{\omega}_i \times r)$. Since $\bar{\nu}(\bar{r}) = \nu(r)$, this implies that

$$\int_{\mathcal{B}} \nu(r)(v_1 + \omega_1 \times r)^T (v_2 + \omega_2 \times r) dV = \int_{\bar{\mathcal{B}}} \bar{\nu}(\bar{r})(\bar{v}_1 + \bar{\omega}_1 \times \bar{r})^T (\bar{v}_2 + \bar{\omega}_2 \times \bar{r}) d\bar{V},$$

and frame-invariance follows. It is trivial to observe that $\langle \dot{q}_1, \dot{q}_2 \rangle$ is a symmetric and non-negative bilinear function, and is therefore a pseudo-Riemannian metric. If ν is positive definite, then $\langle \dot{q}, \dot{q} \rangle = 0$ implies that the velocities of three non-collinear points are zero, which in turn implies that $\dot{q} = 0$. The computation formula is proved by noting that $v + \omega r = [I, -\hat{r}] \binom{v}{\omega}$, and that $\dot{q}_i$ are independent of $r \in \mathcal{B}$. □

This Riemannian metric immediately induces a norm of rigid body velocities, given by

$$\|\dot{q}\|_{rms} = \langle \dot{q}, \dot{q} \rangle^{\frac{1}{2}} = (\dot{q}^T M \dot{q})^{\frac{1}{2}}, \tag{8.4}$$

for a body velocity $\dot{q} = (v, \omega)$. Since $\langle \dot{q}, \dot{q} \rangle$ is frame-invariant, this norm is also frame-invariant. Note that this defines a pseudo-norm if $\langle \dot{q}, \dot{q} \rangle$ is a pseudo-Riemannian metric.

There are two interesting interpretations of this Riemannian metric and its induced norm. If ν is interpreted as the mass density of $\mathcal{B}$, then $\frac{1}{2} \langle \dot{q}, \dot{q} \rangle$ is the *kinetic energy* of the body with velocity $\dot{q}$. On the other hand, one can alternatively interpret this Riemannian metric from a purely kinematic point of view. By interpreting ν as a weighting function on contributions from individual particles of $\mathcal{B}$, the metric can be viewed as a *weighted average*, and the norm is the *root-mean-square (rms)* of the velocities of $\mathcal{B}$'s points. For this reason, $\langle \dot{q}, \dot{q} \rangle$ is called the *weighted-average Riemannian metric*, and as the notation suggests, $\|\dot{q}\|_{rms}$ is termed the rms velocity norm. The weighting function can be chosen to encode certain manufacturing requirements. For example, if one uses uniform weighting by choosing $\nu(r) = (\int_{\mathcal{B}} dV)^{-1}$, then the points of $\mathcal{B}$ are considered equally important. On the other hand, using discrete weighting $\nu(r) = \sum_{i=1}^{k} \nu_i \delta(r - r_i)$, where ν_i are constants such that $\sum_{i=1}^{k} \nu_i = 1$, the contributions of only a finite number of points in the object are included. These points can be chosen as feature points that have the most influence on manufacturing accuracy.

While Riemannian metrics can be used to induce velocity norms, it is important to note that norms in general need *not* be inducible from a Riemannian inner product. We now present two such norms that have interesting physical

interpretations. For a body velocity $\dot{q} = (v, \omega)$, define

$$\|\dot{q}\|_{\max} = \max_{r \in \Omega_B} |\omega \times r + v|, \quad \text{and} \quad \|\dot{q}\|_{\text{avg}} = \int_{\mathcal{B}} \nu(r) |\omega \times r + v| dV \tag{8.5}$$

where $\Omega_B \subset \mathcal{B}$ is a set of feature points of the object, and ν is a non-negative weighting function satisfying the condition $\int_{\mathcal{B}} \nu(r) dV = 1$.

Proposition 8.4.2. *The functions $\|\dot{q}\|_{max}$ and $\|\dot{q}\|_{avg}$ are frame-invariant. If Ω_B contains at least three non-coplanar points and ν is nonzero at no less than three non-coplanar points, $\|\dot{q}\|_{max}$ and $\|\dot{q}\|_{avg}$ are norms on $TSE(3)$. Otherwise they are pseudo-norms.*

Proof. The frame-invariance of these functions can be proved in a manner similar to the weighted-average Riemannian metric. We only prove that $\|\dot{q}\|_{\max}$ is a norm, since a similar proof can be given to $\|\dot{q}\|_{\text{avg}}$. Write $\|\dot{q}\|_{\max} = \max_{r \in \Omega_B} |u_r(\dot{q})|$, where $u_r(\dot{q}) = v + \omega \times r$ is the velocity of the point r. The function $\|\dot{q}\|_{\max}$ is obviously non-negative, and its homogeneity follows directly from the linearity of $u_r(\dot{q})$ in $\dot{q}$. It also satisfies the triangle inequality:

$$\begin{aligned} \|\dot{q}_1 + \dot{q}_2\|_{\max} &= \max_{r \in \Omega_B} |u_r(\dot{q}_1 + \dot{q}_2)| = \max_{r \in \Omega_B} |u_r(\dot{q}_1) + u_r(\dot{q}_2)| \\ &\leqslant \max_{r \in \Omega_B} |u_r(\dot{q}_1)| + \max_{r \in \Omega_B} |u_r(\dot{q}_2)| = \|\dot{q}_1\|_{\max} + \|\dot{q}_2\|_{\max}, \end{aligned}$$

since the norm $|\cdot|$ on $\mathbb{R}^3$ satisfies the triangle inequality. Therefore $\|\dot{q}\|_{\max}$ is a pseudo-norm. If Ω_B contains at least three non-coplanar points, then $\|\dot{q}\|_{\max} = 0$ implies that the velocities of these three points are zero. Hence $\dot{q} = 0$ and $\|\dot{q}\|_{\max}$ becomes a norm. □

We call $\|\dot{q}\|_{\max}$ the *maximum velocity norm*, and $\|\dot{q}\|_{\text{avg}}$ the *average velocity norm* since they have the following interesting physical interpretations.

$\|\dot{q}\|_{\max}$ is the *maximal velocity or instantaneous displacement* of the points in Ω_B, a feature-point set of $\mathcal{B}$. In fact, this norm actually corresponds to the objective norm in Example 7.6.1, and includes the planar case, formula (7.2), as a special case. On the other hand, $\|\dot{q}\|_{\text{avg}}$ is the *weighted-average velocity or instantaneous displacement* of the points in $\mathcal{B}$. Note that these physical interpretations make the two norms very attractive to practical applications, such as fixturing, where workpiece displacements are a major concern in the design process. While the average norm can be computed in terms of closed-form or numerical integration, the maximum norm can be computed from the following formula that is based on the physical meaning of the norm. Given a velocity $\dot{q} = (v, \omega)$,

$$\|\dot{q}\|_{\max} = \begin{cases} |v| & \text{if } \omega = 0, \\ |\omega| \left(\rho_{\max}^2 + h^2\right)^{\frac{1}{2}} & \text{if } \omega \neq 0 \end{cases} \tag{8.6}$$

where in the case of $\omega \neq 0$, $h = \frac{\omega^T v}{|\omega|^2}$ is the pitch associated with $\dot{q}$, and $\rho_{\max}$ is the maximal distance from the screw axis of $\dot{q}$ (Section 3.2.2), given by $\{v \times \omega + \alpha\omega : \ \alpha \in \mathbb{R}\}$, to any point of $\mathcal{B}$.

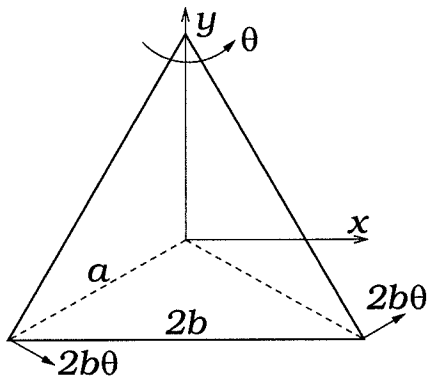

Figure 8.1: An instantaneous rotation of an equilateral triangle.

Example 8.4.1. Suppose that an equilateral triangle whose edges are of length

$2b$ undergoes an instantaneous rotation, of magnitude $0 < \theta \ll 1$, about one of its vertices. We compute the "length" of this velocity using the average, root-mean-square and maximum norms. As shown in Figure 8.1, choose a body frame whose origin is at the triangle's center of symmetry. In this frame, the velocity is given by $\dot{q} = (\theta a, 0, \theta)$, where $a = \frac{2}{\sqrt{3}}b$ is the distance from the origin to the triangle's vertices. To compute the average and rms norms, we use a discrete weighting function $\nu(r) = \sum_{i=1}^{3} \frac{1}{3}\delta(r - r_i)$, where r_i are the triangle's vertices. Denote by $u_{r_i}(\dot{q})$ the velocity of r_i due to $\mathcal{B}$'s velocity $\dot{q}$. By (8.5), the average norm is given by $\|\dot{q}\|_{\text{avg}} = \sum_{i=1}^{3} \frac{1}{3}|u_{r_i}| = \frac{4}{3}\theta\, b$. Now consider the rms norm. It can be shown that the weighting matrix associated with ν is $M = \text{diag}(1, 1, a^2)$, which gives $\|\dot{q}\|_{rms} = (\dot{q}M\dot{q})^{\frac{1}{2}} = \frac{2\sqrt{6}}{3}\theta\, b$. Finally, $\Omega_B = \mathcal{B}$ is taken for the maximum norm. The fact that the maximal velocity of $\mathcal{B}$'s points due to $\dot{q}$ occurs at a bottom vertex, as shown in the figure, implies that $\|\dot{q}\|_{\max} = 2\theta\, b$. Note that $\|\dot{q}\|_{\max} > \|\dot{q}\|_{rms} > \|\dot{q}\|_{\text{avg}}$.

8.5 Frame-Invariant Wrench Norms Induced From Inner Products

Having considered frame-invariant velocity norms, we now turn to frame-invariant wrench norms. First consider a norm that is induced from a wrench inner product.

A wrench inner product can be defined from a Riemannian metric as follows. By the Riez representation theorem in functional analysis [110], every covector, which is a real-valued linear map on the tangent space, corresponds to a unique tangent vector determined by the Riemannian metric. Specifically, let $\langle \dot{q}_1, \dot{q}_2 \rangle$ be a Riemannian metric, expressed in terms of body velocities. Then each body wrench $\boldsymbol{w}$ corresponds to a *unique* body velocity, denoted by $\boldsymbol{w}^\sharp$,

determined from

$$\left\langle \boldsymbol{w}^{\sharp}, \dot{q} \right\rangle = \boldsymbol{w}^{T}\dot{q} \tag{8.7}$$

for all body velocities $\dot{q}$. It follows that an induced inner product of wrenches can be induced by

$$\langle\langle \boldsymbol{w}_1, \boldsymbol{w}_2 \rangle\rangle = \left\langle \boldsymbol{w}_1^{\sharp}, \boldsymbol{w}_2^{\sharp} \right\rangle \tag{8.8}$$

for body wrenches $\boldsymbol{w}_i$. Provided the Riemannian metric $\langle \cdot, \cdot \rangle$ is frame-invariant, the induced wrench product is also *frame-invariant.* We now compute the wrench inner product. Every Riemannian metric can be written in the form $\langle \dot{q}_1, \dot{q}_2 \rangle = \dot{q}_1^T M \dot{q}_2$, where M is a positive definite matrix. For example, for the weighted-average Riemannian metric, M is the weighting matrix corresponding to a given weighting function. According to Equation (8.7), the velocity corresponding to a wrench $\boldsymbol{w}$ is given by $\boldsymbol{w}^{\sharp} = M^{-1}\boldsymbol{w}$. It follows from (8.8) that the induced wrench inner product can be computed from the following formula:

$$\langle\langle \boldsymbol{w}_1, \boldsymbol{w}_2 \rangle\rangle = \boldsymbol{w}_1^T M^{-1} \boldsymbol{w}_2. \tag{8.9}$$

The wrench inner product further induces a wrench norm by the formula

$$\|\boldsymbol{w}\| = \langle\langle \boldsymbol{w}, \boldsymbol{w} \rangle\rangle^{\frac{1}{2}} = (\boldsymbol{w}^T M^{-1} \boldsymbol{w})^{\frac{1}{2}} \tag{8.10}$$

Again, this norm is *invariant* to change of coordinate frames if the Riemannian

metric is frame-invariant.

Recall that a covector is a real-valued linear functional on the tangent space based at the same point. From an elementary result in functional analysis [110], a tangent vector norm induces a covector norm. Specifically, let $\|\cdot\|$ be a tangent vector norm expressed in terms of body velocities. Let $\boldsymbol{w}$ be a body wrench. Then the norm of $\boldsymbol{w}$ induced from the velocity norm is given by

$$\|\boldsymbol{w}\| = \sup\{\frac{|\boldsymbol{w}^T\dot{q}|}{\|\dot{q}\|} : \dot{q} \in T_{g_0}SE(3)\}. \tag{8.11}$$

This wrench norm is *frame-invariant* provided that the tangent vector norm is frame-invariant.

Proposition 8.5.1. *Let $\langle\langle\cdot,\cdot\rangle\rangle$ be the wrench inner product induced from a Riemannian metric $\langle\cdot,\cdot\rangle$. Let $\|\cdot\|_2$ and $\|\cdot\|_2$ be the velocity and wrench norms induced from $\langle\cdot,\cdot\rangle$ and $\langle\langle\cdot,\cdot\rangle\rangle$, respectively. Denote by $\|\cdot\|_2'$ the wrench norm induced from the velocity norm $\|\cdot\|$ according to* (8.11). *Then $\|\boldsymbol{w}\| = \|\boldsymbol{w}\|'$ for any wrench $\boldsymbol{w}$.*

Proof. It follows from (8.11) that

$$\|\boldsymbol{w}\|_2'^2 = \sup_{\dot{q}\in\mathbb{R}^6} \frac{(\boldsymbol{w}^T\dot{q})^2}{\|\dot{q}\|^2} = \sup_{\dot{q}\in\mathbb{R}^6} \frac{\dot{q}^T\boldsymbol{w}\boldsymbol{w}^T\dot{q}}{\dot{q}^TM\dot{q}} = \sup_{x\in\mathbb{R}^6} \frac{x^T(M^{-\frac{1}{2}}\boldsymbol{w}\boldsymbol{w}^TM^{-\frac{1}{2}})x}{x^Tx}.$$

Therefore, $\|\boldsymbol{w}\|_2'^2$ is the largest eigenvalue: $\lambda_{\max}(M^{-\frac{1}{2}}\boldsymbol{w}\boldsymbol{w}^TM^{-\frac{1}{2}})$. Since

$$(M^{-\frac{1}{2}}\boldsymbol{w}\boldsymbol{w}^TM^{-\frac{1}{2}})(M^{-\frac{1}{2}}\boldsymbol{w}) = (\boldsymbol{w}^TM^{-1}\boldsymbol{w})(M^{-\frac{1}{2}}\boldsymbol{w}),$$

$\boldsymbol{w}^TM^{-1}\boldsymbol{w}$ is the only nonzero eigenvalue of $M^{-\frac{1}{2}}\boldsymbol{w}\boldsymbol{w}^TM^{-\frac{1}{2}}$, since $M^{-\frac{1}{2}}\boldsymbol{w}\boldsymbol{w}^TM^{-\frac{1}{2}}$

has rank 1. Therefore, $\lambda_{\max}(M^{-\frac{1}{2}}\boldsymbol{w}\boldsymbol{w}^T M^{-\frac{1}{2}}) = \boldsymbol{w}^T M^{-1}\boldsymbol{w}$. This proves the assertion, since $\|\boldsymbol{w}\|_2^2 = \boldsymbol{w}^T M^{-1}\boldsymbol{w}$. □

Let us now focus on the wrench norm induced from the weighted-average Riemannian metric (8.3). In this case, the matrix M in the wrench norm formula (8.10) is the weighting matrix given by Proposition 8.4.1. To seek a physical interpretation, imagine that a wrench is generated by a distributed force as follows. Define a set of distributed forces by

$$\mathcal{D}_{\boldsymbol{w}}^2 = \Big\{ \mathsf{f} : \mathcal{B} \to \mathbb{R}^3 : \quad \int_{\mathcal{B}} \nu(r)\, D^T(r)\, \mathsf{f}(r)\, dV = \boldsymbol{w}, \ \int_{\mathcal{B}} \nu(r)\, |\mathsf{f}(r)|^2\, dV < \infty \Big\}, \tag{8.12}$$

where $D(r) = [I, -\widehat{r}]$. Note that $\int_{\mathcal{B}} \nu(r)\, D^T(r)\, \mathsf{f}(r)\, dV = \boldsymbol{w}$ is the matrix form of the conditions $\int_{\mathcal{B}} \nu(r)\, \mathsf{f}(r)\, dV = f$ and $\int_{\mathcal{B}} \nu(r)\, r \times \mathsf{f}(r)\, dV = \tau$. A distributed force $\mathsf{f} \in \mathcal{D}_{\boldsymbol{w}}^2$ is said to *generate* $\boldsymbol{w}$. Using this collection of generating distributed forces leads to the following proposition.

Proposition 8.5.2. *Consider an arbitrary body wrench $\boldsymbol{w}$. Let the wrench norm induced from the weighted-average inner product be denoted by $\|\boldsymbol{w}\|_{rms}$. Then $\|\boldsymbol{w}\|_{rms} = (\boldsymbol{w}^T M^{-1}\boldsymbol{w})^{\frac{1}{2}}$, where $M = \int_{\mathcal{B}} \nu(r)\, D^T(r) D(r)\, dV$, and is related to the distributed forces that generate $\boldsymbol{w}$ by*

$$\|\boldsymbol{w}\|_{rms} = \Big(\int_{\mathcal{B}} \nu(r)\, |\mathsf{f}_0(r)|^2\, dV \Big)^{\frac{1}{2}} = \inf_{\mathsf{f} \in \mathcal{D}_{\boldsymbol{w}}^2} \Big(\int_{\mathcal{B}} \nu(r)\, |\mathsf{f}(r)|^2\, dV \Big)^{\frac{1}{2}},$$

where $\mathsf{f}_0(r) = D(r)\, M^{-1}\boldsymbol{w} \in \mathcal{D}_{\boldsymbol{w}}^2$.

Proof. The formula $\|\boldsymbol{w}\|_{rms} = (\boldsymbol{w}^T M^{-1}\boldsymbol{w})^{\frac{1}{2}}$ is given by (8.10). We consider the relation of the wrench norm to distributed forces. For any velocity $\dot{q} = (v, \omega)$,

it can be shown that if $\mathsf{f} \in \mathcal{D}^2_{\boldsymbol{w}}$, then $\boldsymbol{w}(\dot{q}) = \int_{\mathcal{B}} \mathsf{f}(r) \cdot (v + \omega \times r)\, dV$ for any wrench $\boldsymbol{w} = (f, \tau)$. Thus,

$$\frac{|\boldsymbol{w}(\dot{q})|}{\|\dot{q}\|} \leqslant \frac{1}{\|\dot{q}\|} \int_{\mathcal{B}} |\mathsf{f}(r)|\, |(v + \omega \times r)|\, dV \leqslant \left(\int_{\mathcal{B}} |\mathsf{f}(r)|^2\, dV \right)^{\frac{1}{2}}.$$

By Equation (8.11), this implies that

$$\|\boldsymbol{w}\|_{rms} \leqslant \inf_{\mathsf{f} \in \mathcal{D}^2_{\boldsymbol{w}}} \left(\int_{\mathcal{B}} \nu(r)\, |\mathsf{f}(r)|^2\, dV \right)^{\frac{1}{2}}.$$

We now show that $\|\boldsymbol{w}\|_{rms}$ achieves this upper bound at the distributed force $\mathsf{f}_0(r) = D(r) M^{-1} \boldsymbol{w}$. First we verify that f_0 generates $\boldsymbol{w}$. Substituting f_0 for f verifies the first condition of Equation (8.12):

$$\int_{\mathcal{B}} \nu(r)\, D^T(r)\, \mathsf{f}(r)\, dV = \int_{\mathcal{B}} \nu(r)\, D^T(r) D(r) M^{-1} \boldsymbol{w}\, dV = \boldsymbol{w},$$

where we have used the fact that $M = \int_{\mathcal{B}} \nu(r)\, D^T(r) D(r)\, dV$. Thus, $\mathsf{f}_0 \in \mathcal{D}^2_{\boldsymbol{w}}$. Now compute

$$\begin{aligned} \int_{\mathcal{B}} \nu(r)\, |\mathsf{f}_0(r)|^2\, dV &= \int_{\mathcal{B}} \nu(r)\, (D(r) M^{-1} \boldsymbol{w})^T (D(r) M^{-1} \boldsymbol{w})\, dV \\ &= \int_{\mathcal{B}} \nu(r)\, \boldsymbol{w}^T M^{-1}\, D(r) D^T(r)\, M^{-1} \boldsymbol{w}\, dV = \boldsymbol{w}^T M^{-1} \boldsymbol{w} = \|\boldsymbol{w}\|^2_{rms}. \end{aligned}$$

Therefore, $\|\boldsymbol{w}\|_{rms}$ achieves the upper bound at f_0, which completes the proof.

□

It follows from Proposition 8.5.2 that *the wrench norm* $\|\boldsymbol{w}\|_{rms}$ *is the greatest lower bound on the root-mean-square of the magnitude of any distributed force that generates* $\boldsymbol{w}$. For this reason, this norm is called the *rms*

wrench norm, which explains the notation. Since the rms norm has an interesting physical interpretation and affords efficient computation, it can be very attractive in practical applications. Its use has been demonstrated in the minimum-deflection fixturing approach, where it provided well-defined wrench balls. Such wrench balls, as is clear from formula (8.10), are ellipsoids in the wrench space.

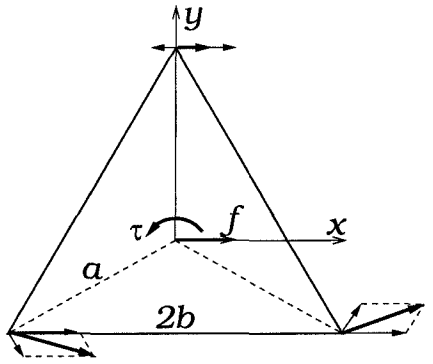

Figure 8.2: The rms norm of wrenches acting on an equilateral triangle is the root mean square of three forces at the vertices.

Example 8.5.1. Consider an equilateral triangle whose edges are of length $2b$, and whose center of symmetry is at a distance $a = \frac{2}{\sqrt{3}}b$ from the vertices. Choose a body frame as shown in Figure 8.2, and choose a weighting function $\nu(r) = \sum_{i=1}^{3} \frac{1}{3}\delta(r - r_i)$, where r_i are the triangle's vertices. The weighting matrix is then given by $M = \mathrm{diag}(1, 1, a^2)$. Consider a family of wrenches $\boldsymbol{w} = (f, 0, \tau)$ where $f > 0$ is fixed and $\tau \geqslant 0$ can vary. By proposition 8.5.2, $\|\boldsymbol{w}\|_{rms} = (\boldsymbol{w}^T M^{-1} \boldsymbol{w})^{\frac{1}{2}} = f\sqrt{1 + \frac{3}{4}\bar{\tau}^2}$, where $\bar{\tau} = \frac{\tau}{fb}$. From the same proposition, the norm is the root mean square of a distributed force $\mathrm{f}_0(r)$, given by $\mathrm{f}_0(r) = f\binom{1}{0} + \frac{\sqrt{3}}{2}\bar{\tau} f \begin{pmatrix} -\sin(\varphi(r)) \\ \cos(\varphi(r)) \end{pmatrix}$, where $\varphi(r)$ is the angle made by r with the x axis. By examining Equation (8.12) and Proposition 8.5.2, we see that the rms norm is in fact the root mean square of three concentrated forces, which are statically equivalent to $\boldsymbol{w}$, acting at the triangle's vertices. These concentrated forces are also shown in the figure.

8.6 The Average Norm of Wrenches Acting on Planar Bodies

The rms wrench norm considered in the preceding section is induced from a wrench inner product. However, similar to velocity norms, there are wrench norms that are *not* induced from wrench inner products. The maximum and average velocity norms (Section 8.4) can be used to induce wrench norms (via the definition of (8.11)) that are not inducible from any wrench inner products.

Unlike the rms wrench norm, the computation of the wrench norms induced from maximum and average velocity norms is very difficult and largely remains open. However, for planar objects, the wrench norm that is induced from the maximum velocity norm has an interesting physical interpretation, which in turn yields an efficient computation algorithm. This section summarizes the main results, while detailed proofs are given in Appendix D.

Recall that the maximum velocity norm is defined by Equation (8.5): $\|\dot{q}\|_{\max} = \max_{r\in\Omega_B} |\omega \times r + v|$, where $\dot{q} = (v, \omega)$ is a body velocity. Without loss of generality, assume that $\Omega_B = \mathcal{B}$, since a given feature-point set Ω_B can be regarded as an "object" for the purpose of norm computation. The norm of a wrench $\boldsymbol{w}$ induced from the maximum velocity norm is given by (8.11): $\|\boldsymbol{w}\|_{\text{avg}} = \sup\{\frac{|\boldsymbol{w}^T\dot{q}|}{\|\dot{q}\|_{\max}} : \dot{q} \in T_{g_0}SE(3)\}$. In a way similar to (8.12), define the following set of distributed forces:

$$\mathcal{D}^1_{\boldsymbol{w}} = \Big\{\mathsf{f} : \mathcal{B} \to \mathbb{R}^3 : \int_{\mathcal{B}} D^T(r)\,\mathsf{f}(r)\,dV = \boldsymbol{w},\ \int_{\mathcal{B}} |\mathsf{f}(r)|\,dV < \infty\Big\}, \qquad (8.13)$$

This allows us to introduce the following upper bound on $\|\boldsymbol{w}\|_{\text{avg}}$ which holds for general three-dimensional bodies.

Lemma 8.6.1. *Consider an arbitrary wrench $\boldsymbol{w}$ acting on an object $\mathcal{B}$. For*

any distributed force $\mathsf{f} \in \mathcal{D}^1_{\boldsymbol{w}}$, *we have the inequality* $\|\boldsymbol{w}\|_{avg} \leqslant \eta(\boldsymbol{w})$, *where* $\eta(\boldsymbol{w}) = \inf_{\mathsf{f}\in\mathcal{D}^1_{\boldsymbol{w}}} \int_{\mathcal{B}} |\mathsf{f}(r)|\, dV$.

Proof. For any velocity $\dot{q}$ and distributed force $\mathsf{f} \in \mathcal{D}^1_{\boldsymbol{w}}$,

$$\begin{aligned}\frac{|\boldsymbol{w}^T\dot{q}|}{\|\dot{q}\|_{\max}} &= \frac{1}{\|\dot{q}\|_{\max}} \int_{\mathcal{B}} \mathsf{f}(r)\cdot(v+\omega\times r)\, dV \\ &\leqslant \frac{1}{\|\dot{q}\|_{\max}} \max_{r\in\mathcal{B}} |v+\omega\times r| \int_{\mathcal{B}} |\mathsf{f}(r)|\, dV = \int_{\mathcal{B}} |\mathsf{f}(r)|\, dV,\end{aligned}$$

where $\|\dot{q}\|_{\max} = \max_{r\in\mathcal{B}} |v+\omega\times r|$ has been used. Taking supremum and infimum as appropriate proves the assertion. □

It is seen that $\|\boldsymbol{w}\|_{\text{avg}}$, called the *average wrench norm*, is a lower bound on the average magnitude of distributed forces that generate $\boldsymbol{w}$. While it is conjectured that the equality in the lemma is achieved for three-dimensional object, we now show that this is indeed true for planar objects. To simplify the notation, the wrench space is hereafter denoted by $\mathcal{W} = T^*_{g_0}SE(3)$. We start with the simplest polygons—triangles.

The three vertices of any triangle lie on the triangle's circumscribing circle. As shown in Figure 8.3(a), specify wrenches with respect to a frame based at O, the center of the circumscribing circle. The triangle's vertices, denoted r_i, and edges, denoted e_i, are ordered counterclockwise, with e_i directing from r_i to r_{i+1} (mod 3). Let α_i be the angle subtended by e_i, and a the radius of the circumscribing circle. Then the length of e_i is $2\ell_i = 2a\sin\alpha_i$. A wrench $\boldsymbol{w} = (f,\tau)$, which is specified in a frame based at O, will transform to $\boldsymbol{w} = (f,\tau_i)$ if specified in a frame that is based at r_i. Let f_i denote the projection of f onto e_i. Then f_i and τ_i are given by

$$f_i = f\cdot\vec{e}_i \quad \text{and} \quad \tau_i = \tau - r_i\times f, \tag{8.14}$$

where $\vec{e}_i$ denotes a unit-magnitude vector aligned with edge e_i, and $r_i \times f \triangleq \det([r_i, f])$ with r_i the position vector of vertex r_i.

Proposition 8.6.2. *Let $\boldsymbol{w} = (f, \tau) \in \mathcal{W}$ be a wrench acting on a triangle. Then $\|\boldsymbol{w}\|_{avg} = \eta(\boldsymbol{w})$, where $\eta(\boldsymbol{w}) = \inf_{\mathsf{f} \in \mathcal{D}^1_{\boldsymbol{w}}} \int_{\mathcal{B}} |\mathsf{f}(r)|\, dV$. Moreover, the wrench space can be decomposed as $\mathcal{W} = \mathcal{W}_0 \cup \mathcal{W}_1 \cup \mathcal{W}_2 \cup \mathcal{W}_3 \cup \mathcal{W}_4$, where $\mathcal{W}_i = \mathcal{W}_i^+ \cup \mathcal{W}_i^-$ are mutually disjoint wrench subsets given as follows.*

$$\mathcal{W}_0^+ = \{\boldsymbol{w} \in \mathcal{W} : \ \tau \geqslant 0, \text{ and } \tau_j \leqslant 0 \text{ for any } j\},$$
$$\mathcal{W}_i^+ = \{\boldsymbol{w} \in \mathcal{W} : \ \tau > 0, \ \tau_j > 0 \ \forall j, \text{ and } f_i \geqslant \frac{\tau}{\ell_i} \sin\alpha_i \cos\alpha_i\} \quad (i = 1, 2, 3),$$
$$\mathcal{W}_4^+ = \{\boldsymbol{w} \in \mathcal{W} : \ \tau > 0, \ \tau_j > 0, \text{ and } f_j < \frac{\tau}{\ell_j} \sin\alpha_j \cos\alpha_j, \ \forall j\},$$

and $\mathcal{W}_i^- = \{\boldsymbol{w} \in \mathcal{W} : \ -\boldsymbol{w} \in \mathcal{W}_i^+\}$ $(i = 0, \ldots, 4)$, where f_i and τ_i are computed using (8.14). *The norm of $\boldsymbol{w}$ is given by*

$$\|\boldsymbol{w}\|_{avg} = \begin{cases} |f| & \text{if } \boldsymbol{w} \in \mathcal{W}_0, \\ \sqrt{(\frac{\tau}{\ell_i})^2 - 2(\frac{\tau}{\ell_j}) f_i \cot\alpha_i + f_i^2 \csc^2\alpha_i} & \text{if } \boldsymbol{w} \in \mathcal{W}_i \quad (i = 1, 2, 3), \\ \frac{|\tau|}{a} & \text{if } \boldsymbol{w} \in \mathcal{W}_4. \end{cases}$$

The proof of this proposition (Appendix D.2) shows that there exists a distributed force $\mathsf{f}(r) = \sum_{i=1}^3 \mathsf{f}_i \delta(r - r_i)$ (i.e., $\mathsf{f}(r)$ vanishes except at the triangle's vertices) such that $\|\boldsymbol{w}\|_{\text{avg}} = \int_{\mathcal{B}} |\mathsf{f}(r)|\, dV = \sum_{i=1}^3 |\mathsf{f}_i|$. A distributed force with this property is said to be *critical*. A wrench $\boldsymbol{w} \in \mathcal{W}_0$ is statically equivalent to a pure force f acting at some point in the triangle, and in this case the components f_i of the critical distributed force are all aligned with f. A wrench $\boldsymbol{w} \in \mathcal{W}_i$ $(i = 1, 2, 3)$ is not statically equivalent to a pure force acting on $\mathcal{B}$, and the critical distributed force is nonzero only at edge e_i's endpoints. Finally, a

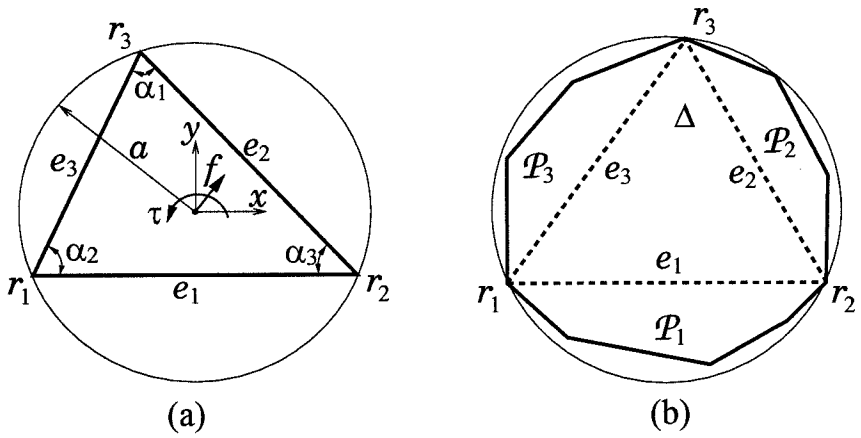

Figure 8.3: Computing the norm of a wrench acting on a (a) triangle and (b) polygon.

wrench $\boldsymbol{w} \in \mathcal{W}_4$ is also not statically equivalent to a pure force acting on $\mathcal{B}$, and the components f_i of the critical distributed force are nonzero at all the vertices of $\mathcal{B}$. Note that $\mathcal{W}_i$ are *subsets* rather than subspaces of wrenches, and every wrench in $\mathcal{W}$ is contained in one of these subsets.

The methodology for triangles can be extended to general polygons as follows. Let $\mathcal{B}$ be an arbitrary polygon, whose convex hull is denoted $\bar{\mathcal{B}}$. As shown in Figure 8.3(b), $\bar{\mathcal{B}}$ can be contained in a circle such that three vertices, denoted r_i, are on the circle. Let r_i be ordered counterclockwise with respect to the triangle, denoted Δ, formed by these vertices. Denote the triangle by Δ and denote its edges by e_i, where each e_i is directed from r_i to r_{i+1} (mod 3), and cuts a convex polygon, denoted $\mathcal{P}_i$, from $\bar{\mathcal{B}}$. For clarity we write $\|\boldsymbol{w}\|_{\text{avg}} = \|\boldsymbol{w}\|^{\mathcal{B}}_{\text{avg}}$ and $\eta(\boldsymbol{w}) = \eta_{\mathcal{B}}(\boldsymbol{w})$, meaning that $\|\boldsymbol{w}\|^{\mathcal{B}}_{\text{avg}}$ is computed with $\boldsymbol{w}$ regarded as a wrench *acting on* $\mathcal{B}$, and $\eta_{\mathcal{B}}(\boldsymbol{w})$ with respect to a force that is *distributed over* $\mathcal{B}$. Similar notation apples to Δ and $\mathcal{P}_i$. For example, $\|\boldsymbol{w}\|^{\Delta}_{\text{avg}}$ and $\eta_{\Delta}(\boldsymbol{w})$ are interpreted in the obvious way.

Proposition 8.6.3. *Let $\boldsymbol{w} = (f, \tau) \in \mathcal{W}$ be a wrench acting on a polygon $\mathcal{B}$. Then $\|\boldsymbol{w}\|^{\mathcal{B}}_{avg} = \eta_{\mathcal{B}}(\boldsymbol{w})$, where $\eta_{\mathcal{B}}(\boldsymbol{w}) = \inf_{\mathsf{f}\in\mathcal{D}^1_{\boldsymbol{w}}} \int_{\mathcal{B}} |\mathsf{f}(r)|\, dV$. Let $\bar{\mathcal{B}}$ be contained in a circle with vertices r_i (i=1,2,3) on the circle. Then $\bar{\mathcal{B}} = \Delta \cup \mathcal{P}_1 \cup \mathcal{P}_2 \cup \mathcal{P}_3$,*

as shown in Figure 8.3(b). By applying Proposition 8.6.2 to the triangle Δ, *the norm can be computed as follows.*

(1) If $\boldsymbol{w} \in \mathcal{W}_i$, $i = 0, 4$, *then* $\|\boldsymbol{w}\|_{avg}^{\mathcal{B}} = \|\boldsymbol{w}\|_{avg}^{\Delta}$.

(2) If $\boldsymbol{w} \in \mathcal{W}_i$, $i = 1, 2, 3$, *and* e_i *is an edge of* $\bar{\mathcal{B}}$, *then* $\|\boldsymbol{w}\|_{avg}^{\mathcal{B}} = \|\boldsymbol{w}\|_{avg}^{\Delta}$.

(3) If $\boldsymbol{w} \in \mathcal{W}_i$, $i = 1, 2, 3$, *and* e_i *is* not *an edge of* $\bar{\mathcal{B}}$, *then* $\|\boldsymbol{w}\|_{avg}^{\mathcal{B}} = \|\boldsymbol{w}\|_{avg}^{\mathcal{P}_i}$.

By applying this proposition in a recursive manner, the problem is reduced to polygons of successively less edges. The problem can eventually be solved by considering a triangle. Clearly, this scheme can be used for approximately computing the average norm of wrenches acting on a curved planar object $\mathcal{B}$ by discretizing the boundary of $\mathcal{B}$ and approximate $\mathcal{B}$ by a polygon with n edges. Moreover, letting $n \to \infty$, the approximation polygon approaches $\mathcal{B}$ and we have the following general conclusion.

Corollary 8.6.4. *Let* $\boldsymbol{w} = (f, \tau) \in \mathcal{W}$ *be a wrench acting on an arbitrary object* $\mathcal{B}$. *Then* $\|\boldsymbol{w}\|_{avg}^{\mathcal{B}} = \eta_{\mathcal{B}}(\boldsymbol{w})$, *where* $\eta_{\mathcal{B}}(\boldsymbol{w}) = \inf_{\mathfrak{f} \in \mathcal{D}_{\boldsymbol{w}}^1} \int_{\mathcal{B}} |\mathfrak{f}(r)|\, dV$.

It follows that the average norm of a wrench acting on a planar object is the *greatest lower bound on the average magnitude of distributed forces that generate the wrench.* Because of this physical interpretation and the efficient computational scheme outlined in Proposition 8.6.3 for polygonal objects, the average wrench norm can be potentially useful in practical applications.

Example 8.6.1. We compute the average norm of the family of wrenches considered in Example 8.5.1. Proposition 8.6.2 can be used to obtain

$$\|\boldsymbol{w}\|_{\text{avg}} = \begin{cases} f & \text{if } \bar{\tau} \leqslant \frac{1}{\sqrt{3}}, \\ f\sqrt{\bar{\tau}^2 - \frac{2}{\sqrt{3}}\bar{\tau} + \frac{4}{3}} & \text{if } \frac{1}{\sqrt{3}} \leqslant \bar{\tau} \leqslant \frac{4}{\sqrt{3}}, \\ \frac{\sqrt{3}}{2} f \bar{\tau} & \text{if } \bar{\tau} > \frac{4}{\sqrt{3}}. \end{cases}$$

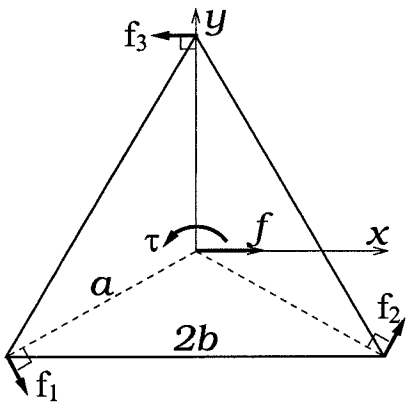

(a) Distributed forces

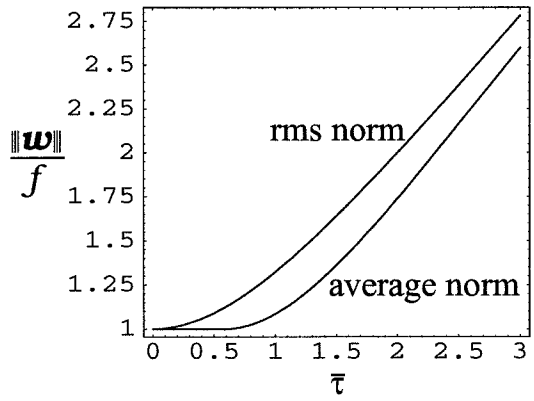

(b) Comparison with the rms wrench norm

Figure 8.4: The average norm of wrenches acting on an equilateral triangle.

where $\bar{\tau} = \frac{\tau}{fb}$. In all the three cases given above, $\|\boldsymbol{w}\|_{\text{avg}} = \eta(\boldsymbol{w})$ holds at distributed forces which vanish except at the triangle's vertices. When $\bar{\tau} \leqslant \frac{1}{\sqrt{3}}$, $\boldsymbol{w}$ is statically equivalent to a pure force acting on the triangle. In this case the norm simply equals f. When $\frac{1}{\sqrt{3}} \leqslant \bar{\tau} \leqslant \frac{4}{\sqrt{3}}$, the norm equals the sum of the magnitudes of forces acting at the two lower vertices, as shown in Figure 8.4(a). If $\bar{\tau} > \frac{4}{\sqrt{3}}$, then the norm is the sum of the magnitudes of forces acting at all the three vertices, also shown in Figure 8.4(a). A comparison of the average and rms norms of these wrenches is given in Figure 8.4(b), which shows that $\|\boldsymbol{w}\|_{\text{avg}} \leqslant \|\boldsymbol{w}\|_{rms}$ for the choice of feature-point set $\Omega_B = \mathcal{B}$ (for computing $\|\boldsymbol{w}\|_{\text{avg}}$) and weighting function ν (for computing $\|\boldsymbol{w}\|_{rms}$).

Summary:

This chapter built upon the equivalence between the notions of objectivity and frame-invariance, as discussed in Chapter 7, to develop well-defined norms of rigid body velocities and wrenches. These norms include the root-mean-square, maximum and average velocity norms as well as the root-mean-square and average wrench norms. These norms are frame-invariant, have interesting physical meanings, and in many cases can be efficiently computed. There-

fore, these norms can potentially be applied to practical engineering problems, as demonstrated by the minimum-deflection fixturing approach discussed in Chapter 6.

Chapter 9

Discussion and Future Work

This thesis presented an approach, based on accurate and efficient physical modelling, to automated planning of workpiece fixturing and robotic grasping, a problem that has remained a major challenge facing manufacturing automation. Several key issues in mechanics and planning of fixtures and grasps were addressed, including the accurate and efficient modelling of compliance, well-defined and practically useful quality measures, and well-defined kinematic metric functions for rigid bodies.

The accurate and efficient modelling of compliance in fixturing and grasping is the foundation for automated fixture and grasp planning systems. In a contribution to this foundation, a closed-form stiffness matrix formula was developed which employs realistic and nonlinear contact models. In particular, the formula incorporates the classical Hertz contact model, which is both theoretically justified and experimentally verified. This is in contrast to the commonly used linear-spring contact model, which is not supported by experimental data or elasticity theory. The stiffness matrix formula is in closed form and can be directly computed from the fixture geometry and basic material properties of the contacting bodies. Consequently, the formula affords both accuracy and efficiency, and is therefore highly desirable for automated fixture and grasp planning systems.

The stiffness matrix formula was used as a basis for a systematic analysis of the role played by first and second-order geometrical effects in the stiffness and stability of a fixture. The effects of the local curvature of the contacting bodies at the contacts on the stability of a fixture were investigated. It was shown that destabilizing effects of local curvatures are practically negligible, and that curvature effects can be used to stabilize, sometimes quite significantly, an otherwise unstable fixture. The investigation of the impact of the choice of contact models showed that stability analysis is in general model-dependent. This model-dependency offers additional evidence that realistic contact models should be preferred in assessing stiffness and stability of fixtures and grasps.

The second issue addressed in this thesis is concerned with theoretically sound and physically meaningful fixture and grasp quality measures and their application to optimal planning algorithms. Recognizing that existing quality measures are limited to rigid grasps and mostly depend on the choice of reference frames, we developed the stiffness and deflection quality measures which are appropriate to compliant fixtures and grasps. These quality measures are frame-invariant, are valid for general compliance models, and apply to two- and three-dimensional workpieces fixtured by any number of fingers. The stiffness quality measure is defined as the worst-case characteristic stiffness of a fixture in terms of the principal translational and rotational stiffness parameters, which are frame-invariant and possess interesting physical and geometrical interpretations. On the other hand, the deflection quality measure is defined, based on frame-invariant norms and pseudo-norms of rigid body velocities and wrenches, as the worst-case deflection of a fixtured workpiece under the action of any wrench in a subset of the wrench space. This subset, which is called the task wrench set and represents a set of manufacturing operations, has been modelled either by the unit wrench ball, or by a class of primitive wrench sets representing basic manufacturing operations.

The stiffness and deflection quality measures were applied to optimal planning, resulting in maximum-stiffness and minimum-deflection fixtures and grasps. Using the stiffness matrix formula mentioned above to analyze three- and four-finger frictionless fixtures of polygonal objects, the qualitative properties of the optimal finger arrangement for such fixtures were characterized. For three-finger fixtures of a polygon modelled by a general contact model, simple graphical and analytical techniques were developed for finding the globally optimal finger arrangement with respect to each quality measure. For four-finger fixtures of a polygon modelled by the linear-spring contact model, a global optimization algorithm was devised with respect to each quality measure in terms of indefinite quadratic programs. Since there are only four independent variables in these indefinite quadratic programs, they can be solved at a reasonable computational cost even though no efficient algorithms are available for large-scale indefinite quadratic programming problems. The usefulness of the stiffness and deflection quality measures was demonstrated by several examples of optimal fixtures that are intuitively effective.

The final issue addressed in this thesis centers on formal conditions as well as practical development methods for well-defined metric functions for rigid body kinematics. Based on an intrinsic, frame-free definition of $\mathcal{C}$, the configuration space of a rigid body, the notion of objectivity was introduced to formalize the natural and fundamental requirement that a well-defined metric function be indifferent to the observers that perform metric measurements. The objectivity notion allowed to clarify the relationship between well-definedness in $\mathcal{C}$ and invariance in $SE(3)$. It was shown that an objective metric function on $\mathcal{C}$ corresponds to a family of left invariant metric functions on $SE(3)$ that are not necessarily right invariant. The necessity of left invariance indicated that bi-invariance on $SE(3)$ is sufficient, but not necessary, for a metric function on $\mathcal{C}$ to be well-defined, and that metric functions on $SE(3)$ that are

merely right invariant in general do not lead to well-defined functions. To facilitate practical development of well-defined metric functions, an accurately defined notion of frame-invariance was also introduced, which was shown to be a necessary and sufficient condition for objectivity. Thus, one may conveniently focus on frame-invariant metric functions on $SE(3)$.

In the framework of objectivity and frame-invariance, this thesis developed well-defined norms and pseudo-norms of rigid body velocities and wrenches. In addition to the well-known fact that there are no bi-invariant Riemannian metrics on $SE(3)$, it was shown that there are no bi-invariant norms on $SE(3)$ as well. Thus, it is expected that well-defined norms are frame-invariant, but not bi-invariant. The thesis further proceeded to actually define several frame-invariant norms and pseudo-norms of rigid body velocities and wrenches. These norms and pseudo-norms have interesting physical interpretations, and are hence practically attractive. The utility of these norms was demonstrated by their application to the deflection quality measure, which allows for the planning of minimum-deflection fixtures and grasps.

The results from this thesis are a step forward toward a fixture and grasp planning paradigm that is based on accurate and efficient physical modelling. However, further research needs to be pursued to enable the development of practical planning systems. In particular, more work is needed on compliance modelling and planning algorithm development.

The open problems in compliance modelling include realistic contact models that augment the Hertz model, more realistic preloading analysis, and incorporation of friction and global deformations. The classical Hertz model offers an accurate compliance relationship, $f = c\delta^{3/2}$, for the contact of two compliant bodies that initially touch at a single point. However, when the compliant bodies initially touch along a line, the Hertz model involves a choice of datum points (Equation (4.10)), and may hence cause significant inaccuracy

to compliance analysis. Since line contacts are quite common in workpiece fixturing, we need to develop compliance models that are appropriate for such contacts. The second open problem involves realistic preloading analysis. The current methodology is restricted to essential fixtures, which are assumed to be preloaded in such a way that the finger forces are normal to the workpiece's surface at known positions and are in constant ratios determined by the normalized finger force magnitudes (Section 4.4.2). As a consequence of this assumption, the workpiece is at the same configuration at the start and end of preloading. However, this assumption may be violated by a practical preloading process, in which some finger forces may not be actively controlled and the workpiece may consequently change its configuration. An efficient method needs to be devised to compute the workpiece's preloading displacement. Such a method would also be useful for the related problem of finding the displacement of a workpiece in a non-preloaded fixture due to a work load.

The most desirable feature of the current stiffness matrix formula lies in its closed-form incorporation of the Hertz contact model, as compared with the use of the linear-spring model by existing formulas. However, the formula leaves out two important factors: friction and global deformations. In some fixturing applications, friction is either negligibly small or can be ignored for a conservative analysis. However, under circumstances where it is desired to explore the beneficial effects of friction, the current formula is no longer valid. Thus, there is a need to incorporate friction in compliance analysis. We should, however, distinguish such an extension of the current work from the traditional approach that models frictional contacts by linear springs in the directions normal and tangential to the contacting surfaces. As has been indicated, such a linear-spring based approach is not theoretically or experimentally supported. In the current stiffness matrix formula, global deformations, i.e., elastic deformations that occur in the regions of the contacting

bodies away from the contact points, have also been neglected. The exclusion of global deformations implies that the formula ceases to be valid for fixtures that possess slender structures. To enable automated planning algorithms for more general fixtures, there is a need to incorporate global deformations in compliance analysis.

We have developed fixture quality measures that apply to general fixtures, but have only developed optimal planning algorithms for the simplest cases, i.e., three- and four-finger fixtures of polygons. In addition to the obvious need for devising practical optimization algorithms for three-dimensional fixtures, there are a few issues that still remain open even for planar fixtures. First, the global optimization algorithms for four-finger polygonal fixtures are based on the assumption that the finger force at a contact is a linear function of the overlap. While globally optimal planning of fixtures that are modelled by nonlinear contact models appears to be extremely difficult, the practical importance of Hertz model based modelling calls for the development of local or approximately global algorithms which allow the planning of adequately effective fixtures.

In addition to the restriction in the choice of contact model, we have only used the root-mean-square velocity and wrench norms to plan minimum-deflection fixtures. Moreover, the task wrench set used for optimal planning has been limited to the unit wrench ball. These restrictions improved the tractability of the optimization problem and served the need for demonstrating the minimum-deflection approach. However, to plan minimum-deflection fixtures that can be used for practical manufacturing operations, there is a need to relax some or all of these restrictions according the given manufacturing task. For example, the maximum velocity norm indicates the largest displacement of the workpiece's feature points, and can directly characterize manufacturing accuracy requirements. Thus, it may be desirable to address

the optimal planning by use of the maximum velocity norm instead of the root-mean-square norm. Moreover, when a set of manufacturing operations is specified, a task wrench set that models these operations in terms of primitive wrench sets is generally preferred in optimal planning over the unit wrench ball.

The efficient computation of the wrench norms for general objects, with the exception of the root-mean-square wrench norm, also remains open. In particular, the average norm of a wrench acting on a planar object has been interpreted as the average magnitude of distributed forces that generate the wrench, and based on this interpretation, a computation algorithm has been devised for a polygon. However, it remains unclear whether the physical interpretation and resulting computation algorithm can be extended to the average norm of wrenches acting on a three-dimensional object. Such an extension would be of practical interest since the physical interpretation is practically attractive.

The results from this thesis have a number of potential applications. First, as their main application domain, these results can be used in the analysis and synthesis of compliant fixtures and grasps. Given a candidate fixture of a workpiece, the compliance model and quality measures can be used to analyze the fixture's compliant behaviors under the action of given work loads. Note that the work loads can be efficiently represented by a task wrench set in term of the primitive wrench sets developed in the thesis. From the analysis of compliance, one can determine whether the fixture will be adequate to avoid contact breakage and meet strength requirements. In addition, the effects of the material, geometry, number, and position of fingers can be investigated. Such an investigation would allow to determine whether the finger material, geometry or location can be varied to obtain improved fixture stiffness and stability, and whether the finger number can be reduced to allow larger freedom in

manufacturing operations while not jeopardizing stiffness and stability. These analysis results can then be used in the fixture synthesis process, in which the optimal choice is made of the material, geometry, number, and position of fingers for the fixture. Such synthesis methods are well-suited to automated planning systems, since the compliance model is in closed-form and directly computable from CAD data on basic geometric and material properties, while the quality measures accurately characterize fixture requirements and can be efficiently computed. The efficiency and accuracy offered by such synthesis methods can also facilitate, in a design-for-manufacture approach, the integration of fixture planning with the planning of manufacturing processes for which the fixture is designed.

The results from this thesis can also be applied to research areas other than the planning of compliant fixtures and grasps. It is believed that objective and frame-invariant kinematic metric functions potentially have a few interesting applications. First, while we have focused on compliant fixtures and grasps, the frame-invariant wrench norms developed in this thesis can be used to define frame-invariant quality measures for rigid grasps, as opposed to prior works that use frame-dependent wrench norms (e.g., [41, 79, 151]). Second, the frame-invariant velocity and wrench norms can also be used to allow well-defined performance evaluation, such as manipulability and dexterity, of rigid or compliant robotic manipulation plans which may or may not involve grasping and fixturing. Third, the objectivity notion leads to frame-invariant distance metrics. Such metrics can be used for motion approximation, obstacle avoidance, and other robot motion planning problems in which it is necessary to measure the distance from a set of goal configurations, or a collection of obstacles, to a candidate path along which an end-effector is to move. Last, the notion of objectivity can be applied to simultaneous control of force and motion which uses "orthogonal complements" of velocity and wrench spaces. The

theory of such control, called hybrid control, has been traditionally based on orthogonality that is defined in terms of the Euclidean inner products on the velocity and wrench spaces. Since these inner products are frame-dependent, the resulting hybrid control theory is not well-defined (Duffy [36]). The notion of objectivity now allows for frame-invariant Riemannian metrics, which would lead to consistent hybrid control theory.

Finally, it is believed that the compliance analysis methodology presented in this thesis can serve as an excellent starting point for analysis and design of other mechanical systems in which compliance plays a significant role. These systems include mechanical part handling tools such as grippers, fasteners, and feeders, medical robotic tools, and in particular, microelectromechanical systems (MEMS). In the MEMS community, there is a trend to use micro compliant mechanisms, which reduce or eliminate the use of joints. Such designs offer improved manufacturability, reduced friction and wear, and decreased need for lubrication and assembly [68, 81]. To facilitate compliant MEMS design, efficient and accurate micro compliance models need to be established, and optimal synthesis algorithms need to be developed based on these models. Research that addresses these needs will benefit from the approaches and ideas of the modelling methods of macro-scale compliance.

Appendix A

Details in Compliance Computation and Analysis

This appendix contains results concerned with the derivation of the formula for $D^2\delta_i(q_0)$ in Section 4.5, and the details of results from Sections 4.5 and 4.6.

A.1 Computation of $D^2\delta_i(q_0)$

Let $q(t) = (d(t), \theta(t))$ be a c-space curve such that $q(0) = q_0$ and $\dot{q}(0) = \dot{q}$. For each t, let $x_i(q(t)) \in \partial\mathcal{B}(q(t))$ be $\mathcal{B}$'s endpoint of the overlap segment. Let $r_i(q(t)) \in \partial\mathcal{B}$ be the coordinates of this point in the body frame $\mathcal{F}_B$, i.e. $x_i(q(t)) = R(\theta(t))\, r_i(q(t)) + d(t)$. We also use the notation $x_i = x_i(q_0)$, $r_i = r_i(q_0)$, $N_i = N(x_i(q_0))$, and $p_i = R_0 r_i$ where R_0 is the orientation of $\mathcal{B}$ at q_0.

We decompose the tangent space at q_0 into the direct sum $T_{q_0}SE(3) = V_1 \oplus V_2$. The subspace V_1 is tangent to the level-set $S_i = \{q \in SE(3) : \delta_i(q) = \delta_i(q_0)\}$, and is given by $V_1 = \{\dot{q} \in T_{q_0}SE(3) : \nabla\delta_i^T(q_0)\,\dot{q} = 0\}$. The subspace V_2 is tangent to the line which passes through q_0 in the direction $\ell = (N_i, 0)$. The subspace V_2 is given by $V_2 = \{\dot{q} : \dot{q} = \alpha(N_i, 0),\ \alpha \in \mathbb{R}\}$. The following lemma asserts that V_1 and V_2 induce a direct-sum decomposition on the tangent space

$T_{q_0}SE(3)$.

Lemma A.1.1. *For any $\dot{q} \in T_{q_0}SE(3)$, there exist unique $\dot{q}_1 \in V_1$ and $\dot{q}_2 \in V_2$ such that $\dot{q} = \dot{q}_1 + \dot{q}_2$. These two components are given by $\dot{q}_1 = P_i\dot{q}$ and $\dot{q}_2 = -(\nabla\delta_i^T(q_0)\dot{q})\ell$ with*

$$P_i = I_{6\times 6} + \ell\,\nabla\delta_i^T(q_0) = \begin{pmatrix} I - N_iN_i^T & N_iN_i^T\widehat{p}_i \\ 0 & I \end{pmatrix}, \tag{A.1}$$

where $I_{6\times 6}$ is the 6×6 identity matrix.

Proof. The decomposition is straightforwardly verified. Its uniqueness follows from the fact that $V_1 \cap V_2 = \{0\}$. □

At this point, it is important to note that $D^2\delta_i(q_0)$ is a *bilinear* function on the tangent space $T_{q_0}SE(3)$, and that what we are seeking is the *matrix representation* of this function with respect to the hybrid coordinates. Let us still denote this matrix by $D^2\delta_i(q_0)$, and denote by Q_i the matrix representation of $D^2\delta_i(q_0)$ as restricted to V_1. The following proposition gives the formula for $D^2\delta_i(q_0)$.

Proposition 4.4.4. *Let $\mathcal{B}(q_0)$ have an overlap of $\delta_i(q_0) > 0$ with $\mathcal{A}_i$. Using the hybrid parametrization* (3.1)*, the 6×6 Hessian matrix of the overlap function δ_i is:*

$$D^2\delta_i(q_0) = P_i^TQ_iP_i \quad \textit{where } P_i = \begin{pmatrix} I - N_iN_i^T & N_iN_i^T\widehat{p}_i \\ 0 & I \end{pmatrix}, \tag{A.2}$$

where Q_i is given in (4.17) *and $p_i = R_0r_i$.*

Proof. Let $q(t)$ be a c-space curve which coincides with the line l, such that $q(0) = q_0$ and $\dot{q}(0) \in V_2$. Clearly $R(\theta(t))r_i(q(t)) \equiv R_0r_i$ and $N(x_i(q(t))) \equiv$

$N(x_i(q_0))$ (Figure 4.5). Hence $\nabla\delta_i(q(t)) \equiv \nabla\delta_i(q_0)$ and $\frac{d}{dt}\big|_{t=0}\nabla\delta_i(q(t)) = 0$. Therefore, if one of two tangent vectors $u, v \in T_{q_0}SE(3)$ lies in V_2, then $u^T D^2\delta_i(q_0)v = 0$. Since the vectors $u, v \in T_{q_0}SE(3)$ can be decomposed using Lemma A.1.1, the bilinearity and symmetry of $D^2\delta_i(q_0)$ imply that

$$u^T D^2\delta_i(q_0)v = u^T P_i^T D^2\delta_i(q_0)P_i v \quad \text{for all } u, v \in T_{q_0}SE(3).$$

Since $P_i u, P_i v \in V_1$, the right-hand side can be written as $u^T P_i^T Q_i P_i v$, and the result follows. □

Remark A.1.1. We have derived a formula for $D^2\delta_i(q_0)$ in Proposition 4.4.4 by considering the actual object $\mathcal{B}$ and an imaginary finger $\bar{\mathcal{A}}_i$. Alternatively, we may consider the actual finger $\mathcal{A}_i$ and an imaginary object obtained by uniformly compressing $\mathcal{B}$ by the amount $\delta_i(q_0)$. It can be shown that the result is identical.

A.2 Details of Stiffness Matrix Analysis

Now consider some details of results from Section 4.5. We first introduce the following two lemmas, which are followed by Lemma A.2.3. Then Proposition 4.5.1 will be proved using the matrix-norm inequalities provided in Lemma A.2.3.

Lemma A.2.1. *Let A and C be symmetric matrices and suppose that C is positive definite. Let $D = C^{-\frac{1}{2}}AC^{-\frac{1}{2}}$. Then*

$$\max\Big\{\frac{\lambda_{\min}(A)}{\|C\|},\ \|C^{-1}\|\lambda_{\min}(A)\Big\} \leqslant \lambda(D) \leqslant \min\Big\{\frac{\lambda_{\max}(A)}{\|C\|},\ \|C^{-1}\|\lambda_{\max}(A)\Big\}.$$

Proof. Since $\lambda_{\min}(A)\,C^{-1} \leqslant D \leqslant \lambda_{\max}(A)\,C^{-1}$, $\lambda_{\max}(C^{-1}) = \|C^{-1}\|$, and $\lambda_{\min}(C^{-1}) = 1/\|C\|$, we have

$$\frac{1}{\|C\|}\lambda_{\min}(A) \leqslant \lambda_{\min}(D) \leqslant \frac{1}{\|C\|}\lambda_{\max}(A), \tag{A.3}$$

$$\|C^{-1}\|\lambda_{\min}(A) \leqslant \lambda_{\max}(D) \leqslant \|C^{-1}\|\lambda_{\max}(A). \tag{A.4}$$

Since $\lambda_{\min}(-A) = -\lambda_{\max}(A)$ and $\lambda_{\max}(-A) = -\lambda_{\min}(A)$, replacing A with $-A$ in (A.3) and (A.4) and rearranging yield

$$\|C^{-1}\|\lambda_{\min}(A) \leqslant \lambda_{\min}(D) \leqslant \|C^{-1}\|\lambda_{\max}(A), \tag{A.5}$$

$$\frac{1}{\|C\|}\lambda_{\min}(A) \leqslant \lambda_{\max}(D) \leqslant \frac{1}{\|C\|}\lambda_{\max}(A). \tag{A.6}$$

Combining (A.3)-(A.6) completes the proof. □

Lemma A.2.2. *Let A and B be symmetric matrices and suppose that $A+B = C > 0$. Then there exist a nonsingular matrix T and a diagonal matrix Λ such that*

(1) $A = T^T\Lambda\,T$, $B = T^T(I-\Lambda)\,T$, and $C = T^TT$.

(2) $\|T\| = \|C\|^{\frac{1}{2}}$, $\|T^{-1}\| = \|C^{-1}\|^{\frac{1}{2}}$, and $\|\Lambda\| \leqslant \frac{\|A\|}{\|C\|}$.

Proof. Let the diagonal entries of Λ consist of the eigenvalues of $D = C^{-\frac{1}{2}}AC^{-\frac{1}{2}}$, and U be an orthogonal matrix such that $U^TD\,U = \Lambda$. Let $T = U^TC^{\frac{1}{2}}$, which is nonsingular. Then Part (1) can be easily verified. The norms of T and T^{-1} are obvious. Using Lemma A.2.1, we have $\lambda_{\max}(\Lambda) \leqslant \frac{1}{\|C\|}\lambda_{\max}(A)$, and $\lambda_{\min}(\Lambda) \geqslant \frac{1}{\|C\|}\lambda_{\min}(A)$. Therefore, using $\|A\| = \max\{\lambda_{\max}(A), -\lambda_{\min}(A)\}$

yields

$$\|\Lambda\| = \max\{\lambda_{\max}(\Lambda), -\lambda_{\min}(\Lambda)\} \leqslant \max\Big\{\frac{\lambda_{\max}(A)}{\|C\|}, -\frac{\lambda_{\min}(A)}{\|C\|}\Big\} = \frac{\|A\|}{\|C\|}. \qquad \square$$

Lemma A.2.3. *For the terms involving the curvature matrices of the contacting surfaces, the following inequalities hold true:*

$$\begin{aligned}
\|\mathcal{L}_{\bar{A}}\bar{L}_{rel}^{-1}\| &\leqslant \|L_{\bar{A}}\|\Big(\frac{\|\bar{L}_{rel}^{-1}\|}{\|\bar{L}_{rel}\|}\Big)^{\frac{1}{2}} \leqslant \|L_{\bar{A}}\|\|\bar{L}_{rel}^{-1}\|,\\
\|\bar{L}_{rel}^{-1}\mathcal{L}_{B}\| &\leqslant \|L_{B}\|\Big(\frac{\|\bar{L}_{rel}^{-1}\|}{\|\bar{L}_{rel}\|}\Big)^{\frac{1}{2}} \leqslant \|L_{B}\|\|\bar{L}_{rel}^{-1}\|,\\
\|\mathcal{L}_{\bar{A}}\bar{L}_{rel}^{-1}\mathcal{L}_{B}\| &\leqslant \min\Big\{\|L_{\bar{A}}\| + \frac{\|L_{\bar{A}}\|^2}{\|\bar{L}_{rel}\|}, \|L_{B}\| + \frac{\|L_{B}\|^2}{\|\bar{L}_{rel}\|}\Big\}.
\end{aligned}$$

Proof. In Lemma A.2.2, set $A = L_{\bar{A}} = T^T\Lambda T$, $B = L_B = T^T(I-\Lambda)T$ and $C = \bar{L}_{rel} = T^TT$. Then

$$\begin{aligned}
\|L_{\bar{A}}\bar{L}_{rel}^{-1}L_{B}\| &= \|T^T\Lambda(I-\Lambda)T\| \leqslant \|T\|^2\|\Lambda\|\,\|I-\Lambda\|\\
&\leqslant \|\bar{L}_{rel}\|\Big(\frac{\|L_{\bar{A}}\|}{\|\bar{L}_{rel}\|}\Big)\Big(1+\frac{\|L_{\bar{A}}\|}{\|\bar{L}_{rel}\|}\Big) = \|L_{\bar{A}}\|\Big(1+\frac{\|L_{\bar{A}}\|}{\|\bar{L}_{rel}\|}\Big).
\end{aligned}$$

Similarly, it can be shown that

$$\|L_{\bar{A}}\bar{L}_{rel}^{-1}\| = \|T^T\Lambda T^{-T}\| \leqslant \|L_{\bar{A}}\|\,\Big(\frac{\|\bar{L}_{rel}^{-1}\|}{\|\bar{L}_{rel}\|}\Big)^{\frac{1}{2}}.$$

By setting $A = L_B$ and $B = L_{\bar{A}}$ instead, we obtain

$$\|L_{\bar{A}}\bar{L}_{rel}^{-1}L_{B}\| \leqslant \|L_{B}\|\Big(1+\frac{\|L_{B}\|}{\|\bar{L}_{rel}\|}\Big), \qquad \|\bar{L}_{rel}^{-1}L_{B}\| \leqslant \|L_{B}\|\,\Big(\frac{\|\bar{L}_{rel}^{-1}\|}{\|\bar{L}_{rel}\|}\Big)^{\frac{1}{2}}.$$

Collecting these inequalities proves the lemma. □

Proposition 4.5.1. *The second-order effects satisfy* $\|\Psi_{ij}\| \ll 1$ *for* $i, j = 1, 2$, *when the following two conditions hold.*

(1) $\delta_0\|L_{\bar{A}}\| \ll 1$ *and* $\delta_0\|L_B\| \ll 1$.

(2) $\frac{\|L_{\bar{A}}\|}{\|\bar{L}_{rel}\|} = \mathcal{O}(1)$, $\frac{\|L_B\|}{\|\bar{L}_{rel}\|} = \mathcal{O}(1)$, *and* $\frac{\|\bar{L}_{rel}^{-1}\|}{l^2\|\bar{L}_{rel}\|} = \mathcal{O}(1)$.

Proof. First consider the term $\Psi_{11} = -\delta_0\mathcal{L}_{\bar{A}}\bar{L}_{rel}^{-1}\mathcal{L}_B$. Using the third inequality of Lemma A.2.3,

$$\delta_0\|\mathcal{L}_{\bar{A}}\bar{L}_{rel}^{-1}\mathcal{L}_B\| \leqslant \delta_0(\|L_{\bar{A}}\| + \frac{\|L_{\bar{A}}\|^2}{\|\bar{L}_{rel}\|}) = \delta_0\|L_{\bar{A}}\|(1 + \frac{\|L_{\bar{A}}\|}{\|\bar{L}_{rel}\|}).$$

But $\delta_0\|L_{\bar{A}}\| \ll 1$ while $\frac{\|L_{\bar{A}}\|}{\|\bar{L}_{rel}\|} = \mathcal{O}(1)$ according to the proposition. Hence $\|\Psi_{11}\| \ll 1$. Next consider the term $\Psi_{12} = \frac{\delta_0}{l}\mathcal{L}_{\bar{A}}\bar{L}_{rel}^{-1}(\mathcal{L}_B\widehat{p} + \widehat{N})$. The first summand in Ψ_{12} can be written as $(\delta_0\mathcal{L}_{\bar{A}}\bar{L}_{rel}^{-1}\mathcal{L}_B)(\frac{1}{l}\widehat{p})$. We have already shown that $\|\delta_0\mathcal{L}_{\bar{A}}\bar{L}_{rel}^{-1}\mathcal{L}_B\| \ll 1$, while $\|\frac{1}{l}\widehat{p}\| = \mathcal{O}(1)$. As for the second summand in Ψ_{12}, the first inequality of Lemma A.2.3 implies: $\frac{\delta_0}{l}\|\mathcal{L}_{\bar{A}}\bar{L}_{rel}^{-1}\widehat{N}\| \leqslant (\delta_0\|L_{\bar{A}}\|)\left(\frac{1}{l^2}\frac{\|\bar{L}_{rel}^{-1}\|}{\|\bar{L}_{rel}\|}\right)^{1/2}$. But $\delta_0\|L_{\bar{A}}\| \ll 1$ and $\frac{1}{l^2}\frac{\|\bar{L}_{rel}^{-1}\|}{\|\bar{L}_{rel}\|} = \mathcal{O}(1)$ according to the proposition. Hence $\|\Psi_{12}\| \ll 1$. Finally, $\|\Psi_{22}\|$ contains three summands. The second and third summands can be treated in a way similar to the treatment of $\|\Psi_{11}\|$ and $\|\Psi_{12}\|$. The first summand satisfies: $\|\frac{\delta_0}{l^2}\widehat{N}^T\bar{L}_{rel}^{-1}\widehat{N}\| \leqslant \frac{\delta_0}{l^2}\|\bar{L}_{rel}^{-1}\|$. From the third item of condition (2) in the proposition, $\|\bar{L}_{rel}^{-1}\| = cl^2\|\bar{L}_{rel}\|$ where $c = \mathcal{O}(1)$ is a scalar. Thus, $\frac{\delta_0}{l^2}\|\bar{L}_{rel}^{-1}\| = c\delta_0\|\bar{L}_{rel}\|$. However, it can be verified that the hypotheses $\delta_0\|L_{\bar{A}}\| \ll 1$ and $\delta_0\|L_B\| \ll 1$ imply that $\delta_0\|\bar{L}_{rel}\| \ll 1$. This leads to the conclusion that $\frac{\delta_0}{l^2}\|\bar{L}_{rel}^{-1}\| \ll 1$, and consequently $\|\Psi_{22}\| \ll 1$. □

Lemma 4.5.3 will now be proved. Based on the decomposition of the nondimensionalized second-order term in the stiffness matrix given in Lemma 4.5.3, Propositions 4.5.4 and 4.5.5 will then be proved.

Lemma 4.5.3. *Let $\mathcal{L}_S = \mathcal{L}_B\widehat{p} + \widehat{N}$. Then the matrix Ψ given in* (4.21) *can be written as:*

$$\begin{aligned}\Psi &= \Psi_a + \Psi_b \\ &= \begin{pmatrix} \delta_0 \mathcal{L}_{\bar{A}}{}^T \bar{L}_{rel}^{-1} \mathcal{L}_{\bar{A}} & \frac{\delta_0}{l} \mathcal{L}_{\bar{A}} \bar{L}_{rel}^{-1} \mathcal{L}_S \\ \frac{\delta_0}{l} \mathcal{L}_S{}^T \bar{L}_{rel}^{-1} \mathcal{L}_{\bar{A}} & \frac{\delta_0}{l^2} \mathcal{L}_S{}^T \bar{L}_{rel}^{-1} \mathcal{L}_S \end{pmatrix} + \begin{pmatrix} -\delta_0 \mathcal{L}_{\bar{A}} & 0 \\ 0 & \frac{\delta_0}{l^2}\Big(- \widehat{p}^T \mathcal{L}_B \widehat{p} + (\widehat{N}\widehat{p})_s \Big) \end{pmatrix}.\end{aligned} \tag{A.7}$$

In this decomposition, Ψ_a is positive semidefinite, and provided that $\delta_0 \|L_{\bar{A}}\| \ll 1$ and $\delta_0 \|L_B\| \ll 1$, the matrix Ψ_b satisfies $\|\Psi_b\| \ll 1$.

Proof. The check that $\Psi = \Psi_a + \Psi_b$ is straightforward. The matrix Ψ_a is positive semidefinite since $\Psi_a = \left(\begin{smallmatrix} A^TA & A^TB \\ B^TA & B^TB \end{smallmatrix}\right) = [A, B]^T[A, B]$, where $A = \delta_0{}^{1/2} \bar{L}_{rel}^{-1/2} \mathcal{L}_{\bar{A}}$ and $B = (\frac{\delta_0}{l^2})^{1/2} \bar{L}_{rel}^{-1/2} \mathcal{L}_B$. As for Ψ_b, we have $\|\delta_0 \mathcal{L}_{\bar{A}}\| \leqslant \delta_0 \|L_{\bar{A}}\| \ll 1$. We also have $\frac{\delta_0}{l^2} \|\widehat{p}^T \mathcal{L}_B \widehat{p}\| \leqslant (\frac{1}{l}\|\widehat{p}\|)^2 (\delta_0 \|L_B\|) \ll 1$ since $\frac{1}{l}\|\widehat{p}\| = \mathcal{O}(1)$ while $\delta_0 \|L_B\| \ll 1$. Finally, $\|(\widehat{N}\widehat{p})_s\| \ll 1$ since $\frac{\delta_0}{l} \ll 1$ and $\frac{1}{l}\|\widehat{p}\| = \mathcal{O}(1)$. □

Proposition 4.5.4. *Let a fixture be first-order stable* (i.e. $\tilde{K}_1 > 0$). *Then the fixture is stable* (i.e. $\tilde{K} = \tilde{K}_1 + \tilde{K}_2 > 0$), *when the following condition holds true:*

$$\sigma_{min}^2(G) \min_{1 \leqslant i \leqslant m} \frac{f_i'(\delta_i(q_0))}{k_0} \gg \max_{1 \leqslant i \leqslant m} \Big\{ \delta_0 \|L_{\bar{A}i}\|, \delta_0 \|L_{Bi}\|, \frac{\delta_0}{l} \Big\}, \tag{A.8}$$

where $G = \mathrm{diag}(I, \frac{1}{l} I)[\nabla \delta_1(q_0), \cdots, \nabla \delta_m(q_0)]$ and $\sigma_{min}(G)$ is the smallest singular value of G.

Proof. We have $\tilde{K} = \tilde{K}_1 + \tilde{K}_2 = \tilde{K}_1 + \sum_{i=1}^m \nu_i \Psi_i$ such that $\Psi_i = \Psi_{a_i} + \Psi_{b_i}$. Since $0 \leqslant \nu_i \leqslant 1$ and $\Psi_a \geqslant 0$, it suffices to show that $\lambda_{\min}(\tilde{K}) \geqslant \lambda_{\min}(\tilde{K}_1) - \sum_{i=1}^m \|\Psi_{b_i}\| > 0$. In particular, it suffices to show that $\lambda_{\min}(\tilde{K}_1) \gg \|\Psi_{b_i}\|$ for

each Ψ_{b_i}. First, $\tilde{K}_1 = GDG^T$ and $GDG^T \geqslant \lambda_{\min}(D)\, GG^T$. Hence

$$\lambda_{\min}(\tilde{K}_1) \geqslant \lambda_{\min}(GG^T)\lambda_{\min}(D) = \sigma^2_{min}(G) \min_{1 \leqslant i \leqslant m} \frac{f_i'(\delta_i(q_0))}{k_0}.$$

Second, from the definition of the matrix Ψ_{b_i} in Equation (A.7), we have:

$$\|\Psi_{b_i}\| \leqslant \max\left\{\delta_0 \|\mathcal{L}_{\bar{A}}\|, \frac{\delta_0}{l^2}\|-\widehat{p}^T \mathcal{L}_B \widehat{p} + (\widehat{N}\widehat{p})\|\right\}.$$

But $\delta_0\|\mathcal{L}_{\bar{A}}\| \leqslant \delta_0\|L_{\bar{A}}\|$ and $\frac{\delta_0}{l^2}\|\widehat{p}^T\mathcal{L}_B\widehat{p}\| \leqslant (\frac{1}{l}\|\widehat{p}\|)^2(\delta_0\|L_B\|)$. Hence

$$\|\Psi_{b_i}\| \leqslant \max\left\{\delta_0\|L_{\bar{A}}\|, (\frac{1}{l}\|\widehat{p}\|)^2\delta_0\|L_B\| + \frac{\delta_0}{l}(\frac{1}{l}\|\widehat{p}\|)\right\}.$$

Since $\|\frac{1}{l}\widehat{p}\| \sim 1$, condition (A.8) implies that $\lambda_{\min}(\tilde{K}_1) \gg \|\Psi_{b_i}\|$. Thus $\lambda_{\min}(\widetilde{K}) > 0$ and the fixture is stable. □

Proposition 4.5.5. *Let a fixture be second-order stable, such that* $\delta_0\|L_{\bar{A}}\| \ll 1$ *and* $\delta_0\|L_B\| \ll 1$. *Then the stabilizing curvature effects are comparable to the stabilizing first-order effects when* $\|\bar{L}_{rel}\|/(\frac{\delta_0}{l^2}) = \mathcal{O}(1)$. *In this case* $\|\Psi_a\| \sim 1$ *(or even* $\|\Psi_a\| > 1$*), while* $\|\Psi_b\| \ll 1$.

Proof. In general, the norm of a matrix is bounded from below by the norm of its diagonal blocks. Hence, to prove that $\|\Psi_a\| \sim 1$, we consider the norm of its lower-right diagonal block. Given a matrix B, the matrix $B^T(A - \lambda_{\min}(A)\, I)B$ is positive semidefinite. Hence $\lambda_{\max}(B^TAB) \geqslant \lambda_{\min}(A)\lambda_{\max}(B^TB)$ or, equivalently, $\|B^TAB\| \geqslant \|B\|/\|A^{-1}\|$, since $\lambda_{\min}(A) = 1/\lambda_{\max}(A^{-1})$. In our case $A = \bar{L}_{rel}^{-1}$ and $B = \mathcal{L}_S$. Thus $\|\mathcal{L}_S{}^T\bar{L}_{rel}^{-1}\mathcal{L}_S\| \geqslant \|\mathcal{L}_S\|/\|\bar{L}_{rel}\|$, which gives for the

lower-right diagonal block of Ψ_a:

$$\frac{\delta_0}{l^2}\|{\mathcal{L}_S}^T \bar{L}_{rel}^{-1}\mathcal{L}_S\| \geqslant \frac{\delta_0}{l^2}\frac{\|\mathcal{L}_S\|}{\|\bar{L}_{rel}\|}.$$

We may write the hypothesis $\|\bar{L}_{rel}\|/(\frac{\delta_0}{l^2}) = \mathcal{O}(1)$ as $\|\bar{L}_{rel}\| \sim \epsilon\frac{\delta_0}{l^2}$ where $\epsilon = \mathcal{O}(1)$. Thus $\frac{\delta_0}{l^2}\|{\mathcal{L}_S}^T \bar{L}_{rel}^{-1}\mathcal{L}_S\| \geqslant \|\mathcal{L}_S\|/\epsilon \sim 1/\epsilon$, where we have used the fact that generically $\|\mathcal{L}_S\| \sim 1$. Since $\|\Psi_a\|$ is bounded from below by the norm of its diagonal blocks, $\|\Psi_a\|$ is at least of the order-of-magnitude of unity. □

A.3 Details of the Impact of Contact Model Choices on Stability Analysis

This section provides a proof of Proposition 4.6.3, which considers second-order stable fixtures in which curvature effects are insignificant under the conditions given in Proposition 4.5.5. In this case $\|\widetilde{K}_2\|$ is very small, and $\widetilde{K}_2$ as such can be considered as a small perturbation to $\widetilde{K}_2$. We hence introduce the following lemma.

Lemma A.3.1. *Let a real symmetric matrix A be perturbed to $A+B$, where B is real symmetric with $\|B\| \ll \|A\|$. Let λ be an eigenvalue of A and T an orthogonal matrix whose columns span the invariant space of A associated with λ. Then $\lambda+\mu$ is approximately an eigenvalue of $A+B$, where μ is an eigenvalue of T^TBT. Equivalently, $\mu = x^TBx$, where $x = Tu$ is a unit-magnitude eigenvector of A associated with λ, and u a unit-magnitude eigenvector of T^TBT.*

Proof. The continuity of eigenvalues implies that there is approximately an eigenvalue $\lambda+\mu$ of $A+B$ with $|\mu|$ very small. It can be shown that an eigenvector of $A+B$ associated with $\lambda+\mu$ can approximately be written as

$Tu + v$, where $\|u\| = 1$ and $T^T v = 0$ with $\|v\| \ll 1$. Thus,

$$(A + B)(Tu + v) = (\lambda + \mu)(Tu + v).$$

Expanding and pre-multiplying both sides by T^T, we obtain

$$T^T B(Tu + v) = \mu u.$$

Since $\|Tu\| = 1$ and $\|v\|$ is very small, we approximately have

$$(T^T BT)\, u = \mu u,$$

and hence μ is an eigenvalue of $T^T BT$. The equivalent expression of μ follows by pre-multiplying by u^T both sides of the above equation. □

We also need the following lemma on the eigenvalues of the first-order stiffness matrix $\widetilde{K}_1$, which is positive semidefinite for second-order stable fixtures. In the lemma the set of eigenvalues of an $n \times n$ symmetric matrix A will be arranged in increasing order: $\lambda_1(A) \leqslant \lambda_2(A) \leqslant \ldots \leqslant \lambda_n(A)$. This lemma is followed by the proof of Proposition 4.6.3.

Lemma A.3.2. *Let $\lambda_j(\widetilde{K}_1) > 0$ be a nonzero eigenvalue of $\widetilde{K}_1$. Then*

$$\lambda_j(\widetilde{K}_1) \geqslant \sigma_0^2(G) \min_{1 \leqslant i \leqslant m} \frac{f_i'(\delta_i(q_0))}{k_0}$$

where $\sigma_0(G)$ is the smallest nonzero singular value of G.

Proof. From a basic result in matrix eigenvalue problems ([61]), if matrices A and B are symmetric with $A \geqslant B$, then $\lambda_j(A) \geqslant \lambda_j(B)$. Now, $\widetilde{K}_1 = GDG^T \geqslant$

$\lambda_{\min}(D)\, GG^T$, where $\lambda_{\min}(D) = \min_{1 \leqslant i \leqslant m} \frac{f_i'(\delta_i(q_0))}{k_0}$ is the smallest eigenvalue of D. We hence have $\lambda_j(\widetilde{K}) \geqslant \lambda_{\min}(D)\lambda_j(GG^T)$. Since D is nonsingular, it can be shown that for a given vector x, $\widetilde{K}_1 x = 0$ if and only if $GG^T x = 0$. Therefore, $\widetilde{K}_1$ and GG^T have the same number of zero and nonzero eigenvalues. Since $\lambda_j(\widetilde{K}_1) > 0$ by assumption, $\lambda_j(GG^T) > 0$. This implies that $\lambda_j(GG^T) \geqslant \sigma_0^2(G)$, which completes the proof. □

Proposition 4.6.3. *Consider an essential fixture that satisfies the geometric conditions* $\frac{\|L_{\bar{A}_i}\|}{\|\bar{L}_{rel_i}\|} = \mathcal{O}(1)$, $\frac{\|L_{B_i}\|}{\|\bar{L}_{rel_i}\|} = \mathcal{O}(1)$, *and* $\frac{\|\bar{L}_{rel_i}^{-1}\|}{l^2\|\bar{L}_{rel_i}\|} = \mathcal{O}(1)$ *at each contact. Suppose that the fixture is second-order stable with respect to a given contact model such that the following inequality holds:*

$$\sigma_0^2(G) \min_{1 \leqslant i \leqslant m} \frac{f_i'(\delta_i(q_0))}{k_0} \gg \max_{1 \leqslant i \leqslant m} \{\delta_0 \|L_{\bar{A}i}\|, \delta_0 \|L_{Bi}\|, \frac{\delta_0}{\ell}\},$$

where $\sigma_0(G)$ *is the smallest nonzero singular value of* G. *Then the fixture is stable for all contact models under which the above inequality remains to hold.*

Proof. We prove that all the eigenvalues of $\widetilde{K}$ are strictly positive for all the contact models under consideration. The inequality in the proposition implies that $\delta_0 \|L_{\bar{A}_i}\| \ll 1$ and $\delta_0 \|L_{B_i}\| \ll 1$. Along with the geometric conditions $\frac{\|L_{\bar{A}}\|}{\|\bar{L}_{rel}\|} = \mathcal{O}(1)$, $\frac{\|L_B\|}{\|\bar{L}_{rel}\|} = \mathcal{O}(1)$, and $\frac{\|\bar{L}_{rel}^{-1}\|}{l^2\|\bar{L}_{rel}\|} = \mathcal{O}(1)$, this leads to $\|\widetilde{K}_2\| \ll 1$ by Proposition 4.5.1. In other words, the curvature effects are small. Lemma A.3.1 then implies that the eigenvalues of $\widetilde{K}$ takes the form

$$\lambda(\widetilde{K}) = \lambda_j(\widetilde{K}_1) + x^T \widetilde{K}_2 x,$$

where x is a unit-magnitude eigenvector of $\widetilde{K}_1$ associated with the eigenvalue $\lambda_j(\widetilde{K}_1)$. First suppose that $\lambda_j(\widetilde{K}_1) = 0$. Then $\lambda(\widetilde{K}) = x^T \widetilde{K}_2 x$ with x lying in the null space of G^T, which is model-independent. It follows that $\lambda(\widetilde{K}) > 0$

for all the contact models under consideration. Now suppose that $\lambda_j(\widetilde{K}_1) > 0$, which implies that $\lambda_j(\widetilde{K}) \geqslant \sigma_0^2(G) \min_{1 \leqslant i \leqslant m} \frac{f_i'(\delta_i(q_0))}{k_0}$ by Lemma A.3.2. Following the proof of Proposition 4.5.1, it can be shown that $\|\widetilde{K}_2\|$ is in the order of $\max_{1 \leqslant i \leqslant m}\{\delta_0 \|L_{\bar{A}i}\|, \delta_0 \|L_{Bi}\|, \frac{\delta_0}{\ell}\}$. Thus, the inequality condition in the proposition implies that $\lambda_j(\widetilde{K}_1) \gg \|\widetilde{K}_2\| \geqslant x^T \widetilde{K}_2 x$. This again indicates that $\lambda(\widetilde{K}) > 0$ for all the contact models under consideration. Summarizing the two cases completes the proof. □

Appendix B

Details in Optimal Planning of Planar Fixtures

This appendix provides details in the planning of maximum-stiffness and minimum-deflection fixtures. We first adapt the compliance computation method of Chapter 4 from hybrid coordinates to body coordinates, and consider the characterization of compliant fixtures of a planar body by three and four fingers. The algorithms are then presented for finding maximum-stiffness and minimum-deflection four-finger fixtures.

B.1 Compliance Computation in Body Coordinates

This section formulates the computation of fixture compliance in body coordinates. Let the stiffness matrix of a fixture be respectively denoted by K_b and K_h with respect to body and hybrid coordinates. That is, $\boldsymbol{w}_b = K_b \dot{q}_b$ and $\boldsymbol{w}_h = K_h \dot{q}_h$, where $\dot{q}_b$ and $\dot{q}_h$ are the body and hybrid coordinates of an instantaneous displacement of $\mathcal{B}$, and $\boldsymbol{w}_b$ and $\boldsymbol{w}_h$ are the body and hybrid coordinates of the corresponding restoring wrench. By Formula (3.5), the matrices K_b and K_h are related by $K_b = T_{bh}^T K_h T_{bh}$, where the matrix T_{bh} is given

by (3.6).

From now on we denote K_b, $\dot{q}_b$ and $\boldsymbol{w}_b$ simply by K, $\dot{q}$ and $\boldsymbol{w}$, respectively. In terms of body representations, the equilibrium condition (4.12) and stiffness matrix formula (4.13) take the form

$$\sum_{i=1}^{m} \nu_i \nabla_b \delta_i(q_0) = 0, \tag{B.1}$$

and

$$K = K_1 + K_2 = \sum_{i=1}^{m} k_i \nabla_b \delta_i(q_0) \nabla_b \delta_i^T(q_0) + f_T \sum_{i=1}^{m} \nu_i D_b^2 \delta_i(q_0), \tag{B.2}$$

where $\nu_i = \frac{f_i(\delta_i(q_0))}{f_T}$ are the normalized preloading finger force magnitudes, $f_T = \sum_{j=1}^{m} f_i(\delta_i(q_0))$ is the total preload, $k_i = f_i'(\delta_i(q_0))$,

$$\nabla_b \delta_i(q_0) \triangleq T_{bh}^T \nabla \delta_i(q_0) \quad \text{and} \quad D_b^2 \delta_i(q_0) \triangleq T_{bh}^T D^2 \delta_i(q_0) T_{bh}. \tag{B.3}$$

The overlap derivatives $\nabla \delta_i(q_0)$ and $D^2 \delta_i(q_0)$ are given in hybrid coordinates by Lemma 4.4.3 and Proposition 4.4.4, respectively.

B.2 Details in Characterization of Planar Fixtures

This section describes the characterization of stable equilibrium fixtures of polygons by three and four disc fingers, and prove Lemmas 5.4.1 and 5.4.2.

B.2.1 Details of Three-Finger Stable Fixtures

We prove Lemma 5.4.1, which gives a closed-form formula for the stiffness matrix of a three-finger stable equilibrium fixture.

Lemma 5.4.1. *Let three disc fingers of radius r hold a polygonal object $\mathcal{B}$ on an edge-triplet in a frictionless equilibrium fixture. Choose the origin of the body frame $\mathcal{F}_B$ at the concurrency point of the lines of the contact normals. Then for a general contact model, the fixture is stable and its stiffness matrix is given by*

$$K = \mathrm{diag}(\sum_{i=1}^{3} k_i N_i N_i^T, \mu) \quad \textit{where } \mu = f_T(2a\zeta + r). \tag{B.4}$$

In the expression for μ, f_T is the total preload, *given by $f_T = \sum_{i=1}^{3} f_i(\delta_i(q_0))$; a is the radius of the triangle's circumscribing circle; and $\zeta = \frac{\prod_{i=1}^{3} \sin\alpha_i}{\sum_{i=1}^{3} \sin\alpha_i}$ is determined from the triangle's three interior angles, denoted α_i $(i = 1, 2, 3)$.*

Proof. Denote the first and second summands in the overlap-based stiffness matrix formula (B.2) by K_1 and K_2, respectively. By the choice of origin, the overlap gradient can be computed from Formulas (4.16) and (B.3): $\nabla_b \delta_i(q_0) = -(N_i, 0)$, from which it follows that $K_1 = \mathrm{diag}(\sum_{i=1}^{3} k_i N_i N_i^T, 0)$. To compute K_2, the overlap Hessian can be computed from Corollary 4.4.5 and Formula (B.3): $D_b^2 \delta_i(q_0) = \mathrm{diag}(0, 0, \rho_i + r)$, where ρ_i is the distance from the concurrency point to the i^{th} contact point (positive if the finger and the concurrency point lie on the opposite sides of the i^{th} edge). Thus, we obtain $K_2 = \mathrm{diag}(0, 0, \mu)$, where $\mu = f_T \sum_{i=1}^{3} \nu_i(\rho_i + r) = f_T(\sum_{i=1}^{3} \nu_i \rho_i + r)$, and $\nu_i = f_i(\delta_i(q_0))/f_T$. When N_i positively span $\mathbb{R}^2$, it can be shown from (B.1) that these normals uniquely determine ν_i by $\nu_i = d_i/(\sum_{j=1}^{3} d_j)$, where $d_i = \det([N_{i+1}, N_{i+2}])$ (mod 3). Using elementary geometry, we can express ν_i in

terms of the triangle's interior angles, and express ρ_i in terms of the triangle's edge lengths and interior angles, as well as the location of the concurrency point. Then we can further show that the sum $\sum_{i=1}^{3} \nu_i \rho_i$ is actually independent of the location of the concurrency point, and is given by $2a\zeta$. Finally, the fact that the contact normals are concurrent and positively span the plane implies that K is positive definite. Therefore, the fixture is stable. □

B.2.2 Details of Four-Finger Stable Fixtures

To prove Lemma 5.4.2, which characterizes the set of first-order stable equilibrium fixtures of a polygon $\mathcal{B}$, we present the following lemma.

Lemma B.2.1. *Given $s \in \mathcal{P}$, the matrix $[h_1(s), h_2(s), h_3(s), h_4(s)]$ has full rank and the condition $\sum_{i=1}^{4} c_i h_i(s) = 0$ holds for some $c_i > 0$ if and only if $d_1(s)$, $-d_2(s)$, $d_3(s)$ and $-d_4(s)$ are all nonzero and have the same sign.*

There is an intuitive interpretation for this lemma. From Formulas (4.16) and (B.3), it can be shown that $\nabla_b \delta_i(q_0) = -h_i$. Thus, $\sum_{i=1}^{4} c_i h_i(s) = 0$ is precisely the equilibrium condition (B.1) with c_i representing the preloading finger forces. Further, it can be shown that $[h_1(s), h_2(s), h_3(s), h_4(s)]$ has full rank precisely when the finger arrangement forms an essential equilibrium fixture (see Section 4.4.2), i.e., in the absence of a disturbing wrench, each finger must apply nonzero force to maintain equilibrium. In the following we prove Lemma B.2.1, which is then used to prove Lemma 5.4.2.

Proof. First suppose that $d_1(s)$, $-d_2(s)$, $d_3(s)$ and $-d_4(s)$ are nonzero and have the same sign. This immediately implies that $[h_1, h_2, h_3, h_4]$ has full rank. It remains to show that $\sum_{i=1}^{4} c_i h_i(s) = 0$ for some $c_i > 0$, or equivalently, there exist $c_1, c_2, c_3 > 0$ such that the vector $c = (c_1, c_2, c_3)$ solves the equation $[h_1\, h_2\, h_3]\, c = -h_4$. Indeed, since $d_4 = \det([h_1\, h_2\, h_3]) \neq 0$, we can use Cramer's rule to obtain $c = -(\frac{d_1}{d_4}, \frac{-d_2}{d_4}, \frac{d_3}{d_4}) > 0$.

Conversely, suppose that the matrix $[h_1(s),\, h_2(s),\, h_3(s),\, h_4(s)]$ has full rank and that the equilibrium condition $\sum_{i=1}^{4} c_i h_i(s) = 0$ holds for some $c_i > 0$. Clearly, at most two contact normals are aligned with any given line in the plane; otherwise all the four contact normals would be aligned with this line and $[h_1(s),\, h_2(s),\, h_3(s),\, h_4(s)]$ would lose rank. It follows that we can always arrange the contact points such that the contact normals N_i and N_{i+1} intersect, and hence $\det([n_i\, n_{i+1}]) \neq 0$, for all i mod 4. Now suppose that $d_i(s) = 0$ for some i. Without loss of generality, we may choose the location of the origin so that it coincides with the intersection of N_{i+1} and N_{i+2}. Thus $s_{i+1} = s_{i+2} = 0$, and the determinant function d_i takes the form $d_i(s) = s_{i+3} \det([N_{i+1}\, N_{i+2}])$. But $d_i(s) = 0$ by assumption, hence $s_{i+3} = 0$. Thus the normals N_{i+1}, N_{i+2} and N_{i+3} intersect at a common point. To maintain equilibrium, N_i must pass through this intersection, hence $s_i = 0$. This implies that the matrix $[h_1,\, h_2,\, h_3,\, h_4]$, whose last row is identically zero, does not have full row rank. Since this contradicts that assumption that $[h_1(s),\, h_2(s),\, h_3(s),\, h_4(s)]$ has full rank, we must have $d_i(s) \neq 0$. In addition, there exist $c_1, \ldots, c_4 > 0$ such that $\sum_{i=1}^{4} c_i h_i = 0$, or $[h_1\, h_2\, h_3]c = -c_4 h_4$ where $c = (c_1, c_2, c_3)$. Using Cramer's rule again gives $c = -c_4(\frac{d_1}{d_4}, -\frac{d_2}{d_4}, \frac{d_3}{d_4}) > 0$. Thus $d_1(s)$, $-d_2(s)$, $d_3(s)$, and $-d_4(s)$ must have the same sign. □

Lemma 5.4.2. *An arrangement $s \in \mathcal{P}$ of four fingers on a polygon $\mathcal{B}$ forms a first-order stable equilibrium fixture if and only if $d_1(s)$, $-d_2(s)$, $d_3(s)$ and $-d_4(s)$ are all nonzero and have the same sign. To the first order, the stiffness matrix in this case approximately takes the form*

$$K = \begin{pmatrix} \sum_{i=1}^{4} k_i N_i N_i^T & \sum_{i=1}^{4} k_i s_i N_i \\ \sum_{i=1}^{4} k_i s_i N_i^T & \sum_{i=1}^{4} k_i s_i^2 \end{pmatrix}, \tag{B.5}$$

where N_i is the inward unit normal at the i^{th} contact, $k_i = f_i'(\delta_i(q_0))$, and the

function f_i represents a general (linear or nonlinear) contact model.

Proof. Let $s \in \mathcal{P}$ be an equilibrium fixture, whose stiffness matrix takes the form $K = K_1 + K_2$ according to Formula (B.2). Since $\nabla_b \delta_i(q_0) = -h_i$, the first-order term is given by $K_1 = \sum_{i=1}^4 k_i h_i h_i^T = H^T \operatorname{diag}(k_1, \ldots, k_4) H$, where $H = [h_1, h_2, h_3, h_4]$. It follows that s gives a first-order stable equilibrium fixture if and only if s satisfies the equilibrium condition $\sum_{i=1}^4 c_i h_i(s) = 0$ ($c_i > 0$) and H has full rank. By Lemma B.2.1, this is equivalent to the condition that $d_1(s)$, $-d_2(s)$, $d_3(s)$ and $-d_4(s)$ be all nonzero and have the same sign. The stiffness matrix formula (B.5) can be obtained by expanding $K \approx K_1 = \sum_{i=1}^4 k_i h_i h_i^T$. In the following we show that $K \approx K_1$ is an excellent approximation for a generic first-order stable fixture. From Formulas (B.3) and (4.19), it can be shown that $K_2 = \operatorname{diag}(0, 0, f_T \sum_{i=1}^4 \nu_i (r_{A_i} + \rho_i))$, where $f_T = \sum_{i=1}^4 f_i(\delta_i(q_0))$, $\nu_i = \frac{f_i(\delta_i(q_0))}{f_T}$, ρ_i is the distance along N_i from $\mathcal{F}_B$'s origin to the i^{th} contact point, and r_{A_i} is the radius of the i^{th} finger tip. Since $f_T \sim k_i \delta_i(q_0)$ and $\delta_i(q_0) \ll l$ where l is a characteristic object length, $f_T \ll k_i l$. This implies that for a generic first-order stable fixture of a polygon by disc fingers, $f_T \sum_{i=1}^4 \nu_i (r_{A_i} + \rho_i)) \ll \sum_{i=1}^4 k_i s_i^2$. Therefore, the contribution of K_2 is very small compared with that of K_1, and the approximation $K \approx K_1$ is justified. □

B.3 Details in Computing Maximum-Stiffness Four-Finger Fixtures

We wish to find the global maximum of $\mu_{eq}(s) = \frac{\mu(s)}{f(s)}$ over $\mathcal{D}$, where $\mathcal{D}$ is a convex polyhedral subset of $\mathbb{R}^4$. Define a function $\phi\colon \mathbb{R} \times \mathcal{D} \to \mathbb{R}$ by $\phi(t, s) = \mu(s) - tf(s)$, which has the following properties. For a given $t \in \mathbb{R}$, there exists $s \in \mathcal{D}$ such that $t = \mu_{eq}(s)$ if and only if $\phi(t, s) = 0$. Thus, maximizing $\mu_{eq}(s)$ over $\mathcal{D}$ is *equivalent* to maximizing $t \in \mathbb{R}$ such that (t, s) is a zero of ϕ

for some $s \in \mathcal{D}$. This equivalent problem is addressed by the scalar function $\psi(t) = \max_{s\in\mathcal{P}} \phi(t, s)$ and Proposition 5.5.1.

Proposition 5.5.1. *The scalar function $\psi(t)$ is strictly monotonic decreasing and has a unique positive zero. In addition, maximizing $\mu_{eq}(s)$ over $\mathcal{D}$ is equivalent to finding the zero of ψ in the following sense. A positive number $t^* > 0$ satisfies $\psi(t^*) = 0$ if and only if $t^* = \max_{s\in\mathcal{D}} \mu_{eq}(s)$. In this case, a contact configuration $s^* \in \mathcal{D}$ maximizes $\phi(t^*, s)$, regarded as a function of s, over $\mathcal{D}$ if and only if it maximizes $\mu_{eq}(s)$ over $\mathcal{D}$.*

Proof. The function ψ is strictly monotonic decreasing since given $\Delta t > 0$,

$$\psi(t + \Delta t) = \max_{s\in\mathcal{D}}(\mu(s) - tf(s) - \Delta f(s)) < \max_{s\in\mathcal{D}}(\mu(s) - tf(s)) = \psi(t),$$

where we have used the fact that $f(s)$ is strictly positive. Now, $\psi(0) = \max_{s\in\mathcal{D}} \mu(s) > 0$, and $\psi(t) \to -\infty$ as $t \to \infty$. We conclude that there exists a unique $t^* > 0$ such that $\psi(t^*) = 0$, i.e., ψ has a unique positive zero. We now prove the second part of the proposition. Suppose that $t^* > 0$ and $s^* \in \mathcal{D}$ are such that $t^* = \mu_{eq}(s^*) = \max_{s\in\mathcal{D}} \mu_{eq}(s)$. This implies that $\phi(t^*, s^*) = 0$. For any $s \in \mathcal{D}$, we have

$$\phi(t^*, s) = \mu(s) - t^* f(s) = f(s)(\mu_{eq}(s) - t^*) \leqslant 0 = \phi(t^*, s^*).$$

Hence $\psi(t^*) = \phi(t^*, s^*) = \max_{s\in\mathcal{D}} \phi(t^*, s) = 0$. Conversely, suppose that $\psi(t^*) = 0$ for some $t^* > 0$. Given any $\Delta t > 0$, we have

$$\phi(t^* + \Delta t, s) \leqslant \psi(t^* + \Delta t) < \psi(t^*) = 0,$$

where the strict monotonicity of ψ has been used. This indicates that there exist no $s \in \mathcal{D}$ such that $\phi(t^* + \Delta t, s) = 0$ for any $\Delta t > 0$. Therefore, $t^* = \max_{s\in\mathcal{D}} \mu_{eq}(s)$. Furthermore, let $s^* \in \mathcal{D}$ be such that $\psi(t^*) = \phi(t^*, s^*) = \max_{s\in\mathcal{D}} \phi(t^*, s)$. Then by definition of ϕ, we have $t^* = \mu(s^*)/f(s^*) = \mu_{eq}(s^*)$. Hence, s^* maximizes μ_{eq}. □

B.4 Details in Computing Minimum-Deflection Four-Finger Fixtures

This section considers the details in maximizing $Q_{defl}(s) = \lambda_{\min}(\widetilde{K}(s))$ over $\mathcal{D}$, where $\mathcal{D}$ is a convex polyhedral subset of $\mathbb{R}^4$. Let $\alpha = \sigma_1/\sigma_2$, and for a parameter $t \in (0, 1)$ define

$$\zeta(t, s) = \widetilde{\mu}(s) + (1 - \frac{1}{1 - \alpha(1 - t)})\sigma_2\widetilde{\xi}^2(s) + (1 - \frac{1}{t})\sigma_1\widetilde{\eta}^2(s),$$
$$\zeta_c(t, s) = \frac{1}{1 - \alpha(1 - t)}\sigma_2\widetilde{\xi}^2(s) + \frac{1}{t}\sigma_1\widetilde{\eta}^2(s).$$

Since $0 < \alpha \leqslant 1$, which implies that $1 - \alpha(1 - t) > 0$, the functions ζ and ζ_c are well-defined. The following decomposition of $\widetilde{K}$ can then be verified: $\widetilde{K}(s) = \widetilde{K}_1(t, s) + \widetilde{K}_2(t, s)$, where

$$\widetilde{K}_1(t, s) = \text{diag}\left((1 - t)\sigma_1,\ (1 - t)\sigma_1,\ \zeta(t, s)\right),$$
$$\widetilde{K}_2(t, s) = \begin{pmatrix} t\sigma_1 & 0 & -\sigma_1\widetilde{\eta}(s) \\ 0 & (1 - \alpha(1 - t))\sigma_2 & \sigma_2\widetilde{\xi}(s) \\ -\sigma_1\widetilde{\eta}(s) & \sigma_2\widetilde{\xi}(s) & \zeta_c(t, s) \end{pmatrix}.$$

The symmetry of $\widetilde{K}_1$ and $\widetilde{K}_2$ implies that $\lambda_{\min}(\widetilde{K}_1) + \lambda_{\min}(\widetilde{K}_2) \leqslant \lambda_{\min}(\widetilde{K}_1 + \widetilde{K}_2) \leqslant \lambda_{\max}(\widetilde{K}_1) + \lambda_{\min}(\widetilde{K}2)$. Further, it can be shown that $\widetilde{K}_2$ is positive semidefinite, and $\lambda_{\min}(\widetilde{K}_2) = 0$. Therefore

$$\min\{(1-t)\sigma_1, \zeta(t,s)\} \leqslant \lambda_{\min}(\widetilde{K}(s)) \leqslant \max\{(1-t)\sigma_1, \zeta(t,s)\}, \qquad \text{(B.6)}$$

which allows the following characterization of $\lambda_{\min}(\widetilde{K})$ for a fixture $s \in \mathcal{D}$.

Lemma B.4.1. *For a fixed $s \in \mathcal{D}$, the function $\zeta(t,s)$ is monotonically increasing in t, and either of the following two cases must be true.*

(1) There is a unique $t \in (0,1)$, such that $\lambda_{\min}(\widetilde{K}(s)) = (1-t)\sigma_1 = \zeta(t,s)$.

(2) $\lambda_{\min}(\widetilde{K}(s))$ achieves the upper bound σ_1, i.e., $\lambda_{\min}(\widetilde{K}(s)) = \sigma_1$.

Proof. Since $\frac{\partial \zeta}{\partial t}(t,s) = \frac{\sigma_1 \widetilde{\xi}^2}{(1-\alpha(1-t))^2} + \frac{\sigma_1 \widetilde{\eta}^2}{t^2} > 0$, the function $\zeta(t,s)$ is monotonically increasing in t. Consider the function (with dependence on s suppressed):

$$\begin{aligned} f(t) &= \zeta(t,s) - (1-t)\sigma_1 \\ &= \widetilde{\mu} + (1 - \frac{1}{1-\alpha(1-t)})\sigma_2 \widetilde{\xi}^2 + (1 - \frac{1}{t})\sigma_1 \widetilde{\eta}^2 - (1-t)\sigma_1, \end{aligned}$$

which is also monotonically increasing in t. If $\widetilde{\eta} \neq 0$, then $f(0^+) = -\infty$ and $f(1) = \widetilde{\mu} > 0$. Hence, f has a unique zero in the interval $(0,1)$. This fact, along with the bounds in (B.6), leads to Case (1). It remains to consider the case $\widetilde{\eta} = 0$. In this case, $\widetilde{K} = \begin{pmatrix} \sigma_1 & 0 \\ 0 & D \end{pmatrix}$, where $D = \begin{pmatrix} \sigma_2 & \sigma_2 \widetilde{\xi} \\ \sigma_2 \widetilde{\xi} & \widetilde{\mu} + \sigma_2 \widetilde{\xi}^2 \end{pmatrix}$. The characteristic equation of the positive definite matrix D is given by $\bar{f}(z) = z^2 - (\widetilde{\mu} + \sigma_2 + \sigma_2 \widetilde{\xi}^2)\, z + \sigma_2 \widetilde{\mu} = 0$, which transforms to the equation $f(t) = 0$ by change of variable $z = (1-t)\sigma_1$. Thus, there is a one-to-one correspondence between the zeros of $f(t)$ or $\bar{f}(t)$ and the eigenvalues of D. If $\lambda_{\min}(D) < \sigma_1$, then $\lambda_{\max}(D) = (\widetilde{\mu} + \sigma_2 + \sigma_2 \widetilde{\xi}^2) - \sigma_1 > \sigma_1$, which implies that $\bar{f}$ has a unique

zero in $(0, \sigma_1)$ and f has a unique zero in $(0, 1)$. This is again Case (1). Otherwise, we have $\lambda_{\min}(D) \geqslant \sigma_1$ and $\lambda_{\min}(\widetilde{K}(s)) = \sigma_1$, which is Case (2). $\square$

It follows from the lemma that maximizing $\lambda_{\min}(\widetilde{K}(s))$ for $s \in \mathcal{D}$ is equivalent to minimizing a scalar $t \in (0, 1)$ that satisfies the following condition: $\zeta(t, s) = 0$ for some $s \in \mathcal{D}$. Moreover, if no such t exists, the maximal value of $\lambda_{\min}(\widetilde{K})$ is then precisely σ_1. Defining $\psi(t) = \max_{s \in \mathcal{D}} \zeta(t, s) - (1 - t)\sigma_1$, we are now in a position to prove Proposition 6.4.3.

Proposition 6.4.3. *The scalar function ψ is strictly monotonic increasing in the interval $(0, 1)$. Moreover, maximizing $\lambda_{\min}(\widetilde{K})$ is equivalent to finding the zero of ψ, if any. Specifically, either of the following two cases must be true.*

(1) There exists a unique scalar $t^* \in (0, 1)$ such that $\psi(t^*) = 0$ if and only if t^* satisfies the condition $\max_{s \in \mathcal{D}} \lambda_{\min}(\widetilde{K}(s)) = (1 - t^*)\sigma_1$. In this case, $s^* \in \mathcal{D}$ maximizes $\zeta(t^*, s)$, regarded as a function of s, if and only if it maximizes $\lambda_{\min}(\widetilde{K}(s))$.

(2) There exists no zero for the function ψ in the interval $(0, 1)$ if and only if $\max_{s \in \mathcal{D}} \lambda_{\min}(\widetilde{K}(s)) = \sigma_1$. In this case, for any fixed $t \in (0, 1)$, any global maximizer s^* of $\zeta(t, s)$ satisfies the condition $(1 - t)\sigma_1 \leqslant \lambda_{\min}(\widetilde{K}(s^*)) \leqslant \sigma_1$. Hence, a global maximizer of $\lambda_{\min}(\widetilde{K}(s))$ can be found by letting $t \to 0$.

Proof. According to Lemma B.4.1, the function $\zeta(t, s)$ is increasing in t. Hence $\max_{s \in \mathcal{D}} \zeta(t, s)$ is also increasing. This implies that ψ is the sum of an increasing function and a strictly monotonic increasing function, $-(1 - t)\sigma_1$. Therefore ψ is strictly monotonic increasing in the interval $(0, 1)$. We now prove the second part of the proposition, starting with Case (1). Suppose that ψ has a unique zero $t^* \in (0, 1)$. Then $\max_s \zeta(t^*, s) = \zeta(t^*, s^*) = (1 - t^*)\sigma_1$ for some

stable fixture s^*. Using Lemma B.4.1, we have

$$\begin{aligned}\lambda_{\min}(\widetilde{K}(s)) &\leqslant \max\{(1-t^*)\sigma_1,\, \zeta(t^*,s)\} \\ &\leqslant \max\left\{(1-t^*)\sigma_1,\, \max_{s\in\mathcal{D}} \zeta(t^*,s)\right\} \\ &= (1-t^*)\sigma_1.\end{aligned}$$

But from the same lemma, $\lambda_{\min}(\widetilde{K}(s^*)) = (1-t^*)\sigma_1$. Therefore, s^* is the desired optimal fixture. Conversely, let s^* be the optimal fixture such that for any $s \in \mathcal{D}$, we have $\lambda_{\min}(\widetilde{K}(s)) \leqslant \lambda_{\min}(\widetilde{K}(s^*)) < \sigma_1$. By Lemma B.4.1, there exist t^* and t in $(0,1)$, with $t^* \leqslant t$, such that $\lambda_{\min}(\widetilde{K}(s^*)) = \zeta(t^*,s^*) = (1-t^*)\sigma_1$, and $\lambda_{\min}(\widetilde{K}(s)) = \zeta(t,s) = (1-t)\sigma_1$. This implies that

$$\zeta(t^*,s) \leqslant \zeta(t,s) = (1-t)\sigma_1 \leqslant (1-t^*)\sigma_1 = \zeta(t^*,s^*).$$

Therefore, $\max_s \zeta(t^*,s) = \zeta(t^*,s^*) = (1-t^*)\sigma_1$, and $\psi(t^*) = 0$.

Now consider Case (2). If ψ has no zero in (0,1), then suppose that $\max_s \lambda_{\min}(\widetilde{K}(s)) < \sigma_1$. From Case (1), ψ would have a zero in $(0,1)$, a contradiction. Conversely, let $\max_s \lambda_{\min}(\widetilde{K}(s)) = \sigma_1$. If ψ had a zero in $(0,1)$, then Case (1) would imply that $\max_s \lambda_{\min}(\widetilde{K}(s)) < \sigma_1$, again a contradiction. Thus, $\max_s \lambda_{\min}(\widetilde{K}(s)) = \sigma_1$. To prove the second assertion in this case, let $s^* \in \mathcal{D}$ be such that $\zeta(t,s^*) = \max_s \zeta(t,s)$ for a given $t \in (0,1)$. Clearly, $\lambda_{\min}(\widetilde{K}(s^*)) \leqslant \sigma_1$. Suppose that $\zeta(t,s^*) < (1-t)\sigma_1$. Thus, $\zeta(t,s) < (1-t)\sigma_1$ for all $s \in \mathcal{D}$. According to the upper bound given in (B.6), this implies that $\lambda_{\min}(\widetilde{K}(s)) \leqslant (1-t)\sigma_1 < \sigma_1$, a contradiction. Hence $\zeta(t,s^*) \geqslant (1-t)\sigma_1$, and by the lower bound in (B.6) we obtain $\lambda_{\min}(\widetilde{K}(s^*)) \geqslant (1-t)\sigma_1$. □

Appendix C

Axiomatically Defined Euclidean Space

C.1 Summary of the Axioms

The five systems of axioms on points, lines and planes in Euclidean space $\mathbb{E}^3$ are summarized as follows. The summary is not intended to be complete; rather, it is aimed at demonstrating the frame-free axiomatic definition of $\mathbb{E}^3$. See [55, 124] for a complete presentation of these axioms.

The *axioms of incidence* postulate that two distinct points determine one and only one straight line, and that three points not situated in the same line determine one and only one plane. The *axioms of order* establish the notion of betweenness: given two distinct points p_1 and p_2 on a straight line, there always exist distinct points p_3 and p_4 on the line such that p_3 lies between p_1 and p_2, and p_2 lies between p_1 and p_4. The *axioms of congruence* postulate congruence relations of segments, where a *segment*, denoted p_1p_2, on a line between points p_1 and p_2 is the part of the line all points of which lie between p_1 and p_2. The *axiom of continuity* states that given three distinct collinear points p_1, p_2 and p_3 on a straight line such that p_2 lies between p_1 and p_3, there exist a point p_4 on the line such that p_3 lies between p_1 and p_4, and the

segment p_1p_4 is a concatenation of a finite number of segments congruent to p_1p_2. Finally, the *axiom of parallels* postulates that in a plane for any point p_1 outside a straight line ℓ, there exists one and only one straight line which passes through p_1 and which is parallel to ℓ.

C.2 Distance and Orientation in $\mathbb{E}^3$

The notions of distance and orientation are defined in $\mathbb{E}^3$. The *distance* between any two points $p_1, p_2 \in \mathbb{E}^3$ is defined as the length of the segment p_1p_2, where the notion of length is defined as follows. Given a segment p_0q_0 in $\mathbb{E}^3$, there exists a unique real-valued function μ, defined on all segments, satisfying the following properties. First, $\mu(p_0q_0) = 1$; next, for every segment pq, $\mu(pq) > 0$; third, if segments p_1p_2 and q_1q_2 are congruent, then $\mu(p_1q_1) = \mu(p_2q_2)$; finally, if q lies between p_1 and p_2, then $\mu(p_1q) + \mu(qp_2) = \mu(p_1p_2)$. The number $\mu(pq)$ is called the *length* of the segment pq, and the segment p_0q_0 is called the *unit* of length. Now, consider the notion of orientation. Given non-coplanar points $p_i \in \mathbb{E}^3$ $(i = 1, \ldots, 4)$, the triple (p_1, p_2, p_3) is said to have *clockwise (or counterclockwise) orientation* with respect to p_4 if the directed circuit $(\overrightarrow{p_1p_2}, \overrightarrow{p_2p_3}, \overrightarrow{p_3p_1})$, where $\overrightarrow{p_ip_j}$ denotes the directed segment from p_i to p_j, is clockwise (or counterclockwise) when the observer and p_4 are on the same side of the plane determined by p_1, p_2 and p_3.

Let $\widetilde{g}\colon U \to V$ be a bijection, where $U, V \subset \mathbb{E}^3$ are subsets of Euclidean space each containing at least 4 non-coplanar points. The map $\widetilde{g}$ is said to be *distance-preserving* if any $p_1, p_2 \in U$ have the same distance as $\widetilde{g}(p_1), \widetilde{g}(p_2) \in V$, and is said to be *orientation-preserving* if it satisfies the following condition: if $p_i \in \chi_1(\mathcal{B})$ $(i = 1, \ldots, 4)$ are non-coplanar, then $\widetilde{g}(p_i) \in \chi_2(\mathcal{B})$ are non-coplanar as well, and the orientation of (p_1, p_2, p_3) with respect to p_4 is the same as the orientation of $(\widetilde{g}(p_1), \widetilde{g}(p_2), \widetilde{g}(p_3))$ with respect to $\widetilde{g}(p_4)$.

Appendix D

Details of the Average Wrench Norm

This appendix proves the main results, Propositions 8.6.2 and 8.6.3, on the average wrench norm for planar objects. We first consider convex polygonal objects, and later extend the results to arbitrary polygons.

D.1 Preliminaries

Let $\mathcal{B}$ be a polygon, and let the region in $\mathbb{R}^2$ occupied by the polygon also be denoted by $\mathcal{B}$. Given a wrench $\boldsymbol{w}$ acting on $\mathcal{B}$, we focus on a subset of $\mathcal{D}^1_{\boldsymbol{w}}$, rather than the entirety of $\mathcal{D}^1_{\boldsymbol{w}}$, which consists of distributed forces of the form

$$\mathsf{f}(r) = \sum_{i=1}^{k} \mathsf{f}_i \, \delta(r - r_i), \tag{D.1}$$

where $r_i \in \mathcal{B}$ is the coordinates of a *vertex* of $\mathcal{B}$. It will become clear later that this subset is sufficient to contain the desired distributed forces.

Definition D.1.1 (Critical Distributed Forces and Velocities). Let f be a distributed force generating a wrench $\boldsymbol{w}$, and $\dot{q}$ a rigid body velocity. We say that f and $\dot{q}$ are *critical* with respect to each other if they satisfy $|\boldsymbol{w}^T \dot{q}| = \|\dot{q}\|_{\max} \int_{\mathcal{B}} |\mathsf{f}(r)| \, dA$.

Note that if $\boldsymbol{w}$ admits a critical velocity and distributed force, then $\|\boldsymbol{w}\|_{\text{avg}} = \eta(\boldsymbol{w})$ by Lemma 8.6.1. We now characterize the relationship between critical distributed forces and critical velocities. In the following lemma, $\rho_{\max}$ is the maximal distance from the instantaneous center of rotation (ICR) associated with $\dot{q}$ to any point in $\mathcal{B}$, ρ_{r_i} is the distance from the ICR to vertex r_i of $\mathcal{B}$, and φ_{r_i} is the angle made by f_i with the velocity of r_i associated with $\dot{q}$.

Lemma D.1.1. *Consider a distributed force* f *of the form* (D.1)*, which generates some wrench* $\boldsymbol{w} \in \mathcal{W}$.

(1) f *is critical with respect to a pure translation* $\dot{q} = (v, 0)$ *if and only if* $\mathsf{f}_i \cdot v = |\mathsf{f}_i||v|$ *for all* i*, or* $\mathsf{f}_i \cdot v = -|\mathsf{f}_i||v|$ *for all* i.

(2) f *is critical with respect to an instantaneous rotation* $\dot{q} = (v, \omega)$ $(\omega \neq 0)$ *if and only if* (a) $\rho_{\max} = \rho_{r_i}$ *for all* i*, and* (b) $\varphi_{r_i} = 0$ *for all* i *or* $\varphi_{r_i} = \pi$ *for all* i.

Proof. In Case 1, $|\boldsymbol{w}^T\dot{q}| = \left|(\sum_{i=1}^k \mathsf{f}_i)\cdot v\right|$, while $\|\dot{q}\|_{\max} \int_{\mathcal{B}} |\mathsf{f}(r)|\, dA = |v| \sum_{i=1}^k |\mathsf{f}_i|$. The criticality condition can be written as $\left|(\sum_{i=1}^k \mathsf{f}_i) \cdot \frac{v}{|v|}\right| = \sum_{i=1}^k |\mathsf{f}_i|$, from which necessity and sufficiency are readily verified.

In Case 2, by writing $\dot{q} = \theta(v, 1)$, we have $|\boldsymbol{w}^T\dot{q}| = \left|\sum_{i=1}^k \|\mathsf{f}_i\|(\rho_{r_i}\theta)\cos\varphi_{r_i}\right|$. Since $\|\dot{q}\|_{\max} = \rho_{\max}|\theta|$ and $\int_{\mathcal{B}} |\mathsf{f}(r)|\, dA = \sum_{i=1}^k \|\mathsf{f}_i\|$, the criticality condition can be written as $\left|\sum_{i=1}^k \|\mathsf{f}_i\|(\frac{\rho_{r_i}}{\rho_{\max}}\cos\varphi_{r_i})\right| = \sum_{i=1}^k \|\mathsf{f}_i\|$. Noting that $|\cos\phi_{r_i}| \leqslant 1$ and $\rho_{r_i} \leqslant \rho_{\max}$ yields both necessity and sufficiency. □

D.2 The Average Wrench Norm for Triangles

This section considers the case when $\mathcal{B}$ is a triangle, and by seeking critical distributed forces and velocities as characterized in Lemma D.1.1, proves Proposition 8.6.2.

Proposition 8.6.2. *Let $\boldsymbol{w} = (f, \tau) \in \mathcal{W}$ be a wrench acting on a triangle. Then $\|\boldsymbol{w}\|_{avg} = \eta(\boldsymbol{w})$, where $\eta(\boldsymbol{w}) = \inf_{\mathsf{f} \in \mathcal{D}^1_{\boldsymbol{w}}} \int_{\mathcal{B}} |\mathsf{f}(r)|\, dV$. Moreover, the wrench space can be decomposed as $\mathcal{W} = \mathcal{W}_0 \cup \mathcal{W}_1 \cup \mathcal{W}_2 \cup \mathcal{W}_3 \cup \mathcal{W}_4$, where $\mathcal{W}_i = \mathcal{W}_i^+ \cup \mathcal{W}_i^-$ are mutually disjoint wrench subsets given as follows.*

$$\mathcal{W}_0^+ = \{\boldsymbol{w} \in \mathcal{W} :\ \tau \geqslant 0,\ \text{and } \tau_j \leqslant 0 \text{ for any } j\},$$
$$\mathcal{W}_i^+ = \{\boldsymbol{w} \in \mathcal{W} :\ \tau > 0,\ \tau_j > 0\ \forall j,\ \text{and } f_i \geqslant \frac{\tau}{\ell_i} \sin\alpha_i \cos\alpha_i\} \quad (i = 1, 2, 3),$$
$$\mathcal{W}_4^+ = \{\boldsymbol{w} \in \mathcal{W} :\ \tau > 0,\ \tau_j > 0,\ \text{and } f_j < \frac{\tau}{\ell_j} \sin\alpha_j \cos\alpha_j,\ \forall j\},$$

and $\mathcal{W}_i^- = \{\boldsymbol{w} \in \mathcal{W} :\ -\boldsymbol{w} \in \mathcal{W}_i^+\}$ $(i = 0, \ldots, 4)$, where f_i and τ_i are computed using (8.14). *The norm of $\boldsymbol{w}$ is given by*

$$\|\boldsymbol{w}\|_{avg} = \begin{cases} |f| & \text{if } \boldsymbol{w} \in \mathcal{W}_0, \\ \sqrt{(\frac{\tau}{\ell_i})^2 - 2(\frac{\tau}{\ell_j}) f_i \cot\alpha_i + f_i^2 \csc^2\alpha_i} & \text{if } \boldsymbol{w} \in \mathcal{W}_i \quad (i = 1, 2, 3), \\ \frac{|\tau|}{a} & \text{if } \boldsymbol{w} \in \mathcal{W}_4. \end{cases}$$

Proof. Choose a body frame as shown in Figure D.1. We derive the wrench subsets $\mathcal{W}_i^+$ and consider a wrench $\boldsymbol{w} = (f_x, f_y, \tau)$ with $\tau \geqslant 0$. By the choice of frame, $f_1 = f_x$, where f_1 is the projection of f onto the edge directing from r_1 to r_2. Note that while $\tau \geqslant 0$, the vertex torques τ_j may be negative. In the following cases, we show that wrenches in each of $\mathcal{W}_i^+$ admit critical distributed forces and velocities of a certain form.

Case 1: $\tau_j \leqslant 0$ for any j. The wrench $\boldsymbol{w}$ is statically equivalent to a pure force f acting at some point r_0 in the triangle. Then $\mathsf{f}(r) = \sum_{j=1}^{3} \mathsf{f}_j \delta(r - r_j)$, where f_j are aligned with f and apply zero torque about r_0, and $\dot{q} = (cf, 0)$ are critical. Thus $\|\boldsymbol{w}\|_{\text{avg}} = \eta(\boldsymbol{w}) = |f|$ and this gives us the wrench subset

$\mathcal{W}_0^+$.

Case 2: $\tau_j > 0$ for all $i \in \{1, 2, 3\}$, which implies that $\boldsymbol{w}$ is not equivalent to a pure force acting at some point in the triangle.

Case 2(a): There is a critical distributed force $\mathsf{f}(r) = \mathsf{f}_1\delta(r - r_1) + \mathsf{f}_2\delta(r - r_2)$, i.e., f is nonzero at vertices r_1 and r_2 (Figure D.1(a)). Note that the conditions $\tau_1 > 0$ and $\tau_2 > 0$ are necessary for this distributed force. Let $\dot{q}$ be an instantaneous rotation. By Lemma D.1.1, f and $\dot{q}$ are critical if the ICR associated with $\dot{q}$ lies on the positive y-axis with coordinate $y \geqslant 0$, and each f_j is aligned with the velocity of r_j induced by $\dot{q}$, as shown in Figure D.1(a). For f to generate $\boldsymbol{w}$, we have $(|\mathsf{f}_1| + |\mathsf{f}_2|)\cos\beta = f_1$, $(-|\mathsf{f}_1| + |\mathsf{f}_2|)\sin\beta = f_y$, and $(|\mathsf{f}_1| + |\mathsf{f}_2|)\rho_{\max} = \tau + f_1 y$, where $\cos\beta = \frac{\ell_1}{\rho_{\max}}$ and $\rho_{\max}^2 = \ell_1^2 + (y + \ell_1 \cot\alpha_1)^2$. These equations determine $y = \frac{f_1\ell_1 \csc\alpha_1 - \tau\cos\alpha_1}{\tau - f_1\ell_1\cot\alpha_1}$, along with $|\mathsf{f}_j|$. Since $\tau_1, \tau_2 > 0$ implies that $\tau - f_1\ell_1\cot\alpha_1 > 0$, $y \geqslant 0$ if and only if

$$f_1 \geqslant \frac{\tau}{\ell_1}\sin\alpha_1\cos\alpha_1$$

This condition leads to the wrench subset $\mathcal{W}_1^+$, and as can be shown implies that $\tau_3 > 0$ when $\tau_1, \tau_2 > 0$. Since f and $\dot{q}$ are critical for $\boldsymbol{w}$, $\|\boldsymbol{w}\|_{\text{avg}} = \eta(\boldsymbol{w}) = |\mathsf{f}_1| + |\mathsf{f}_2|$. Thus, solving for $|\mathsf{f}_j|$ gives

$$\|\boldsymbol{w}\|_{\text{avg}} = \sqrt{\left(\frac{\tau}{\ell_1}\right)^2 - 2\left(\frac{\tau}{\ell_1}\right)f_1\cot\alpha_1 + f_1^2\csc^2\alpha_1}.$$

Case 2(b): There is a critical distributed force $\mathsf{f}(r) = \mathsf{f}_2\delta(r - r_2) + \mathsf{f}_3\delta(r - r_3)$, i.e., f is nonzero at vertices r_2 and r_3. This is analogous to Case 2(a). By replacing f_1 and α_2 with f_2 and α_2, respectively, we obtain $f_2 \geqslant \frac{\tau}{\ell_2}\sin\alpha_2\cos\alpha_2$, which determines $\mathcal{W}_2^+$, and $\|\boldsymbol{w}\|_{\text{avg}} = \eta(\boldsymbol{w}) = \sqrt{(\frac{\tau}{\ell_2})^2 - 2(\frac{\tau}{\ell_2})f_2\cot\alpha_2 + f_2^2\csc^2\alpha_2}$.

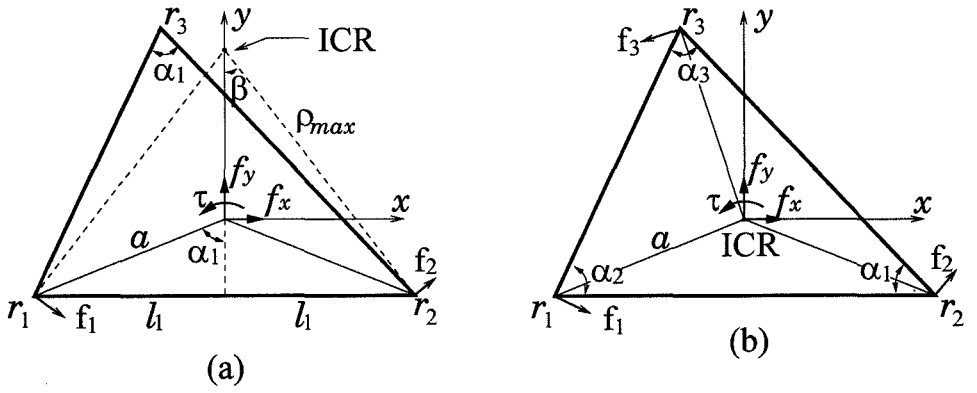

Figure D.1: A distributed force nonzero at (a) r_1 and r_2, and (b) r_1, r_2 and r_3.

Case 2(c): There is a critical distributed force $\mathsf{f}(r) = \mathsf{f}_3\delta(r - r_3) + \mathsf{f}_1\delta(r - r_1)$, i.e., f is nonzero at vertices r_3 and r_1. This is again analogous to Case 2(a). By replacing f_1 and α_3 with f_3 and α_3, respectively, we obtain $f_3 \geqslant \frac{\tau}{\ell_3}\sin\alpha_3\cos\alpha_3$, which determines $\mathcal{W}_3^+$, and $\|\boldsymbol{w}\|_{\text{avg}} = \eta(\boldsymbol{w}) = \sqrt{(\frac{\tau}{\ell_3})^2 - 2(\frac{\tau}{\ell_3})f_3\cot\alpha_3 + f_3^2\csc^2\alpha_3}$.

Case 2(d): There is a critical force $\mathsf{f}(r) = \sum_{j=1}^{3}\mathsf{f}_j\,\delta(r - r_j)$, i.e., f is nonzero at every vertex of the triangle. Let $\dot{q}$ be an instantaneous rotation. By Lemma D.1.1, f and $\dot{q}$ are critical if the ICR associated with $\dot{q}$ is equidistant, at a distance a, to the three vertices, and each f_j is aligned with the velocity of r_j induced by $\dot{q}$, as shown in Figure D.1(b). The distributed force f generates $\boldsymbol{w}$ if $|\mathsf{f}_1|\cos\alpha_1 + |\mathsf{f}_2|\cos\alpha_1 - |\mathsf{f}_3|\cos(\alpha_2 - \alpha_3) = f_1$, $-|\mathsf{f}_1|\sin\alpha_1 + |\mathsf{f}_2|\sin\alpha_1 - |\mathsf{f}_3|\sin(\alpha_2 - \alpha_3) = f_y$, and $(|\mathsf{f}_1| + |\mathsf{f}_2| + |\mathsf{f}_3|)a = \tau$. It can be shown that $|\mathsf{f}_j|$ solved from this set of equations are all positive if $f_j < \frac{\tau}{\ell_j}\sin\alpha_j\cos\alpha_j$ at all the three vertices. This gives the wrench subset $\mathcal{W}_4^+$. Since f and $\dot{q}$ are critical for $\boldsymbol{w}$, $\|\boldsymbol{w}\|_{\text{avg}} = \eta(\boldsymbol{w}) = |\mathsf{f}_1| + |\mathsf{f}_2| + |\mathsf{f}_3|$. Solving for $|\mathsf{f}_j|$ yields

$$\|\boldsymbol{w}\|_{\text{avg}} = \frac{\tau}{a}.$$

Having obtained $\mathcal{W}_i^+$, the consideration of $\mathcal{W}_i^-$ is straightforward. For each $\boldsymbol{w} \in \mathcal{W}_i^-$, it admits a critical distributed force and velocity that are critical for $-\boldsymbol{w} \in \mathcal{W}^+$. Thus, $\|-\boldsymbol{w}\|_{\text{avg}} = \eta(-\boldsymbol{w}) = \|\boldsymbol{w}\|_{\text{avg}}$. We finally consider the relations among these wrench subsets. It is straightforward to observe that $\mathcal{W}_i^+$ and $\mathcal{W}_i^-$ are disjoint for each $i = 0, \ldots, 4$. We also observe that $\mathcal{W}_0^+$ and $\mathcal{W}_4^+$ are disjoint from each other and from $\mathcal{W}_1^+$, $\mathcal{W}_2^+$ and $\mathcal{W}_3^+$. In addition, it can be shown that if $\tau_j > 0$ for all $j \in \{1, 2, 3\}$, the conditions $f_i > \frac{\tau}{\ell_i} \sin\alpha_i \cos\alpha_i$ are mutually exclusive, which implies that $\mathcal{W}_1^+$, $\mathcal{W}_2^+$ and $\mathcal{W}_3^+$ are mutually disjoint. Thus, $\mathcal{W}_i^+$, and hence $\mathcal{W}_i^-$, are mutually disjoint for $i = 0, \ldots, 4$. This implies the mutual disjointness of $\mathcal{W}_i = \mathcal{W}_i^+ \cup \mathcal{W}_i^-$ $(i = 0, \ldots, 4)$, whose union is the entire wrench space: $\mathcal{W} = \mathcal{W}_0 \cup \mathcal{W}_1 \cup \mathcal{W}_2 \cup \mathcal{W}_3 \cup \mathcal{W}_4$. □

D.3 The Average Wrench Norm for Polygons

This section extends the methodology for triangles to polygons. For clarity we first consider a convex polygon $\mathcal{B}$, and later remove the convexity condition (Corollary D.3.4). Denote by $\rho_{\max}(\dot{q})$ the maximal distance from the ICR associated with a velocity $\dot{q}$ to $\mathcal{B}$'s vertices, and by $\rho_A(\dot{q})$ the distance from the ICR of $\dot{q}$ to a particular vertex A of $\mathcal{B}$. The following lemma characterizes the relationship between wrenches and their critical distributed forces and velocities, *if* such distributed forces and velocities exist. The characterization is made in terms of a containing circle of $\mathcal{B}$, centered at O, such that the edge e_{AB} is on the circle, as shown in Figure D.2(a).

Lemma D.3.1. *Consider a convex polygon $\mathcal{B}$. Suppose that each wrench $\boldsymbol{w} \in \mathcal{W}$ has a critical distributed force of the form* (D.1) *and a critical velocity $\dot{q}$. Then $\mathcal{W} = \mathcal{W}_{KQ}^{e_{AB}} \cup \mathcal{W}_c^{\mathcal{B}}$, where $\mathcal{W}_{KQ}^{e_{AB}}$ and $\mathcal{W}_c^{\mathcal{B}}$ are given as follows.*

(1) A wrench $\boldsymbol{w}$ is said to be in $\mathcal{W}_{KQ}^{e_{AB}} \subset \mathcal{W}$ if it admits a critical velocity $\dot{q} = (v, \omega)$ $(\omega \neq 0)$ with ICR lying on the ray KQ, where K is at or

below O, such that $\rho_{\max}(\dot{q}) = \rho_A(\dot{q}) = \rho_B(\dot{q})$.

(2) A wrench $\boldsymbol{w}$ is said to be in $\mathcal{W}_c^{\mathcal{B}} \in \mathcal{W}$ if it admits a critical velocity that is a pure translation or an instantaneous rotation. In the latter case, the ICR is equidistant to two or more vertices of $\mathcal{B}$, at least *one of which is* different *from A and B, such that $\rho_{\max}(\dot{q})$ equals this distance.*

Proof. By assumption, for any wrench $\boldsymbol{w}$ there is a critical distributed force $\mathsf{f} = \sum_{i=1}^{k} \mathsf{f}_i \, \delta(r - r_i)$, where r_i are vertices of $\mathcal{B}$, with respect to a critical velocity $\dot{q}$. We consider the following cases of f.

Case 1: $k = 1$, i.e., f has only a single component, or $k \geqslant 2$ with all f_i aligned in the *same* direction. In this case $\boldsymbol{w}$ is statically equivalent to a pure force acting at some point in $\mathcal{B}$, and a pure translation $\dot{q} = (c\mathsf{f}_1, 0)$ is a critical velocity. Thus, $\boldsymbol{w} \in \mathcal{W}_c^{\mathcal{B}}$.

Case 2: $k \geqslant 2$, f_i are not in the same direction, and $\{r_i\}$ includes *both* r_A and r_B, the coordinates of A and B. Then by Lemma D.1.1, $\dot{q}$ must be an instantaneous rotation such that $\rho_{\max}(\dot{q}) = \rho_A(\dot{q}) = \rho_B(\dot{q})$. Thus, the ICR lies on the bisector of e_{AB}. In addition, since $\rho_{\max}$ is achieved by ρ_A and ρ_B, the ICR must be located on the bisector of the edge e_{AB} and above any line that bisects the segment AV or BV, where V is any vertex of the polygon other than A and B. Since $\mathcal{B}$ is contained in the circle, the *uppermost* intersection of these lines with the bisector of e_{AB}, denoted K, must be *at or below* O (Figure D.2(a)). In this case, $\boldsymbol{w} \in \mathcal{W}_{KQ}^{e_{AB}}$.

Case 3: $k \geqslant 2$, f_i are not in the same direction, and at least one of r_A and r_B, say r_A, is *not* contained in $\{r_i\}$. Then $\{r_i\}$ includes at least a vertex V *different* from A and B. Again by Lemma D.1.1, $\dot{q}$ must be an instantaneous rotation such that $\rho_{\max}(\dot{q}) = \rho_V(\dot{q}) > \rho_A(\dot{q})$. In this case, $\boldsymbol{w} \in \mathcal{W}_c^{\mathcal{B}}$.

Finally, we have considered all possibilities of distributed forces, and therefore all wrenches in $\mathcal{W}$. It follows that $\mathcal{W} = \mathcal{W}_{KQ}^{e_{AB}} \cup \mathcal{W}_c^{\mathcal{B}}$ □

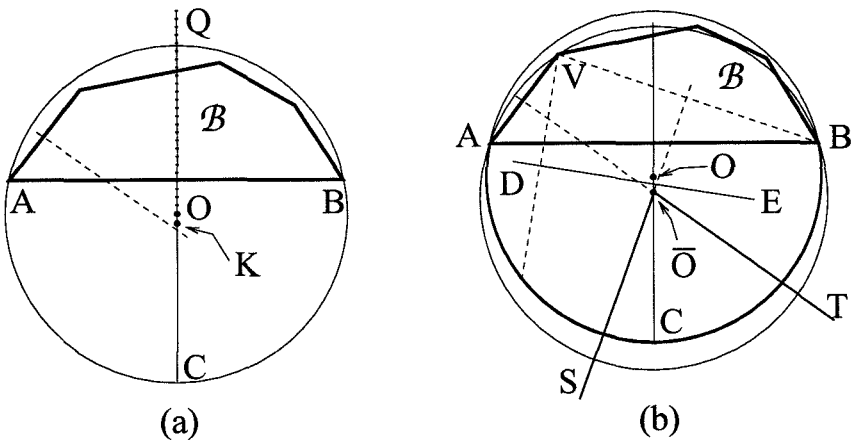

Figure D.2: (a) $\mathcal{B}$'s edge e_{AB} lies on a circle containing $\mathcal{B}$; (b) The arc ACB is glued to $\mathcal{B}$: if $\rho_{\max}(\dot{q}) = \rho_V(\dot{q})$, the ICR lies in the cone $S\bar{O}T$, which is below the line DE.

As another convex polygon is glued to $\mathcal{B}$ on edge e_{AB} to form a new convex polygon $\bar{\mathcal{B}}$, the maximal distance $\rho_{\max}$ associated with a given velocity is in general different. Accordingly for a wrench $\boldsymbol{w}$, a distributed force and velocity that are critical for $\mathcal{B}$ may not remain critical for $\bar{\mathcal{B}}$. Therefore, even if $\boldsymbol{w}$ admits critical forces and velocities with respect to both $\mathcal{B}$ and $\bar{\mathcal{B}}$, $\|\boldsymbol{w}\|^{\mathcal{B}}_{\text{avg}}$ is in general *different* from $\|\boldsymbol{w}\|^{\bar{\mathcal{B}}}_{\text{avg}}$, where the subscripts denote norms computed for different polygons. The following lemma gives a condition allowing the two norms to agree.

Lemma D.3.2. *For both polygons $\mathcal{B}$ and $\tilde{\mathcal{B}}$, suppose that each wrench $\boldsymbol{w} \in \mathcal{W}$ admits a critical distributed force of the form* (D.1) *and a critical velocity. If the new polygon $\tilde{\mathcal{B}}$ remains in the circle O, then for any wrench $\boldsymbol{w} \in \mathcal{W}_c^{\mathcal{B}}$, a velocity $\dot{q}$ and a distributed force* f *that are critical for $\mathcal{B}$ remain critical for $\tilde{\mathcal{B}}$. Consequently,*

$$\|\boldsymbol{w}\|^{\mathcal{B}}_{avg} = \|\boldsymbol{w}\|^{\tilde{\mathcal{B}}}_{avg} = \eta_{\mathcal{B}}(\boldsymbol{w}) = \eta_{\tilde{\mathcal{B}}}(\boldsymbol{w}),$$

where subscripts are also used for the upper bound η to indicate computation with respect to different polygons.

Proof. Let f be a critical distributed force and $\dot{q}$ a critical velocity for $\mathcal{B}$. As illustrated in Figure D.2(b), it is sufficient to show that f and $\dot{q}$ remain critical for the geometric object $\mathcal{G}$ whose boundary consists of the arc ACB and the edges of $\mathcal{B}$ (excluding e_{AB}).

When $\dot{q}$ is a pure translation, the assertion is obviously true. It remains to consider the case where $\dot{q}$ is an instantaneous rotation. Then $\rho^{\mathcal{B}}_{\max}(\dot{q}) = \rho_V(\dot{q})$, where V is a vertex of $\mathcal{B}$ *different* from A and B, and the superscript $\mathcal{B}$ denotes computation with respect to $\mathcal{B}$. For this reason, the ICR of $\dot{q}$ must lie *on or below* the bisector of the segment connecting V with any other vertex, including A and B, of $\mathcal{B}$. Thus, the ICR must lie inside the cone $S\bar{O}T$, where $\bar{O}$ is the center of the circle determined by the points A, B and V. This indicates that $\rho^{\mathcal{G}}_{\max}(\dot{q}) = \rho_V(\dot{q})$. Indeed, any line whose points are equidistant to V and a point on the arc ACB lies *above* $\bar{O}$, as illustrated by the line DE in Figure D.2(b). □

Lemmas D.3.1 and D.3.2 allow us to extend the results for triangles to arbitrary convex polygons in the following proposition.

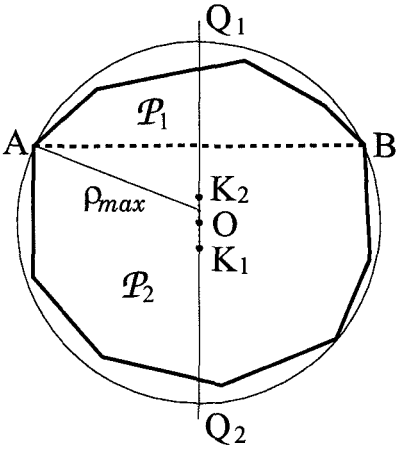

Figure D.3: A polygon cut into two by the segment e_{AB}.

Proposition D.3.3. *Given an arbitrary convex polygon $\mathcal{B}$, there is a critical velocity and a critical distributed force of the form* (D.1) *for any wrench $\boldsymbol{w} \in \mathcal{W}$. Consequently, $\|\boldsymbol{w}\|_{avg} = \eta(\boldsymbol{w})$.*

Proof. We prove this proposition by induction for a polygon with j edges. The assertion is true for $j = 3$, thanks to Proposition 8.6.2. Now assume that the assertion is true for a polygon with $j \leqslant n$ edges ($n \geqslant 3$) and consider a polygon $\mathcal{B}$ with $j = n + 1$ edges.

The convex polygon $\mathcal{B}$ can always be contained in a circle, centered at O, such that two non-adjacent vertices A and B are on the circle (Figure D.5). The segment e_{AB} cuts $\mathcal{B}$ into two adjacent polygons, denoted $\mathcal{P}_1$ and $\mathcal{P}_2$, both with no more than n edges. Let Q_1Q_2 be the bisector of e_{AB}, and let K_1 be a point on Q_1Q_2 such that A and B are the farthest vertices of $\mathcal{P}_1$ from any point on the ray K_1Q_1. Likewise we have a point K_2 on Q_1Q_2 associated with $\mathcal{P}_2$. Lemma D.3.1 and our assumption for polygons with $j \leqslant n$ yield

$$\mathcal{W} = \mathcal{W}^{e_{AB}}_{K_1Q_1} \cup \mathcal{W}^{\mathcal{P}_1}_c \quad \text{and} \quad \mathcal{W} = \mathcal{W}^{e_{AB}}_{K_2Q_2} \cup \mathcal{W}^{\mathcal{P}_2}_c.$$

This implies that $\mathcal{W}$ can be written in the form

$$\mathcal{W} = \mathcal{W}^{e_{AB}}_{K_1K_2} \cup \mathcal{W}^{\mathcal{P}_1}_c \cup \mathcal{W}^{\mathcal{P}_2}_c,$$

where $\mathcal{W}^{e_{AB}}_{K_1K_2} = \mathcal{W}^{e_{AB}}_{K_1Q_1} \cap \mathcal{W}^{e_{AB}}_{K_2Q_2}$. Lemma D.3.1 implies that the rays K_1Q_1 and K_2Q_2 overlap. If $\boldsymbol{w} \in \mathcal{W}^{e_{AB}}_{K_1K_2}$, then $\boldsymbol{w}$ admits a critical velocity whose ICR lies within the segment K_1K_2. As can be seen in Figure D.5, $\dot{q}$ remains to be a critical velocity with respect to $\mathcal{B}$, since $\rho_{\max}(\dot{q}) = \rho_A = \rho_B$ remains to hold for $\mathcal{B}$. Meanwhile, by Lemma D.3.2, if $\boldsymbol{w} \in \mathcal{W}^{\mathcal{P}_1}_c$ or $\boldsymbol{w} \in \mathcal{W}^{\mathcal{P}_2}_c$, then a critical distributed force and velocity for $\mathcal{P}_1$ or $\mathcal{P}_2$ remain critical for $\mathcal{B}$. It

follows that any $\boldsymbol{w} \in \mathcal{W}$ admits a critical distributed force of the form (D.1) and a critical velocity for the body $\mathcal{B}$. □

The above results for convex polygons can be further extended to nonconvex polygons as follows.

Corollary D.3.4. *Let $\mathcal{B}$ be a nonconvex polygon and $\boldsymbol{w}$ a wrench acting on $\mathcal{B}$. Then $\boldsymbol{w}$ admits a critical distributed force and a critical velocity. The critical distributed force is of the form* (D.1)*, and vanishes except at the vertices of $\mathcal{B}$'s convex hull. Consequently, $\|\boldsymbol{w}\|_{avg}^{\mathcal{B}} = \|\boldsymbol{w}\|_{avg}^{\bar{\mathcal{B}}} = \eta_{\mathcal{B}}(\boldsymbol{w}) = \eta_{\bar{\mathcal{B}}}(\boldsymbol{w})$, where $\bar{\mathcal{B}}$ is the convex hull of $\mathcal{B}$.*

Proof. From Proposition D.3.3, $\boldsymbol{w}$, regarded as a wrench acting on $\bar{\mathcal{B}}$, admits a critical velocity $\dot{q}$ and a critical distributed force f, which vanishes except at the vertices of $\bar{\mathcal{B}}$. Clearly, these vertices also belong to $\mathcal{B}$, and $\rho_{\max}^{\mathcal{B}}(\dot{q}) = \rho_{\max}^{\bar{\mathcal{B}}}(\dot{q}) = \rho_A(\dot{q})$, where A represents vertices at which f is nonzero. Therefore, f is a force distributed over $\mathcal{B}$ and remains critical with respect to $\dot{q}$, and the proof is completed. □

Now consider computing the wrench norm for polygonal objects. We first introduce a lemma which characterizes the set of wrenches acting on a special object—a line segment. As shown in Figure D.4, one can choose a body frame such that the segment e_{AB} lies on the x-axis and is bisected by the y-axis. Let us consider wrench subsets $\mathcal{W}_{y0+}^{e_{AB}} \in \mathcal{W}$ and $\mathcal{W}_{y0-}^{e_{AB}} \in \mathcal{W}$. A wrench $\boldsymbol{w}$ is said to be in $\mathcal{W}_{y0+}^{e_{AB}}$ (or $\mathcal{W}_{y0-}^{e_{AB}}$) if it admits a critical velocity whose ICR is on the y-axis with coordinate $y > y_0$ (or $y < y_0$).

Lemma D.3.5. *The wrench subsets $\mathcal{W}_{y0+}^{e_{AB}}$ and $\mathcal{W}_{y0-}^{e_{AB}}$ are mutually exclusive, i.e., $\mathcal{W}_{y0+}^{e_{AB}} \cap \mathcal{W}_{y0-}^{e_{AB}} = \emptyset$.*

Proof. As shown in Figure D.4, by considering the ICR lying on the positive and negative y-axis and performing a case analysis, we can obtain $\mathcal{W}_{y0+}^{e_{AB}} =$

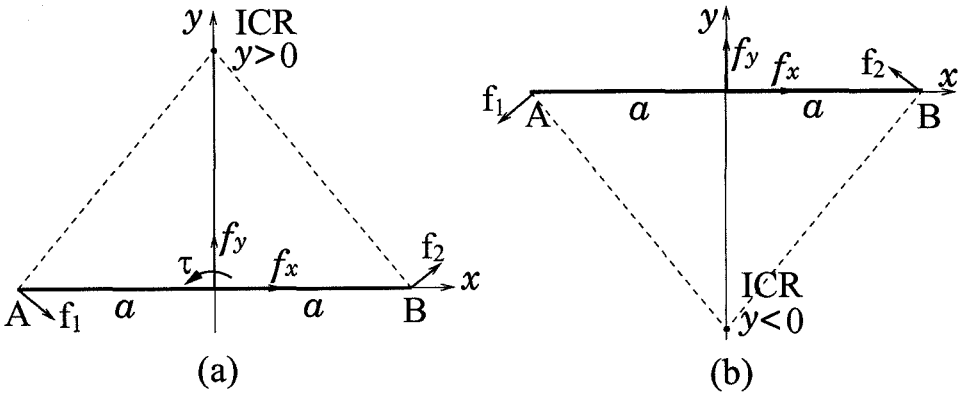

Figure D.4: Critical velocities for a segment: ICR has coordinate (a) $y > 0$ and (b) $y < 0$.

$\{(f_x, f_y, \tau) : \tau > 0, f_x > \frac{\tau y_0}{a^2}, |f_y| \leqslant \frac{\tau}{a}$; or $\tau < 0, f_x < \frac{\tau y_0}{a^2}, |f_y| \leqslant \frac{|\tau|}{a}\}$, and $\mathcal{W}^{e_{AB}}_{y_0-} = \{(f_x, f_y, \tau) : \tau > 0, f_x < \frac{\tau y_0}{a^2}, |f_y| \leqslant \frac{\tau}{a}$; or $\tau < 0, f_x > \frac{\tau y_0}{a^2}, |f_y| \leqslant \frac{|\tau|}{a}\}$
Thus, $\mathcal{W}^{e_{AB}}_{y_0+} \cap \mathcal{W}^{e_{AB}}_{y_0-} = \emptyset$. □

We are now in a position to compute the wrench norm for a general polygonal object.

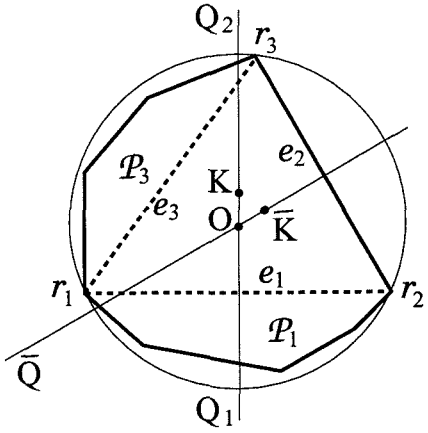

Figure D.5: Three vertices of a convex polygon lie on a containing circle.

Proposition 8.6.3. *Let $\boldsymbol{w} = (f, \tau) \in \mathcal{W}$ be a wrench acting on a polygon $\mathcal{B}$. Then $\|\boldsymbol{w}\|^{\mathcal{B}}_{avg} = \eta_{\mathcal{B}}(\boldsymbol{w})$, where $\eta_{\mathcal{B}}(\boldsymbol{w}) = \inf_{\mathsf{f} \in \mathcal{D}^1_w} \int_{\mathcal{B}} |\mathsf{f}(r)|\, dV$. Let $\bar{\mathcal{B}}$ be contained in a circle with vertices r_i (i=1,2,3) on the circle. Then $\bar{\mathcal{B}} = \Delta \cup \mathcal{P}_1 \cup \mathcal{P}_2 \cup \mathcal{P}_3$,*

as shown in Figure 8.3(b). By applying Proposition 8.6.2 to the triangle Δ, the norm can be computed as follows.

(1) If $\boldsymbol{w} \in \mathcal{W}_i$, $i = 0, 4$, then $\|\boldsymbol{w}\|^{\mathcal{B}}_{avg} = \|\boldsymbol{w}\|^{\Delta}_{avg}$.

(2) If $\boldsymbol{w} \in \mathcal{W}_i$, $i = 1, 2, 3$, and e_i is an edge of $\bar{\mathcal{B}}$, then $\|\boldsymbol{w}\|^{\mathcal{B}}_{avg} = \|\boldsymbol{w}\|^{\Delta}_{avg}$.

(3) If $\boldsymbol{w} \in \mathcal{W}_i$, $i = 1, 2, 3$, and e_i is not *an edge of $\bar{\mathcal{B}}$, then $\|\boldsymbol{w}\|^{\mathcal{B}}_{avg} = \|\boldsymbol{w}\|^{\mathcal{P}_i}_{avg}$.*

Proof. The fact that $\|\boldsymbol{w}\|^{\mathcal{B}}_{\text{avg}} = \eta_{\mathcal{B}}(\boldsymbol{w})$ and the computation can be performed with respect to $\mathcal{B}$'s convex hull follows from Corollary D.3.4.

Case 1: $\boldsymbol{w} \in \mathcal{W}_i$, $i = 0, 4$. If $\boldsymbol{w} \in \mathcal{W}_0$, then $\boldsymbol{w}$ admits a pure translation $\dot{q} = (v, 0)$ as a critical velocity, and a critical distributed force f aligned with v. Since f and $\dot{q}$ remain critical for $\mathcal{B}$, $\|\boldsymbol{w}\|^{\mathcal{B}}_{\text{avg}} = \|\boldsymbol{w}\|^{\Delta}_{\text{avg}}$. On the other hand, if $\boldsymbol{w} \in \mathcal{W}_4$, then $\boldsymbol{w}$ admits a critical velocity with ICR at O which is equidistant to r_i. Since $\mathcal{B}$ is contained in the circle, the maximal distance from the ICR to $\mathcal{B}$'s points remains to be the radius of the circle. Thus, $\dot{q}$, along with its associated critical distributed force, remain critical for $\mathcal{B}$. This again implies $\|\boldsymbol{w}\|^{\mathcal{B}}_{\text{avg}} = \|\boldsymbol{w}\|^{\Delta}_{\text{avg}}$.

Case 2: $\boldsymbol{w} \in \mathcal{W}_i$ (i=1,2,3), e_i is an edge of $\bar{\mathcal{B}}$. As shown in Figure D.5, suppose that e_2 is such an edge. Then $\boldsymbol{w}$ admits a critical velocity with ICR on the ray $O\bar{Q}$. Since the ray $\bar{K}\bar{Q}$ contains $O\bar{Q}$, by Lemma D.3.1, this velocity, along with its associated critical distributed force, remains critical for $\mathcal{B}$. Hence $\|\boldsymbol{w}\|^{\mathcal{B}}_{\text{avg}} = \|\boldsymbol{w}\|^{\Delta}_{\text{avg}}$.

Case 3. $\boldsymbol{w} \in \mathcal{W}_i$ (i=1,2,3), e_i is *not* an edge of $\bar{\mathcal{B}}$. Suppose that the segment e_1 is such an edge of the triangle (Figure D.5), which cuts the polygon $\mathcal{P}_1$ from $\mathcal{B}$. Thus, there is a critical velocity with ICR on the ray OQ_2, and $\boldsymbol{w} \in \mathcal{W}^{e_1}_{OQ_2}$. By Proposition D.3.3, $\mathcal{W} = \mathcal{W}^{e_1}_{KQ_1} \cup \mathcal{W}^{\mathcal{P}_1}_{c}$ for some point K below O. If $\boldsymbol{w} \in \mathcal{W}^{e_1}_{OK}$, $\boldsymbol{w}$ admits the same critical force and velocity with respect to both $\mathcal{B}$ and $\mathcal{P}_1$ since r_1 and r_2 are the farthest vertices of both $\mathcal{B}$ and $\mathcal{P}_1$ to a point on OK. It remains to consider $\boldsymbol{w} \in \mathcal{W}^{e_1}_{KQ_2}$ which admits a

critical velocity with ICR on the ray KQ_2 (excluding K). By Lemma D.3.5, $\boldsymbol{w} \notin \mathcal{W}^{e_2}_{KQ_1}$. This implies that $\boldsymbol{w} \in \mathcal{W}^{\mathcal{P}_1}_c$ since $\mathcal{W} = \mathcal{W}^{e_1}_{KQ_1} \cup \mathcal{W}^{\mathcal{P}_1}_c$. Therefore, $\|\boldsymbol{w}\|^{\mathcal{B}}_{\text{avg}} = \|\boldsymbol{w}\|^{\mathcal{P}_1}_{\text{avg}}$ by Lemma D.3.2. $\square$

Bibliography

[1] R. Abraham, J. E. Marsden, and T. S. Ratiu. *Manifolds, Tensor Analysis, and Applications.* Springer-Verlag, 2nd edition, 1988.

[2] A. Allcock. Case for modular fixtures. *Mach. Prod. Eng.*, 147(3759):64–65, 1989.

[3] H. Asada and A. B. By. Kinematic analysis of workpart fixturing for flexible assembly with automatically reconfigurable fixtures. *IEEE Trans. on Robotics and Automation*, 1(2):86–94, 1989.

[4] H. Asada and A. Fields. Design of flexible fixtures reconfigured by robot manipulators. In *Proc. Robotics and Manufacturing Automation, ASME Winter Annual Meeting*, pages 251–257, 1985.

[5] A. Bagchi and R. L. Lewis. On fixturing issues for the factory of the future. Proc. Computers in Industry, 1986.

[6] B. S. Baker, S. Fortune, and E. Grosse. Stable prehension with a multifingered hand. In *Proc. Int. Conf. on Robotics and Automation*, pages 570–575, 1985.

[7] D. Baraff, R. Mattikalli, and P. Khosla. Minimal fixturing of frictionless assemblies: Complexity and algorithms. *Algorithmica*, 19:4–39, 1997.

[8] D. P. Baron. Quadratic programming with quadratic constraints. *Naval Research Logistics Quarterly*, 19:253–260, 1972.

[9] J. J. Bausch and K. Youcef-Toumi. Kinematic methods for automated fixture reconfiguration planning. In *Proc. Int. Conf. on Robotics and Automation*, pages 1396–1401, Cincinnati, OH, 1990.

[10] B. Benhabib, K. C. Chan, and M. Q. Dai. A modular programmable fixturing system. *ASME J. of Engineering for Industry*, 113:93–100, 1991.

[11] A. Bicchi. Optimal control of robotic grasping. In *Proc. American Control Conf.*, pages 778–779, 1992.

[12] A. Bicchi. On the closure properties of robotic grasping. *Int. J. of Robotics Research*, 14(4):319–334, 1995.

[13] P. Bison, C. Ferrari, E. Pagello, and L. Stocchiero. Heuristic approach to automatic grasp planning for a 3-fingered hand. *J. of Intelligent and Robotic Systems: Theory and Applications*, 13(1):45–74, 1995.

[14] W. M. Boothby. *An Introduction to Differentiable Manifolds and Riemannian Geometry.* Academic Press, 2nd edition, 1986.

[15] R. C. Brost and K. Y. Goldberg. A complete algorithm for synthesizing modular fixtures for polygonal parts. In *Proc. Int. Conf. on Robotics and Automation*, pages 535–542, San Diego, CA, May 1994.

[16] R. C. Brost and R. R. Peters. Automatic design of 3d fixtures and assembly pallets. Technical Report SAND 95-2411, Sandia National Labs., Albuquerque, NM, 1997.

[17] R. G. Brown and R. C. Brost. A 3d modular gripper design tool. Technical Report SAND 97-0063, Sandia National Labs., Albuquerque, NM, 1997.

[18] J. H. Buitrago and K. Toucef-Toumi. Design of active modular and adaptable fixtures operated by robot manipulators. In *ASME USA-Japan Symp. on Flexible Automation*, pages 467–474, Minneapolis, MN, 1988.

[19] M. Buss, H. Hashimoto, and J. B. Moore. Dextrous hand grasping force optimization. *IEEE Trans. on Robotics and Automation*, 12(3):406–418, 1996.

[20] W. Cai, S. J. Hu, and J. X. Yuan. Deformable sheet metal fixturing: Principles, algorithms, and simulations. *J. of Manufacturing Science and Engineering*, 118:318–324, 1996.

[21] W. Cai, S. J. Hu, and J. X. Yuan. A variational method of robust fixture configuration design for 3-D workpieces. *J. of Manufacturing Science and Engineering*, 119:593–602, 1997.

[22] E. Caillaud, D. Noyes, G. Anglerot, and P. Padilla. Concurrent engineering: an expert system for fixture design. In *Proc. INRIA/IEEE Symp. on Emerging Technologies and Factory Automation*, pages 137–144, Paris, 1995.

[23] I.-M. Chen and J. W. Burdick. Finding antipodal point grasps on irregularly shaped objects. In *Proc. Int. Conf. on Robotics and Automation*, pages 2278–2283, Nice, France, April 1992.

[24] Y.-C. Chen, I. D. Walker, and J. B. Cheatham. Grasp synthesis for planar and solid objects. *Journal of Robotic Systems*, 10(2):153–186, 1993.

[25] F.-T. Cheng and D. E. Orin. Efficient algorithm for optimal force distribution—the compact-dual LP method. *IEEE Trans. on Robotics and Automation*, 6(2):178–187, 1990.

[26] Y.-C. Chou. Automated planning and design of fixtures for complex parts. *Int. J. of Computer Applications in Technology*, 10:183–197, 1997.

[27] Y.-C. Chou, V. Chandru, and M. M. Barash. A mathematical approach to automatic configuration of machining fixtures: Analysis and synthesis. *ASME J. of Engineering for Industry*, 111:299–306, 1989.

[28] C.-H. Chu, M. W. Trethewey, E. C. De Meter, and C.-Y. Wu. Modeling and analysis of workpiece static and dynamic structural characteristics for machining operations. In *Proc. Int. Modal Analysis Conf.*, pages 325–331, Orlando, FL, 1997.

[29] J. A. Coelho and R. A. Grupen. Optimal multifingered grasp synthesis. In *Proc. Int. Conf. on Robotics and Automation*, pages 1937–1942, San Diego, CA, May 1994.

[30] M. R. Cutkosky. *Robotic Grasping and Fine Manipulation.* Kluwer Academic Publishers, 1985.

[31] M. R. Cutkosky and I. Kao. Computing and controlling the compliance of a robotic hand. *IEEE Trans. on Robotics and Automation*, 5(2):151–165, 1989.

[32] M. R. Cutkosky, E. Kurokawa, and P. K. Wright. Programmable conformable clamps. In *Proc. AUTOFACT 4*, pages 1151–1158, 1982.

[33] M. R. Cutkosky and P. Wright. Friction, stability and the design of robotic fingers. *Int. J. of Robotics Research*, 5(4):20–37, 1986.

[34] J. Czyzowicz, I. Stojmenovic, and J. Urrutia. Immobilizing a polytope. In *Lecture Notes in Computer Science*, volume 519, pages 214–227. 1991.

[35] J. P. Donoghue, W. S. Howard, and V. Kumar. Stable workpiece fixturing. In *Proc. ASME Design Technical Conferences*, Minneapolis, MN, Sept. 1994.

[36] J. Duffy. The fallacy of modern hybrid control theory that is based on "orthogonal complements" of twist and wrench spaces. *Journal of Robotic Systems*, 7(2):139–144, 1990.

[37] P. J. Englert and P. K. Wright. Applications of artificial intelligence and the design of fixtures for automated manufacturing. In *Proc. Int. Conf. on Robotics and Automation*, pages 345–351, San Francisco, CA, 1986.

[38] K. R. Etzel and J. M. McCarthy. A metric for spatial displacements using biquaternions on $so(4)$. In *Proc. Int. Conf. on Robotics and Automation*, pages 3185–3190, Minneapolis, MN, April 1996.

[39] E. Faldella, B. Fringuelli, D. Passeri, and F. Zanichelli. Robot grasp synthesis tool based on neural computational models. In *Proc. Int. Conf. on Industrial Electronics, Control and Instrumentation.*, pages 930–935, Bologna, Italy, 1994.

[40] B. Faverjon and J. Ponce. On computing two-finger force-closure grasps of curved 2D objects. In *Proc. Int. Conf. on Robotics and Automation*, pages 424–429, Sacramento, CA, 1991.

[41] C. Ferrari and J. Canny. Planning optimal grasps. In *Proc. Int. Conf. on Robotics and Automation*, pages 2290–2295, Nice, France, May 1992.

[42] P. M. Ferreria, B. Kochar, C. R. Liu, and V. Chandra. Aifix: an expert systems approach to fixture design. In *ASME Winter Annual Meeting, Computer-Aided/Intelligent Process Planning*, pages 73–82, 1985.

[43] H. Fessler and E. Ollerton. Contact stresses in toroids under radial loads. *Brit. J. of Applied Physics*, 8:387, 1957.

[44] C. A. Floudas and V. Visweswaran. Quadratic optimization. In R. Horst and P. M. Pardalos, editors, *Handbook of Global Optimization.* Kluwer Academic Publishers, 1995.

[45] A. Friedman. The modular fixturing system, a profitable investment. In *Proc. Int. Conf. on Advances in Manufacturing*, pages 165–173, 1984.

[46] M. V. Gandhi and B. S. Thompson. Phase change fixturing for flexible manufacturing systems. *J. of Manufacturing Systems*, 4(1):29–39, 1985.

[47] M. V. Gandhi and B. S. Thompson. Automated design of modular fixtures for flexible manufacturing systems. *J. of Manufacturing Systems*, 5(4):243–252, 1986.

[48] A. Gesley. From cad/cam to simulation: Automatic model generation for mechanical devices. In P. Fishwick and R. Modjeski, editors, *Knowledge-Based Simulation: Methods and Applications.* Springer-Verlag, 1989.

[49] L. E. Goodman and L. M. Keer. The contact stress problem for an elastic sphere indenting an elastic cavity. *Int. J. of Solids Structures*, 1(4):407–415, 1965.

[50] B. Grunbaum. *Convex Polytopes.* Wiley-Intersciences, 1967.

[51] M. E. Gurtin. *An Introduction to Continuum Mechanics.* Academic Press, 1972.

[52] H. Hanafusa and H. Asada. Stable prehension by a robot hand with elastic fingers. In *Proc. 7^{th} Int. Symp. on Industrial Robots*, pages 361–368, Tokyo, October 1977.

[53] F. B. Hazen and P. K. Wright. Workholding automation: Innovations in analysis, design, and planning. *Manufacturing Review*, 3(4):224–237, 1990.

[54] H. Hertz. On the contact of rigid elastic solids and on hardness. In *Misc. Papers by H. Hertz.* Jones and Schott, Macmillan, London, 1896. English translation.

[55] D. Hilbert. *The Foundations of Geometry.* Translated by E. J. Townsend. Open Court Publ. Co., LaSalle, Illinois, 1965.

[56] M. J. Hockenberger and E. C. De Meter. Effect of machining fixture design parameters on workpiece displacement. *Manufacturing Review*, 8(1):22–32, 1993.

[57] M. J. Hockenberger and E. C. De Meter. Preliminary experimentation and modeling of workpiece displacement during machining. *NAMRI/SME*, 21:351–357, 1993.

[58] M. J. Hockenberger and E. C. De Meter. Application of meta functions to the quasi-static analysis of workpiece displacement within a machining fixture. *J. of Manufacturing Science and Engineering*, 118(3):325–331, 1996.

[59] M. J. Hockenberger and E. C. De Meter. Impact of rigid body workpiece displacement on the geometric errors of milled surfaces. *Int. J. of Computer Applications in Technology*, 10:170–182, 1997.

[60] E. G. Hoffman. *Modular Fixturing.* Manufacturing Technology Press, Lake Geneva, WI, 1987.

[61] R. A. Horn and C. R. Johnson. *Matrix Analysis.* Cambridge University Press, 1985.

[62] J.-L. Hou and A. J. C. Trappey. The illustration of systematic fixture design approach for automotive part machining. *J. of Chinese Society of Mechanical Engineers*, 18(6):499–511, 1997.

[63] W. S. Howard and V. Kumar. A minimum principle for the dynamics analysis of systems with frictional contacts. In *Proc. Int. Conf. on Robotics and Automation*, pages 437–442, Atlanta, GA, May 1993.

[64] W. S. Howard and V. Kumar. Stability of planar grasps. In *Proc. Int. Conf. on Robotics and Automation*, pages 2822–2827, San Diego, CA, May 1994.

[65] W. S. Howard, M. Zefran, and V. Kumar. On the 6x6 stiffness matrix for three dimensional motions. In *9th World Congress of the IFToMM*, Milano, Italy, August 1995.

[66] C. Icking, G. Rote, E. Welzl, and C. Yap. Shortest paths for line segments. *Algorithmica*, 10:182–200, 1993.

[67] S.-L. Jeng, L.-G. Chen, and W.-H. Chieng. Analysis of minimum clamping force. *Int. J. of Machine Tools and Manufacture*, 35:1213–1224, 1995.

[68] B. D. Jensen, L. L. Howell, D. B. Gunyan, and L. G. Salmon. The design and analysis of compliant mems using the pseudo-rigid-body model. In *Proc. ASME Int. Mechanical Eng. Congress and Exposition*, pages 119–126, Dallas, TX, 1997.

[69] Z. Ji and B. Roth. Contact force in grasping and kinematic constraints. In *7th IFToMM World Congress*, pages 1219–1222, Sevilla, Spain, 1987.

[70] Z. Ji and B. Roth. Direct computation of grasping force for three-finger tip-prehension grasps. *ASME J. of Mechanisms, Transmissions, Automation in Design*, 110:405–413, 1988.

[71] K. L. Johnson. One hundred years of hertz contact. *Proc. Inst. Mechanical Engineers*, 196:363–378, 1982.

[72] K. L. Johnson. *Contact Mechanics.* Cambridge University Press, 1985.

[73] K. Kazerounian and J. Rastegar. Object norms: A class of coordinate and metric independent norms for displacements. In G. Kinzel et al., editor, *Flexible Mechanisms, Dynamics and Analysis: ASME Design Technical Conferences, 22nd Biennial Mechanisms Conference*, volume 47, pages 271–275, Scottsdale, AZ, September 1992.

[74] D. R. Kerr and D. J. Sanger. Restraint analysis of a rigid body using frictional elastic contacts. *ASME J. of Mechanisms, Transmissions, Automation in Design*, 109:450–454, 1987.

[75] J. Kerr and B. Roth. Analysis of multifingered hands. *Int. J. of Robotics Research*, 4(4):3–17, 1986.

[76] K. H. Kim. *A System for Automated Fixture Planning.* PhD thesis, Carnegie Mellon University, 1993.

[77] L. S.-B. King and I. Hutter. Theoretical approach for generating optimal fixturing locations for prismatic workparts in automated assembly. *J. of Manufacturing Systems*, 12(5):409–416, 1993.

[78] L. S.-B. King and F. F. Ling. Force analysis based analytical framework for automatic fixture configuration. In *Proc. ASME Int. Mechanical Eng. Congress and Exposition*, pages 789–800, New York, NY, 1995.

[79] D. G. Kirkpatrick, B. Mishra, and C. K. Yap. Quantitative steinitz's theorems with applications to multifingered grasping. In *Proc.* 20^{th} *ACM Symp. on Theory of Computing*, pages 341–351, Baltimore, MD, May 1990.

[80] J. K. Knowles. Advanced mathematical elasticity theory. Lecture notes. Department of Applied Mechanics, California Inst. of Technology, 1992.

[81] S. Kota, G. K. Ananthasuresh, S. B. Crary, and K. D. Wise. Design and fabrication of microelectromechanical systems. *ASME J. of Mechanical Design*, 116:1081–1088, 1994.

[82] K. Kurz, K. Craig, B. Wolf, and F. Stolfi. Developing a flexible automated fixturing device. *Mechanical Engineering*, 116(7):59–63, 1994.

[83] K. Lakshminarayana. Mechanics of form closure. ASME Paper No. 78-DET-32, 1978.

[84] P. Larochelle and J. M. McCarthy. Planar motion synthesis using an approximate bi-invariant metric. *ASME J. of Mechanical Design*, 117(4):646–651, 1995.

[85] J.-C. Latombe. *Robot Motion Planning.* Kluwer Academic Publishers, 1991.

[86] J. D. Lee and L. S. Haynes. Finite-element analysis of flexible fixturing system. *ASME J. of Engineering for Industry*, 109:134–139, 1987.

[87] S. H. Lee and M. R. Cutkosky. Fixture planning with friction. *ASME J. of Engineering for Industry*, 113:320–327, 1991.

[88] Z. Li. Geometrical considerations of robot kinematics. *IEEE J. of Robotics and Automation*, 5(3):139–145, 1990.

[89] Z. Li and S. Sastry. Task oriented optimal grasping by multifingered robot hands. In *Proc. Int. Conf. on Robotics and Automation*, pages 389–394, Raleigh, NC, April 1987.

[90] Z. Li and S. Sastry. Task oriented optimal grasping by multifingered robot hands. *IEEE Trans. on Robotics and Automation*, 4(1):32–44, 1988.

[91] Z.-C. Lin and C.-B. Yang. Expert system for fixturing design for face milling using modular fixture. *Int. J. of Advanced Manufacturing Technology*, 10(6):379–388, 1995.

[92] J. Loncaric. *Geometric Analysis of Compliant Mechanisms in Robotics.* PhD thesis, Harvard University, 1985.

[93] J. Loncaric. Normal forms of stiffness and compliance matrices. *IEEE J. of Robotics and Automation*, RA-3(6):567–572, 1987.

[94] B. Madewell. The flexibility of modular fixturing. *Cutting Tool Engineering*, 48(7), 1996.

[95] M. Mani and W. R. D. Wilson. A programmable orenting systems for flat parts. In *Proc. 13th NAMRC*, pages 427–432, 1985.

[96] X. Markenscoff, L. Ni, and C. H. Papadimitriou. The geometry of grasping. *Int. J. of Robotics Research*, 9(1):61–74, 1990.

[97] X. Markenscoff and C. H. Papadimitriou. Optimum grip of a polygon. *Int. J. of Robotics Research*, 8(2):17–29, 1989.

[98] A. Markus, A. Markusz, and J. Farkas. Fixture design using prolog: An expert system. *Robotics and Computer Integrated Manufacturing*, 1(2):167–172, 1984.

[99] J. E. Marsden and T. J. R. Hughes. *Mathematical Foundations of Elasticity.* Prentice-Hall, 1983.

[100] J. M. R. Martinez and J. Duffy. On the metrics of rigid body displacements for infinite and finite bodies. *ASME J. of Mechanical Design*, 117(1):41–47, 1995.

[101] R. Mason, E. Rimon, and J. W. Burdick. Stability of heavy objects with multiple contacts. In *Proc. Int. Conf. on Robotics and Automation*, pages 439–445, Nagoya, Japan, May 1995.

[102] R. Mason, E. Rimon, and J. W. Burdick. Stable poses of 3-dimensional objects. In *Proc. Int. Conf. on Robotics and Automation*, pages 391–398, Albuquerque, NM, April 1997.

[103] R. J. Menassa and W. R. DeVries. Optimization methods applied to selecting support positions in fixture design. *ASME J. of Engineering for Industry*, 113:412–418, 1991.

[104] E. C. De Meter. Min-max load model for optimizing machining fixture performance. *ASME J. of Engineering for Industry*, 117(2):186–193, 1995.

[105] B. Mirtich and J. Canny. Easily computable optimum grasps in 2-D and 3-D. In *Proc. Int. Conf. on Robotics and Automation*, pages 739–747, San Diego, CA, May 1994.

[106] B. Mishra. Grasp metrics: Optimality and complexity. In *1994 Workshop on Algorithmic Foundations of Robotics*, pages 137–165, A. K. Peters, Wellseley MA, 1995.

[107] B. Mishra, J. T. Schwartz, and M. Sharir. On the existence and synthesis of multifinger positive grips. *Algorithmica*, 2(4):541–558, 1987.

[108] B. Mishra and N. Silver. Some discussion of static gripping and its stability. *IEEE Trans. on Systems, Man and Cybernetics*, 19(4):783–796, 1989.

[109] R. M. Murray, Z. Li, and S. S. Sastry. *A Mathematical Introduction to Robotic Manipulation.* CRC Press, Boca Raton, Florida, 1994.

[110] A. W. Naylor and G. R. Sell. *Linear Operator Theory in Engineering and Science.* Springer-Verlag, 1982.

[111] A. Y. C. Nee, N. Bhattacharyya, and A. N. Poo. Applying AI in jig and fixture design. *Robotics and Computer Integrated Manufacturing*, 3(2):195–200, 1987.

[112] Y. E. Nesterov and A. S. Nemirovsky. *Interior Point Polynomial Methods in Convex Programming: Theory and Applications.* Springer Verlag, 1992.

[113] V.-D. Nguyen. Constructing force-closure grasps. *Int. J. of Robotics Research*, 7(3):3–16, 1988.

[114] V.-D. Nguyen. Constructing stable grasps. *Int. J. of Robotics Research*, 8(1):26–37, 1989.

[115] K. Nikpur and R. Gohar. Deflexion of a roller compressed between platens. *Tribology International*, 8(2):2–8, 1975.

[116] B. Nnaji, S. Alladin, and P. Lyu. A framework for a rule-based expert fixturing systems for face milling planar surfaces on a cad system using flexible fixtures. *J. of Manufacturing Systems*, 7(1):193–207, 1988.

[117] W. Noll. Lectures on the foundations of continuum mechanics and thermodynamics. *Archive for Rational Mechanics and Analysis*, 52:62–92, 1973.

[118] E. Oberg, F. D. Jones, H. L. Horton, and H. H. Ryffel. *Machinery's Handbook.* Industrial Press, 24th edition, 1992.

[119] M. S. Ohwovoriole and B. Roth. An extension of screw theory. *ASME J. of Mechanical Design*, 103:725–735, 1981.

[120] F. C. Park. Distance metrics on the rigid body motions with applications to mechanism design. *ASME J. of Mechanical Design*, 117(1):48–54, 1995.

[121] Y. C. Park and G. P. Starr. Grasp synthesis of polygonal objects using a three-fingered robot hand. *Int. J. of Robotics Research*, 11(3):163–184, 1992.

[122] T. Patterson and H. Lipkin. Structure of robot compliance. *ASME J. of Mechanical Design*, 115(3):576–580, 1993.

[123] G. A. Pfeifer and F. W. Liou. Investigation resulting in guidelines to optimize fluidized-bed fixture performance. In *Proc. of the 1990 ASME Design Technical Confs.—2nd Conf. in Flexible Assembly Systems*, pages 37–44, Chicago, IL, September 1990.

[124] A. V. Pogorelov. *Lecutures on the Foundations of Geometry.* Translated from the 2nd Russian edition by L. F. Boron. P. Noordhoff Ltd., Groningen, the Netherlands, 1966.

[125] J. Ponce. On planning immobilizing fixtures for 3d polyhedral parts. In *IEEE Int. Conf. on Robotics and Automation*, pages 509–514, 1996.

[126] J. Ponce, J. W. Burdick, and E. Rimon. Computing the immobilizing three-finger grasps of planar objects. Proc. 2^{nd} Workshop on Comp. Kinematics, 1995.

[127] J. Ponce and B. Faverjon. On computing three-finger force-closure grasps of polygonal objects. In *Proc. Int. Conf. on Robotics and Automation*, pages 1018–1023, Sacramento, CA, 1991.

[128] J. Ponce, S. Sullivan, J-D. Boissonnat, and J-P. Merlet. On characterizing and computing three- and four-finger force-closure grasps of polyhedral objects. In *Proc. Int. Conf. on Robotics and Automation*, pages 821–827, Atlanta, GA, May 1993.

[129] P. C. Pong, R. R. Barton, and P. H. Cohen. Optimum fixture design. In *Proc. 2nd Industrial Eng. Research Conf.*, pages 6–10, Los Angeles, CA, May 1993.

[130] Poritsky. Stresses and deflections of cylindrical bodies in contact. *ASME J. of Applied Mechanics*, 18:191–201, 1950.

[131] D. Prattichizzo, J. K. Salisbury, and A. Bicchi. Contact and grasp robustness measures: Analysis and experiments. In *Proc. 4th Int. Symp. on Experimental Robotics*, pages 50–60, Stanford, CA, 1995.

[132] F. Reuleaux. *The Kinematics of Machinery.* MacMillan, 1876. Reprint: Dover, 1963.

[133] E. Rimon and A. Blake. Caging 2D bodies by 1-parameter two-fingered gripping systems. In *Proc. Int. Conf. on Robotics and Automation*, pages 1795–1800, May 1996. Minneapolis, MN.

[134] E. Rimon and J. Burdick. New bounds on the number of frictionless fingers required to immobilize planar objects. *J. Robotic Systems*, 12(6):433–451, 1995.

[135] E. Rimon and J. W. Burdick. Mobility of bodies in contact—i: A new 2^{nd} order mobility index for multiple-finger grasps. In *Proc. Int. Conf.*

on Robotics and Automation, pages 2329–2335, San Diego, CA, May 1994.

[136] E. Rimon and J. W. Burdick. Mobility of bodies in contact—ii: How forces are generated by curvature effects. In *Proc. Int. Conf. on Robotics and Automation*, pages 2336–2341, San Diego, CA, May 1994.

[137] E. Rimon and J. W. Burdick. Configuration space analysis of bodies in contact - i. 1^{st} order mobility. *Mechanism and Machine Theory*, 30(6):897–912, 1995.

[138] E. Rimon and J. W. Burdick. Configuration space analysis of bodies in contact - ii. $2^n d$ order mobility. *Mechanism and Machine Theory*, 30(6):913–928, 1995.

[139] E. Rimon and J. W. Burdick. Mobility of bodies in contact—i: A 2^{nd} order mobility index for multiple-finger grasps. *IEEE Trans. on Robotics and Automation*, To appear.

[140] A. J. Rosakis. Continuum mechanics of fluids and solids. Lecture notes. Department of Aeronautics, California Inst. of Technology, 1993.

[141] J. K. Salisbury. *Kinematic and Force Analysis of Articulated Hands.* PhD thesis, Stanford University, 1982.

[142] J. K. Salisbury and B. Roth. Kinematic and force analysis of articulated hands. *ASME J. of Mechanisms, Transmissions, Automation in Design*, 105:33–41, 1982.

[143] M. N. Sela, O. Gaudry, E. Dombre, and B. Benhabib. A reconfigurable modular fixturing system for thin-walled flexible objects. *Int. J. of Advanced Manufacturing Technology*, 13:611–617, 1997.

[144] A. Senthil kumar and A. Y. C. Nee. Framework for a variant fixture design system using case-based reasoning technique. In *Proc. ASME Int. Mechanical Eng. Congress and Exposition*, pages 763–775, New York, NY, 1995.

[145] G. S. A. Shawki and M. M. Abdel-Aal. Effect of fixture rigidity and wear on dimensional accuracy. *Ing. J. Mach. Toll Design and Research*, 5:183–202, 1965.

[146] P. R. Sinha and J. M. Abel. A contact stress model for multifingered grasps of rough objects. *IEEE Trans. on Robotics and Automation*, 8(1):7–22, 1992.

[147] A. H. Slocum, J. Peris, and A. Donmez. Development of a flexible automated fixturing system. SME Technical Paper MR86-126, 1986.

[148] P. Somoff. Uber gebiete von schraubengeschwindigkeiten eines starren korpers bie verschidener zahl von stutzflachen. *Z. Mathematik und Physik*, 45:245–306, 1900.

[149] Z. J. Tao, A. Senthil kumar, A. Y. C. Nee, and M. A. Mannan. Modelling and experimental investigation of a sensor-integrated workpiece-fixture system. *Int. J. of Computer Applications in Technology*, 10:237–250, 1997.

[150] K. Tchon and I. Duleba. Definition of a kinematic metric for robot manipulators. *Journal of Robotic Systems*, 11:211–221, 1994.

[151] M. Teichmann. A grasp metric invariant under rigid motions. In *Proc. Int. Conf. on Robotics and Automation*, pages 2143–2148, Minneapolis, MN, April 1996.

[152] B. S. Thompson and M. V. Gandhi. Commentary on flexible fixturing. *Applied Mechanics Reviews*, 39(9):1365–1369, 1986.

[153] J. A. Thorpe. *Elementary Topics in Differential Geometry.* Springer-Verlag, 1979.

[154] S. P. Timoshenko and D. H. Young. *Elements of Strength of Materials.* Van Nostrand, New York, 5th edition, 1968.

[155] K. Toucef-Toumi, K. S. Liu, and H. Asada. A computer integration of reconfigurable fixturing systems for drilling of sheet metal parts. In *2nd Robotics and Factories of the Future Conf.*, pages 751–759, San Diego, CA, 1987.

[156] A. J. C. Trappey, D. S. Su, and J. L. Hou. Computer-aided fixture analysis using finite element analysis and mathematical optimization modeling. In *Proc. ASME Int. Mechanical Eng. Congress and Exposition*, pages 777–787, New York, NY, 1995.

[157] J. C. Trinkle. On the stability and instantaneous velocity of grasped frictionless objects. *IEEE Trans. on Robotics and Automation*, 8(5):560–572, 1992.

[158] J. C. Trinkle, A. O. Farahat, and P. F. Stiller. Second-order stability cells for frictionless rigid body systems. In *Proc. Int. Conf. on Robotics and Automation*, pages 2815–2821, San Diego, CA, May 1994.

[159] J.C. Trinkle, A.O. Farahat, and P.F. Stiller. First-order stability cells of active multi-rigid-body systems. *IEEE Trans. on Robotics and Automation*, 11(4):545–557, 1995.

[160] C. Truesdell. *A First Course in Rational Continuum Mechanics.* Academic Press, 1977.

[161] K. Tuffentsammer. Automatic loading of machining systems and automatic clamping of workpieces. *CIRP Annals*, 30(2):553–558, 1981.

[162] V. K. Varma and U. Tasch. A new representation for a robot grasping quality measure. *Robotica*, 13:287–295, 1995.

[163] S. Vavasis. *Nonlinear Optimization: Complexity Issues.* Oxford University Press, 1991.

[164] I. D. Walker, J. B. Cheatham, and Y.-C. Chen. Efficient method for computing the force distribution of a three-fingered grasp. In *Proc. SPIE - Int. Society for Optical Eng. Cooperative Intelligent Robotics in Space*, volume 1387, pages 974–989, Bellingham WA, 1990.

[165] I. D. Walker, J. B. Cheatham, and Y.-C. Chen. Intelligent grasp planning strategy for robotic hands. In *Proc. SPIE - Int. Society for Optical Eng. Applications of Artificial Intelligence IX*, volume 1468, pages 974–989, Orlando, FL, 1991.

[166] A. S. Wallack and J. F. Canny. Planning for modular and hybrid fixtures. In *Proc. Int. Conf. on Robotics and Automation*, pages 520–527, San Diego, CA, May 1994.

[167] C.-C. Wang and C. Truesdell. *Introduction to Rational Elasticity.* Noordhoff International Publishing, Leyden, The Netherlands, 1973.

[168] D. E. Whitney. Quasi-static assembly of compliantly supported rigid parts. *ASME J. of Dynamic Systems, Measurement, and Control*, 104(1):65–77, 1982.

[169] J. D. Wolter and J. C. Trinkle. Automatic selection of fixture points for frictionless assemblies. In *Proc. Int. Conf. on Robotics and Automation*, pages 528–534, San Diego, CA, May 1994.

[170] Y. Wu, Y. Rong, and T. C. Chu. Automated generation of dedicated fixture design. *Int. J. of Computer Applications in Technology*, 10:213–235, 1997.

[171] M. Yeong, X. Dong, R. J. Menassa, and W. R. DeVries. Techniques to reduce lead time in fixture design. In *Proc. Manufacturing International, ASME*, pages 445–458, Dallas, TX, 1992.

[172] M. Yeong, L. Ruff, and W. R. DeVries. A survey of part presentation, feeding and fixturing in automated assembly systems. In *Proc. 3rd ASME Conf. on Flexible Assembly Systems, 1991 ASME Design Technical Conferences*, volume DE-Vol. 33, pages 83–90, Miami, FL, 1991.

[173] M. Zefran and V. Kumar. Affine connections for the cartesian stiffness matrix. In *Proc. Int. Conf. on Robotics and Automation*, Albuquerque, NM, April 1997.

[174] Y. Zhuang and K. Y. Goldberg. Design rules for tolerance-insensitive and multi-purpose fixtures. In *Proc. Int. Conf. on Advanced Robotics*, pages 681–686, 1997.

[175] Y. Zhuang, K. Y. Goldberg, and Y.-C. Wong. Planning for modular and hybrid fixtures. In *Proc. Int. Conf. on Robotics and Automation*, pages 543–549, San Diego, CA, May 1994.